Fast Transient Fluid Structure Interaction Vibration of Immersed Structures in Typical Liquid Metal Fast Breeder Reactor

By

SUMATHI V

Enrolment Number: ENGG02201304011

Indira Gandhi Center for Atomic Research, Kalpakkam, India

A thesis submitted to the Board of Studies in Engineering Sciences

In partial fulfillment of requirements

For the Degree of

DOCTOR OF PHILOSOPHY

of

HOMI BHABHA NATIONAL INSTITUTE

June, 2019

Homi Bhabha National Institute[1]

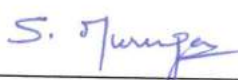## Recommendations of the Viva Voce Committee

As members of the Viva Voce Committee, we certify that we have read the dissertation prepared by **Sumathi V** entitled **"Fast Transient Fluid Structure Interaction Vibration of Immersed Structures in Typical Liquid Metal Fast Breeder Reactor"** and recommend that it may be accepted as fulfilling the thesis requirement for the award of Degree of Doctor of Philosophy.

Chairman – **Dr. K Velusamy**		Date : 19/7/2019
Guide / Convener - **Dr. S. Murugan**		Date : 19.7. 2019
Examiner - **Dr. Amiya Ranjan Mohanty**		Date : 19/7/2019
Member 1- **Dr. Anil Kumar Sharma**		Date : 19/7/2019
Member 2- **Dr. Anish Kumar**		Date : 19/7/19
Technology Adviser- **Dr. P. Selvaraj**		Date : 19/7/19
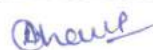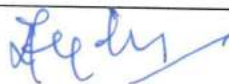
Final approval and acceptance of this thesis is contingent upon the candidate's submission of the final copies of the thesis to HBNI.

I hereby certify that I have read this thesis prepared under my direction and recommend that it may be accepted as fulfilling the thesis requirement.

Date: 19/07/2019

Place: Kalpakkam

Dr. S. Murugan

(Guide)

---

[1] This page is to be included only for final submission after successful completion of viva voce.

STATEMENT BY AUTHOR

This dissertation has been submitted in partial fulfillment of requirements for an advanced degree at Homi Bhabha National Institute (HBNI) and is deposited in the Library to be made available to borrowers under rules of the HBNI.

Brief quotations from this dissertation are allowable without special permission, provided that accurate acknowledgement of source is made. Requests for permission for extended quotation from or reproduction of this manuscript in whole or in part may be granted by the Competent Authority of HBNI when in his or her judgment the proposed use of the material is in the interests of scholarship. In all other instances, however, permission must be obtained from the author.

Sumathi V

DECLARATION

I hereby declare that the investigation presented in the thesis has been carried out by me. The work is original and has not been submitted earlier as a whole or in part for a degree / diploma at this or any other Institution / University.

Sumathi V

LIST OF PUBLICATIONS

Journals

a. Published

1. **Sumathi V,** Jalaldeen S, Selvaraj P and Murugan S, "Vibration of core subassemblies due to large sodium-water reaction in the steam generator of an LMFBR" Progress in Nuclear Energy, Vol. 106, July 2018, Pages: 231-239. https://doi.org/10.1016/j.pnucene.2018.03.005

2. **Sumathi V,** Jalaldeen S, Selvaraj P and Murugan S, "Implications of large scale sodium water reactions in an LMFBR", Nuclear Engineering and Design, Vol 337, October 2018, Pages: 364-377. https://doi.org/10.1016/j.nucengdes.2018.07.013

b. Communicated

Sumathi V, Jalaldeen S, Selvaraj P and Murugan S, "Forced vibration transmission analyses of two parallel plates immersed in fluid with Fluid Structure Interaction" (International Journal of structural Integrity).

c. To be communicated

1. **Sumathi V,** Jalaldeen S, Selvaraj P and Murugan S, "Experimental and numerical simulation of vibration response of cantilever plates immersed in a fluid", (Journal of Pressure vessel technology-ASME).

Conference proceedings

1. **Sumathi V,** Jalaldeen S, Selvaraj P and Murugan S "Investigation of Vibration Transmission in Cantilevered Structures Submerged in Fluid Considering Fluid Structure Interaction" in sixth International congress on Computational Mechanics and simulation ICCMS 2016 held in IIT Bombay on June 27-July 01, 2016.

2. **Sumathi V,** Jalaldeen S, Selvaraj P and Murugan S "Experimental and Numerical investigation of vibration transmission between two parallel plate partially immersed in a fluid" in Turbomachinery Technical conference and Exposition ASME-TURBOEXPO 2017 held in Charlotte, USA on June 26-30, 2017. doi:10.1115/GT2017-63391

3. **Sumathi V,** Jalaldeen S, Selvaraj P and Murugan S "Analysis of fluid structure interaction vibration response for plate and rod structures excited by sinusoidal and impulse loads" in International conference on Power Engineering ASME-ICOPE 2017 held in Charlotte, USA on June 26-30, 2017.

4. **Sumathi V,** Jalaldeen S, Selvaraj P and Murugan S "Investigation of Vibration response in cantilever plates partially immersed in a fluid" in HBNI RSM-MSENM - 2018 held in IGCAR, Kalpakkam on May 07-09, 2018.

Sumathi V

Dedicated to my Parents and

Husband

ACKNOWLEDGEMENTS

CONTENTS

SYNOPSIS

In a Liquid Metal Fast Breeder Reactor (LMFBR), the heat generated in the reactor core is removed by liquid sodium in the primary circuit, which is transferred to secondary sodium in the Intermediate heat exchanger (IHX). The secondary sodium flows through the steam generator exchanging heat with the steam water system. When steam/water leaks into the shell side of sodium, due to defects or ruptures of the steam generator heat transfer tubes, sodium water reaction will occur. The sodium water reaction will cause various phenomena depending on the amount of water coming out and will have different effects on steam generator and primary circuit.

Since IHX is hanging freely from top, it vibrates when a high-pressure wave due to large sodium water reaction passes through it. Through sodium and inner vessel this vibration can get transmitted to subassemblies leading to possible reactivity oscillations. In connection to this investigation, the hydrodynamics of structures partially or fully immersed in liquid medium and the phenomenon of vibration transmission between immersed structures have to be studied. To analyze the behavior of large components immersed in liquid sodium, the phenomenon of Fluid Structure Interaction (FSI) vibration is studied using finite element code CAST3M. Experiments have been conducted to study vibration transmission between plate structures and plate and tube structures partially immersed in a fluid.

This work focuses on the evaluation of subassemblies displacement and consequent changes in the reactivity in a fast breeder reactor in case of design basis and beyond design basis sodium water reaction.

Vibration transmissions between plate and tube structures immersed in fluid have been found experimentally and the results were compared with CAST3M results. The results are closely matching, and it provides validation of / applicability of CAST3M for the present study. When the plate is excited close to its resonance frequency, the amplitude of vibration of the response plate is found to be higher and it is much lower when excited far away from its resonance frequency in immersed conditions. Parametric studies were carried out with change in width and depth of plates immersed in medium. Further in the study of tubular structures, the vibration transmission between plate and tube were studied. Transmissibility ratios close to resonance frequency showed higher values.

Investigations on the response of various reactor assembly components due to design and beyond design basis sodium water reactions have been studied. Evaluation of displacement of subassemblies in the reactor for design basis leak and beyond design basis leak shows a maximum displacement of 0.07 mm and 0.3 mm respectively. Reactivity perturbations due to displacement of subassemblies are found to be negligible. From these investigations, it is concluded that sufficient margin exists in the design to take care of transient event like large scale sodium water reactions to the extent of simultaneous double-ended guillotine failure of 15 tubes in the steam generator.

LIST OF FIGURES

LIST OF TABLES

CHAPTER 1

Introduction

<div style="text-align: right; font-size: large;">**1**</div>

1.0 FOREWORD

Energy availability is essential for human development and is the prime concern of economic growth. In developing countries like India with rapid industrialization and growing population, the energy consumption rate is growing at a faster pace creating a large energy deficit. To meet this demand, new energy sources and technologies are being developed. Among the energy generation methods, non-conventional, renewable, and environment friendly methods are preferred globally. Nuclear energy is considered to be one of the clean and sustainable sources of such energy. India has formulated the well-known three-stage nuclear power programme as depicted in Fig. 1.1 (Kakodkar, 2008).
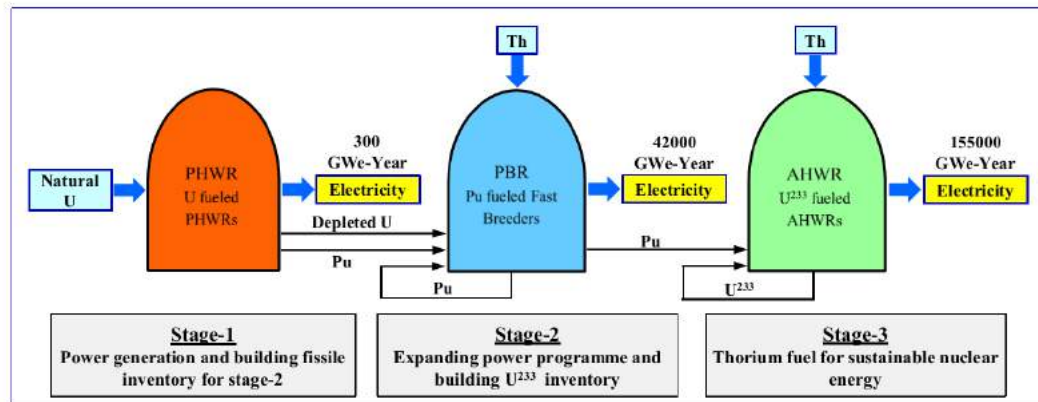
Fig.1.1 Three-stage nuclear power programme

First stage comprises of thermal reactors fueled by natural Uranium containing 0.7% of fissile isotope of U^{235} and they are based on Pressurized Heavy Water Reactor

(PHWR) technology. PHWR's have been chosen for the first stage, as these are efficient producers of Plutonium required for the second stage. In the second-stage of nuclear programme, the energy from natural Uranium can be increased to about 3,00,000 MW in the coming years through Fast Breeder Reactors (FBR). Fast Breeder Reactors form the second-stage of the program linking the first phase with natural Uranium and third phase with Thorium fuels. By adopting Th^{232}-U^{233} cycle in the third-stage, the energy potential for sustainable electricity generation will be further increased that would last for few centuries.

Currently second-stage of nuclear programme with Fast Breeder Reactor technology is being recognized before launching a large scale programme on fast reactors. Fast reactor concepts are typically categorized by their coolant. The commonly used coolants for the fast reactors are (i) Sodium-cooled Fast Reactor (SFR); (ii) Lead or Lead-Bismuth cooled Fast Reactor (LFR); (iii) Gas-cooled Fast Reactor (GFR). For the second-stage of nuclear programme, Sodium cooled Fast Reactor concept has been considered reliable and economical.

1.1 SODIUM COOLED FAST REACTOR

Sodium cooled Fast Reactor concept has been considered for its following characteristics,

➢ Liquid metal sodium coolant is ~100 times more effective heat transfer medium compared to water with wide range of boiling (upto 800^{0} C) and its compatibility with structural components and metallic fuels.

➢ High temperature operation (>500^{0} C) and greater thermal efficiency for energy conversion.

- Low pressure primary and intermediate coolant system.

- Low design pressure for containment on the basis of heat produced by potential sodium fire.

- Simpler operation and accident management.

Overview of currently operating SFRs and their various applications are discussed (Banerjee, 2017). SFR's have two major configurations, the Loop type and the Pool type. A 40 MW thermal capacity loop type Fast Breeder Test Reactor (FBTR) was constructed at Kalpakkam, India in the year 1985 (Srinivasan et.al, 2006). As a follow up to FBTR, a pool type 500 MW electric power Prototype Fast Breeder Reactor (PFBR) was designed and presently it is under construction in Kalpakkam, India (Chetal et al., 2011), (Chetal, 2006, 2011).
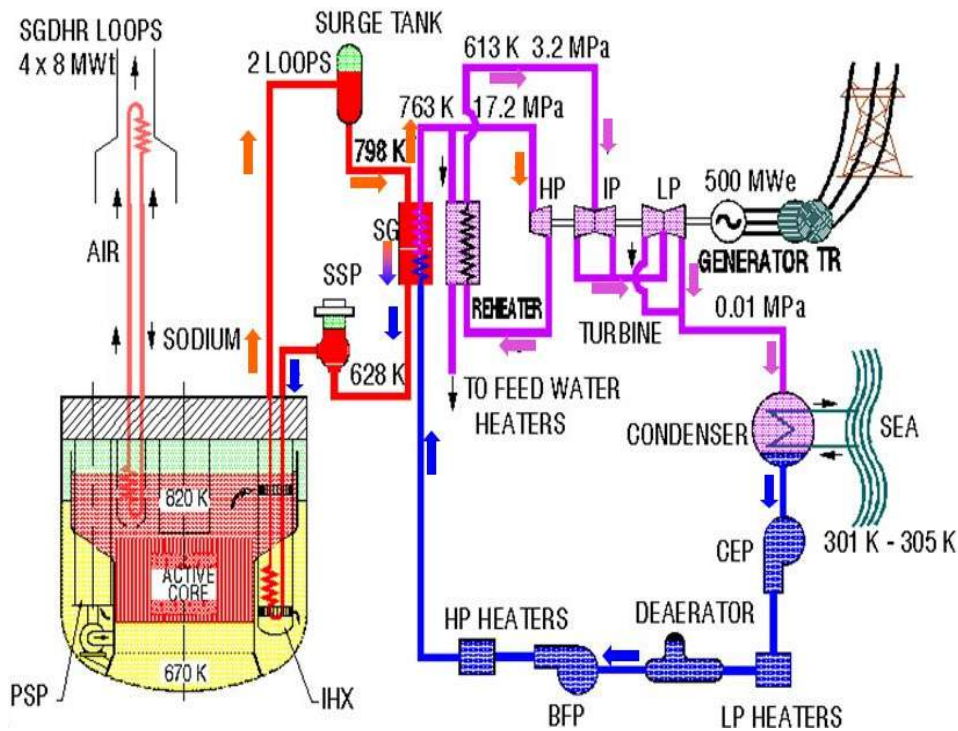
Fig.1.2 Flow sheet of typical Sodium cooled Fast Reactor

SFRs generally have three heat transfer systems, (i) Primary heat transfer system which cools the core; (ii) Intermediate heat transfer systems which transfer heat from the primary loop to the Steam Generator; (iii) Energy conversion systems to generate electricity with a turbine. The flow sheet of typical SFR is depicted in Fig. 1.2 (Padmakumar et al., 2013). It consists of three circuit's viz., two sodium circuits to transfer the nuclear heat generated in the core to the steam water system and power plant circuit to produce steam to run the turbine. The two sodium circuits are known as primary and secondary circuits. Among these two circuits, the primary circuit is entirely inside the pool of sodium. An expanded view of primary circuit assembly is depicted in Fig. 1.3.

The primary sodium is contained in a large diameter vessel called Main vessel, and consists of core, primary pumps, Intermediate Heat Exchanger (IHX) and primary pipe connecting the pumps and grid plate. The vessel has no penetrations and it is welded at the top to the roof slab. The vessel is cooled using cold sodium to enhance its structural integrity. The core subassemblies are supported on grid plate, which in turn is supported on core support structure. The Main vessel is surrounded by a Safety vessel, following the shape of the Main vessel closely, with a nominal gap to permit robotic and ultrasonic inspection. The Safety vessel helps to keep the sodium level above the inlet windows of the Intermediate Heat Exchanger ensuring continued cooling of core in case of a leak in Main vessel. The inner space between Main and Safety vessel is filled with inert nitrogen. The main vessel is closed at its top by a top shield, which includes roof slab, large and small rotary plugs and control plug. The reactor vault concrete ensures the biological shielding in the radial and bottom axial direction outside of the Main vessel.
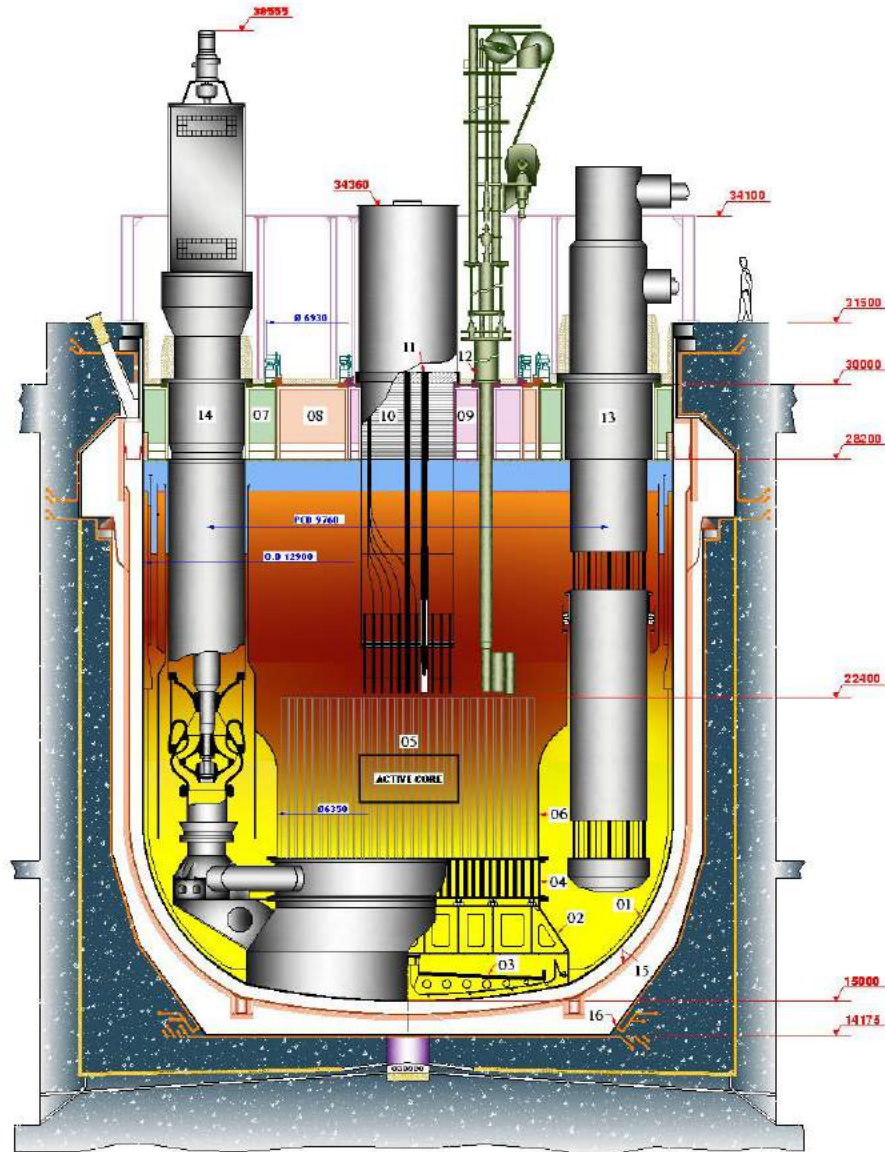
Fig.1.3 Primary Circuit assembly of Pool type Fast Breeder Reactor*

*
  LEGEND

01	MAIN VESSEL	09	SMALL ROTATABLE PLUG
02	CORE SUPPORT STRUCTURE	10	CONTROL PLUG
03	CORE CATCHER	11	CONTROL AND SAFETY ROD MECHANISM
04	GRID PLATE	12	IN-VESSEL TRANSFER MACHINE
05	CORE	13	INTERMEDIATE HEAT EXCHANGER
06	INNER VESSEL	14	PRIMARY SODIUM PUMP
07	ROOF SLAB	15	SAFETY VESSEL
08	LARGE ROTATABLE PLUG	16	REACTOR VAULT

Safe operation of the reactor is of prime importance for which number of transient event analyses are carried out. With advancement of numerical methods and computing technology in the recent past, Finite Element Method (FEM) has been harnessed to address and solve many challenges in the design and safety evaluation of SFR's. This is evident from the published work (Puthiyavinayagam et al., 2017) for Indian FBR's.

1.2 SODIUM - WATER REACTION

In a SFR, liquid sodium is used as a primary and secondary coolant. When steam/water leaks into the shell side of Steam Generator containing secondary sodium, sodium-water reaction will occur. This problem has been considered as one of the most critical problems for a wide use of SFR's. Sodium-water reaction is an exothermal reaction which is composed of three reactions:

$$H_2O + Na \rightarrow NaOH + \frac{1}{2} H_2 \quad \ldots\ldots\ldots\ldots\ldots\ldots\ldots\ldots\ldots\ldots\ldots\ldots\ldots\ldots\ldots\ldots\ldots\ldots\ldots ...(1.1)$$

$$H_2 + 2 Na \rightarrow 2 NaH \ldots\ldots\ldots\ldots\ldots\ldots\ldots\ldots\ldots\ldots\ldots\ldots\ldots\ldots\ldots\ldots\ldots\ldots\ldots.(1.2)$$

$$NaOH + 2 Na \rightarrow NaH + Na_2O \ldots\ldots\ldots\ldots\ldots\ldots\ldots\ldots\ldots\ldots\ldots\ldots\ldots\ldots..(1.3)$$
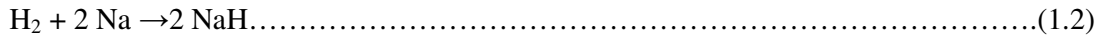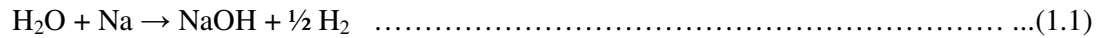
The first reaction is the primary chemical reaction, which occurs instantaneously, and the following two reactions would occur as secondary reactions. From the chemical analyses, the reaction products of large scale sodium-water reaction contain NaOH, Na_2O and NaH. The reason of sodium-water reaction includes tube corrosion with loss of tube wall thickness due to stress corrosion cracking (mainly in welded zones), thermal shocks when under-saturated water is injected at inlet inducing thermal fatigue, restraint tube expansion induced by differential expansion, and tube bundle vibrations due to hydraulic

effect of sodium flow inducing tube wear (Hori, M., 1980). The effects of sodium-water reaction can be categorized as Chemical effects, Mechanical, and Overheating effects. Chemical effects are stress corrosion cracking due to NaOH, and local corrosion/erosion. Mechanical effects are overpressure, and vibration. Overheating effects are deformation, swelling and bursting of tubes.

The sodium-water reaction will cause various phenomena depending on the amount of water/steam released and will have different effects on Steam Generator and primary circuit. Depending on the leak rate and its effect, sodium-water reaction is classified into four types (Hori, M., 1980) : (i) Micro leak where only self-wastage occurs, (ii) Small leak where impingement wastage of a tube which is directly opposite to the leaking tube occurs, (iii) Intermediate leak where wastage occurs on multiple tubes due to overheating and also causes pressure increase, and (iv) Large leak where pressure rise due to hydrogen generation is more dominant.

Table 1.1 Comparison of leak rate with diameter of hole and dominant threat of the event

Leak	Diameter (Hole/m)	Dominant threat
Micro leak (<0.05 g/s)	$< 0.7 \times 10^{-3}$	Too small to detect, bubbling may occur, no threat to other adjacent tubes. Enlargement of leaking hole occurs.
Small leak (0.05-10 g/s)	$(0.7-1.0) \times 10^{-3}$	Generate corrosive sodium-water jet, damage to adjacent tubes.
Intermediate leak (10-2000g/s)	$(1.0-7.0) \times 10^{-3}$	Damage of adjacent tubes, tube failure by overheating and pressurization due to hydrogen production in single tube
Large leak (>2000 g/s)	$>7.0 \times 10^{-3}$	Tube failure by overheating and overpressure, rapid pressurization due to hydrogen production in multiple tubes

In case of large leak, high pressure waves are generated. These waves travel throughout the secondary sodium system causing pressurization and vibration of the components and piping.

1.3 OBJECTIVES AND SCOPE OF THE THESIS WORK

In LMFBR's of rated power 500 MWe or more, pool type concept is used for the primary system where Main vessel, IHX, and other components are supported from the top. Supporting from the top allows free expansion of the components when reactor temperature increases from room temperature to the maximum operating temperature of around 550 ℃.

When the steam generator tubes leak or break, the leakage of water into the sodium may occur, resulting in a sodium-water reaction. The sodium-water reaction produces hydrogen and heat, thus generating high pressure waves near the leak. The hydrogen gas produced causes rapid pressure buildup inside the steam generator. The pressure generated in the steam generator propagates to the secondary heat-transport system components through the sodium coolant piping. Further the pressure gets propagated to the intermediate heat exchanger (IHX) through the coolant piping connected to inlet and outlet of IHX. IHX inlet and outlet experiences sudden rise in pressure due to this pressure wave propagation.

Since IHX is hanging freely from top, it vibrates when a high pressure wave due to large sodium-water reaction passes through it. Through sodium and Inner vessel this vibration can get transmitted to the subassemblies in the core (Fig. 1.4) leading to possible reactivity oscillations. In connection to this investigation, the hydrodynamics of

structures partially or fully immersed in liquid medium and the phenomenon of vibration transmission between structures need to be studied. To analyze the behavior of large components immersed in liquid sodium, the phenomenon of Fluid Structure Interaction (FSI) vibration is studied using FEM code CAST3M, and experiments with plate and tube structures have also been conducted.
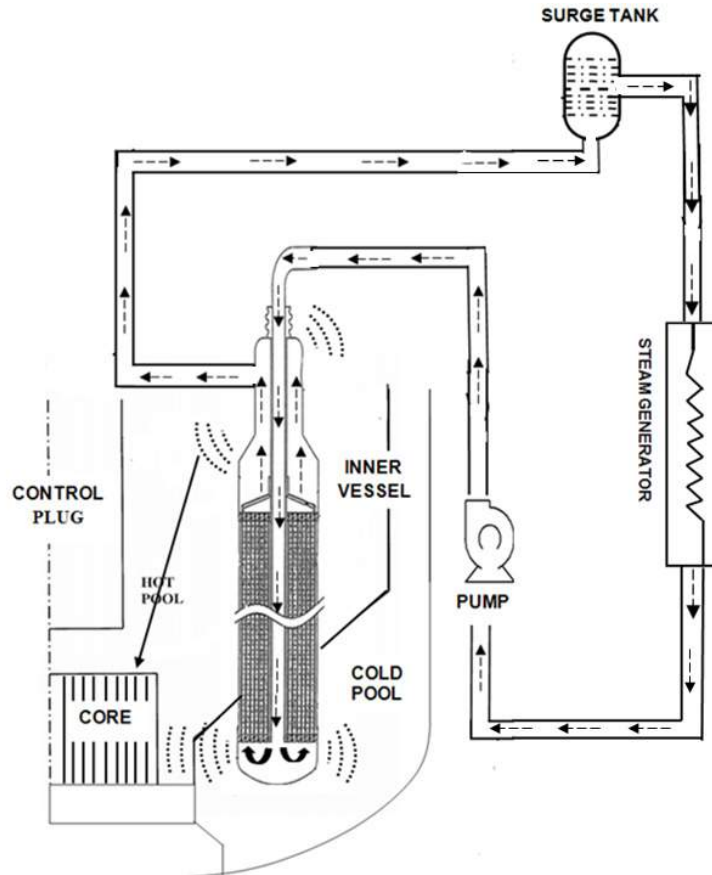
Fig. 1.4 Transmission of vibration from IHX to the core

The objectives of the present research are:

(i)   To use the numerical code CAST3M for the FSI vibration problems through benchmark studies and experiments.

(ii)   To study numerically the vibration transmission between walls of tank structure partially filled with a fluid.

(iii)   To validate the above numerical work through an experimental work.

(iv)   To study vibration transmission between cantilevered plate structures partially immersed in a fluid with an experimental setup established for this purpose.

(v)   To study numerically the above experimental work in CAST3M

(vi)   To study vibration transmission between plate and tube structures immersed in a fluid with an experimental setup.

(vii)   To investigate the vibration in core subassemblies due to large leak sodium water reaction in a typical LMFBR.

1.4 ORGANIZATION OF THE THESIS

Present thesis is divided into four major parts. The first part comprises of two chapters with introduction of the problem (Chapter - 1) and literature survey (Chapter - 2). The second part comprises of two chapters dealing with use of FEM code for the study of FSI phenomenon in immersed structures (Chapter - 3) and usage of the code to study vibration transmission with experimental works (Chapter - 4). Third part comprises the investigation of FSI vibration in reactor assembly components for Design basis event (Chapter - 5) and Beyond Design basis event (Chapter - 6) sodium-water reactions. The final part of the thesis (Chapter - 7) focuses on the summary of the major findings of this thesis and future scope of the work.

* * *

CHAPTER 2

Literature Survey   **2**

2.0 INTRODUCTION

The pool type fast reactors have specific favourable features, such as operation at low pressures and high thermal inertia. However, the general safety concerns for SFRs require serious attention because some potential accident may lead to reactivity insertion and power increase. Therefore, extensive studies have been carried out on reactivity point of view through large experimental works and theoretical developments. SFR uses liquid sodium as the coolant which is a very reactive metal and must be carefully controlled to avoid leaks that can trigger damaging events such as fire. Liquid sodium is advantageous because it has excellent heat removal capability and, non-corrosive to stainless steels. However it has significant disadvantages as well as it ignites spontaneously upon contact with air and reacts violently with water. As a result, the SFR system presents distinct challenges that the nuclear power industry needs to address as it develops this technology. Sodium-water reaction is one such event which has to be studied in detail in a SFR. Some of the significant literatures related to sodium-water reactions and their effects on the reactor components are discussed in this chapter.

In addition, the dynamics of immersed structures and recent advancements in the field of vibration analysis of immersed structures have also been discussed here.

2.1 SODIUM-WATER REACTION & VIBRATION STUDY IN LMFBR

2.1.1 Sodium-Water reaction

SFR utilizes a primary coolant loop that transfers heat via steam generator to a secondary loop. In the steam generators, high temperature sodium exchanges heat with water and water is converted to saturated or superheated steam. The sodium and water are separated by the wall of thin transfer tubes. Therefore, if hole or breach occurs in the heat transfer tube, leakage of water into the sodium will occur, resulting in a sodium-water reaction. The reaction between sodium and water is violent. Studies have been carried out 1950 on the effects of the reaction between sodium and water so as to facilitate the safe handling of sodium as a coolant for nuclear reactors. Computer codes to analyze the pressure transients caused by sodium-water reactions in a steam generator and its related systems have been developed in various countries, and used for the safety analysis of SFR steam generators. Details of research on sodium-water reaction event, its consequences, threat and design considerations to the steam generators have been elaborated (Hori, M., 1980). Safety analysis and response of the secondary sodium system of the Experimental Breeder Reactor-II to postulated leaks of steam and water into sodium is hypothesized (S Srinivas and P.S Chopra, 1977) to calculate the dynamic pressures in the system and the stresses in the components. Mathematical formulations for water leak model and steam leak model for pressure transients resulting from sodium-water reaction following a large leak in a SFR have been presented (Rajput, 1983). Dynamics of a sodium-water reaction bubble in the sodium of a steam generator of SFR is analytically solved using bubble dynamics model (Shin et al., 1988). This paper also explains the dynamics of the sodium-

water reactions coupled to the response of intermediate heat transport system. Mathematical model of the sodium-water reactions and pressure transients in an SFR with spherical and columnar bubble models in the reaction site have been compared with the experimental results (Selvaraj et al., 1990). Vapour mass flow rate and corresponding hydrogen production rate for the sodium-water reaction have been numerically approached using CFD (Computational Fluid Dynamics) code and, also a comparison with the 1-D models for a SFR steam generator have been presented (SeyunKim et al., 2007). Evaluation of steam generator tube rupture accident has been carried out as part of safety analysis with investigations in structural integrity of the immersed components (S.Wang et al., 2008). Experiments simulating steam leaks into sodium to study the phenomenon of impingement wastage and its effect to the adjacent tubes have been studied (Kishore et al., 2012).

2.1.2 Vibration studies due to Sodium-Water reaction

Experimental and theoretical approach have been used to the study the flow induced vibrations in fuel pins of SFR. Variations in the natural frequencies and modes shapes are found to occur due to random pressure fluctuations in the coolant (Kadlec and Appelt, 1970). Analyses for coupled vibration of a group of cylinders in liquids with emphasis on fuel bundle vibration have been carried out (Shoei-sheng Chen, 1975). Numerical calculations for the fluid structure coupling of the fuel subassemblies have been examined to study the resonance frequencies of the core (Planchard, 1985). Using the analysis of flow induced vibration and fluid structure interaction in reactor internals, the structural vibration caused by bulging and the sloshing phenomenon has been

explained (Fujita, 1990). A computer code SAFA was developed to analyze the vibration of SFR components during seismic excitation to calculate the impact forces during such an event (Horiuchi et al., 1995). Consequences of sodium-water reaction in the secondary sodium circuit for a typical pool type reactor and pressure propagation to IHX and surge tank have been presented (Selvaraj P. et al., 1996). In the work of (Aizawa, 1998), the importance of safety study of sodium-water reactions and examples of fluid structure coupled vibration due to water leakage in the secondary circuit of fast reactors have been discussed. Mechanical excitations of reactor assembly components due to primary sodium pump vibration have been studied (Chellapandi et al., 2003). Various structural dynamic studies for a typical SFR including the response of intermediate heat transport system components due to sodium water reaction have been reported (Bhoje, 2003). Seismic analyses of reactor internals in a pool type SFR with core displacement have been studied (Chellapandi et al., 2007). Flow induced vibration experiments for intermediate heat exchanger for a typical SFR have been carried out (Prakash et al., 2009). Fluid structure interaction studies in the interspace between main vessel and safety vessel for a typical SFR have been reported (Chellapandi et al., 2012) for the dynamic pressure developed. Evaluation of temperature rise in the subassemblies due to rupture in steam generator tubes caused by sodium-water reaction for prototype Generation IV sodium cooled fast reactor has been presented (Ahn et al., 2016). The importance of the phenomenon of Fluid Structure Interaction (FSI) in design and analysis of future nuclear power plants has been explained using numerical studies (Song et al., 2017). Dynamic characteristics of plate type fuel subassemblies immersed in water are numerically investigated (GauravVerma et al., 2017).

2.2 VIBRATION STUDIES IN IMMERSED STRUCTURES

2.2.1 Vibration studies in plates

Fluid around a structure can significantly alter the vibrational characteristics of the structure. The presence of fluid decreases the natural frequencies and increases the damping effect of the structure. The fluid couples the vibration of elastic structures which are adjacent to each other, thus a fluid flow can induce vibration. A vibration induced by the fluid flow is due to Fluid Structure Interaction (FSI) phenomena. FSI can simply be defined as the effect of fluid on structure and the resulting effect exerted by the structure on the fluid. Thus strong fluid structure interaction phenomena results when the fluid force on a structure induces a significant response which in turn alters the fluid force.

An accurate understanding of the dynamic interaction between elastic structures and fluid is necessary in various engineering problems. Plates and shells are simple mechanical structures which are commonly considered in modeling, analysis and experimental works through which an approximate behavior of complex structures can be understood. Examples of FSI include vibration of floating structures (ships, offshore platforms etc.) excited by wave impact, water retaining structures (dams, storage vessels etc.) under earthquake loading etc. The local resonant vibration behavior of individual structures is a significant concern for the designers. Plate structures have wide applications in areas such as, modern construction engineering, aerospace and aeronautical industries, aircraft construction, ship building and the components of nuclear power plants. In recent literature, there has been renewed interest in the problem of plates

vibrating in contact with fluid. Experimental investigation of the resonance frequencies of cantilever plates in air, totally or partially immersed in water have been carried out (U.S. Lindholm et al., 1965) and, the results are compared with the theoretical predictions using a strip-theory approach. Free vibration of submerged cantilever plates including the effects of partial submergence and liquid free level surface have been presented (Marcus M.S, 1978) using finite element simulation. The finite element method has also been applied to solve fluid structure interaction problems for completely immersed plates (Muthuveerappan et al., 1979). Parametric studies with change in boundary conditions and fluid medium of different densities have been considered in the prediction of natural frequency and mode shapes of cantilever plates (Muthuveerappan et al., 1980). Towards the analysis of vertical shaft pump, the vibrations of a non-uniform cantilever beam immersed in the fluid have been analyzed using a spline interpolation technique (Narita, 1982). Vibration of immersed plates with six type of temperature distributions has been studied to calculate the natural frequencies using finite element method (Rao and Ganesan, 1985). Dynamic behavior of a vertical or horizontal cantilever plate totally or partially immersed in fluid have been studied (Fu and Price, 1987). In the analyses, they calculate the generalized fluid loading to assess the influences of free surface and submerged plate length on the dynamic characteristics. Vibrations of square composite plates immersed in the fluid have been considered to calculate the Eigen frequencies and Eigen vectors using finite element method (Joseph et al., 1990). Experimental and theoretical observations on a waveguide/sensor immersed in fluid and its characteristics depending on fluid viscosity have been studied (Kim et al., 1991). Numerical investigations on vibration of a flexible plate coupled with acoustics wave propagation

have been carried out (Frendi et al., 1992). Resonance characteristics of cantilever plates vibrating in fluid have been investigated using an optical detection method (Inaba et al., 1993). Considering surface wave effects and compressibility of water, vibration of immersed uniform columns with arbitrary cross sections is solved for the Eigen frequencies (Zhou, 1993). Using finite element method, evaluation of non-linear hydrodynamic damping effects of the off shore structures have been presented (Venkataramana and Kawano, 1995). Dynamic response of flat horizontal plates vibrating in air and under water has been investigated experimentally and analytically. Added masses and natural frequency of the rectangular plates are determined. Using added mass approach, free vibration analysis of annular plates immersed in the fluid medium has been carried out and Hankel transform has been used to solve the fluid-plate coupled system (Amabili et al., 1996). Using displacement variable for solid and the fluid, computation of Eigen frequencies in the case of incompressible fluid-elastic structures have been studied, and a numerical solution for fluid structure interaction problem has been presented (Bermúdez et al., 1997). Using Rayleigh-Ritz method, the forced vibration analysis of a thin plate floating in an infinite fluid medium has been carried out (Meylan, 1997). Numerical computations of hydroelastic vibration with displacement formulation and including the effects of gravity on free surface of the fluid as well as on the liquid–solid interface have been presented (Bermúdez and Rodríguez, 1999). They have used finite element method to calculate the Eigen frequencies and sloshing frequencies. Analytical and numerical study for the vibrations of cantilever plates in air and water using added mass formulation for various aspect ratios and thickness ratios of the plates have been presented (Liang et al., 2001). Using finite element method, vibrations in a fluid coupled

system subjected to an external harmonic excitation with interface damping have been computed (Bermúdez et al., 2001). Plates with uniformly distributed mass and concentrated mass have been analyzed for free vibration in comparison with cantilever plates partially or fully immersed in the fluid (Kopmaz and Telli, 2002).The dynamic characteristics of a vertical cantilever plate partially in contact with the fluid were investigated (Ergin and Uğurlu, 2003). A three dimensional vibration analysis of two identical rectangular plates coupled with fluid has been validated using an analytical method. Natural frequency of the fluid structure coupled system has been obtained using a finite Fourier series expansion method (Jeong et al., 2004). For cantilever beams immersed in a fluid, it was observed that the resonant frequencies are unaffected by the fluid in the limit of higher modes in comparison with the lower modes (Van Eysden and Sader, 2006). Fluid structure interaction studies in impulsive loading in the fluid medium and the response of the structure due to this effect have been reported (Espinosa et al., 2006).Using Neumann-Kelvin formulation in time domain, the dynamic analysis of a cantilever plate has been described (Kara and Vassalos, 2007). Analyses of a rectangular cantilever plate in contact with a fluid with a crack have been carried out using Rayleigh Ritz method (SeyunKim et al., 2007). Natural frequency analysis of two rectangular plates coupled with the fluid with different depth of immersion using Rayleigh Ritz method has been carried out and it was observed that the normalized natural frequencies increase with the liquid thickness for out-of-phase mode shapes and decreases for in-phase mode shapes for the two identical plates (Jeong and Kim, 2009). Using finite element method and Sander's shell theory, the natural frequencies of the rectangular plates immersed in the fluid for different immersion depths have been carried out with the

numerical model (Kerboua et al., 2008). Frequency response of micro cantilever plates have been studied and it was established that compressibility has a significant effect on the frequency response of micro cantilever beams immersed in gas, whereas in liquid the effects of compressibility are negligible in practice (Van Eysden and Sader, 2009). Free vibration analysis of vertical rectangular moderately thick plates resting on elastic foundation and fully or partially in contact with fluid on their one side have been studied by using the well-known Ritz method (HosseiniHashemi et al., 2010). Natural frequencies of rectangular plates are studied for different fluid levels, foundation parameters, aspect ratios, thickness to width ratios and boundary conditions. A study on transmission of vibration between two beams immersed in a fluid and connected by a mechanical link has been carried out (Zhang et al., 2012) considering FSI. Natural frequency, mode shapes and pressure distribution in the fluid have also been studied. Free vibration of horizontal plates on the free surface of the fluid and the influence of fluid depths, fluid densities, aspect ratios and thickness to length ratios has been studied through simulation and analytical work (Hosseini-Hashemi et al., 2012). Dynamic response of the cantilever beam such as resonant frequency, and frequency amplitude, and compared as functions of the rheological properties (density and viscosity) of fluid media have been presented (Hossain et al., 2012). The resonant frequency of the beam was found to be decreased with the increasing fluid density and viscosity. Vibration analysis of a bundle of identical rectangular plates fully in contact with an ideal liquid have been presented (Jeong and Kang, 2013). It was remarkable that the lowest natural frequency of the liquid-coupled multiple rectangular plates is the same as that of a single plate with a half gap between the rigid walls and plate. The above study represents the

fuel assemblies of a research reactor consist of a number of rectangular fuel plates with an equal gap with coolant flow between the fuel plates for exchange of heat generated in the fuel plate. Vibration analysis of a composite cantilevered plate for both in-air and in-water cases have been studied via combined analytical and numerical analysis (Kramer et al., 2013). This paper highlights the importance of considering added mass effects for composite plates and beams immersed in fluid. Vibrational characteristics of composite beams immersed in fluid with FSI using different materials have been presented (Kwon et al., 2013). Vibrating steel strip partially immersed in liquid zinc during the continuous hot-dip galvanizing process has been studied (Li et al., 2013). The results show the effects on natural frequencies and mode shapes of vibrating steel strips partially immersed into a liquid. The influences of parameters such as the submergence depth, the position of strip in the container and the dimension of the container on the dynamic behavior of the strip are discussed. The effect of fluid-structure interaction on the free vibration frequencies of a micro-beam in contact with incompressible bounded fluid was investigated (Shabani et al., 2013). The above study helps in the design of micro devices and it shows that the higher modes are important in dense fluids. The effect of finite amplitude forced vibrations of a cantilever beam of rectangular cross section immersed in a viscous fluid under harmonic base excitation has been studied (Phan et al., 2013). Vibration analysis of a supported rectangular plate immersed in a fluid have been discussed (Tubaldi and Amabili, 2013). Eigen frequencies have been calculated for the axial flow of fluid. Flexural vibration of two thin beams that are coupled through an viscous fluid has been studied by through an experimental work (Intartaglia et al., 2013). It was found that hydrodynamic damping decreases with the increase of the gap and the oscillatory

Reynolds number. Investigation on the response of a flexible plate in a uniform flow, when its leading edge is forced into a harmonic motion have been carried out using an experimental setup (Paraz et al., 2014). The study shows that for this type of condition non-linear effects have to be considered along with FSI. Non-linear effects on the resonance of a periodically-forced cantilevered plate immersed in a fluid at rest have been studied experimentally and theoretically (Arellano Castro et al., 2014). The frequencies at resonances decrease when the forcing amplitude is increased, revealing the presence of non-linear effects. Natural frequency analysis of rectangular bottom plate structures in contact with fluid have been presented (Cho et al., 2015a). FSI was considered by a semi-analytical method using the fluid velocity potential, derived from the boundary conditions for the fluid and structure and the results are compared with FEM analysis. The effect of forced vibration analysis of bottom and vertical rectangular plate structures in contact with fluid, subjected to internal point harmonic excitation force have been presented (Cho et al., 2015b). It is noticed that increase infilling level reduces not only plate wet natural frequencies, but also velocity amplitudes. Natural frequencies of the immersed composite structures under force vibrations has been estimated using an experimental setup (Stenius et al., 2016). The experiment is carried out for 19 specimens that are made from various materials including aluminium, steel, glass-fibre, and carbon-fibre with aspect ratios varying from 3.7 to 11.2 and breadth to thickness ratios ranging from 2.7 to 20.5. A theoretical study of the modal analysis of microbeams partially immersed in a viscous fluid has been presented (Abassi et al., 2016). The results are validated with finite element method using COMSOL Multiphysics software results. Free vibration analyses of thick rectangular composite plates in contact with a bounded fluid have been presented

(Canales and Mantari, 2017). The plate displacement field is analyzed using Carrera Unified Formulation and validation is performed with results reported in the open literature and by using 3D finite element software. Response of a thin rectangular plate in contact with fluid have been experimentally studied using Acoustic and Modal tests (Khorshidi et al., 2017).

2.2.2 Vibration studies in Tube structures

A numerical solution technique for determining the dynamic response of a thin, elastic, circular, cylindrical shell of constant wall thickness and density, immersed in a potential fluid has been presented (Cummings, 1978). The phenomenon of flow induced vibrations of cylindrical structures in nuclear reactors have been detailed (Chen, 1985).Natural frequency changes of a partially liquid filled cantilever tube of constant diameter due to changes in liquid length have been calculated (Chan and Zhang, 1995). Added mass representation for a flexible cylinder vibrating in a fluid medium has been discussed (Han and others, 1996). The fluid-structure interaction problem under the influence of harmonic ground and inertia dominated hydrodynamic loading is studied. Interaction between the torsional vibration of the rod and the fluid theoretically in terms of mechanical impedance have been studied (Kim and Chun, 2003).Dynamic response of partially submerged vertical circular cantilever beam undergoing flexural oscillations has been studied (Da Lozzo et al., 2012). Natural frequency of pipe structures has been demonstrated (Chambers, 2013). Added mass effect of on disc vibrating in water which could be calculated by comparing the vibrating frequency in water with the one in air and Eigen value have been investigated (Intartaglia et al., 2013). Dynamic response of

both thick-walled and thin-walled cylindrical composite structures subjected to underwater impulsive loads have been analyzed (Qu et al., 2017).

2.3 CLOSURE

It is evident from the literature that sodium-water reaction event in a SFR can significantly affect the structural integrity of the components of the intermediate heat transport system and the safety of the primary heat transfer system. Pressure wave propagation from the steam generator to the intermediate heat exchanger is a dynamic phenomenon. Since the components in the reactor assembly are partially or fully immersed in the liquid sodium, the phenomenon of flow induced vibration and Fluid Structure interaction plays a significant role. Core subassemblies vibration due to large leak sodium-water reaction in the steam generator is a new phenomenon recently attracted the attention of designers and researchers. The current work focuses on the evaluation of displacement of subassemblies and consequent changes in the reactivity in a fast breeder reactor in case of large leak sodium-water reaction.

For the plate and tube structures, the transmission of vibration between structures for instance, from one plate to adjacent plate immersed in a finite volume of fluid is scarcely reported. In order to understand the coupled vibration transmission in plates immersed in fluid, experimental and numerical studies have been carried out in the present work, as given below:

➤ Use of numerical tool CAST3M for FSI vibration studies using literature and experimental setup has been explained in Chapter – 3.

➤ Study on vibration transmission between plate and tube structures has been presented in Chapter – 4.

➤ Introduction of sodium water reaction and investigation on the response of reactor assembly components for design basis sodium-water reaction has been elaborated in Chapter – 5.

➤ Investigations for beyond design basis sodium-water reaction event have been discussed in Chapter – 6.

* * *

CHAPTER 3

Use of CAST3M for FSI Vibration Studies

3

3.0 INTRODUCTION

Fluid Structure Interaction (FSI) vibration in immersed structures is an important phenomenon that affects the dynamic characteristics of structures. In problems with Fluid Structure Interaction, a solid structure interacts with surrounding fluid. The solid structure displacement will cause pressure differences in the fluid and these pressure differences will force, or damp, the motion of the structure. A vibrating plate induces vibrations of the surrounding fluid which in turn generates additional inertia forces due to the fluid mass. To study and understand the phenomenon of FSI vibration in structures, the numerical Finite Element Method (FEM) tool CAST3M has been chosen. Coupled problems of fluid-structure type such as interaction of plates and tubes with fluid have been studied. Benchmarks studies validating using literature results and experimental works have been presented in detail in this chapter.

CAST3M is a toolbox for finite element computations developed by CEA, France. The toolbox contains the essential elements in order to perform a finite element computation. Its main application area is mechanics including elasticity, elasto-visco-plasticity, buckling, vibration or dynamics (CAST3M, 2000). Other application areas include thermal, hydraulic or electromagnetic analysis. Its modular character permits to program new applications in an easy and comfortable manner, which make the tool adapted for coupled multiphysics problems. The language used to define the processing

functional instructions is GIBIANE. It is an advanced language as it favors data exchanges between user and program, and the easy usage of code. CAST3M is comparable with codes like Mathematica, Matlab, Scilab, Octave, Mapple etc.

Cast3M is a multi-physics code using finite element method. It specially focuses on nuclear reactor applications, including solid and structural mechanics, and fluid and heat transfer. It consists of various elemental bricks called procedures that can be organized together for the resolution of more complex problems or equations.

In spite of the large flexibility of the CAST3M, the user needs to learn to formulate calculation problems according to the method adopted by the code. As a result, it is important for the user to understand how a finite element analysis is structured and organized, so as to be able to establish a direct connection between the mathematical or logical operation to be formulated and the operators to be used.

The fluid structure interaction element used in CAST3M is found to be efficient and the effect of free level fluid surface can also be modelled for fluid structure interaction studies. Also the sequence of operations performed in the CAST3M code is user friendly similar to other computer programming languages like C++.

3.1 MATHEMATICAL FORMULATION

A general method to calculate the dynamic behavior of fluid structure coupled systems is necessary. In FEM the fluid elements are represented by fluid volume elements and the most important part of coupling of fluid and structural elements is achieved by using surface elements between the fluid and the solid. Based on the formulation (Combescure et al., 1980, 1982, Cast3M, 2017, Grzegorz Kępisty, et. al., 2017), the

phenomenon of Fluid Structure Interaction is solved in CAST3M by a functional approach for fluids and structural systems. The method of approach is limited to linear range problems, for the systems with small displacement of the structures and with small pressure fluctuations.

The wave equation which governs the small pressure fluctuations is given by,

$$\nabla \frac{1}{\rho_f} \nabla p - \frac{1}{\rho_f c^2} \frac{\partial^2 p}{\partial t^2} = 0 \quad \text{...(3.1)}$$

Where 'c' is sound velocity and 'p' is fluctuating pressure, 'ρ_f' is the fluid density, 't' is the time

Its associated boundary conditions are given by,

$$\frac{1}{\rho_f} \frac{\partial p}{\partial n_s} = - \overrightarrow{n_s} \frac{\partial^2 \vec{u}}{\partial t^2} \text{for the moving boundary} \quad \text{.....................................} \quad (3.2)$$

$\overrightarrow{n_s}$ is unit vector normal to the boundary S, $\vec{u}$ is the boundary displacement

$$p = \rho_f g Z \text{...(3.3)}$$

$$\frac{\partial p}{\partial n_\in} = -\rho_f \frac{\partial^2 z}{\partial t^2} \text{for free surface 'Σ' in the gravity field...............................} \quad (3.4)$$

'g' is the acceleration due to gravity, 'Z' is the fluid level fluctuation

$p = p_s$ for fixed pressure on the surface

A numerical approximation of the system of equations is solved by a functional approach. The fluid functional and the structure functional are formulated to give a general form of structural system,

$$(K - \omega^2 M = F) \dots\dots\dots\dots\dots\dots\dots\dots\dots\dots\dots\dots\dots\dots\dots\dots \text{ (3.5)}$$

'K' is singular stiffness matrix, 'M' is the mass matrix, 'ω' is the natural frequency and 'F' is the surface forces acting.The above equation can be solved using numerical methods employed for the dynamic analysis of the structural systems by the finite element approach.

3.2 BENCHMARK STUDY – 1 (using Literature results)

3.2.1 Vertical plate vibration
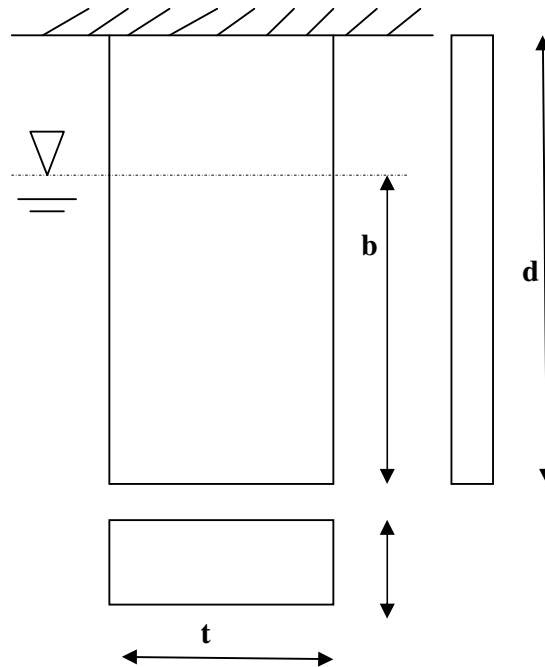
Fig. 3.1(a) A vertical cantilever plate

A Vertical plate (Fig.3.1 (a)) with the dimensions of length 'a' = 1.0 m, width 'b' = 0.2 m, thickness 't' =0.005 m has been experimentally analyzed by U.S. Lindholm, et al., 1965for free vibration of the plate immersed in an infinite fluid medium. The fluid medium considered here is water at the atmospheric conditions. The material properties of the plate are, Density of Steel 'ρ'=7830 kg/m^3, Modulus of elasticity of steel 'E'=2.1x10^{11} N/m^2, Poisson ratio 'μ'=0.3, Density of water 'ρ$_w$'=1000 kg/m^3. The submergence depth of the plate is taken as the ratio of depth of immersion to length. The natural frequency of the cantilever plate immersed in the fluid has been studied for various submergence depth ratio. The above problem is taken as a benchmark study and the numerical analysis is carried out in CAST3M.

Finite element model of the cantilever plate with immersion depth =0.5 is shown in Fig. 3.1.(b) The plate is given fixed boundary condition at the top. The plate is modeled using four noded elastic shell elements and the fluid is modeled using eight noded brick elements. The fluid nodes and structure nodes are connected by fluid-structure transition element. The three-dimensional finite element model consists of the contained fluid element 'LCU8' and the elastic shell element 'COQ4'. 'LCU8' is an eight nodded brick element with six degrees of freedom (U_x, U_y, U_z, R_x, R_y, R_z). 'COQ4' is a four nodded element with six degrees of freedom (U_x, U_y, U_z, R_x, R_y, R_z). The fluid nodes and structure nodes are connected by fluid-structure transition element 'LIC4'. The elements are specific to the FEM code CAST3M.
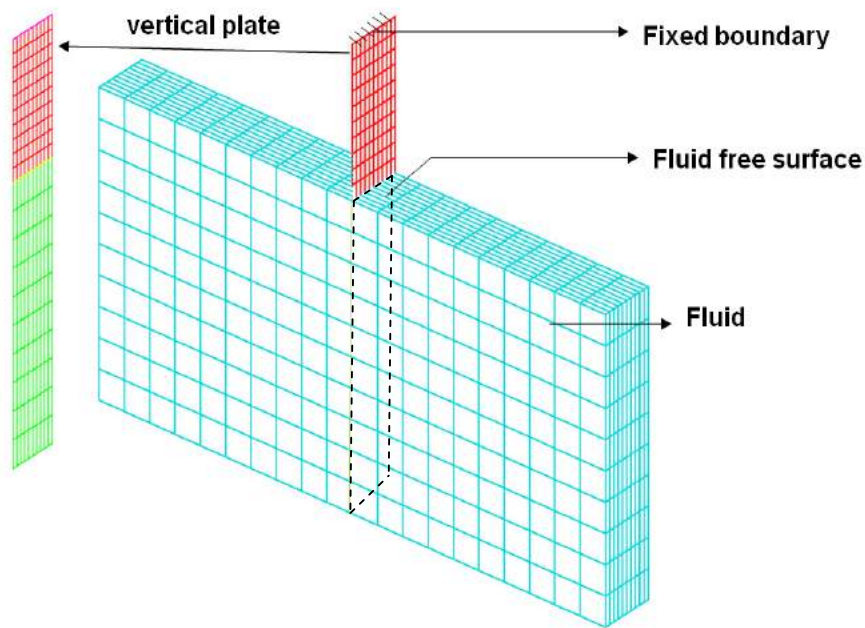
Fig. 3.1(b) Finite element model of the vertical cantilever plate

(i) In air
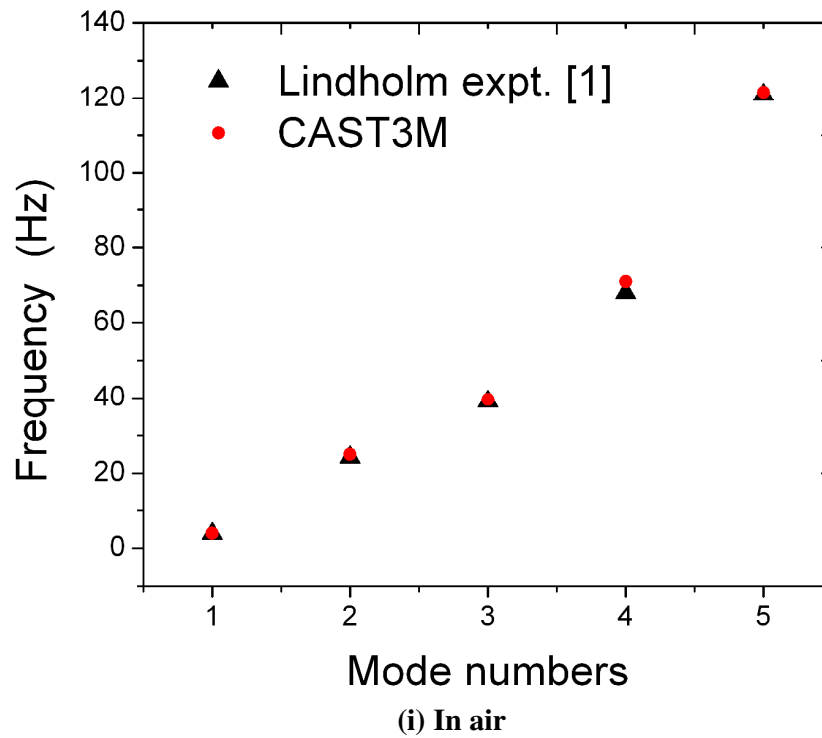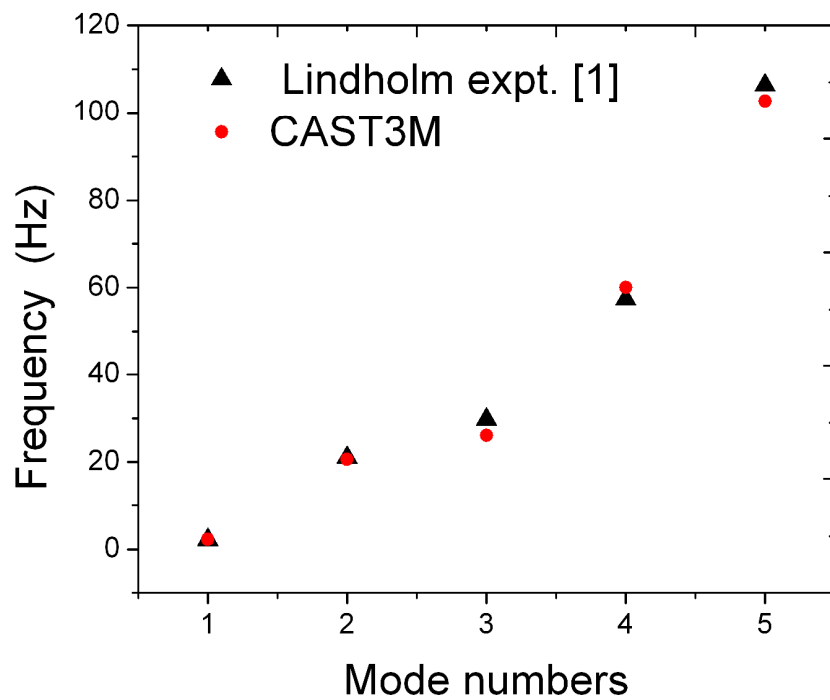
(ii) d/a = 0.25
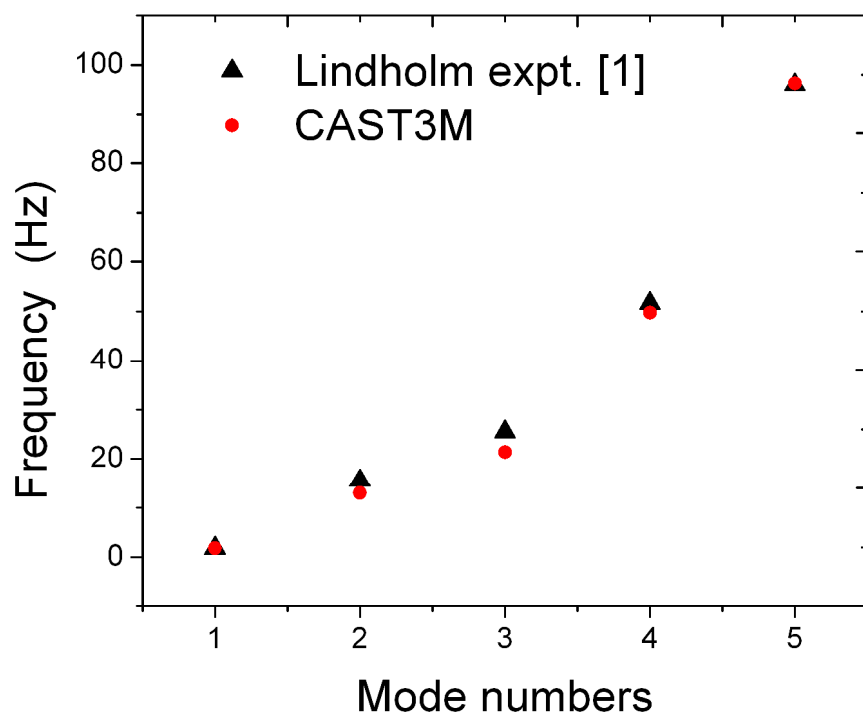
(iii)   d/a = 0.50
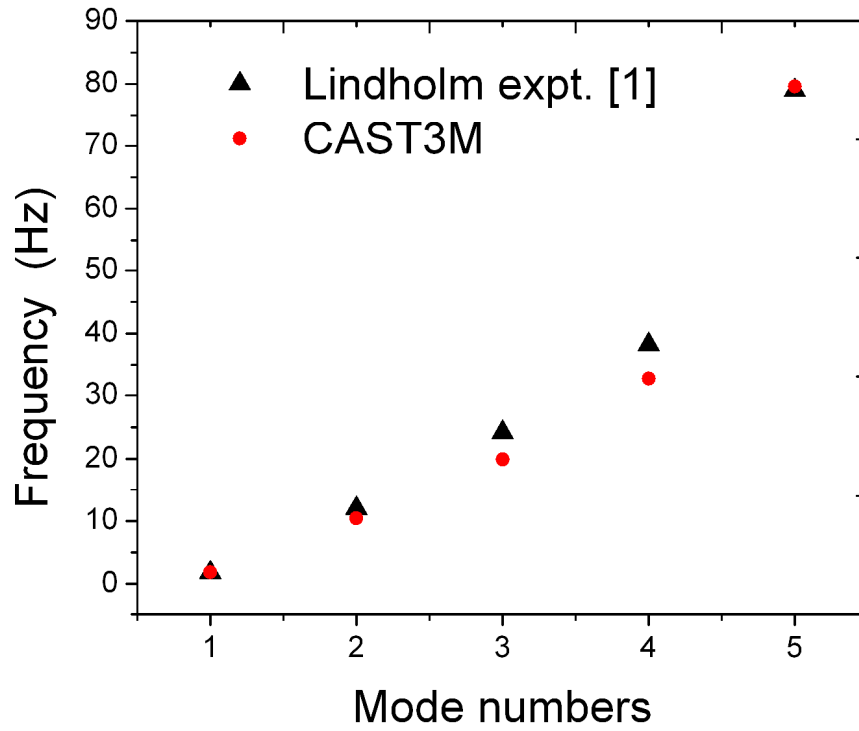
(iv) d/a = 0.75
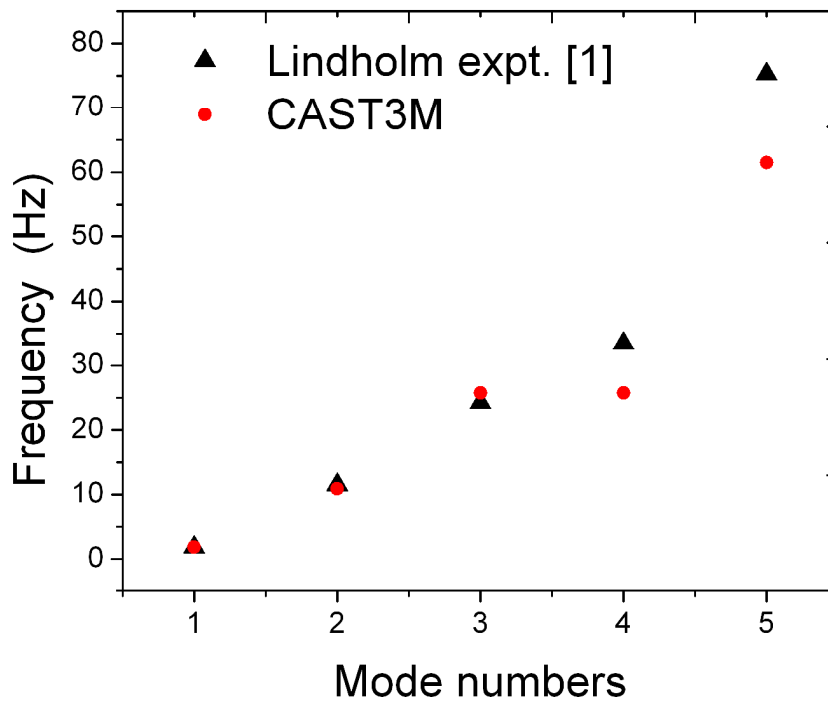
(v) d/a = 1.0

Fig. 3.2 Variation of natural frequencies for various submergence depth ratios

Fig. 3.2 shows the comparison of natural frequencies at different submergence depths. Analysis was carried out using CAST3M code for the same input conditions. Predicted results with CAST3M are closely matching within ± 3% from the experimental results reported by U.S. Lindholm, et al.

(i)

(ii)

(iii)

(iv)

(v)

(vi)

Fig.3.3 Mode shapes for dry natural frequencies obtained from CAST3M. (i) first mode frequency (3.98Hz); (ii) second mode frequency (25.03 Hz); (iii) third mode frequency (39.61 Hz); (iv) fourth mode frequency(71.05Hz); (v) fifth mode frequency (96.31Hz) ;(vi) sixth mode frequency (142.25Hz)

In dry analysis, the dynamic characteristics of the cantilever plate are determined in vacuum in the absence of internal damping and external forces. The wet analysis describes the analysis of the cantilever plate with the fluid surrounding it. The corresponding frequency and mode shape are called as wet natural frequency and wet mode shape respectively. Dry and wet analyses of the cantilever plate are carried out in CAST3M.

From the dry mode shapes of the plate in (Fig. 3.3), it is observed that the 1st ,2nd, 4th and 6th modes corresponds to bending mode shapes, the 3rd and 5th modes corresponds to torsion mode shapes. The same pattern of mode shapes with wet natural frequencies (Fig. 3.4) is obtained by wet analysis. It is observed that the wet natural frequencies decrease with increase in the depth of immersion and we can find the lowest wet natural frequency for the fully immersed condition where the d/a=1.0.

(i)

(ii)

(iii)

(iv)

(v)   **(vi)**
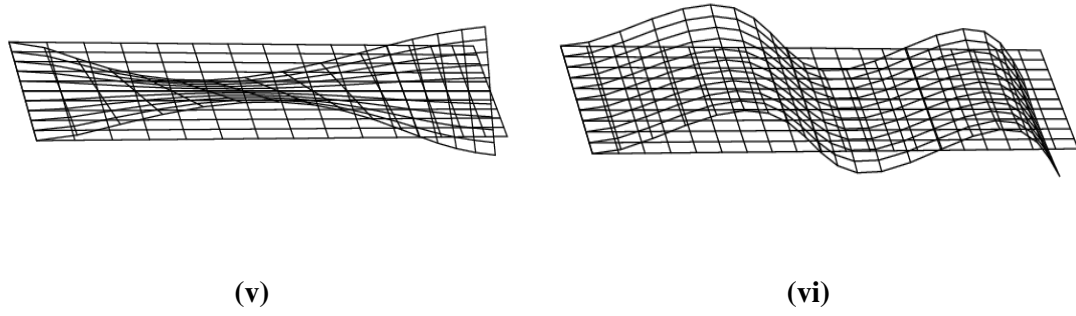
Fig. 3.4 Mode shapes for Wet natural frequencies with depth ratio (d/a=0.5) obtained from CAST3M. (i) first mode frequency (1.84Hz); (ii) second mode frequency (12.97 Hz); (iii) third mode frequency (21.35 Hz); (iv) fourth mode frequency (49.76Hz); (v) fifth mode frequency (96.31 Hz); (vi) sixth mode frequency (96.32Hz)

3.2.2 Horizontal plate vibration

To understand the phenomenon of FSI in horizontal plate, a benchmark problem from literature by Fu and Price, 1987 has been studied using CAST3M computer code. Fig. 3.5 shows the horizontal cantilever plate with steel as material. The physical properties of the material are as follows: Young's modulus 'E' = 206.8 GPa, Poisson's ratio'μ' = 0.3, and mass density 'ρ'= 7830 kg/m^3. The fluid considered is water with a density 'ρ_w' = 1000 kg/m^3, the viscosity and compressibility of water is neglected in the analysis. The finite element analysis was performed to obtain the natural frequencies and mode shapes of the plate with different depths of immersion. The results from the literature and CAST3M are given in Table 3.1. There is fairly good match between CAST3M and literature. It is observed that the natural frequency decreases with increase in depth ratio due to more added mass of the plate immersed in fluid. The lowest frequency is observed for the fully immersed plate.
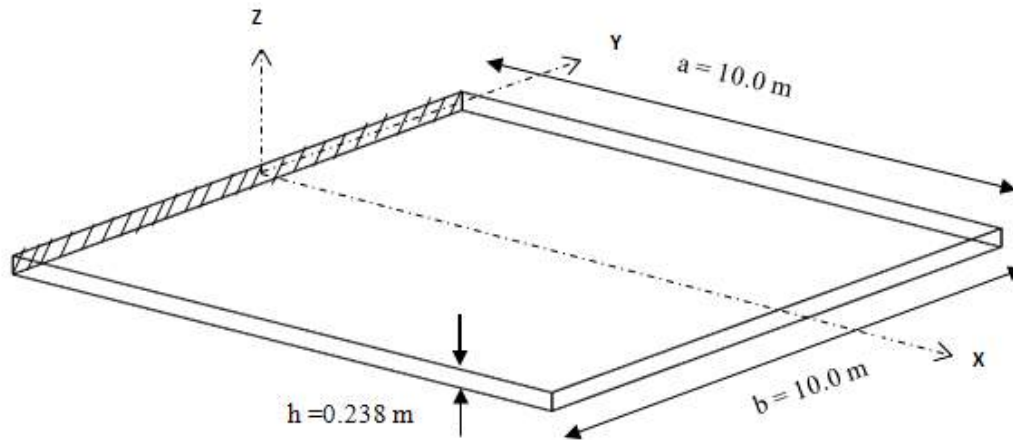
Fig. 3.5 Horizontal cantilever plate (Fu and Price, 1987)

Table 3.1 Comparison of dry and wet natural frequencies in Hz

Modes	From CAST3M coding					Fu and price [4] (1987)				
	In air	Depth ratio (d/a)				In air	Depth ratio (d/a)			
		0.25	0.5	0.75	1		0.25	0.5	0.75	1
1	2.063	1.485	1.298	1.205	1.178	2.06	1.63	1.31	1.21	1.17
2	5.052	3.734	2.858	2.555	2.471	5.05	4.20	3.48	3.26	3.22
3	12.885	11.192	9.769	7.944	6.984	12.70	11.66	10.41	8.70	8.03
4	16.341	12.739	11.223	11.989	10.890	16.10	13.86	12.20	11.38	11.21
5	18.648	16.085	14.714	11.989	10.890	18.40	16.81	15.62	13.25	12.55
6	32.684	29.028	27.099	22.746	23.536	-	-	-	-	-
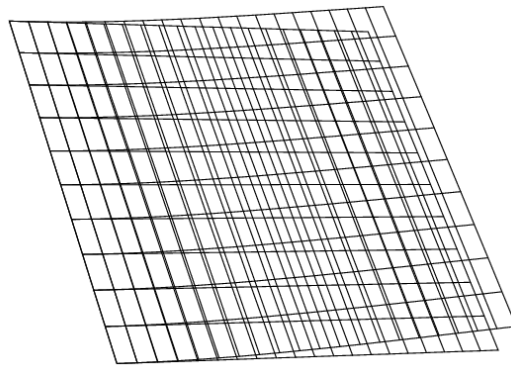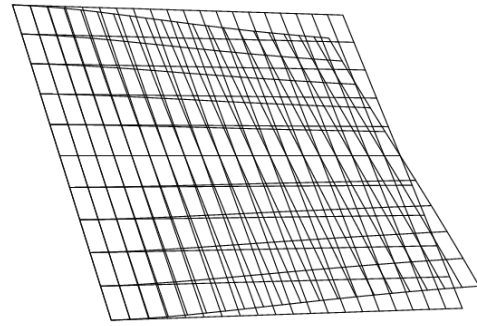
(i)   (ii)
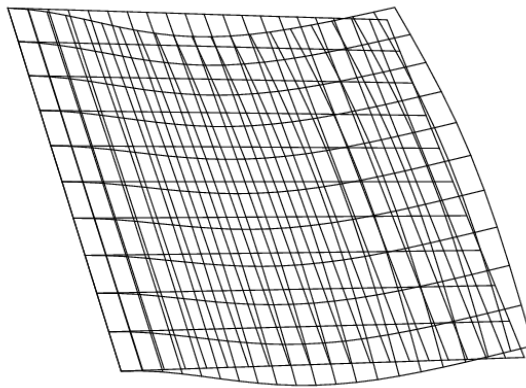
(iii)

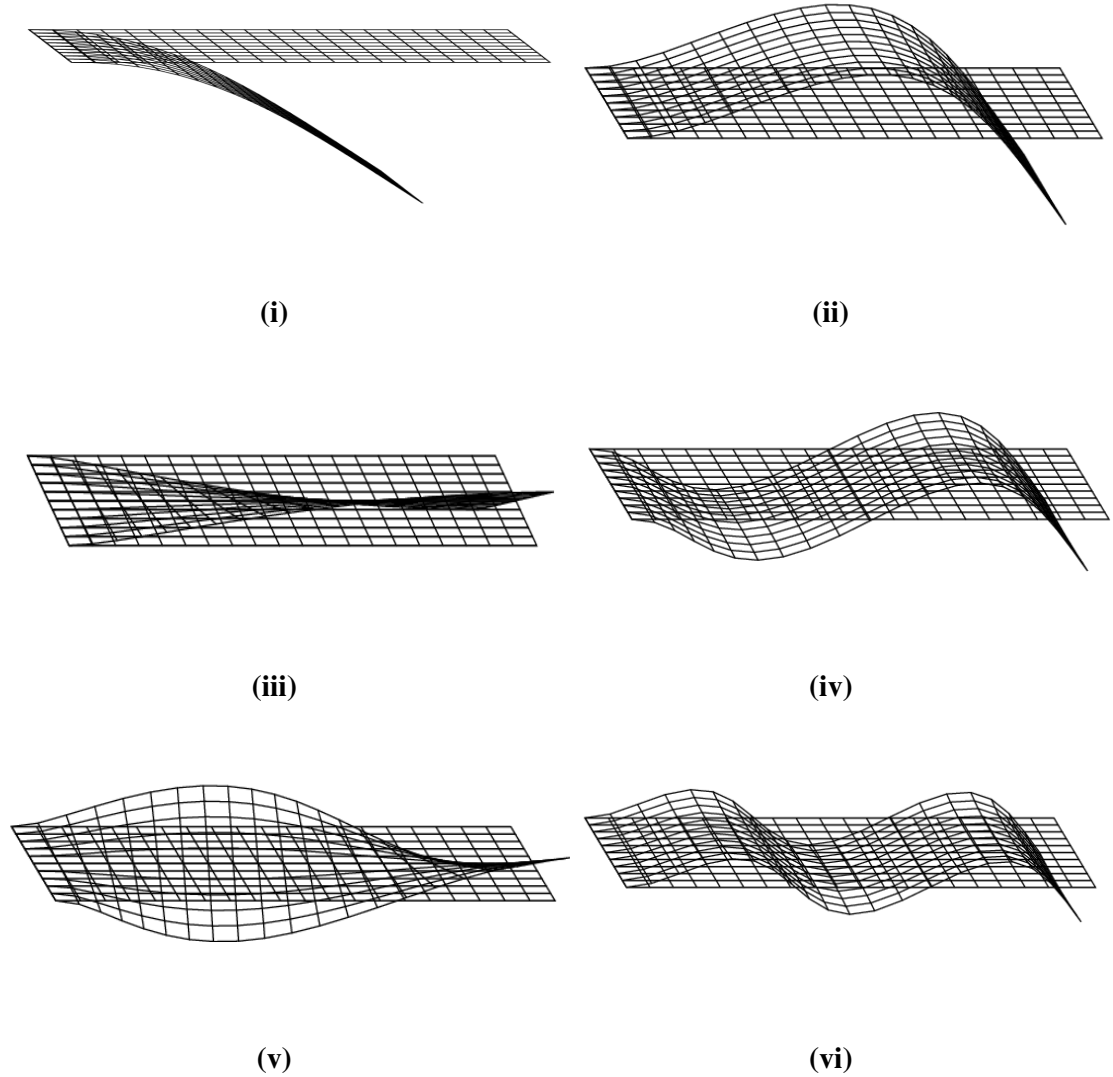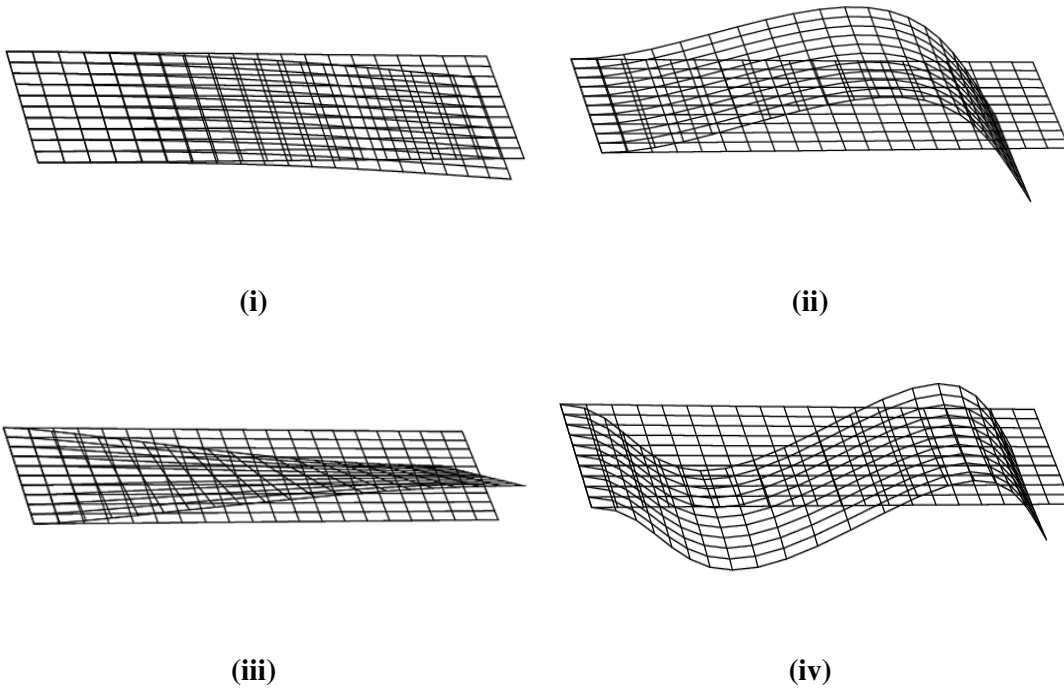**Fig. 3.6 Mode shapes for dry natural frequencies obtained from CAST3M (i) first mode frequency; (ii) second mode frequency; (iii) third mode frequency**
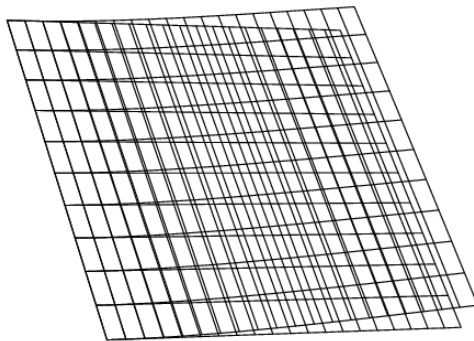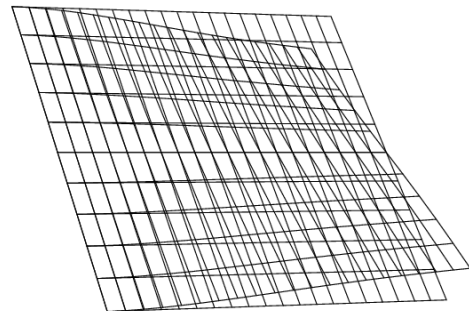
(i)   (ii)
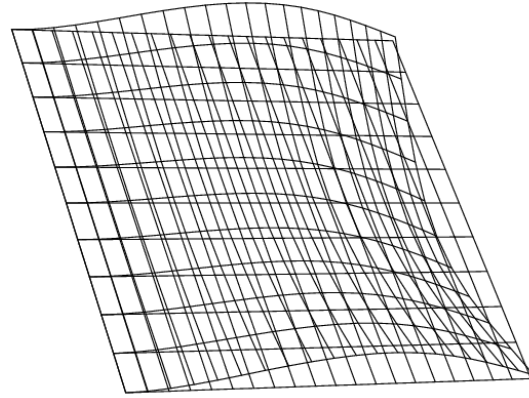
(iii)

Fig. 3.7 Mode shapes for wet natural frequencies obtained from CAST3M (i) first mode frequency; (ii) second mode frequency; (iii) third mode frequency

The mode shapes of the horizontal cantilever plate in air and in water for depth ratio 0.5 is shown in Fig. 3.6 and Fig. 3.7 respectively.

3.3 BENCHMARK STUDY – 2 (using an experimental setup)

3.3.1 Experimental setup

Experimental validation has been carried out to verify the results predicted by CAST3M. The experimental setup consists of a fabricated rectangular tank, an Impact hammer, accelerometers and laser sensors connected to the Data Acquisition System. The technical specifications of the sensors are listed in Table 3.2. Two plates (side walls of the rectangular tank of 1 mm thick) immersed in water have been considered. Plate-1 was excited and the response of Plate-2 for this excitation is measured. The laser sensors are placed on both the plates to measure the displacement during impact. The Impact hammer delivers the excitation force. Water is the fluid medium. The experiment is repeated for various depth of immersion of the plates as 280 mm, 380 mm, 480 mm and 580 mm.

Table 3.2 Technical specifications of Impact hammer and Laser sensors

Impact Hammer	
Make	DJB Instruments
Model	IH-02
Measuring range	2000 N
Sensitivity (with impedance inverter)	2.50 mV/N
Non-Linearity	≤1% FS
Hammer mass & Housing material	180 gram & stainless steel
Purpose	Force excitation
Laser sensors	
Make	RIFTEK
Model	RF603-60/100-485-I-IN-AL-CC
Range	100 mm
Base distance	60 mm
Linearity (%)	±0.05 of the range
Resolution (%)	0.01 of the range
Max.measurement frequency	9400 Hz
Laser type	≤ 1 mW, 60 nm, Class 2
Purpose	Displacement measurement

The fluid considered is incompressible, inviscid and irrotational, the fluid motion is assumed to be small with small pressure fluctuations. The rectangular plates are made of linearly elastic, homogeneous and isotropic material. The shear deformation and rotary inertia are negligible. The physical properties of the material are tabulated in Table 3.3.
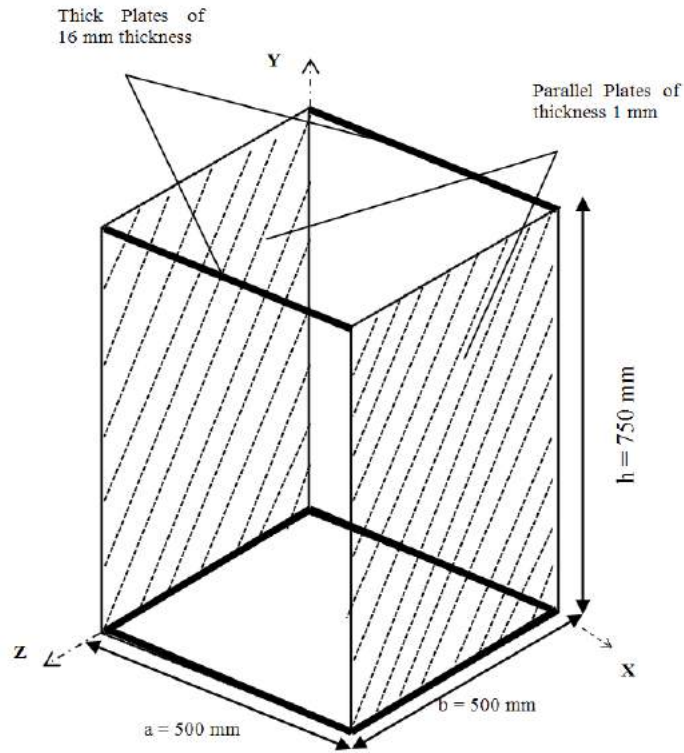
Fig. 3.8 Schematic of experimental setup

| (i) | (ii) |
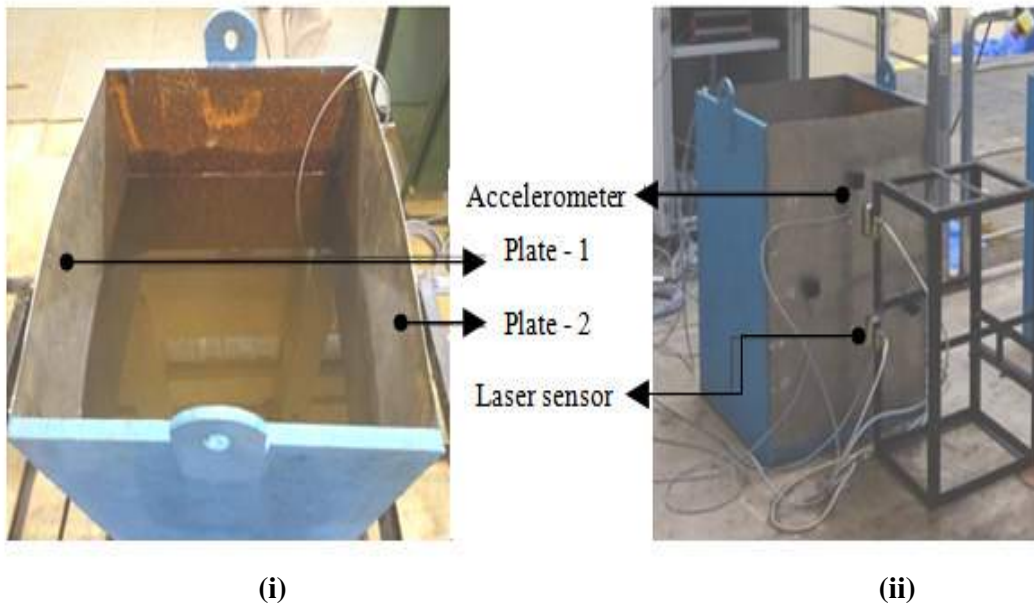
Fig. 3.9 Experimental setup (i) Top view of the tank; (ii) Rectangular tank with

sensors

3.3.2 Modeling

The thin plates are welded to the side walls of thick plate to form a rigid rectangular tank. Since the plates are welded, only the base of the tank is applied with rigid boundary conditions. The plates are modelled with their actual thickness in the simulation. The thin plates can vibrate more as compared to the thick plates.

The three-dimensional finite element model consists of the contained fluid element 'LCU8' and the elastic shell element 'COQ4'. 'LCU8' is an eight nodded brick element and 'COQ4' is a four nodded element with six degrees of freedom (U_x, U_y, U_z, R_x, R_y, R_z). The fluid nodes and structure nodes are connected by fluid-structure transition element 'LIC4'. The elements are specific to the FEM code CAST3M. The rectangular plates have been meshed identically and a fixed boundary condition to the bottom of the tank is applied.

Table 3.3 Material properties

Material	Steel
Fluid	Water
Thickness of side plates (steel)	1 mm
Thickness of adjacent plates (carbon steel)	6 mm
Modulus of Elasticity 'E'	$2.1 \times 10^{11}\,\text{N/m}^2$
Mass density of steel 'ρ'	$7830\,\text{kg/m}^3$
Mass density of carbon steel 'ρ'	$7850\,\text{kg/m}^3$
Density of fluid medium 'ρ_w'	$1000\,\text{kg/m}^3$
Poisson ratio 'μ'	0.3

3.3.3 Results and Discussion

Experimental results obtained have been compared with the numerical results for four different depths of immersion of the plates in the fluid medium.

Immersion depth = 280 mm

(i)

(ii)
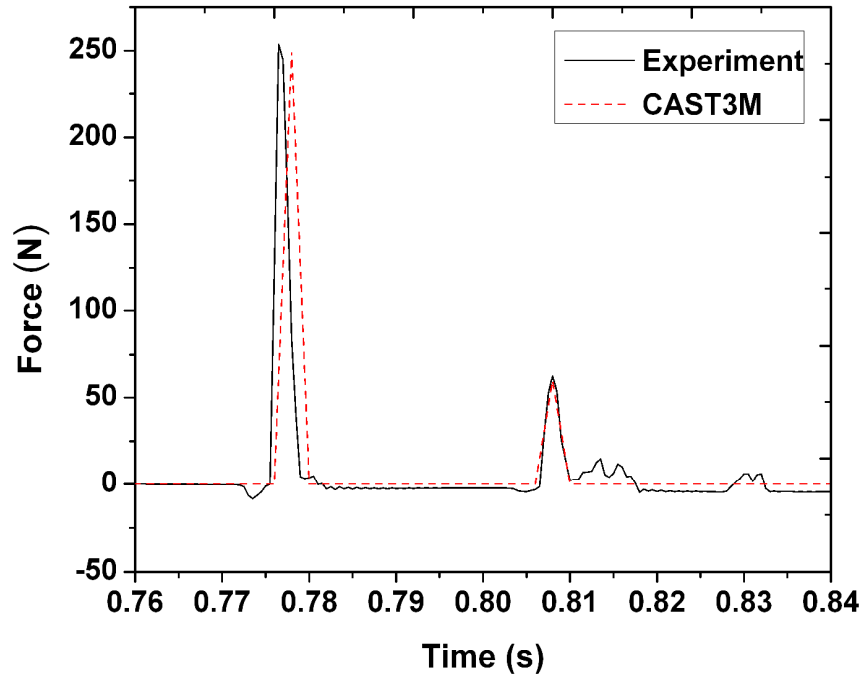
(iii)

Fig. 3.10 (a) For Immersion depth = 280 mm (i) Impact force to plate-1 (ii) Dynamic

displacement of plate-1(iii) Dynamic displacement of plate-2

(i)

(ii)

Fig. 3.10 (b) Frequency spectrum of the plates for immersion depth = 280 mm

Fig. 3.10 (a) presents the excitation and response vibration of the plates to an Impact load of 250 N. The pattern of displacement of plates matches well with the

experiment and the ratio of maximum displacement of plate-2 to plate-1 is found to be 0.2. Two impacts are observed from Fig. 3.10 (a) (i). This is because the modal hammer is handled manually. Only one impact is given to the plate as excitation. Within a short period of time the plate gets in contact with the hammer before it is removed. This is seen as another impact. Achieving a single impact force is difficult manually and, the same input has been used in numerical analysis. Fig. 3.10 (b) shows the frequency spectrum of the plates from experiment and CAST3M. From experiment and analyses, it is found that the plate-1 and plate-2 moves at the same frequency.

Immersion depth = 380 mm

(i)

(ii)
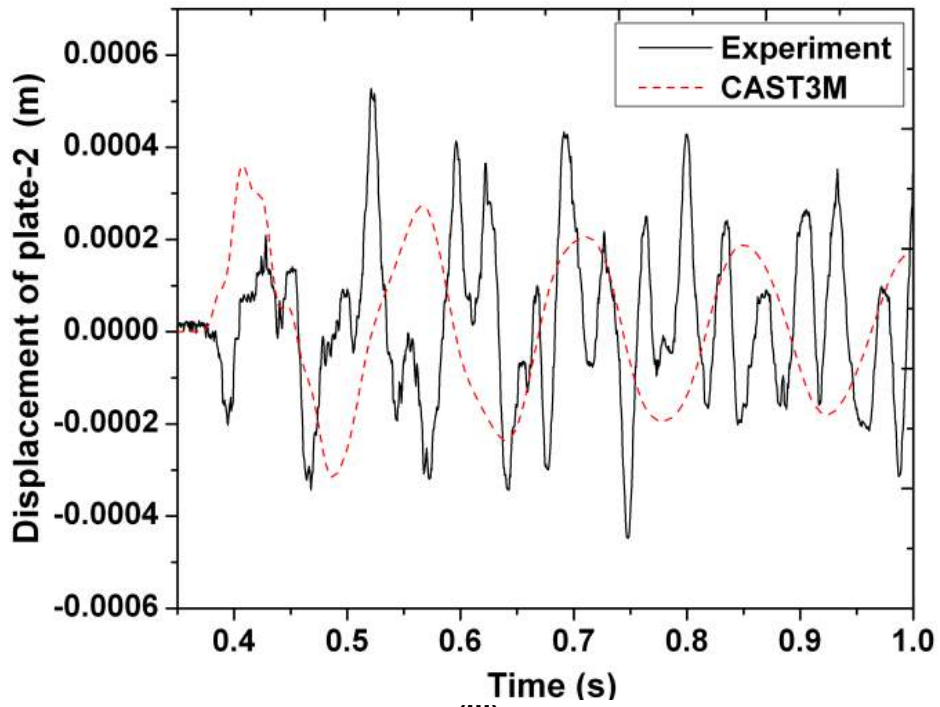
(iii)

Fig. 3.11(a) For Immersion depth = 380 mm (i) Impact force to plate-1 (ii) Dynamic displacement of plate-1 (iii) Dynamic displacement of plate-2

(i)

(ii)
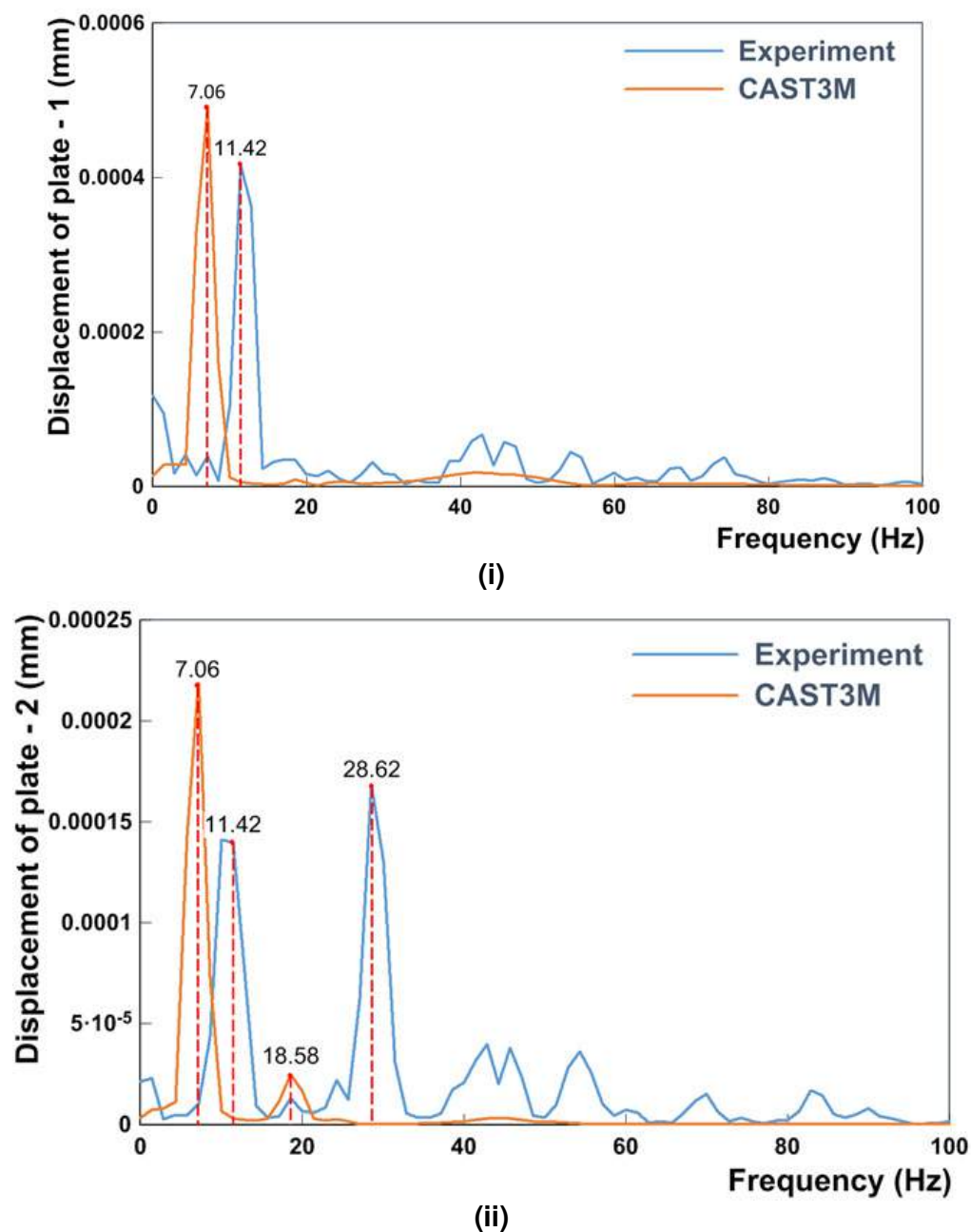
Fig. 3.11 (b) Frequency response of the plates for immersion depth = 380 mm

Fig. 3.11 (a) presents the excitation and response vibration of the plates to an Impact load of 200N. Since the input load is given manually, same value of Input load is not achieved and therefore we have a difference in the input force. The ratio of maximum

displacement of plate-2 to plate-1 is found to be 0.36. The range of amplitude of displacement from experiment and numerical analysis is comparable with a discrepancy in the pattern of displacement. Variation in displacement pattern between experiment and CAST3M results is due to the deformed configuration of thin plates with an increase in the level of the water in the rigid tank. Fig. 3.11 (b) presents the frequency spectrum of the plates from experiment and CAST3M. Additional frequency of 28.62 Hz is observed from the experiment in Plate-2. This is due to the deformation of the plate -2 with increase in the water level, since it is very thin compared to the adjacent plate.

Immersion depth = 480 mm
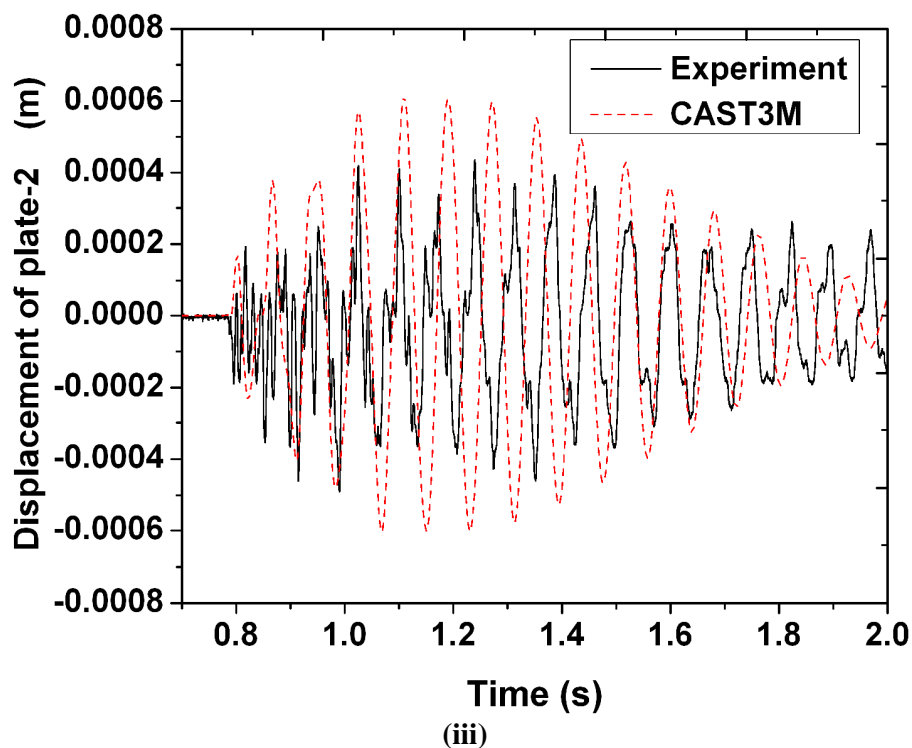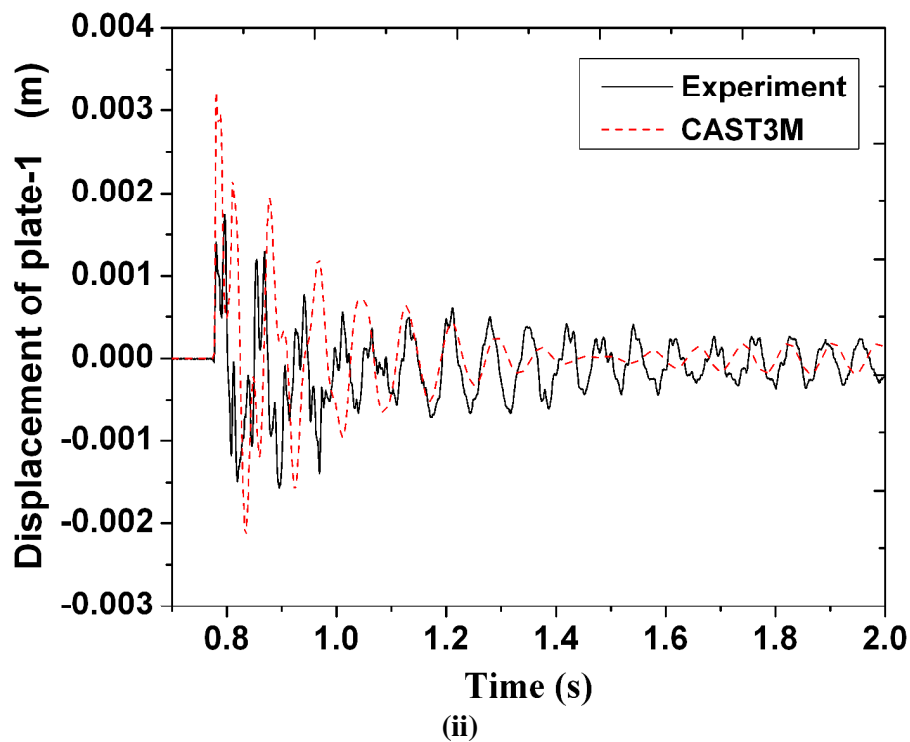

(i)

(ii)

(iii)
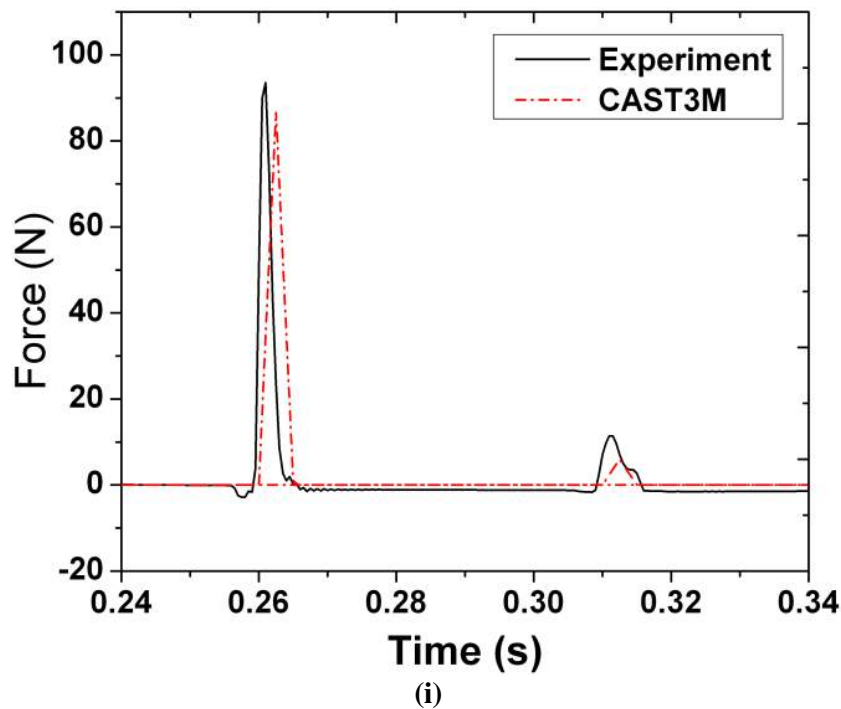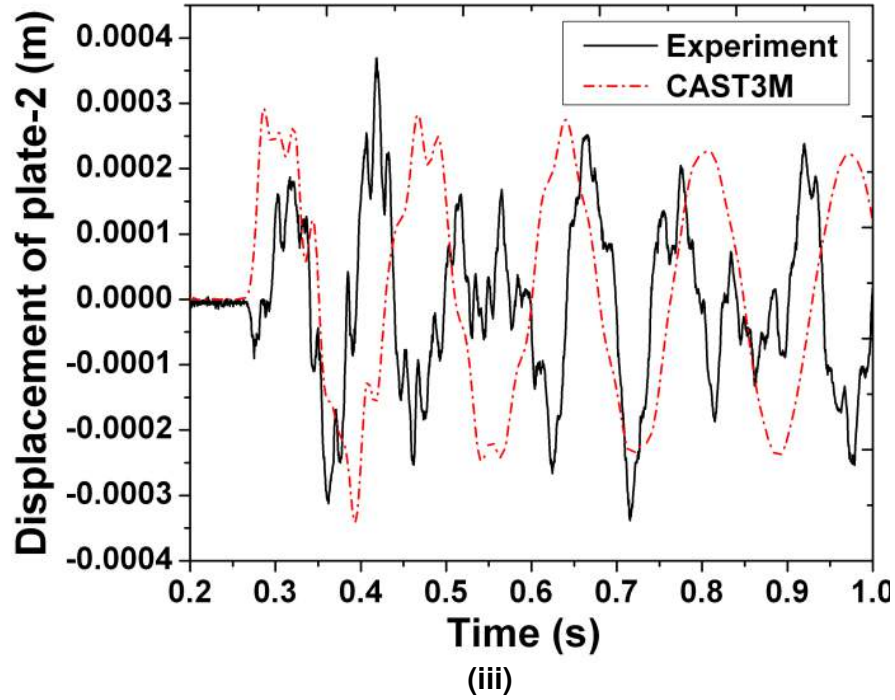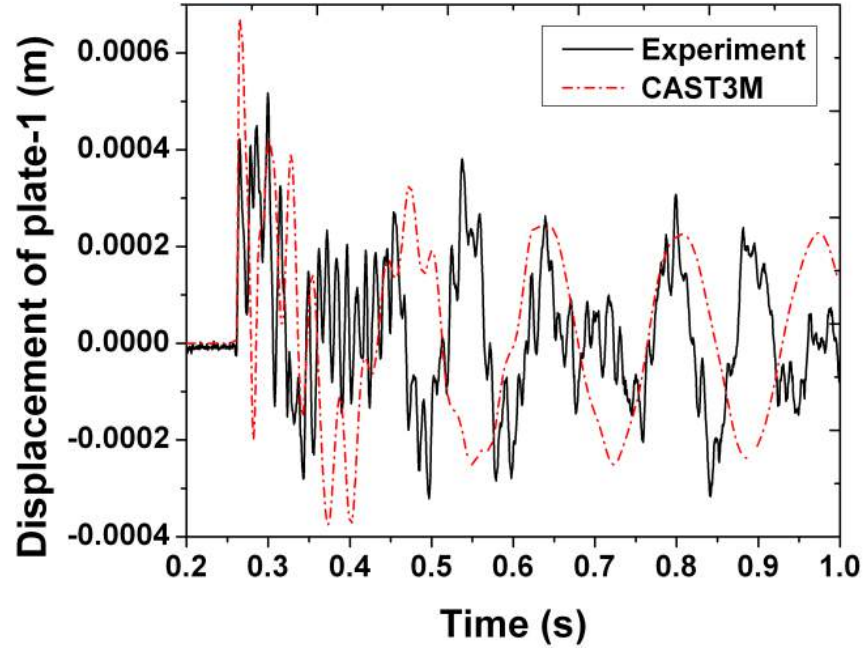
Fig. 3.12 (a) For Immersion depth = 480 mm (i) Impact force to plate-1 (ii) Dynamic displacement of plate-1 (iii) Dynamic displacement of plate-2
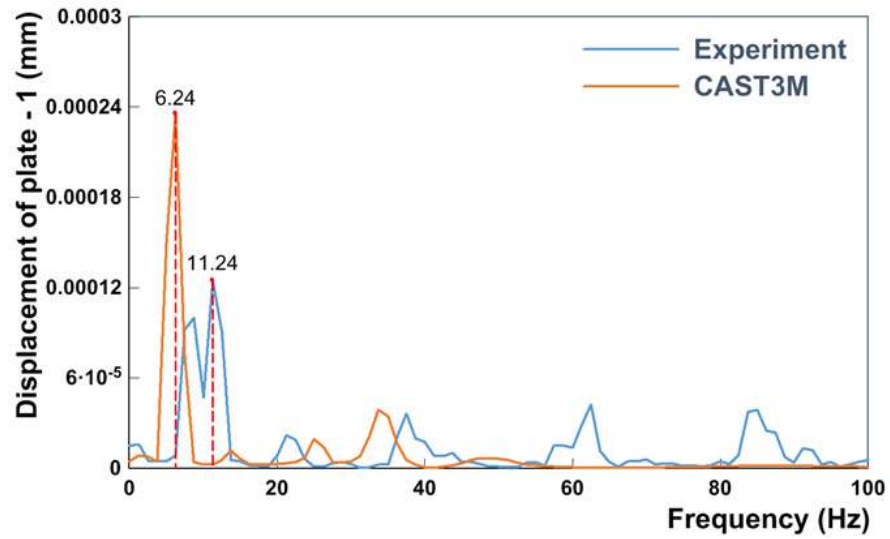
(i)
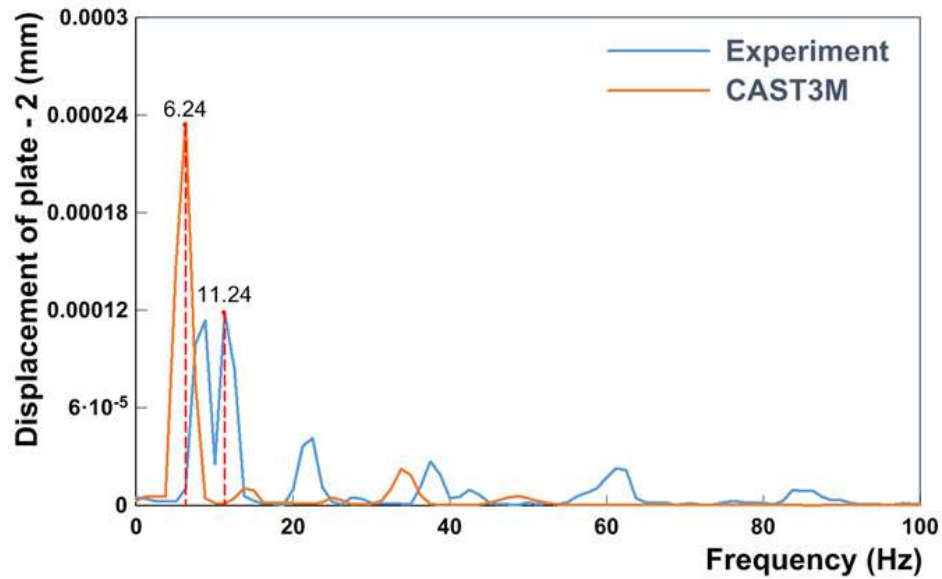
(ii)

Fig. 3.12 (b) Frequency response of the plates for immersion depth = 480 mm

Fig. 3.12(a) presents the excitation and response vibration of the plates to an Impact load of 90N. The pattern of displacement of plates matches with the experiment for the initial

phase and then deviates at later phase showing a shift in phase and amplitude. The ratio of maximum displacement of plate-2 to plate-1 is found to be 0.41. Fig. 3.12 (b) presents the frequency spectrum of the plates from experiment and CAST3M. The plates vibrate at the same frequency, the amplitude of displacement obtained from CAST3M is found be higher than the experiment.
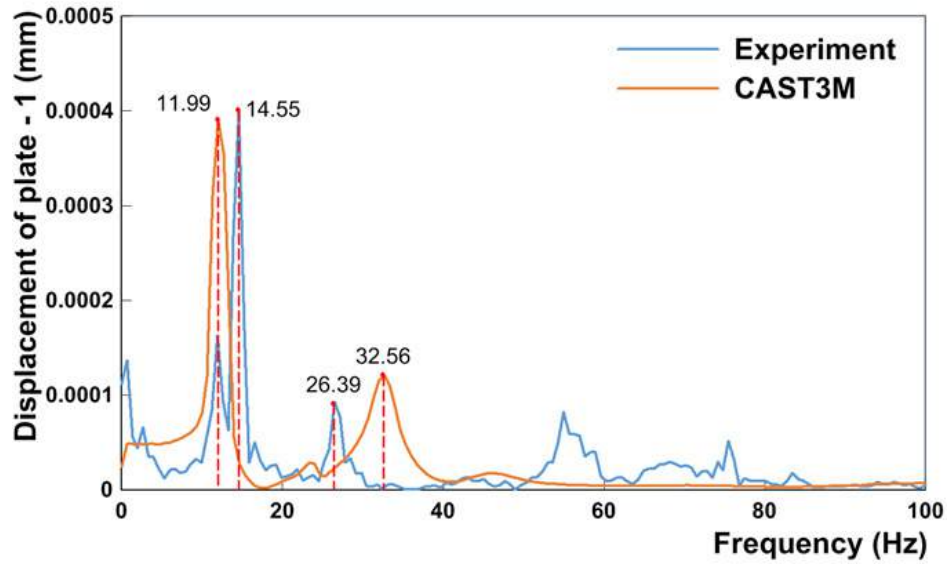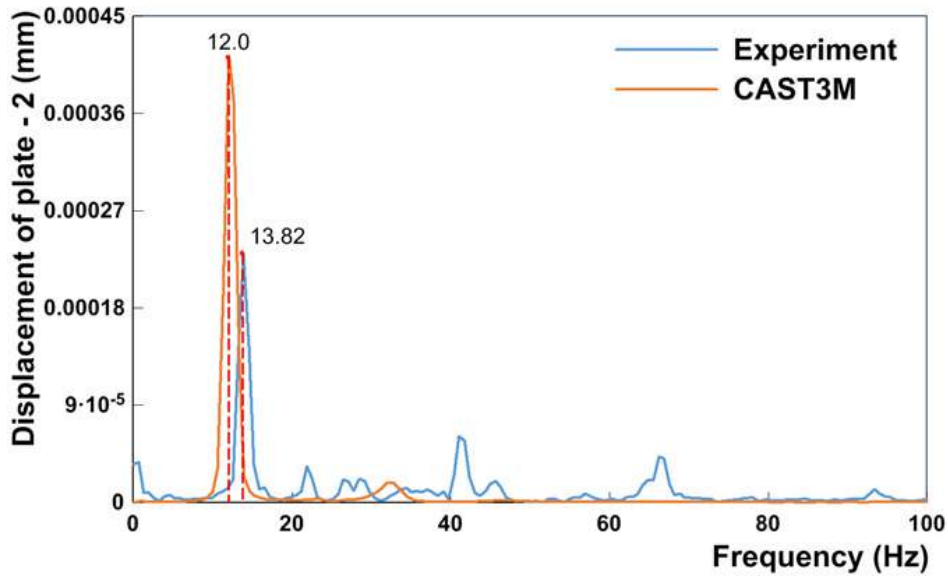
Immersion depth = 580 mm

(i)

(ii)

(iii)
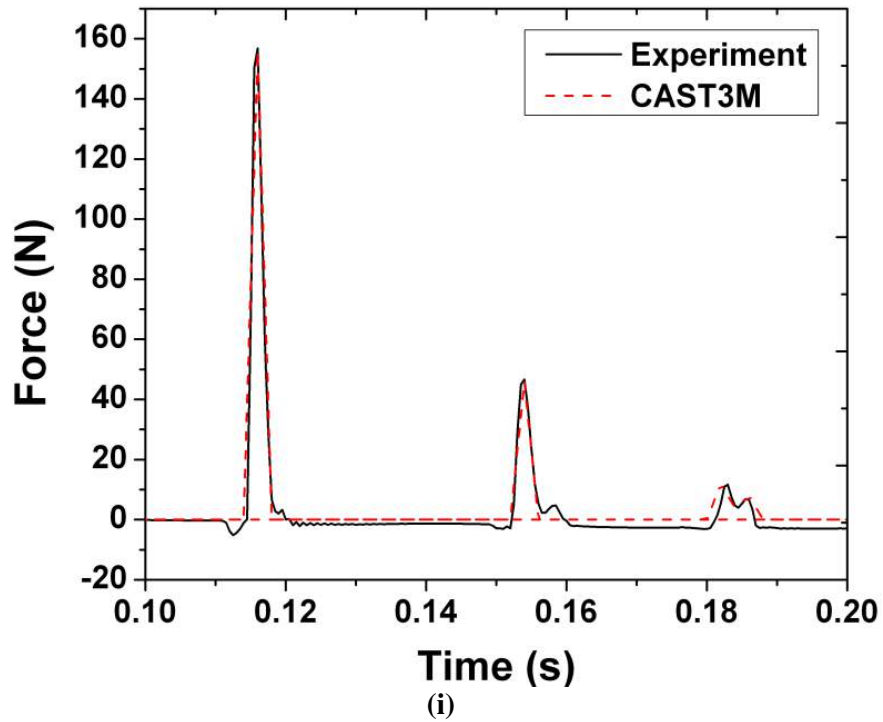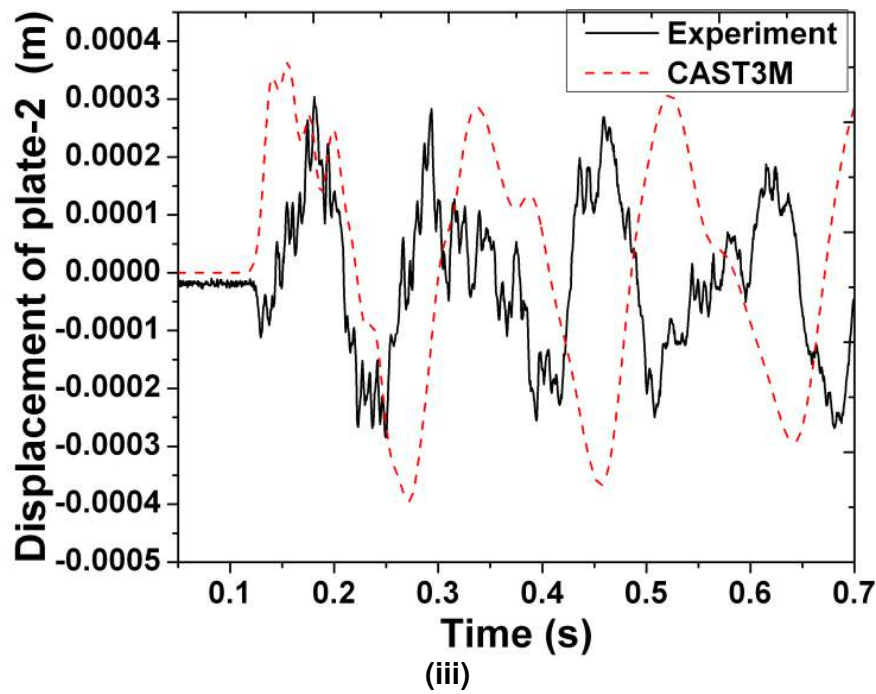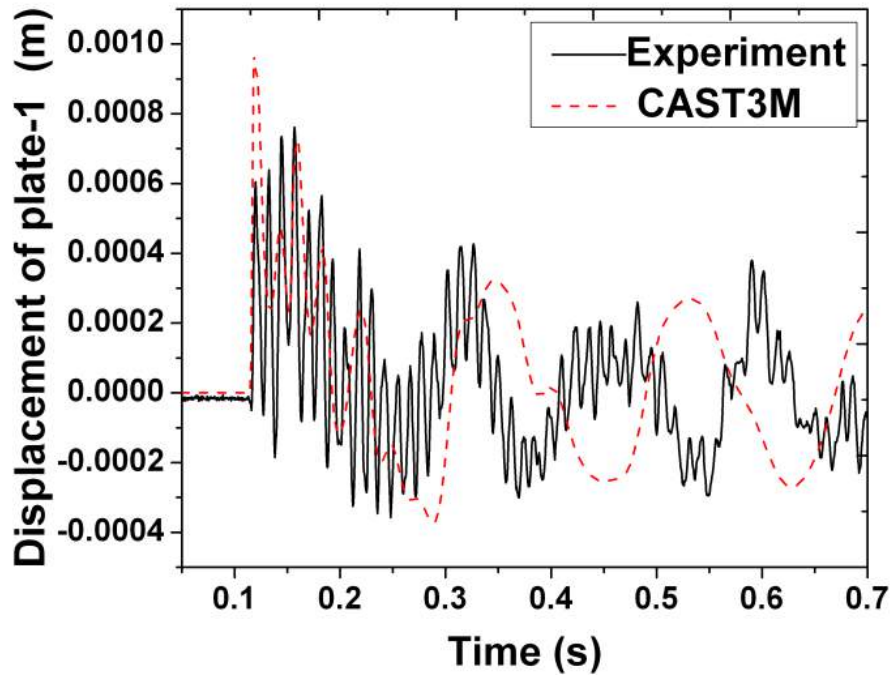
Fig. 3.13 (a) For Immersion depth = 580 mm (i) Impact force to plate-1 (ii) Dynamic displacement of plate-1 (iii) Dynamic displacement of plate-2
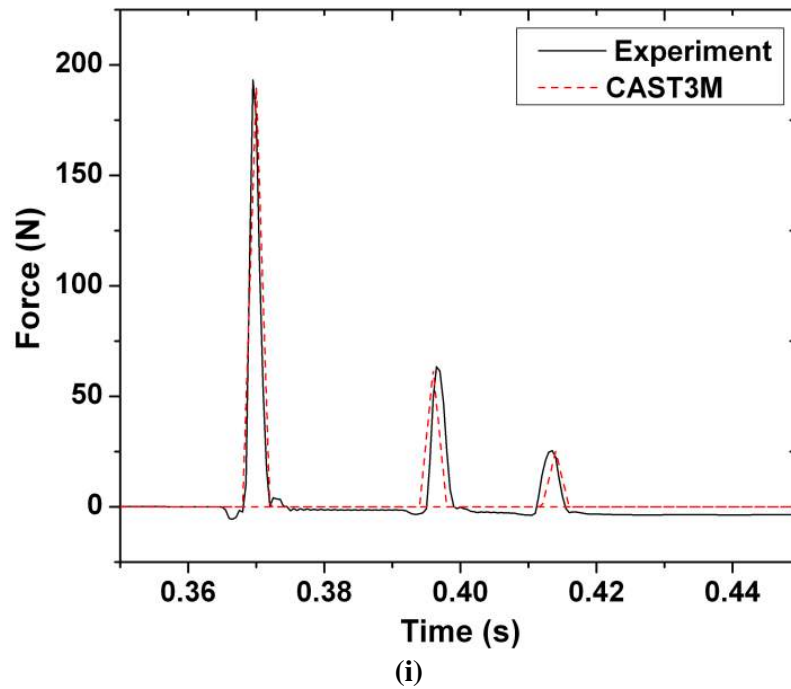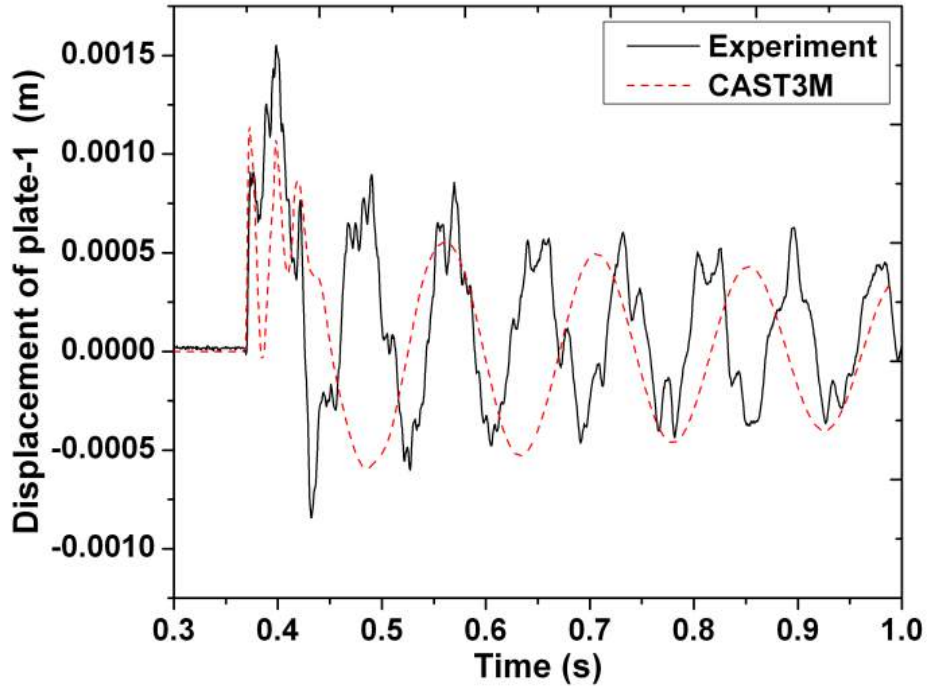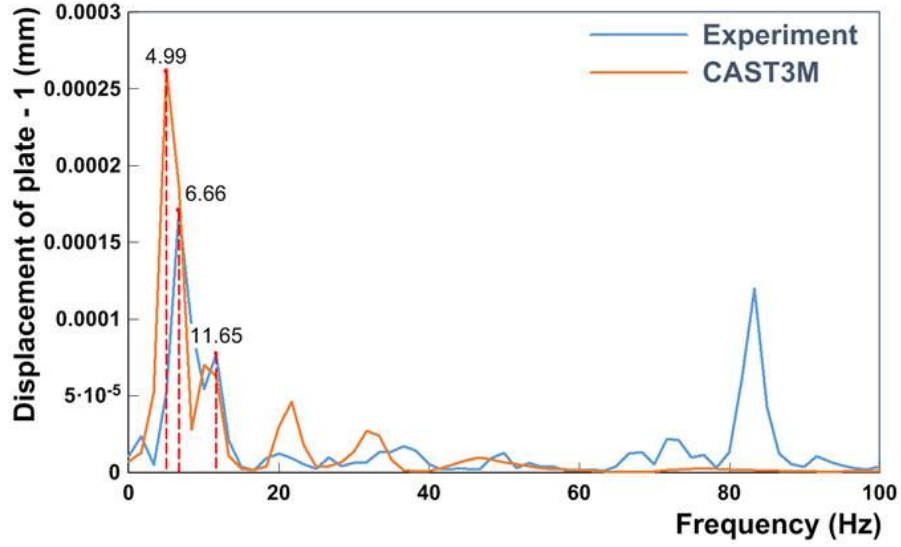
(i)
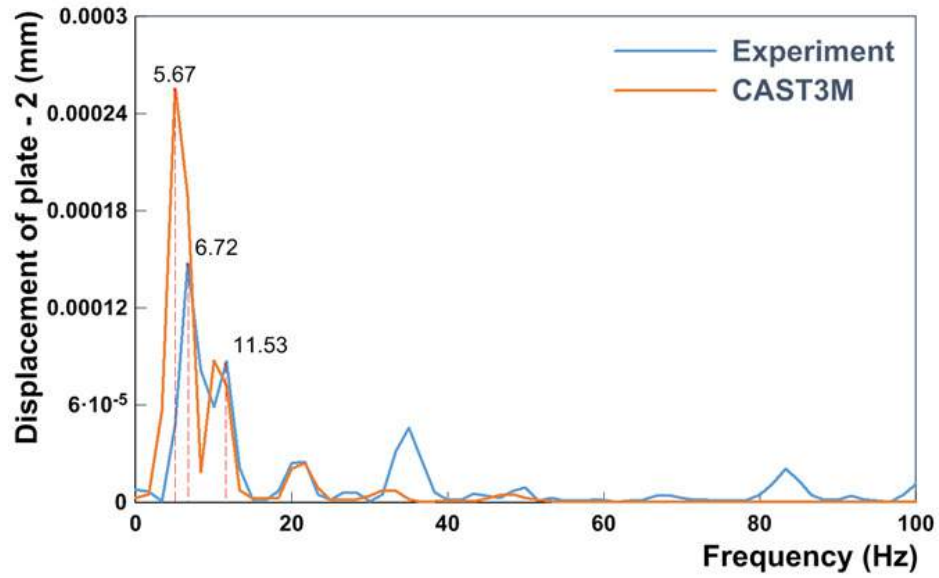
(ii)

Fig. 3.13 (b) Frequency response of the plates for immersion depth = 580 mm

Fig. 3.13(a) presents the excitation and response vibration of the plates to an Impact load of 160N. It is observed that the pattern of displacement finds to be the same with higher displacement compared to the earlier case and the ratio of maximum displacement of plate-2 to plate-1 is found to be 0.39. Fig. 3.13 (b) shows the frequency

spectrum of displacement obtained from experiment and CAST3M. we find that the difference in frequency of vibration is due to the change in geometry of the plate-2 to a curved shape with increase in immersion depth. Analysis was carried out with a curved shape geometry for the plate-2, showing decrease in frequency than the straight plate. Damping of 1% is assumed for all the cases.

From the experimental study, we find that the ratio of displacement of the response plate to the adjacent plate increases with increase in fluid level in the container. The variation of the ratio is due to the fluid coupling.

3.4 CLOSURE

Three-dimensional FEM analyses in CAST3M are compared with literature and experimental work. Natural frequency and mode shapes of vertical and horizontal cantilevered plate immersed in fluid have been studied. Benchmark study from literature predicts 3% error with CAST3M results. Sensitivity analysis for the grid (change in the number of divisions) and material properties (5 % change in the value Young's Modulus and density of the material) has been carried out for the cantilever plate immersed in the fluid. Much variation in the results was not observed. Experimental results show fairly good agreement and the deviation in results may be due to the change in geometry of the plate-2, which is very thin results in curved geometry with increase in the immersion depth. The use of CAST3M code has also been validated to solve dynamic problems with FSI and the same method can be applied to analyze the dynamic characteristics of complex components immersed in the fluid and its effect on the surrounding structures.

* * *

CHAPTER 4

Experimental Studies on Vibration in Structures

4

4.0 INTRODUCTION

In general, for any undamped free vibration of elastic structures in air with small amplitude of motion, its natural frequencies are investigated accounting for the overall stiffness and mass of the system. But when the same system is vibrating in a fluid medium, the Eigen values and Eigen vectors are affected and also the coupling between the structure and the surrounding fluid medium takes the form of an induced pressure at the interface. The dynamic characteristic such as natural frequency, mode shapes, and resonant behavior of individual structures has been a great concern to the designers. At the same time, the dynamic response of the unexcited adjacent structure due to the excited structure present in the same fluid medium is of paramount importance during transient loads. Especially mechanical structures in nuclear reactors when exposed to transient loads, the adjacent structures which are with distinguishing features of operations if get excited may lead to serious consequences. In fact, when the immersed structure interacts with the surrounding fluid medium the natural frequency decreases significantly with increase in the immersion depth. The phenomenon of interaction of fluid with structure and the resulting effect imposed by the structure on the fluid is referred to as Fluid Structure Interaction (FSI). The accurate modeling of FSI is highly challenging because of the computational difficulties in analyzing the two coupled fields (fluid and structure) which mutually interact with each other. In this chapter, vibrational responses of structures partially immersed in the fluid have been studied for impact and sinusoidal

loads. Both experimental and numerical analyses towards the study of vibration transmission in structures have been discussed here.

4.1 VIBRATION BETWEEN SIDE WALLS OF A RECTANGULAR TANK

Experimental and numerical works has been carried out to study vibration transmission between side walls of a rectangular tank filled with a fluid. Numerical analyses have been carried out in CAST3M. Natural frequency, transmission ratio and damping ratio for different depths of fluid level in the tank have been investigated. The results from experiment and numerical analysis are compared.

4.1.1 Experimental Setup
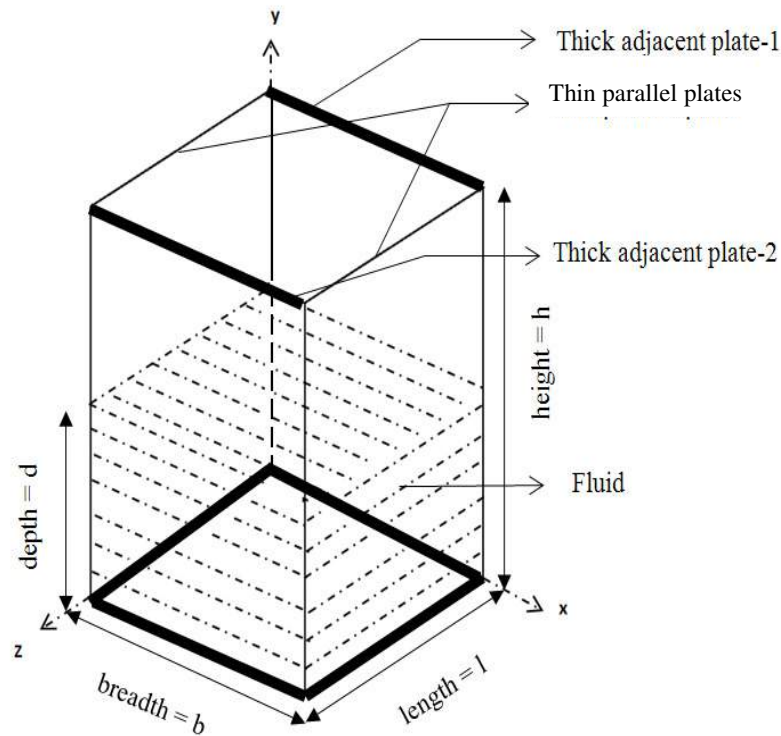
Fig. 4.1 Schematic of the rectangular tank

Two thin (thickness = 3 mm) rectangular plates are welded along their edges to two thick (thickness = 6 mm) plates to form a rigid rectangular tank. Fig. 4.1 shows the schematic of the rectangular tank with dimensions of length 'a'=500mm, width 'b'=500 mm, height 'h'=750mm and depth of immersion='d'. The rectangular tank is filled with the fluid. An impact force of vibration to one thin plate (Plate-1) results in the response vibration to the opposite plate (Plate-2). Impact hammer and piezoelectric accelerometers are used in the experiment. The impact force is given by the impact hammer handled manually. The impact hammer delivers the input excitation force. The accelerometers are fixed on the faces of the thin plates. The response is measured for a minimum period of 10 s. The sampling rate chosen is 10000 Hz. The experiments are carried out in air and in water with four depth ratios. The technical specifications of accelerometers and Impact hammer used are listed in Table 3.2. Specification of accelerometers used are listed in Table 4.1. The position of accelerometers and the position of impact are shown in experimental setup as illustrated in Fig. 4.2.

Table 4.1 Technical specifications of Accelerometers and Underwater

accelerometers

Accelerometers	
Make	Measurement specialties, Inc
Model	4803A
Frequency range	±2g (0-200Hz)
Sensitivity	1000 mV/g
Mounted frequency	700 Hz
Type	Resistive
Purpose	Acceleration measurement

Under water Accelerometers	
Make	Measurement specialities, Inc
Model	4332M1-010
Frequency range	±10g (0-200Hz)
Sensitivity	200 mV/g
Mounted frequency	1000 Hz
Type	Resistive
Purpose	Acceleration measurement

(i)   (ii)
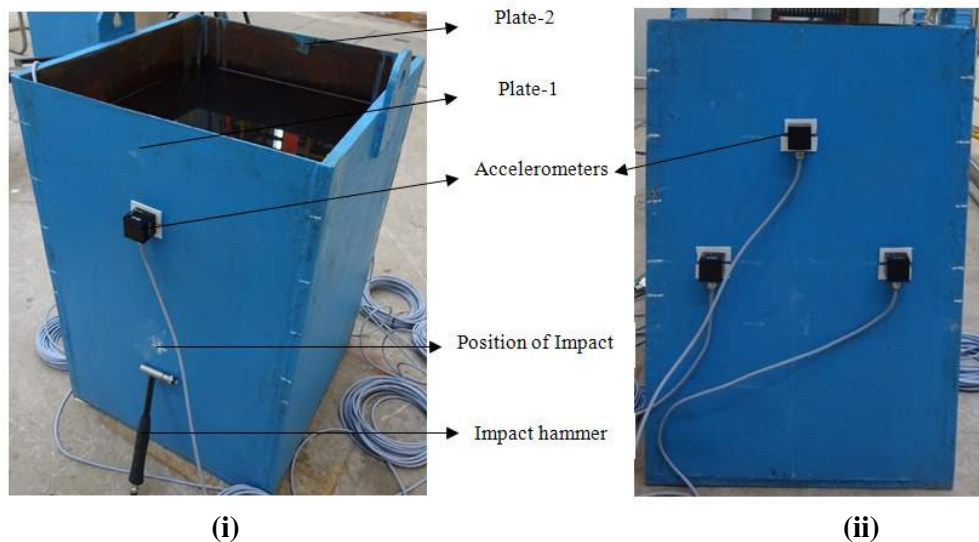
Fig. 4.2 Experimental tank set-up (i) Excited plate with Impact hammer and sensor

(ii) Response plate with sensors

4.1.2 Modeling & Analysis

The rectangular tank is modeled and analyzed using Finite Element Method in CAST3M. It is assumed that the fluid is inviscid, incompressible and motion of the fluid is irrotational. Further small movements of the structure and small pressure fluctuations

are considered. The thin plates are made of stainless steel while the other plates are made of carbon steel. The fluid considered is water with a density of 1000 kg/m^3. The three-dimensional model consists of fluid elements and elastic shell elements. The thin plates are welded to the side walls of thick plate to form a rigid rectangular tank. Since the plates are welded, only the base of the tank is applied with rigid boundary conditions. The plates are modelled with their actual thickness in the simulation. The thin plates can vibrate more as compared to the thick plates. The fluid element is eight noded brick element and plate element is four noded element with six degrees of freedom. At the fluid-solid interface, the fluid nodes and the solid nodes are joined by the liquid transition elements. The free surface of the fluid is modeled using the free surface elements. Each rectangular plate has been meshed identically. A fixed boundary condition for the bottom plate of the tank is given arresting displacement and rotation.

Free vibration analysis

Free vibration analyses have been carried out for different depth ratio (d/h) to obtain the natural frequency and mode shapes of the tank. Natural frequency of the tank for different depth ratio is tabulated in Table 4.2 and the mode shapes for the depth ratio (d/h) = 0.6 are shown in Fig. 4.3.

Table 4.2 Natural frequencies for the model in Hz

Modes	In air	depth ratio (d/h)			
		0.47	0.60	0.73	0.87
1	69.788	35.645	30.686	27.996	26.141
2	70.363	71.077	64.196	50.333	39.324
3	89.554	72.512	67.331	54.411	44.245
4	136.48	95.852	82.700	83.505	76.815
5	160.83	100.09	84.382	85.090	94.485
6	172.85	100.96	93.665	89.568	94.974

(i)　　　　　　　　　　　(ii)

(iii)
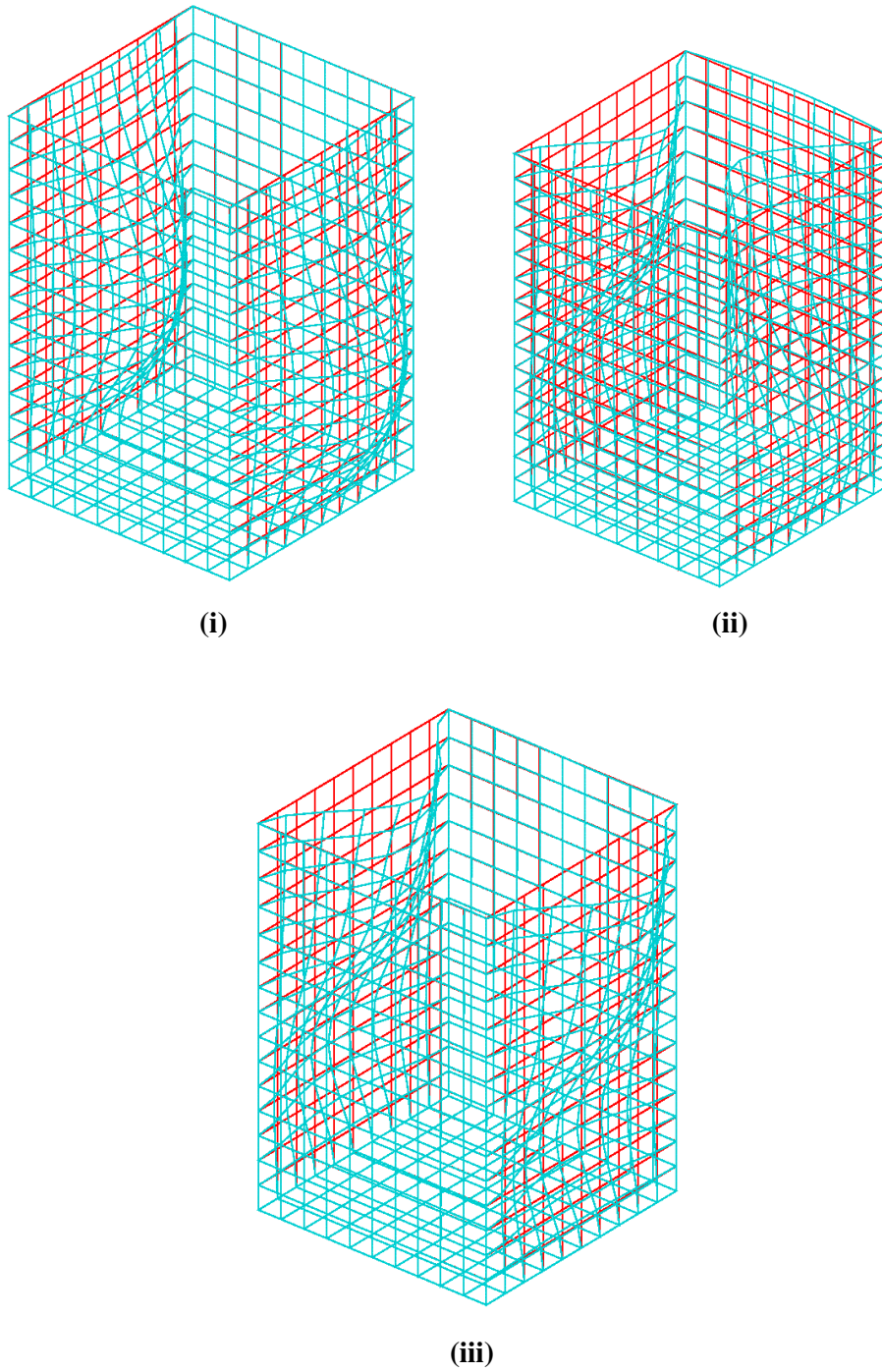
Fig. 4.3 Wet mode shapes of rectangular tank for immersion depth ratio = 0.60 (i) first mode frequency (30.686 Hz); (ii) second mode frequency (64.196 Hz); (iii) third mode frequency (67.331 Hz)

Impact analysis

Plate-1 was excited with an impact and the response of plate-2 for this excitation is measured. The finite element analysis is performed to obtain the response of the plates when excited by an impact load. The frequency of vibration and dynamic displacement of the plates for different depth ratios are calculated.

When the system is set into free vibration after an impact, the damping ratio can be determined from the ratio of two displacement amplitudes measured at an interval of 'm' cycles. If 'x_n' is the amplitude of vibration at any time and 'x_m' is the amplitude 'm' cycles later, the damping ratio 'ζ' is given by,

$$\zeta = \left(\frac{\delta}{2\pi m}\right) \text{ where '}\delta\text{'} = \frac{1}{n}\ln\left(\frac{x_n}{x_m}\right) \text{ is the logarithmic decrement}$$

Using the value of 'ζ', the coefficients for mass and stiffness matrices in Rayleigh damping(Ray W. Clough, 1975)are calculated considering 1st and 10th mode of natural frequencies and used in CAST3M.

4.1.3 Results and discussion

Experiment

The plate is excited using the Impact hammer with a metallic tip. Approximately 10N is set as trigger level for the impact hammer measurement. Response of the plates is measured in parallel during the impact. The frequency range of excitation considered is 2500 Hz. Fig. 4.4 (a) gives the excitation and its spectrum from experiment. The impact excitation spectrum is plotted in logarithmic scale up to 100 Hz. The same excitation force is used in the analyses. Fig. 4.4 (b) shows the acceleration - time history obtained from the experiment for all the cases. The Frequency Response Function (FRF) and phase response of the plates are shown in Fig. 4.5. For all the cases, the first peak corresponds

to the fundamental mode frequency. The natural frequency is found to decrease with increase in the depth ratio. Comparing the experimental values with the calculated (Table 4.1), it is found that for air the difference is only 3 Hz. For water for depth ratio = 0.47 it closely matches, and the difference is 0.1 Hz. With increasing depth ratio, the difference increases and for depth ratio = 0.87, the difference is 9 Hz. It can be seen that from Fig. 4.5 (iv) and Fig.4.5 (v), when the depth ratio increases to 0.73 and 0.87 excitation of higher modes is observed.
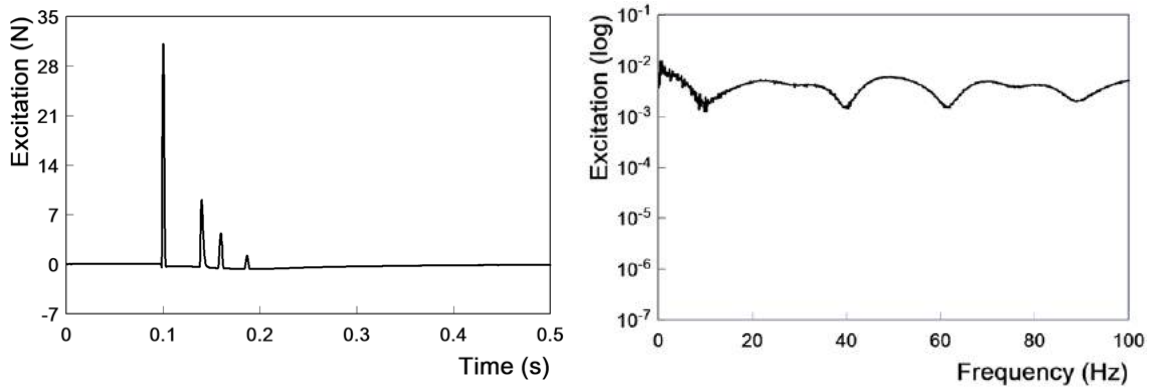
(i) In air
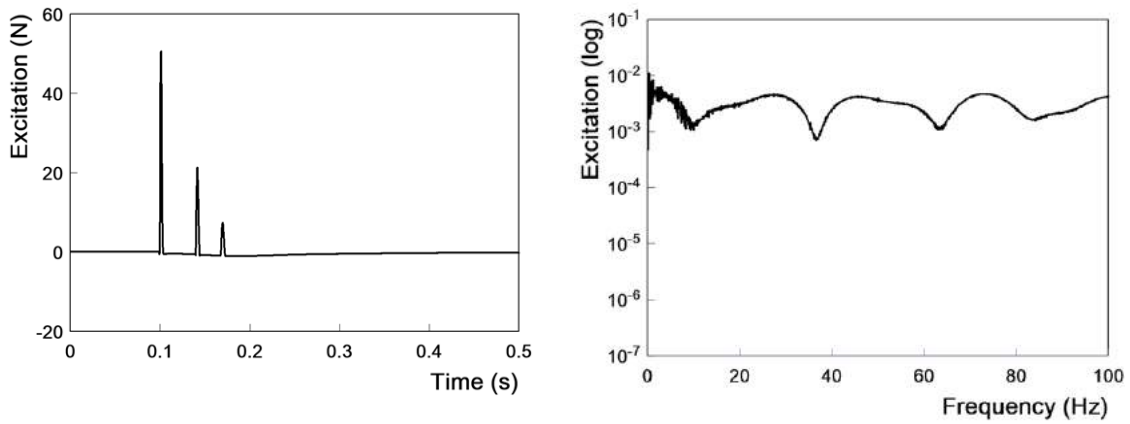
(ii) d/h = 0.43
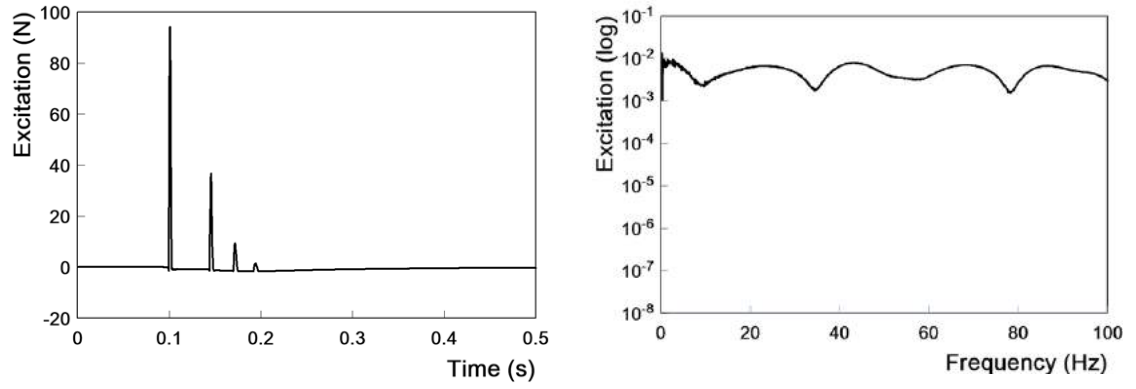
(iii) d/h = 0.60
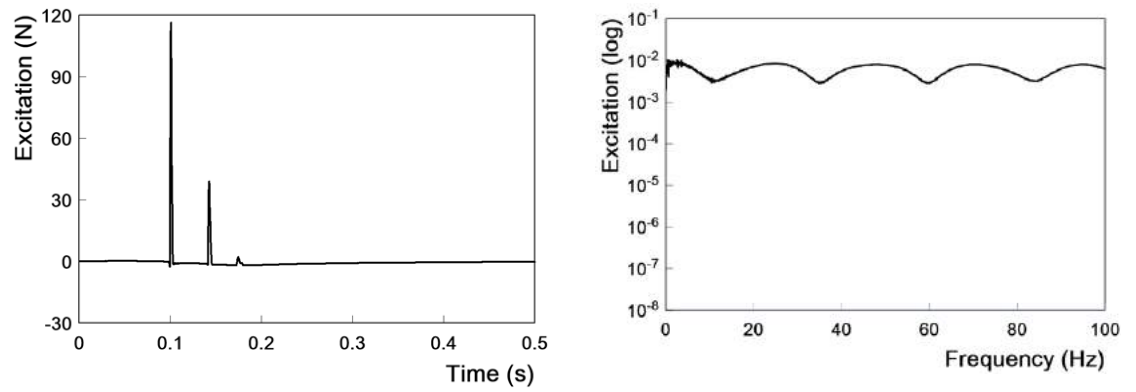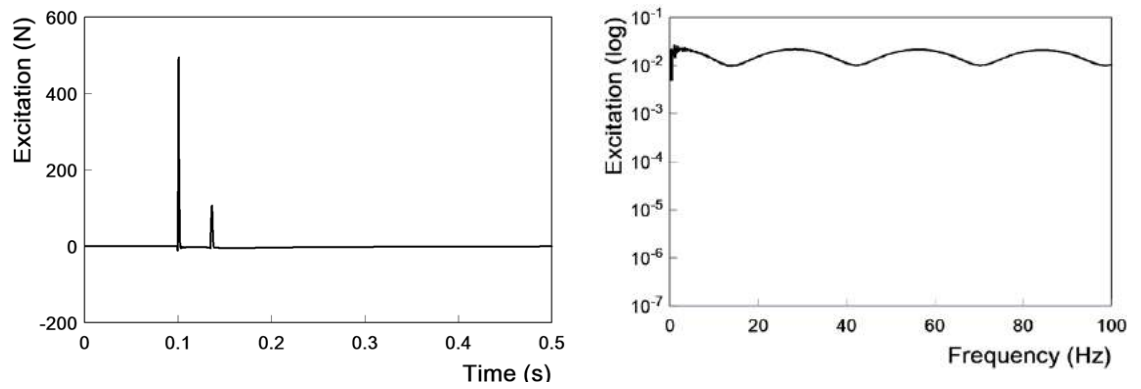
(iv) d/h = 0.73

(v) d/h = 0.87

Fig. 4.4 (a) Excitation and its spectrum for the plate-1 from experiment
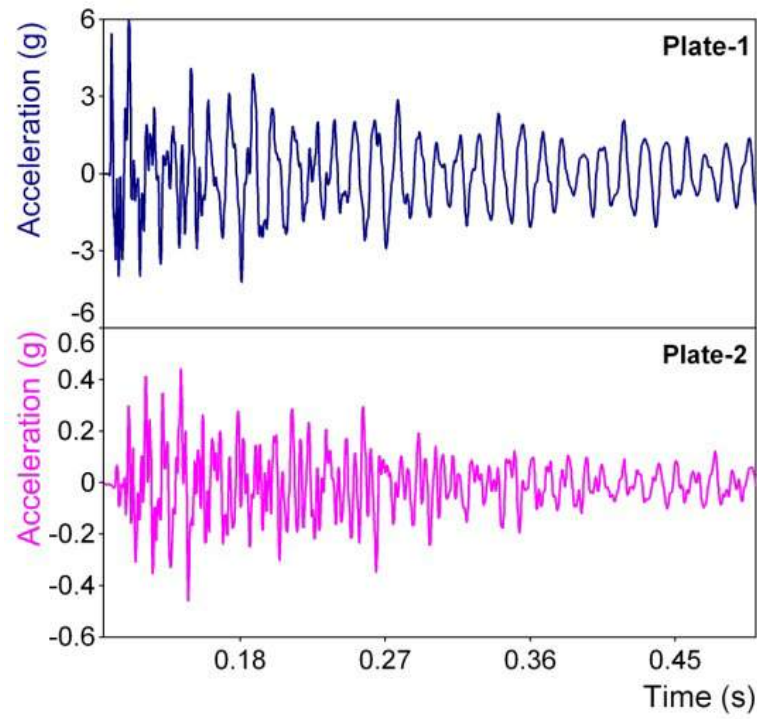
(i) In air
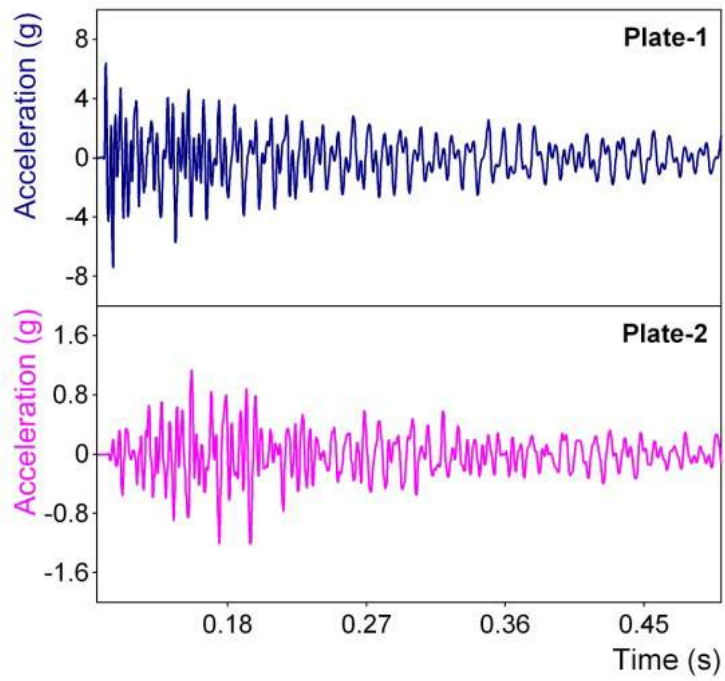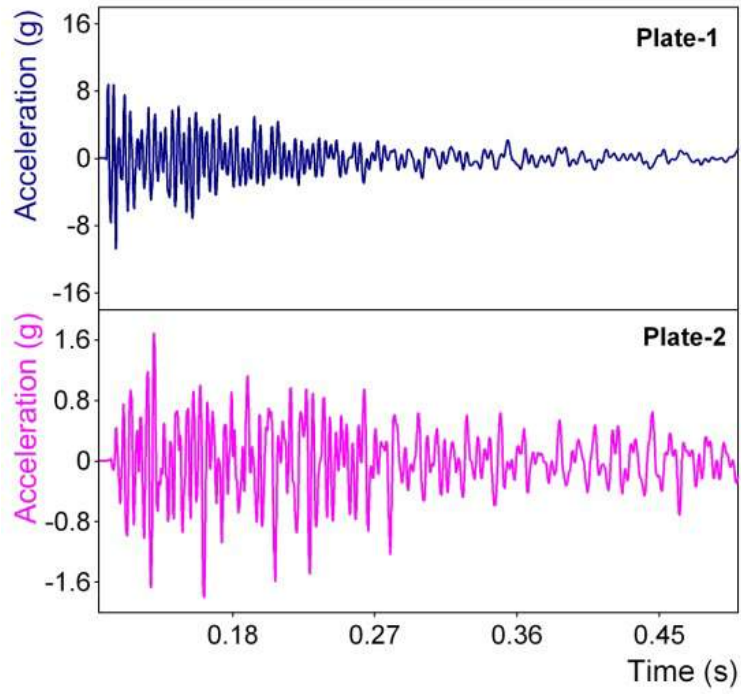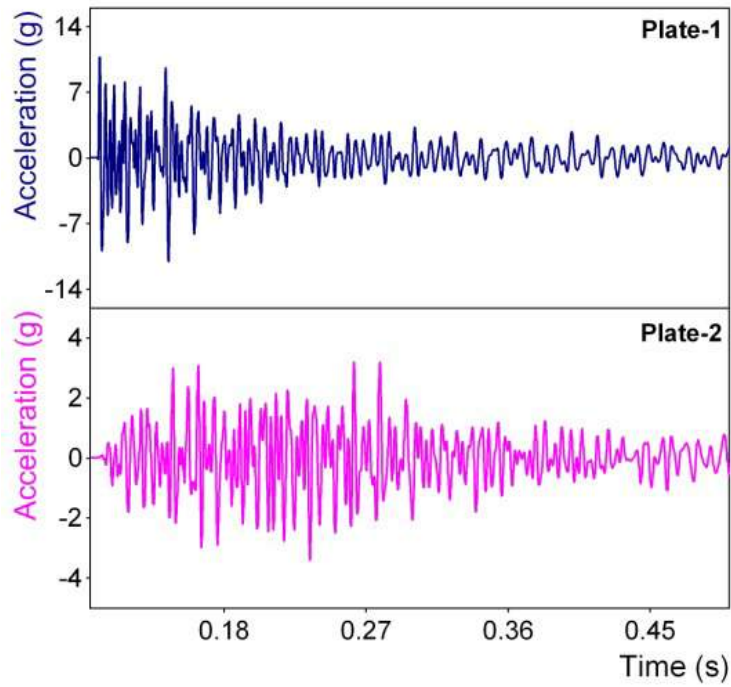
(ii) d/h = 0.47
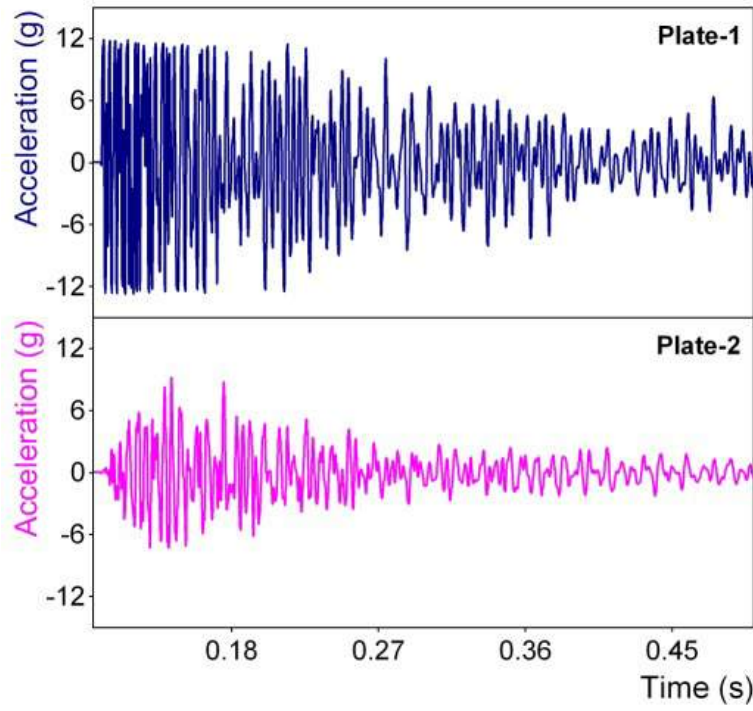
(iii) d/h = 0.60

(iv) d/h = 0.73

(v) d/h =0.87

Fig. 4.4 (b) Acceleration of plate-1 and plate-2 from experiment
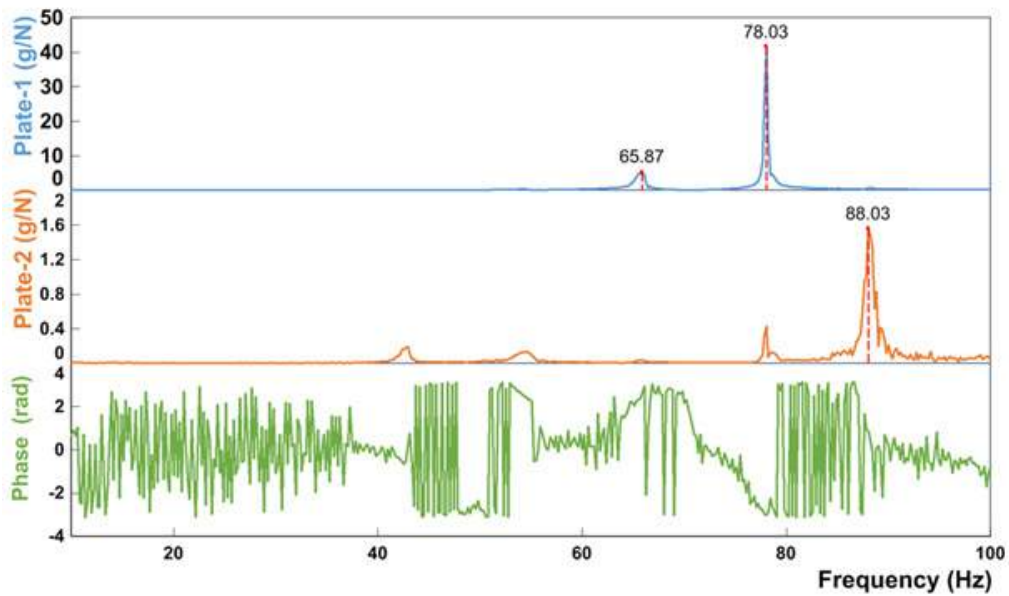
(i) In air
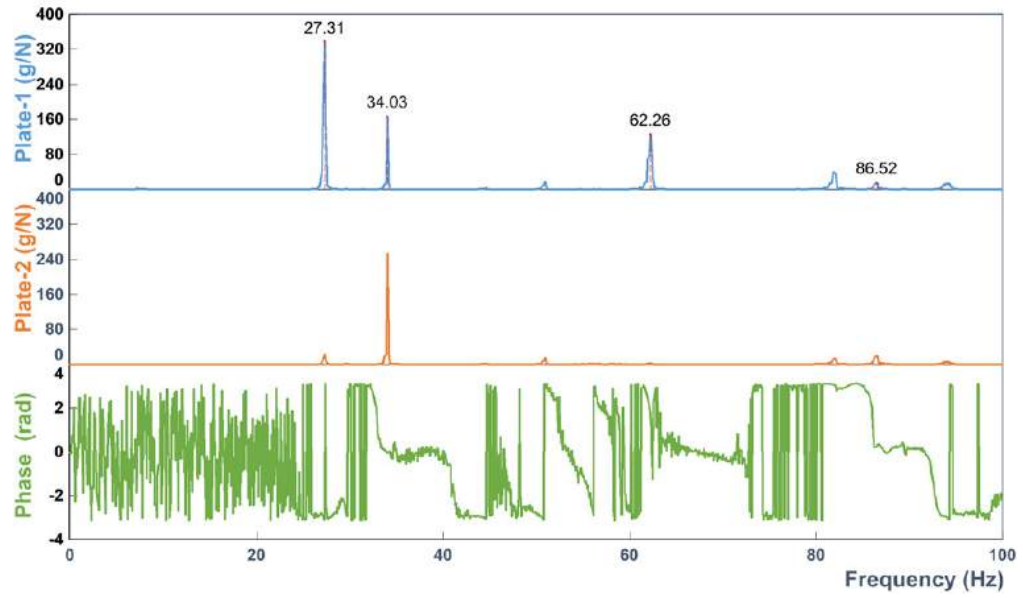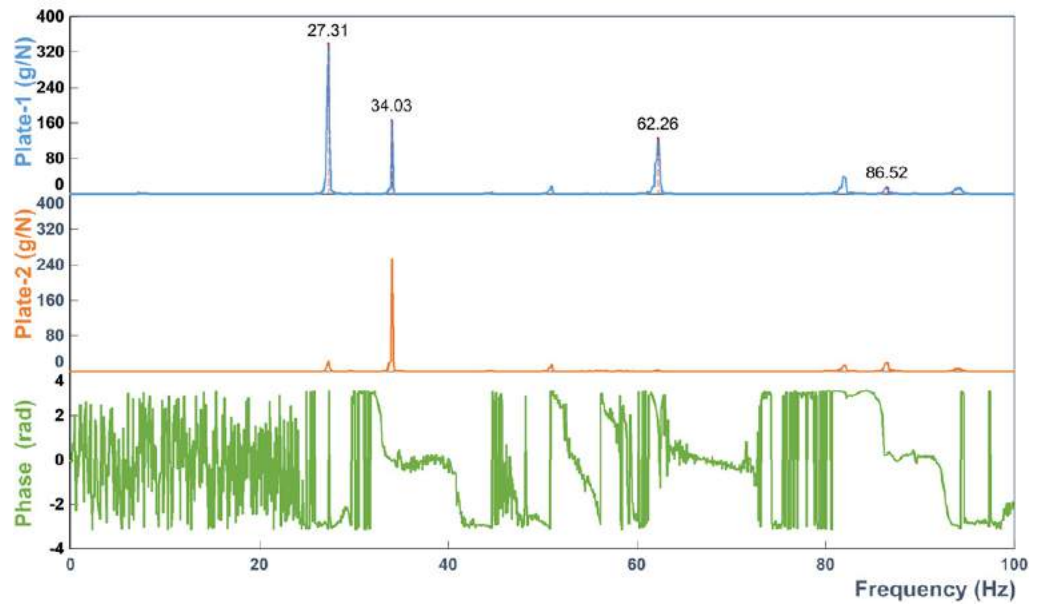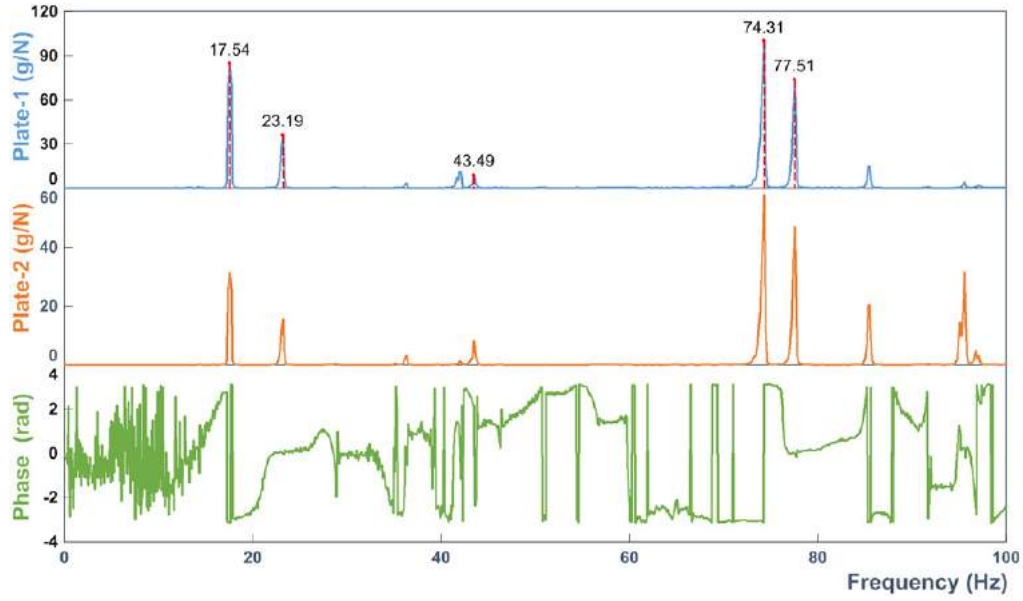
(ii) d/h = 0.47
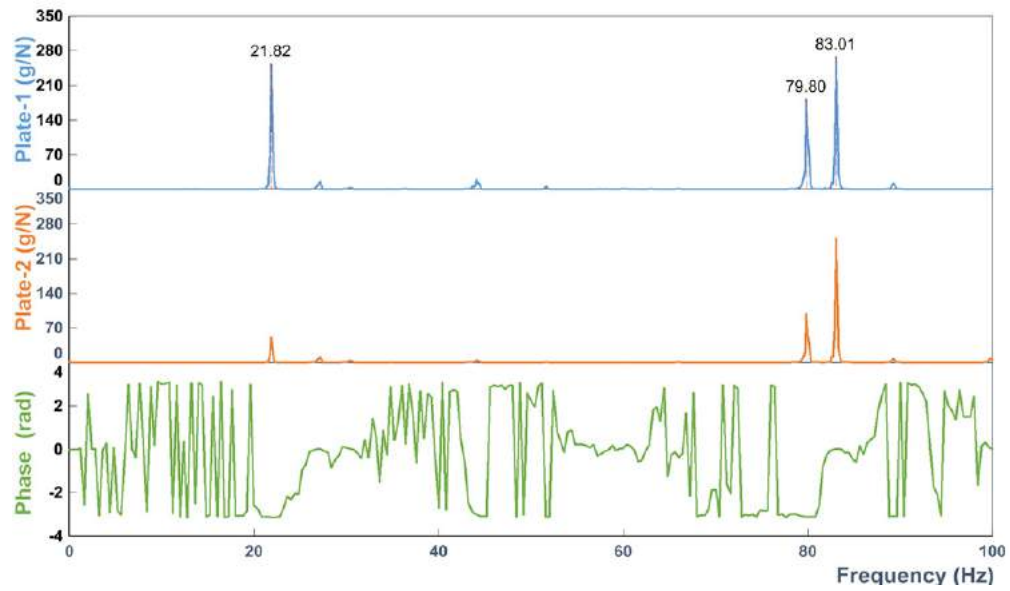
(iii) d/h = 0.60

(iv) d/h = 0.73

(v) d/h = 0.87

Fig. 4.5 FRF and phase response of plate-1 and plate-2 from experiment

Analysis
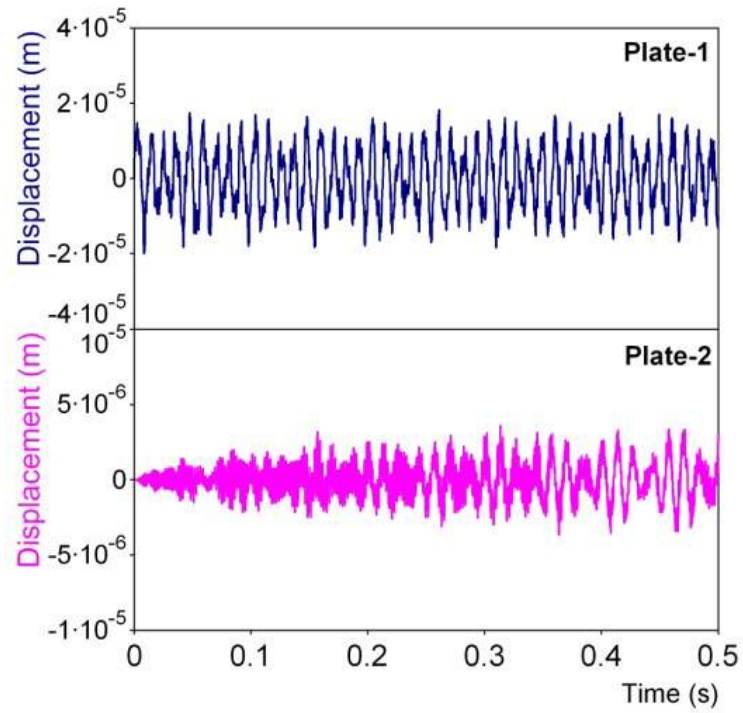
(i) In air
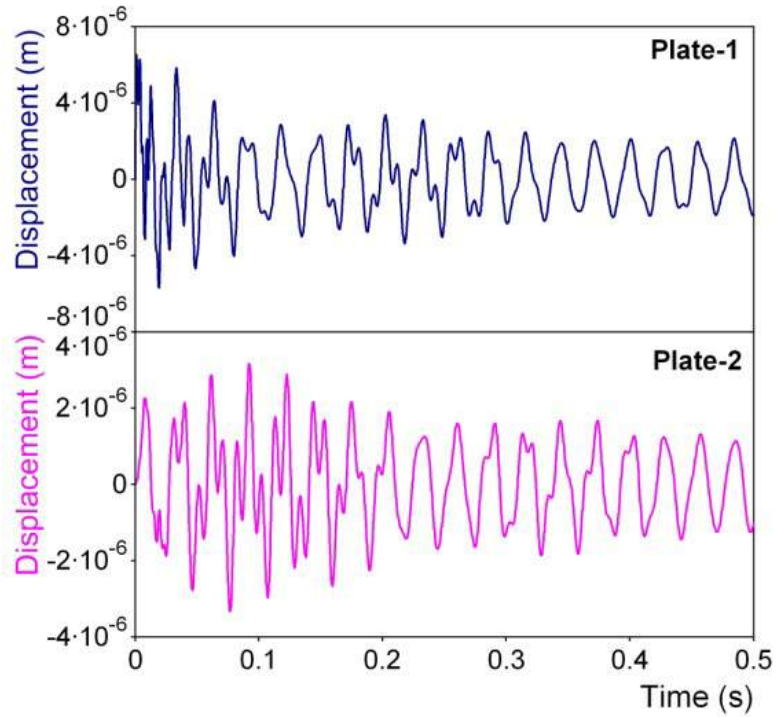
(ii) d/h = 0.47
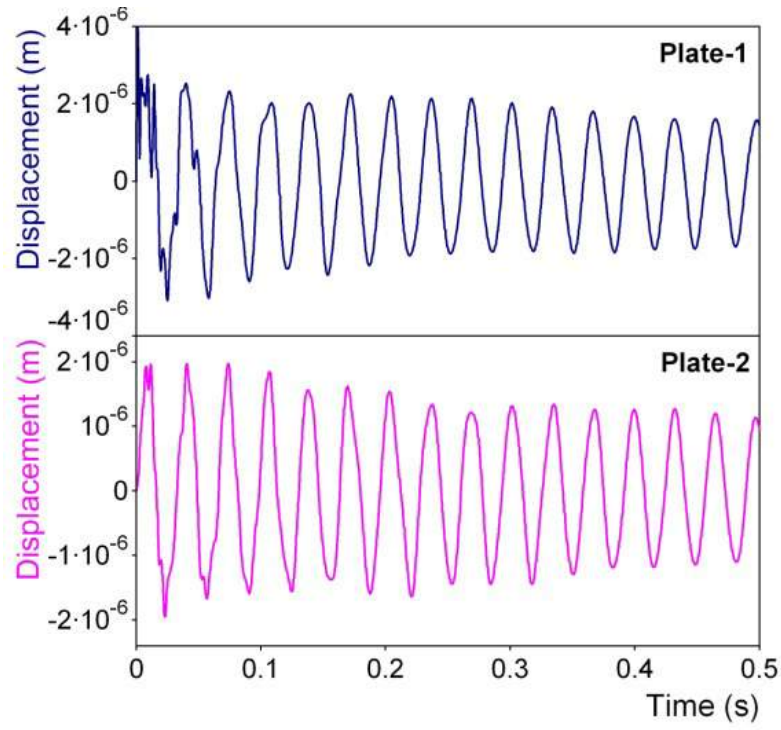
(iii) d/h = 0.60
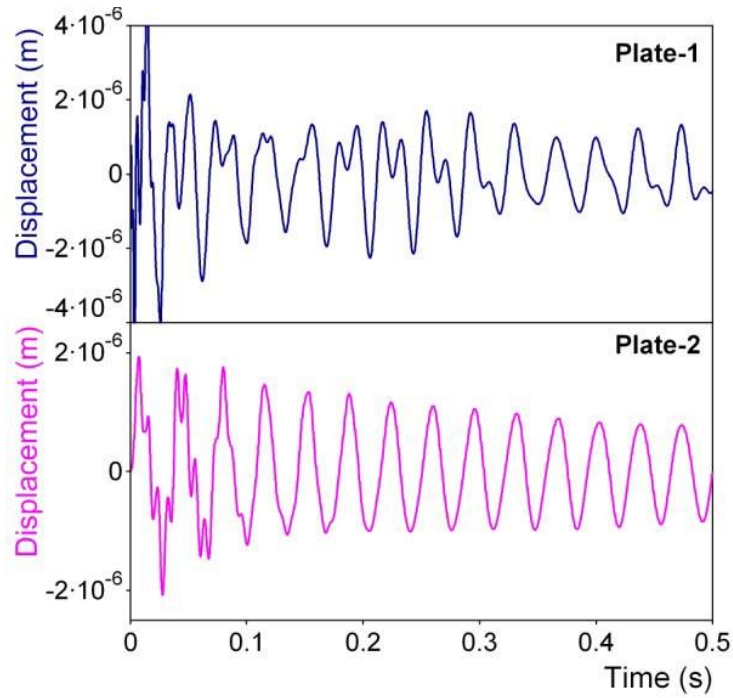
(iv) d/h = 0.73
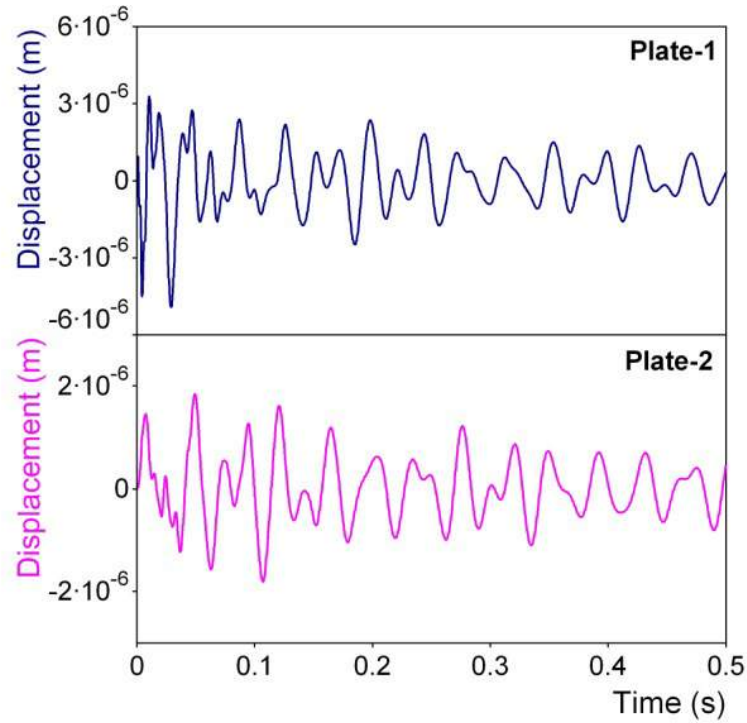
(v) d/h =0.87

Fig. 4.6 Displacement of plate-1 and plate-2 from analysis

Fig. 4.6 gives the displacement time history from CAST3M. The distinct peaks are corresponding to the first mode frequency. FRF of the plates from displacement spectra is shown in Fig. 4.7. Multiple peaks observed in the experiment (Fig.4.5) shows predominant excitation of higher modes. The modal frequencies calculated are in close agreement with the experiment and also match with the natural frequency analysis given in Table 4.2.
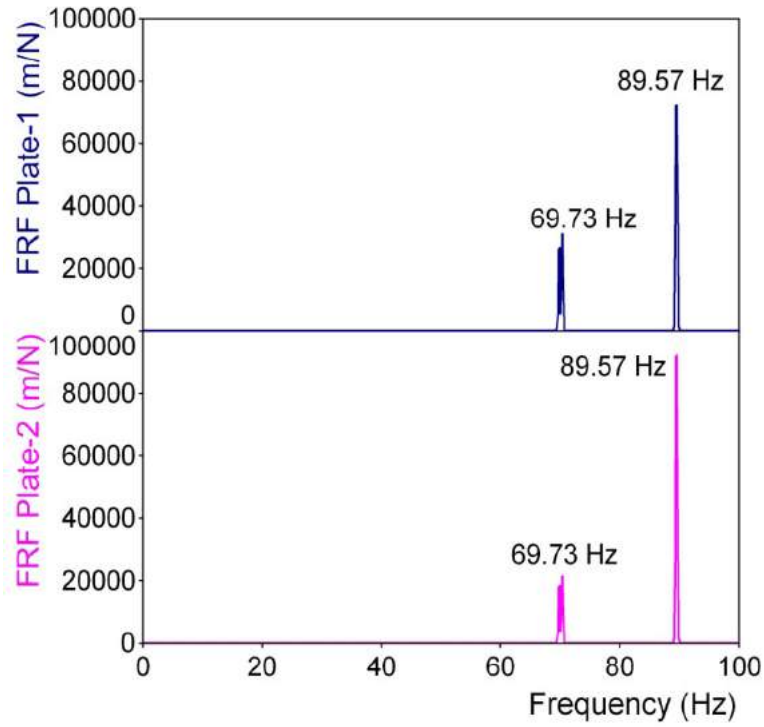
(i) In air
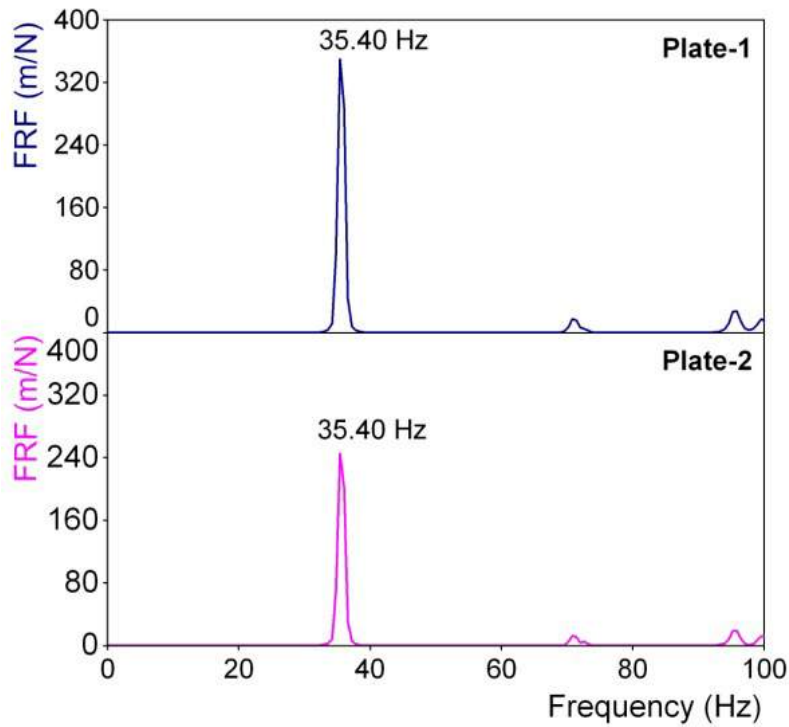
(ii) d/h = 0.47
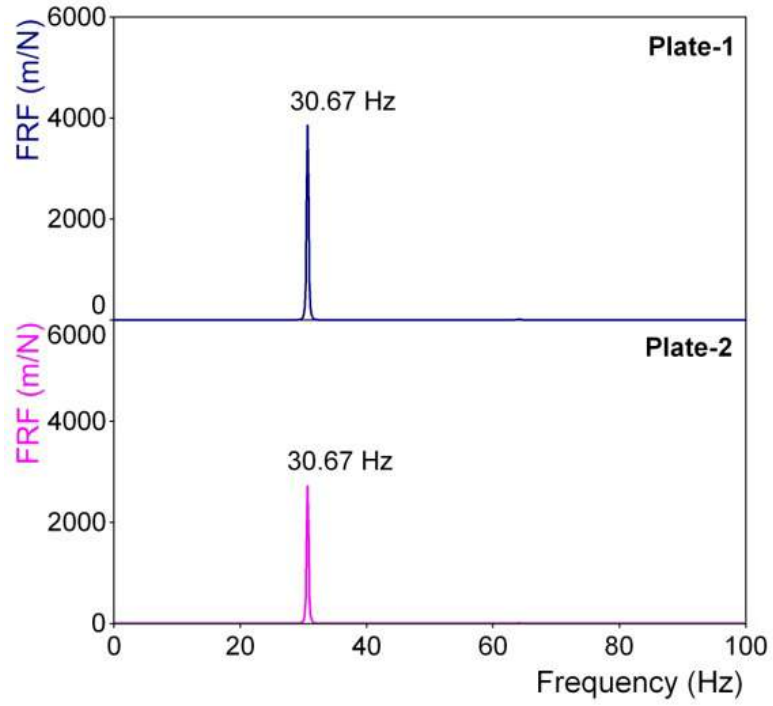
(iii) d/h = 0.60
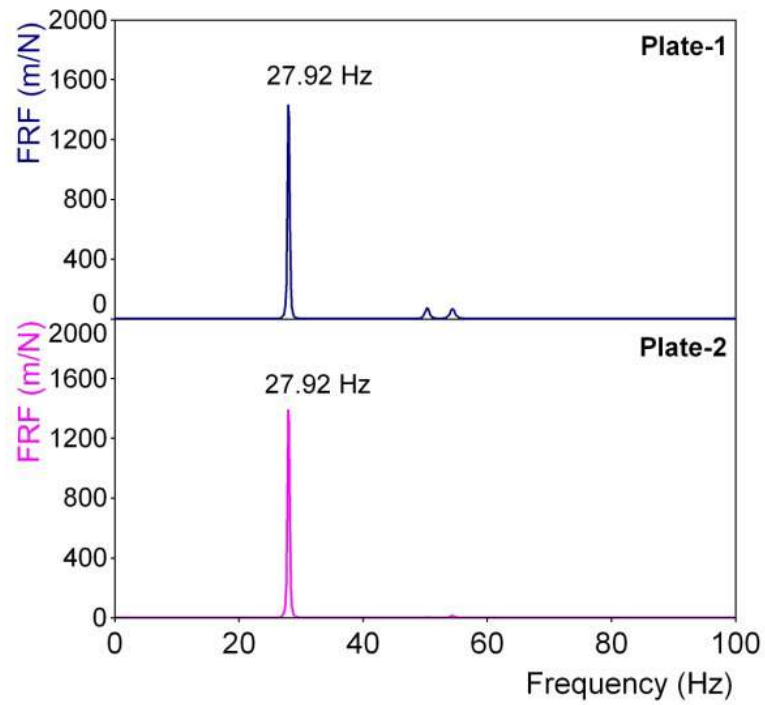
(iv) d/h = 0.73
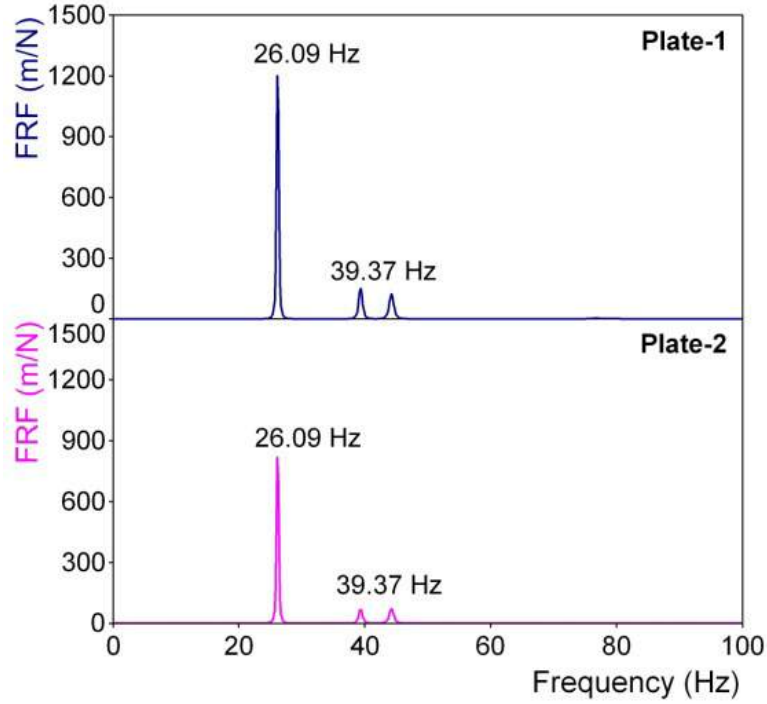
(v) d/h =0.87

Fig. 4.7 FRF of plate-1 and plate-2 from analysis

Vibration transmission ratio between two plates

Transmission ratio is defined as the ratio of displacement of the response plate to the displacement of the excited plate. The ratio of displacement of the plate-2 to plate-1 for a given impact is calculated as the transmission ratio (Max. Disp. of plate-2/Max. Disp. of plate-1). The transmission ratio from plate-1 to plate-2 is shown in Fig. 4.8 from experiment, CAST3M. The position of impact is chosen at the centre of the plate for all the immersion depth ratio. When the position of impact is chosen as centre of submergence depth, it is found that the transmission ratio increases with increase in the depth. This shows that the impact position over the metal and over the immersed portion of the metal plays a significant role. A separate curve with impact position at the centre of immersion depth is included in the Fig. 4.8 using CAST3M analysis. Less transmission is

observed in air, because the transmission takes place only through the adjacent plates. When the fluid level is increased, the transmission ratio increases and then decreases. For both experiment and analysis, the value of transmission ratio with different immersion depth is plotted in Fig. 4.8 including the case with impact at the centre of the immersion depth. The study shows that tendency of increase and decrease in transmission ratio is associated impact position in the rectangular tank.
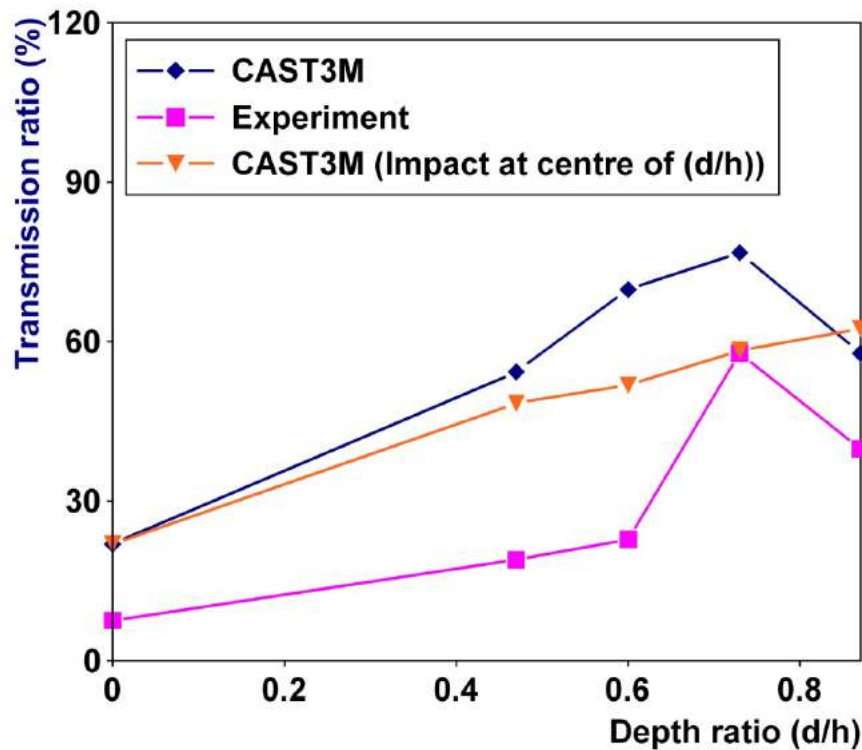
Fig. 4.8 Transmission ratio of plates
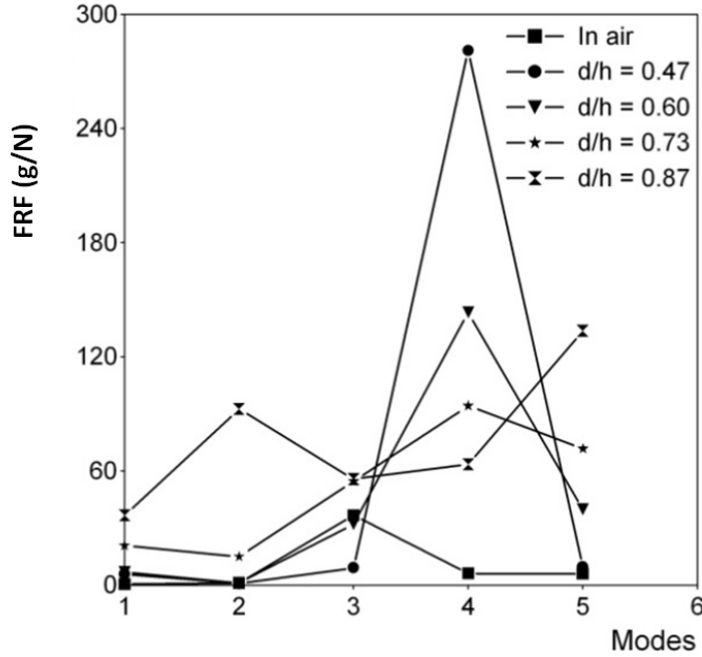
Fig.4.9 Transmission ratio with modes

To understand the mechanism of increase and decrease in the ratio, the transmission ratio is plotted for the first 5 mode shapes associated with both the plates. The ratio is calculated from the FRF (Frequency Response Function) of the plates from various immersion depths and given in Fig. 4.9. It is observed that the transmission ratio reduces at the 5th mode for all the cases except for the depth ratio of 0.87. At higher depth ratio, excitation of higher modes are predominant as observed from Fig. 4.5. Transmissibility ratio obtained from displacement and mode shape showed a similar trend as shown in Fig. 4.8. Fig. 4.10 is plotted by taking RMS (Root mean square) values at the respective mode shapes. This graph is plotted to show the comparison between Fig. 4.8 and Fig. 4.10. Therefore the impact position of the rectangular tank is related with the critical depth ratio.
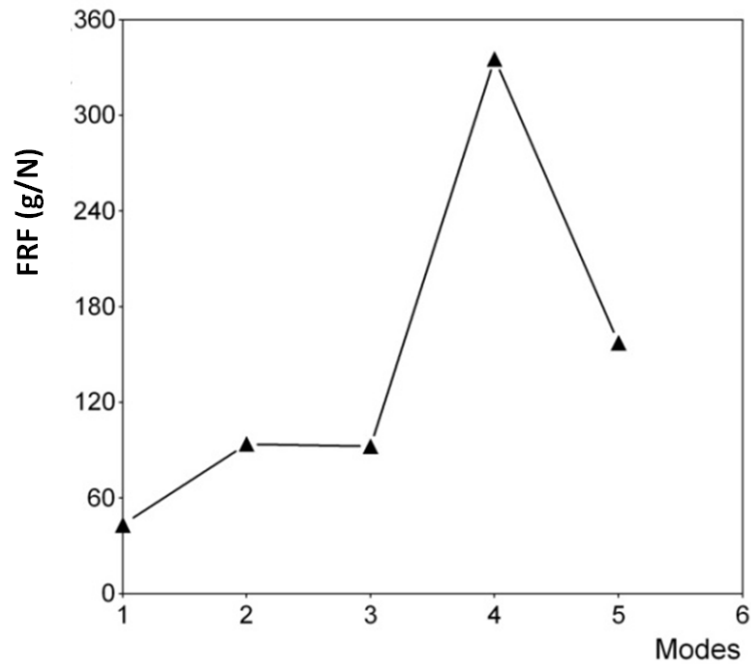
Fig.4.10 Resultant Transmission ratio

Damping and transit time delay of transmission between plates

Fig. 4.11 shows the value of damping ratio for various depth of immersion. The damping ratio is calculated using half power bandwidth method. The half power bandwidth method uses the transfer function (or FRF) trace of the structure to estimate the amount of damping at each mode. In the present study, the peak of first mode frequency is taken to calculate the damping ratio. It is found that the damping increases with increase of depth ratio as expected.
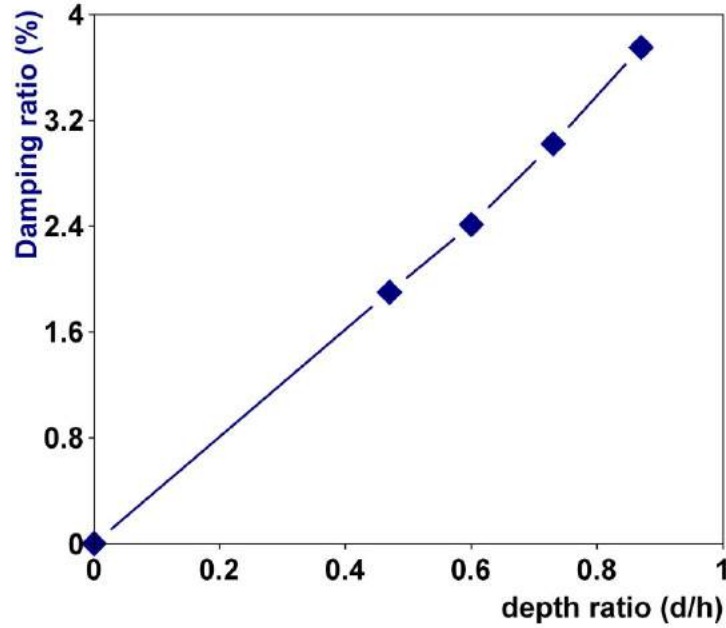
Fig. 4.11 Damping ratio

Transit time of vibration between the two plates has been calculated by the method of cross-correlation. Fig. 4.12 shows the cross correlation curves. Table 4.3 lists the time delay between excitation of first plate and the response of second plate. The first peak from the Fig.4.12 corresponds to the delay time. It is observed that the time delay increases with increase in the depth ratio. Estimated transit time in air was observed to be much lesser compared to transit time in fluid. This shows that the transmission path from plate-1 to plate-2 in case of air is through the adjacent metallic plate of the tank. With increase in the level of the fluid, the transit time is found to be higher, as the transmission path is mainly through the fluid in the tank.
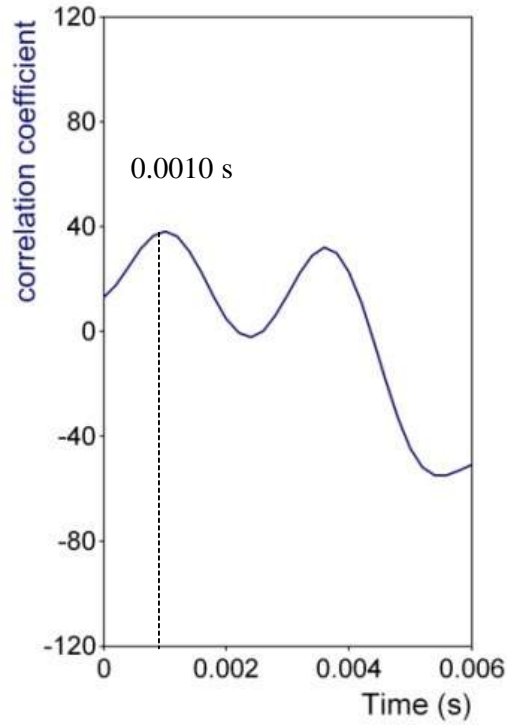
(i) In air
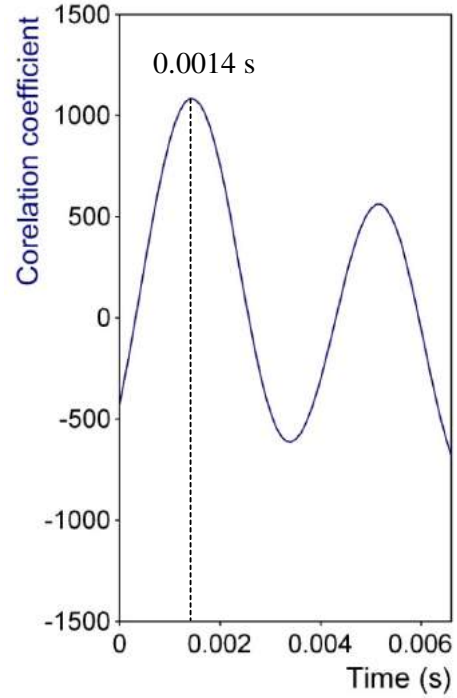
(ii) d/h = 0.43
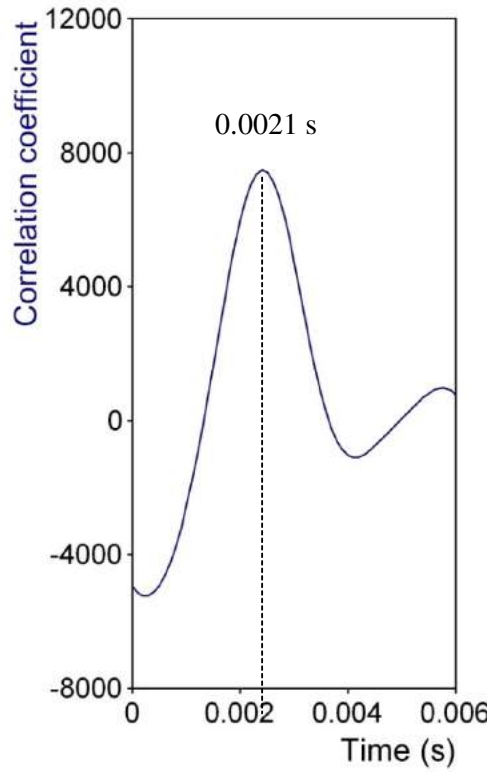
(iii) d/h =0.60
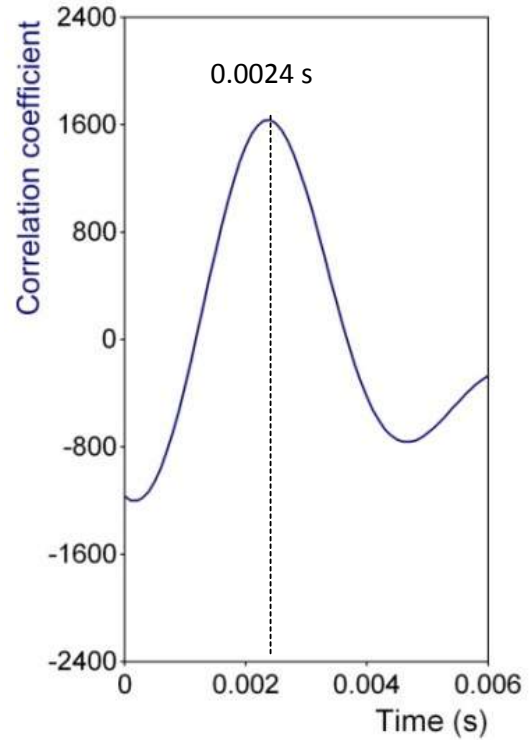
(iv) d/h =0.73
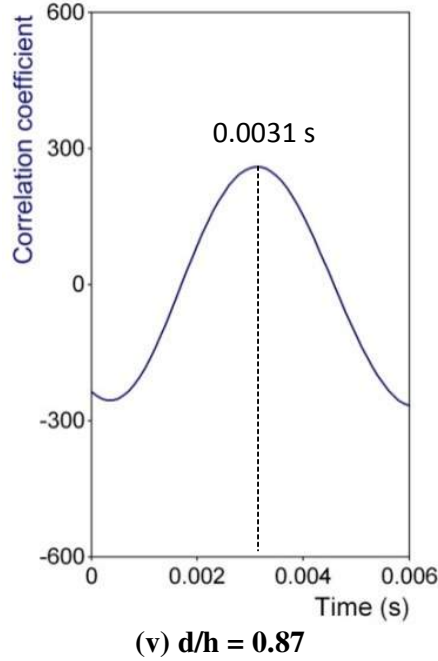
(v) d/h = 0.87

Fig. 4.12 Time delay between plate-1 and plate-2

Table 4.3 Transit time delay between plates

Cases	Correlation time (s)
Air	0.0010
d/h= 0.47	0.0014
d/h= 0.60	0.0021
d/h= 0.73	0.0024
d/h= 0.87	0.0031

The important finding of the study is the energy transmission between plate-1 and plate-2 increases with depth ratio up to a critical depth and reduces beyond that as shown in Fig. 4.8. This shows that for a critical depth ratio the energy transmission is maximum. From study it is also found that the damping ratio and transit time delay increases with increase in the depth ratio.

4.2 VIBRATION BETWEEN CANTILEVERED PLATE STRUCTURES

Investigation of vibration transmission between cantilever plates when they are excited close to resonance frequency for different immersion depth of plates in a finite volume of fluid is studied with an experimental setup established for this purpose. Three-dimensional dynamic analyses simulating the experiment have been carried out using Finite Element Method (FEM) in CAST3M. Vibration transmission in immersed cantilever plates with variations in the width of plate and depth of immersion of the plates have been discussed in this chapter elaborating experimental and numerical works involved.

4.2.1 Experimental Setup
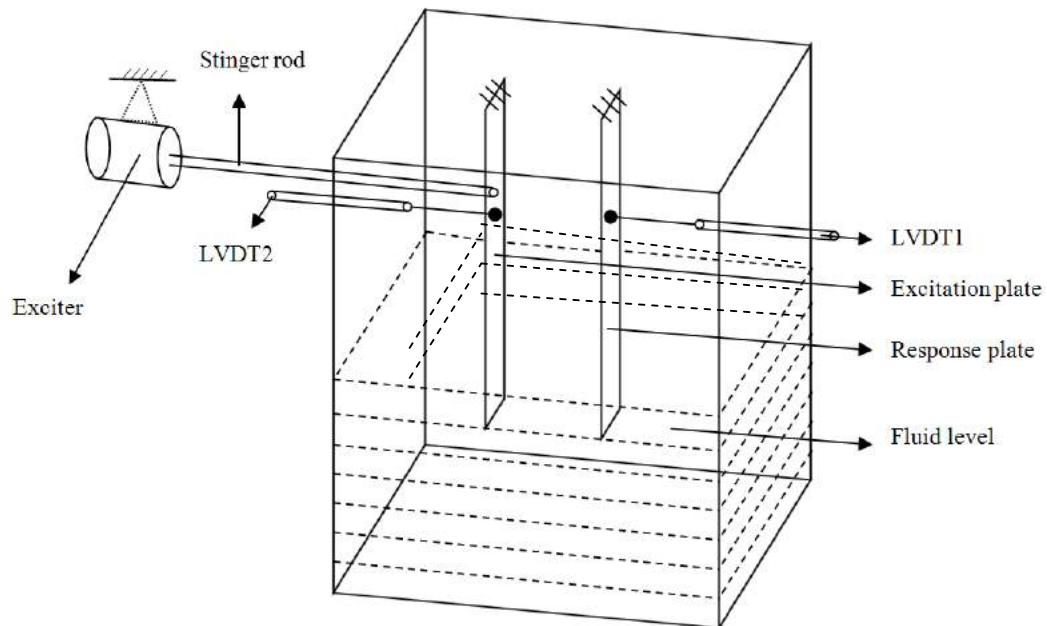
Fig. 4.13 Schematic of the experimental setup

The experimental setup consists of a rectangular tank of dimensions 1000 x 1000 x 1500 mm deep with rectangular cantilever plates welded to top plate of the tank, an electro dynamic exciter and LVDT (Linear variable differential transformers) as shown in the Fig. 4.13.The two cantilever plates are placed independently ensuring that there is no mechanical contact between the plates except fluid coupling. The actual experimental setup is shown in Fig. 4.14. Technical specifications of Electrodynamic shaker, LVDT and Force transducer are listed in Table 4.4.

Table 4.4 Technical specifications of Electrodynamic shaker, LVDT and Force transducer

Electrodynamic shaker	
Make	Spectral Dynamics, Inc
Model	M1600W
Force rating	200 N
Maximum stroke	19.2 mm, 6.75 inch peak to peak
Maximum acceleration	80 g
Fundamental axial resonance	> 5000 Hz
Purpose	Input excitation
LVDT	
Make	Honey well
Model	DW7U DC-DC
Range	± 4 inches
Sensitivity	1.2 V/ inch
case	Stainless steel
weight	21.26 gram
Purpose	Displacement measurement

Force transducer	
Make	PCB Piezotronics
Model	201 B02
Sensitivity	11.2 mV/N
Purpose	Force measurement

Force measurement

The electro dynamic exciter with a stinger rod attached with a force transducer is actuated by a power amplifier of 200 W. The force rating is 200 N which is connected to a function generator for tuning precise frequency of excitation and waveform. The force transducer measures the input force at a distance of 800 mm from the bottom of the plate (i.e. above the fluid level).

Displacement measurement

The two rectangular plates are parallel to each other and centered inside the tank. The LVDTs are positioned at a distance of 700 mm from bottom (i.e. above the fluid level) of the plate at the mid location. The dynamic displacement of the plate is measured above the level of the fluid.

Data Acquisition system

Dewesoft is measurement software which can acquire data from many different measurement hardware and enables the user to do processing, storage and analysis in a simple way. DEWESoft Smart Interfaces (DSI) bring an expanded level of flexibility of measurement system in dynamic signal analysis, combustion analysis and networked data acquisition. It facilitates measurements like voltage & current, sensors with voltage output, temperature, vibration, strain gage, counter, frequency measurement, video

acquisition, CAN bus measurement and GPS acquisition. Dynamic signal analysis covers a wide range of measurements in the field of structural dynamics, industrial acoustics and machine diagnostics.

Test cases and conditions

An input sinusoidal excitation with force amplitude is given to plate-1 and the response is measured in terms of dynamic displacement vs. time history on the plate-2. The experiment is carried out for different immersion depths. Width of the response plate is varied and the width of the excitation plate remains the same for the three different cases. The distance of separation between the plates is taken as 300 mm so that the plates inside the tank would be centered. Table 4.5 gives the test conditions considered.

(i) Front view of tank
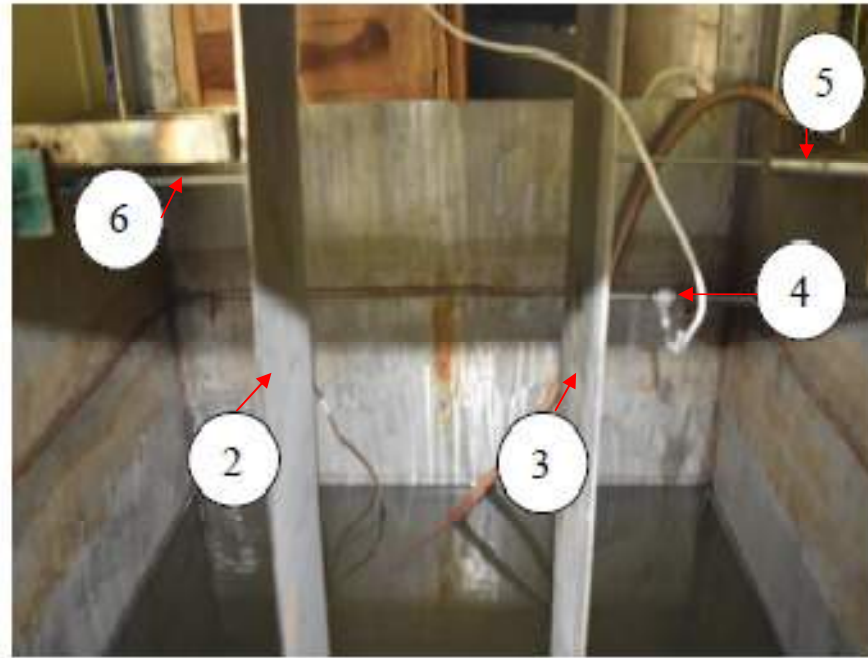
(ii) Interior view of tank
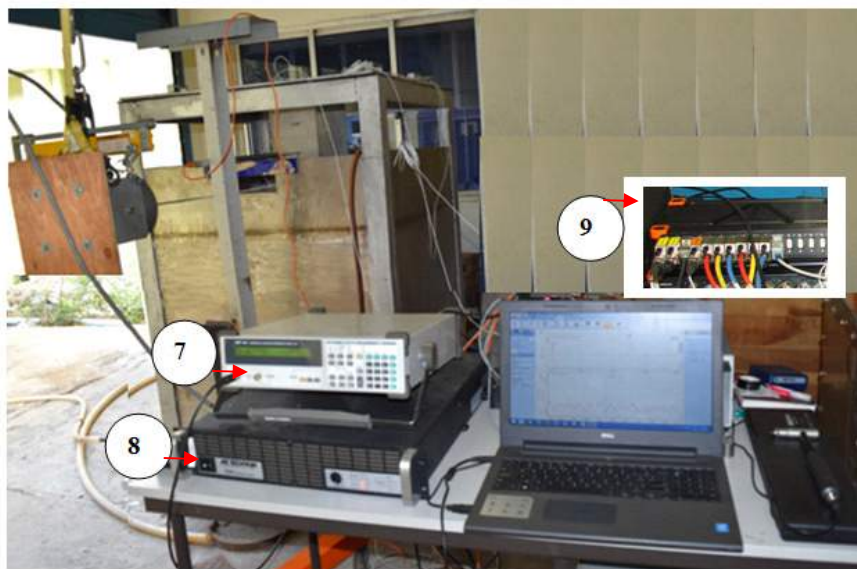
(iii) Isometric view of tank

Fig. 4.14 Experimental setup

1– Electro dynamic exciter	2– Excited plate	3– Response plate
4– Stinger rod with force sensor	5– LVDT at excited plate	6– LVDT at response plate
7-Function Generator	8-Transducer	9-Data acquisition system

Table 4.5 Test conditions

cases	Immersion depth ratio (d/l)	Plate-1 (Excited plate)	Plate-2 (Response plate)
1	0.2, 0.3, 0.4, 0.5 & 0.6	l = 1000 mm, b = 203.2 mm, t = 4.84 mm	l = 1000 mm, **b = 203.2 mm,** t = 4.84 mm
2	0.2, 0.3, 0.4, 0.5 & 0.6	l = 1000 mm, b = 203.2 mm, t = 4.84 mm	l = 1000 mm, **b = 101.6 mm,** t = 4.84mm
3	0.2, 0.3, 0.4, 0.5 & 0.6	l = 1000 mm, b = 203.2 mm, t = 4.84 mm	l = 1000 mm, **b = 50.8 mm,** t = 4.84 mm
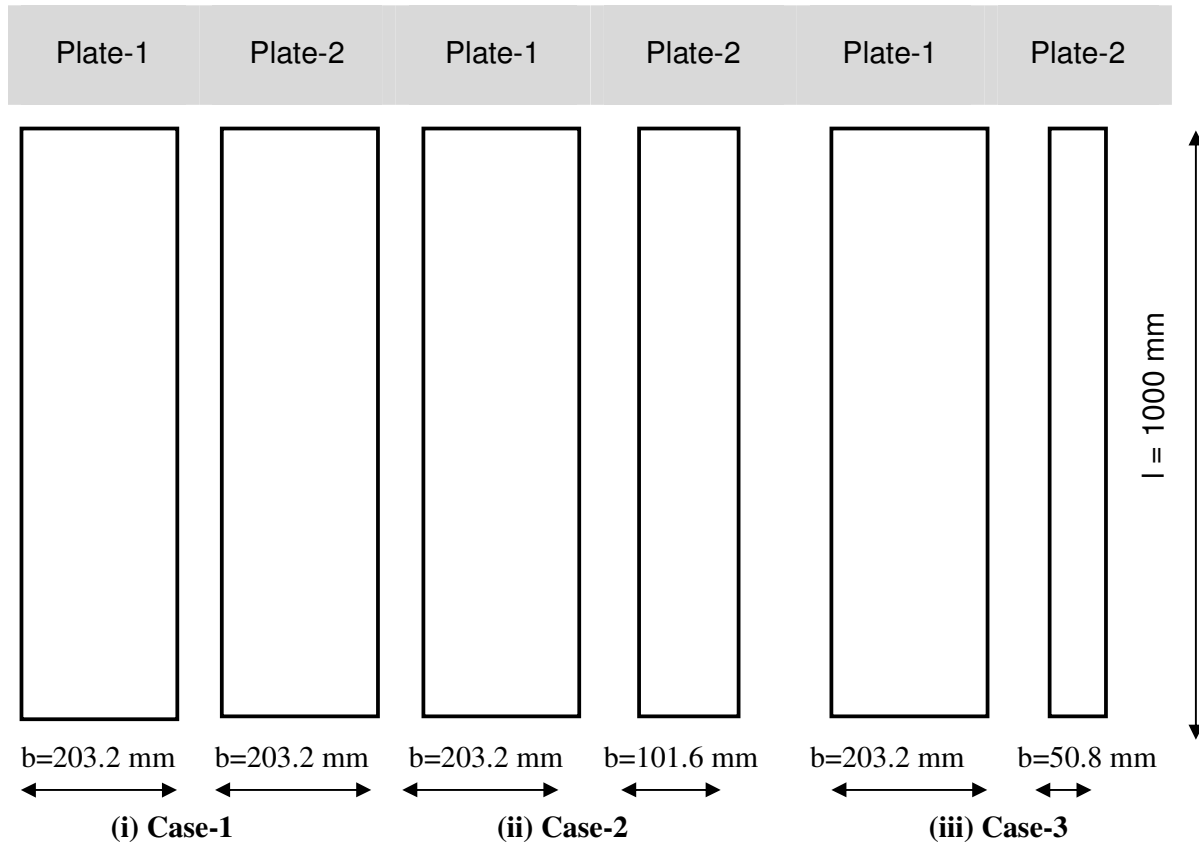
Fig. 4.15 Configuration of plates for various cases

4.2.2 Modeling & Analysis

Natural frequency of the plates considered in test cases

Natural frequencies for the cantilever plates considered for the test cases are determined experimentally and by simulation using CAST3M. The natural frequencies obtained are tabulated in Table 4.6. It can be observed that the frequencies calculated in air remains the same for all geometry of the plates. This shows that with change in width of the plate, there is no change in natural frequency. When the plates are immersed in the fluid with different immersion depth, the natural frequency varies and this is due to the added mass acting on the plate. It is also inferred that with decrease in width of the plate for same thickness, the natural frequency increases.

Table 4.6 Natural frequency of the plates with their geometry in Hz

Immersion depth (d/l)	Case-1		Case-2		Case-3	
	Experiment	CAST3M	Experiment	CAST3M	Experiment	CAST3M
air	3.158	3.3006	3.158	3.3006	3.158	3.3006
0.2	1.95	1.6598	2.20	1.92	2.25	2.25
0.3	1.71	1.5906	1.85	1.85	2.15	2.22
0.4	1.47	1.4969	1.83	1.83	2.12	2.21
0.5	1.46	1.4635	1.77	1.81	2.08	2.20
0.6	1.40	1.4353	1.65	1.79	2.06	2.16

Meshing and Material properties

The plate is modeled using four noded shell element and fluid volume is modeled using eight noded brick element. At the fluid solid interface, the fluid nodes and the solid nodes are joined by liquid shell transition element. The free surface level of the fluid is

modeled using free surface element which is a liquid shell. Water at atmospheric conditions is used. Fig.4.16 shows the FEM model. The material properties of the plate are in   Table 4.7.

Table 4.7 Material properties

Density of Steel 'ρ'	7830 kg/m^3
Modulus of elasticity of steel 'E'	2.1x10^{11} N/m^2
Poisson ratio 'μ'	0.3
Density of fluid 'ρ$_w$'	1000 kg/m^3
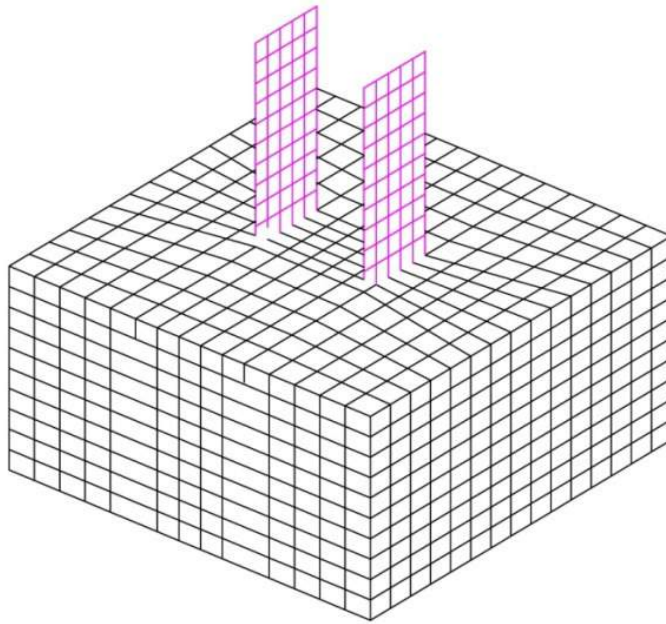
(i)Two cantilever plates with fluid
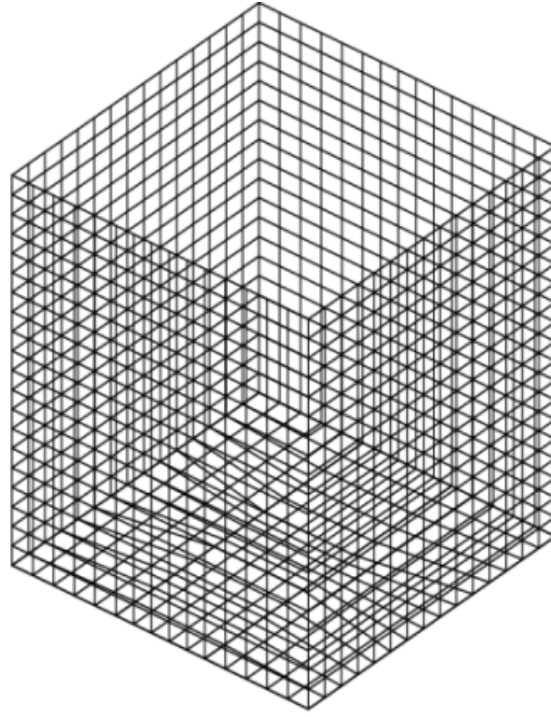
(ii) Rectangular tank

Fig. 4.16 Finite element model

4.2.3 Results and discussion

Sinusoidal excitation of the plates

A sinusoidal input of excitation close to resonance frequency is given to the plate-1 and the response of the plate-2 is observed for all cases considered in Table-4.4. The natural frequency of the plates for various geometries used are determined using experiment and analysis. To understand the transmission of vibration in immersed plates from one plate to the other plate during resonance, the excited plate is vibrated at natural frequency of the response plate. Thus the excited frequency are the resonance frequency of the response plate for various immersion depths.

CASE:1

For different immersion depth ratio (d/l), the plate-1 is excited at its resonance frequency with a force amplitude of 10 N. Fig. 4.17 (a) and Fig. 4.18 (b) show the time history for force, excitation and response of the cantilever plates from experiment and CAST3M respectively for (d/l) = 0.3 excited at frequency of 1.71 Hz. Fig. 4.17 (b) shows the FFT and coherence spectrum of the plates. When the plate-1 is excited by the shaker, the plate-2 gets displaced due to the fluid force with some amplitude. With continuous excitation, superimposition from the backward reflected waves with the plate occurs resulting in coupled amplitude of vibration of the fluid and the plate. Simulation of the experiment was carried out in CAST3M showing similar movement of the plates. Since FSI simulations assume 1-3 % damping, conservative damping of 2 % is considered in the simulation. Since the excitation plate is excited at the resonance frequency of the response plate, the amplitude of vibration of response plate is found to be higher than the excited plate and so the transmission ratio exceeds unity. This can be referred as resonance oscillation. Similar type of phenomenon was observed for other immersion depth ratios. In this case, it is to be noted that the resonance frequencies of both plates are the same.
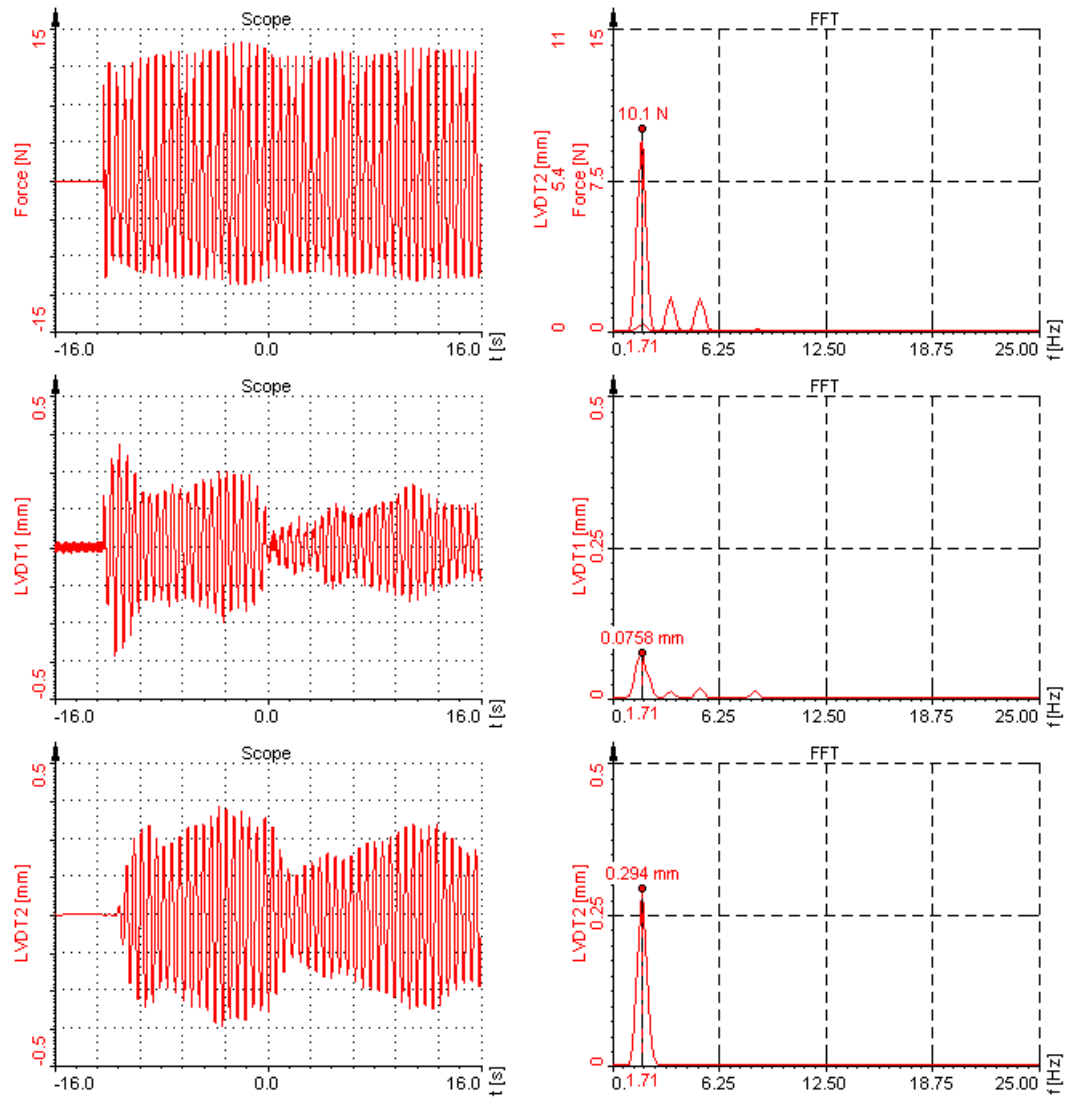
Fig. 4.17 (a) Force, excitation and response of the plates for (d/l) = 0.3 from experiment
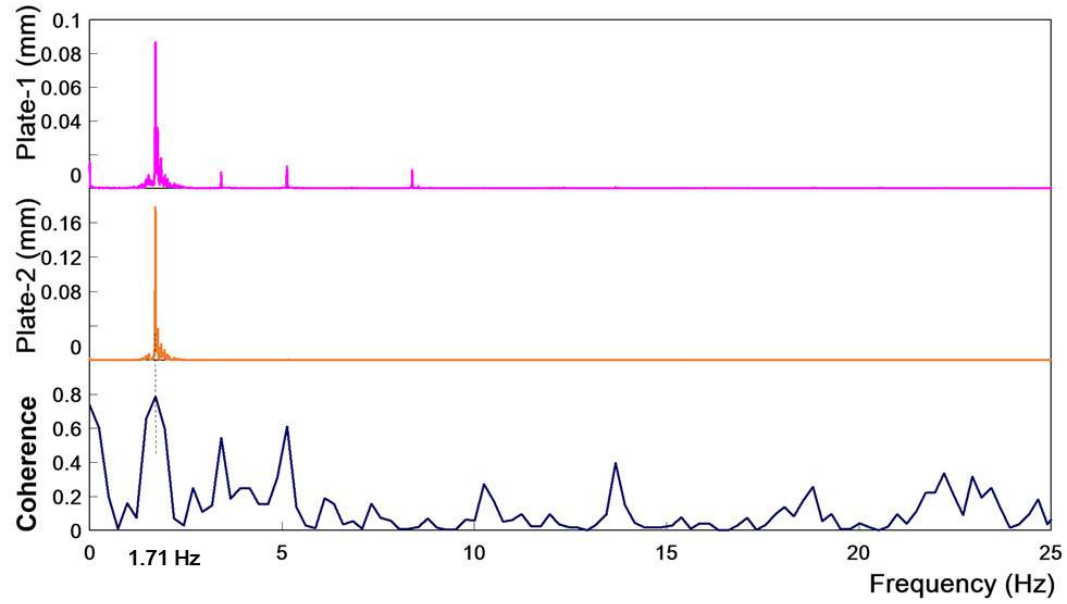
Fig. 4.17 (b) FFT and coherence spectrum of plates for (d/l) = 0.3 from experiment
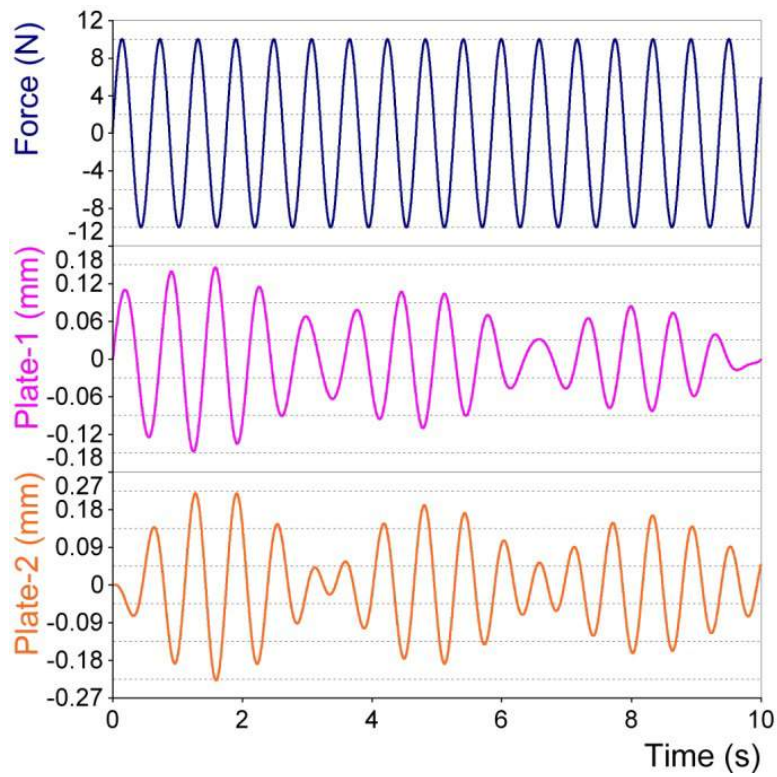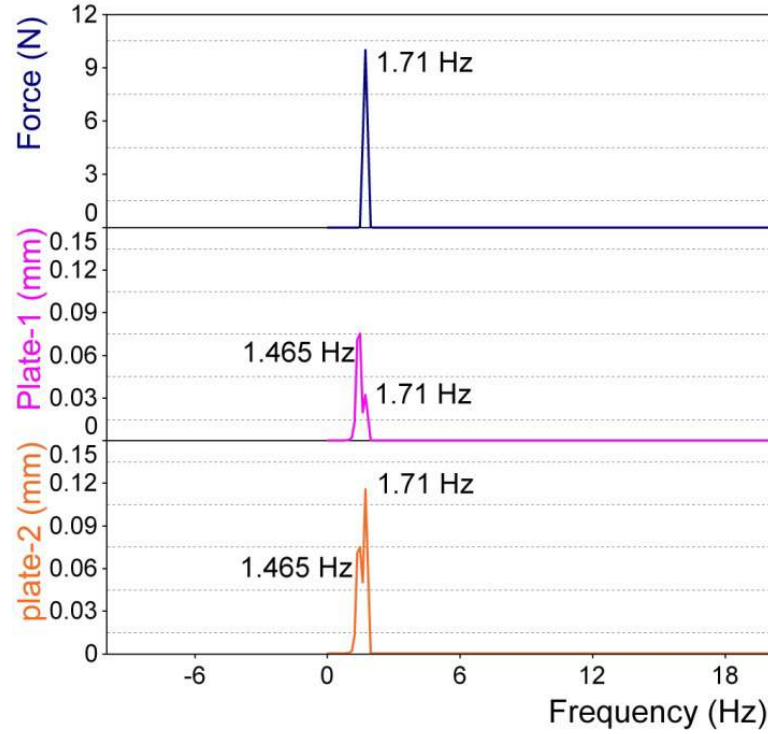
Fig. 4.18 Force, excitation and response of the plates for (d/l) = 0.3 from CAST3M

CASE:2

Now, the width of plate-2 is reduced to half and response of the plate is observed. Fig. 4.19 (a) and Fig. 4.20 show the time history of force, excitation and response of the cantilever plates from experiment and CAST3M respectively for (d/l) = 0.3. Fig. 4.19 (b) shows the FFT and coherence spectrum of the plates. In this case, the coupled vibration for the response plate is found to be much higher than the excited plate. In addition, it is to be noted that the resonance frequency of both the plates are not the same when immersed in the fluid. Maximum transmission of energy to the plate-2 is observed, since the plate-2 is close to resonance frequency of plate-1. Similar observation from simulation results shows higher displacement of the response plates.
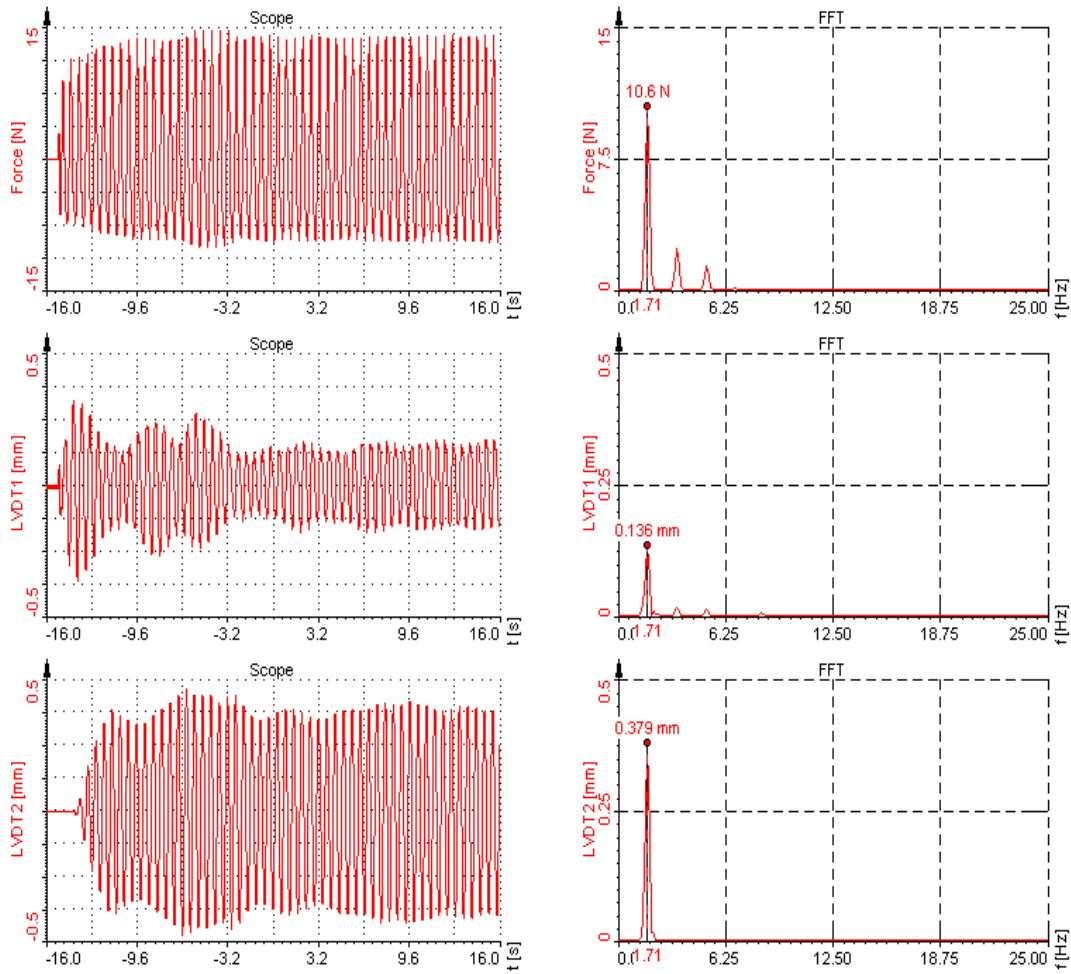
Fig. 4.19 (a) Force, excitation and response of the plates for the (d/l) = 0.3 from experiment
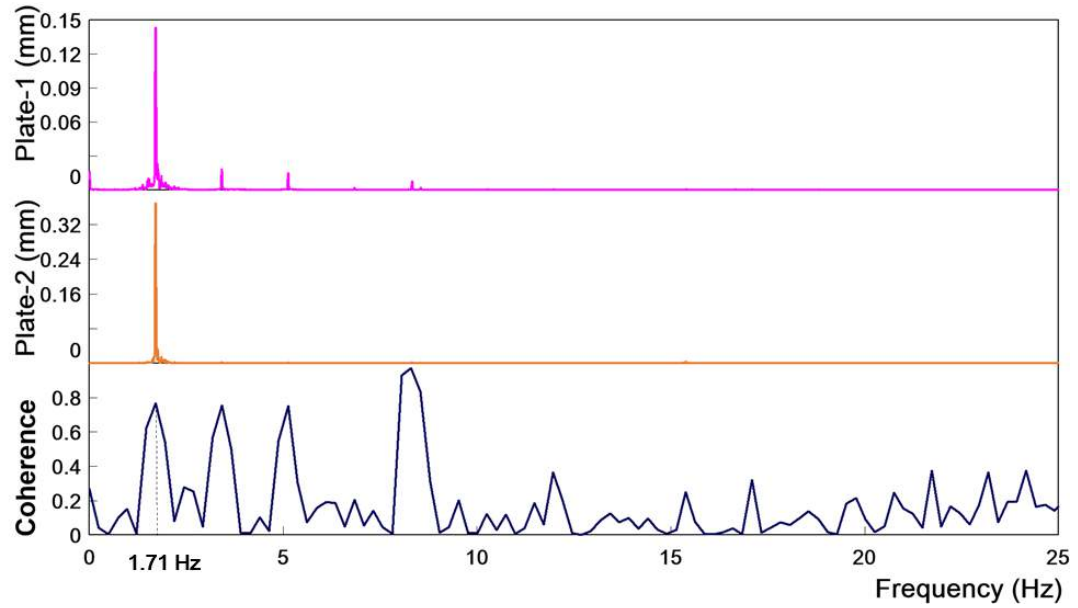
Fig. 4.19 (b) FFT and coherence spectrum of plates for (d/l) = 0.3 from experiment
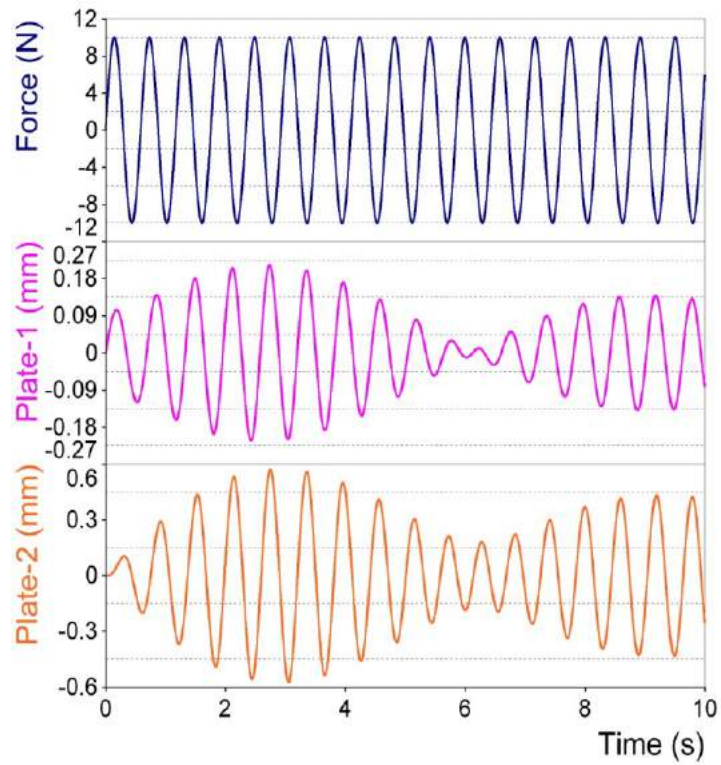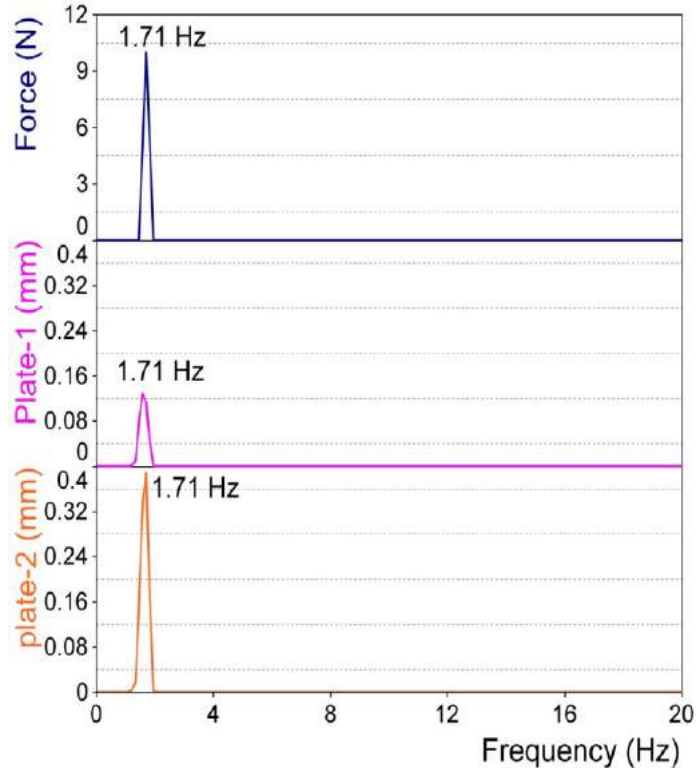
Fig. 4.20 Force, excitation and response of the plates for (d/l) =0.3 from CAST3M

CASE:3

Finally, the width of plate-2 is reduced to one-fourth of original width to investigate the response of the plate. Fig. 4.21(a) and Fig. 4.22 show the time history of force, excitation and response of the cantilever plates from experiment and CAST3M respectively for (d/l) = 0.3. Fig. 4.21 (b) shows the FFT and coherence spectrum of the plates. This case shows a less amplitude of vibration of the response plate in comparison with the excited plate. Since the resonant frequency of the plate-2 is far away from the exciting frequency, the transmission of energy is found to be less from both experiment and simulation.
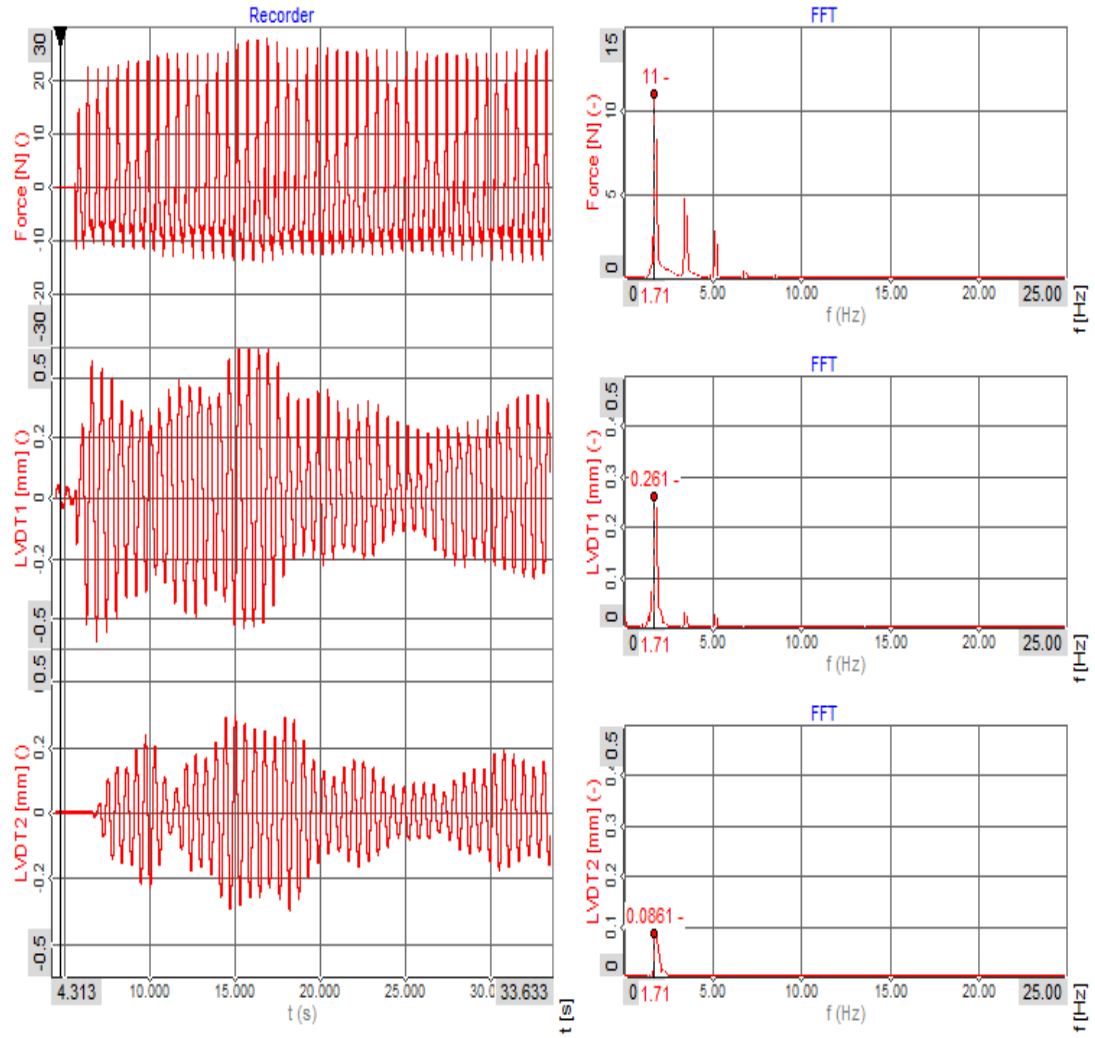
Fig. 4.21 (a) Force, excitation and response of the plates for (d/l) = 0.3 from
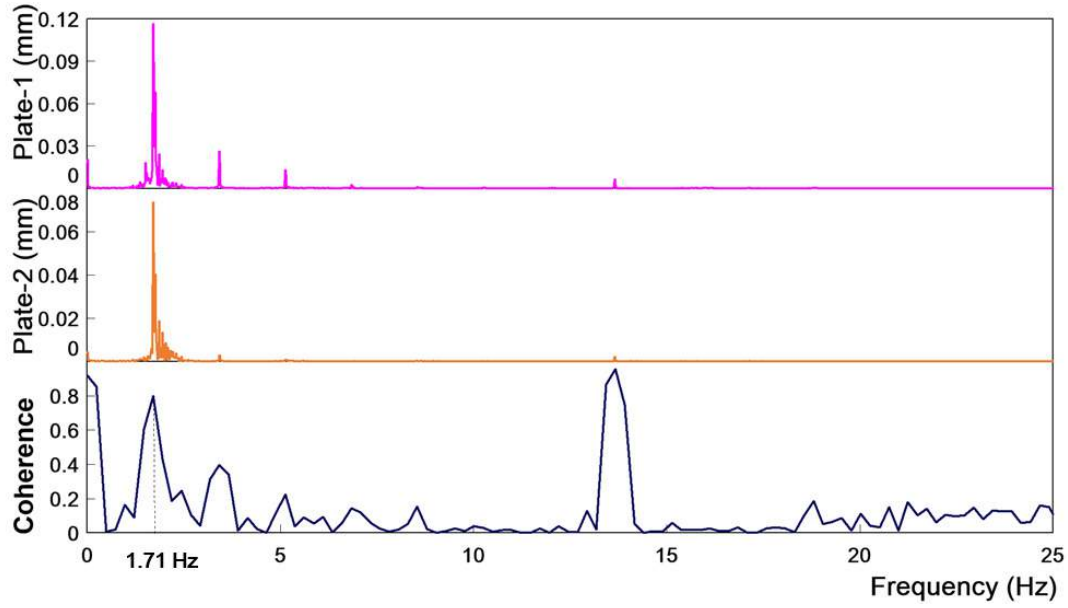
experiment

Fig. 4.21 (b) FFT and coherence spectrum of plates for (d/l) = 0.3 from experiment
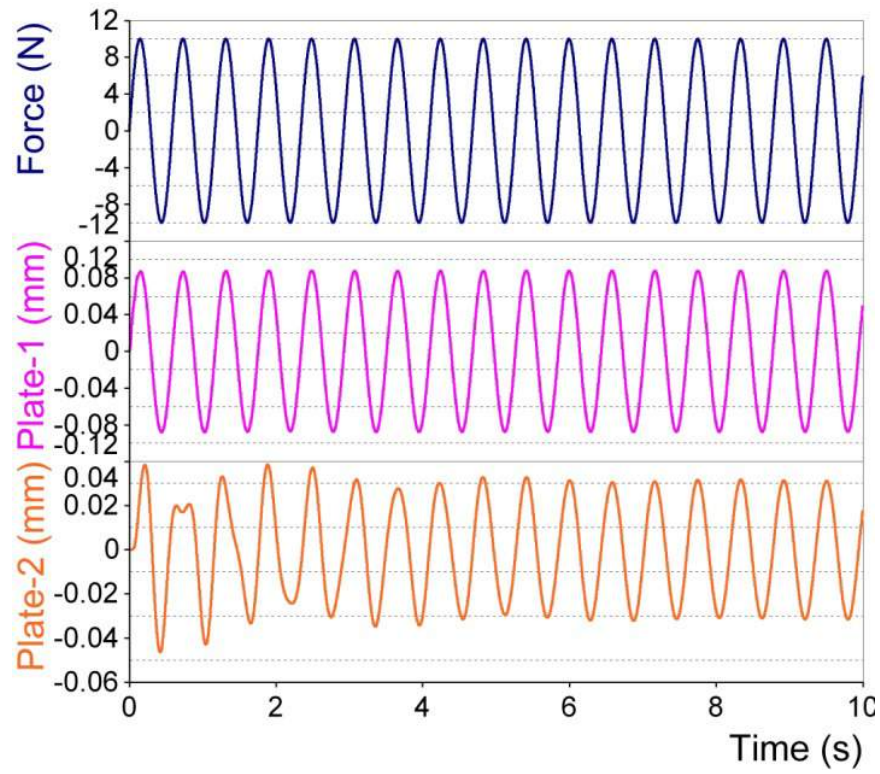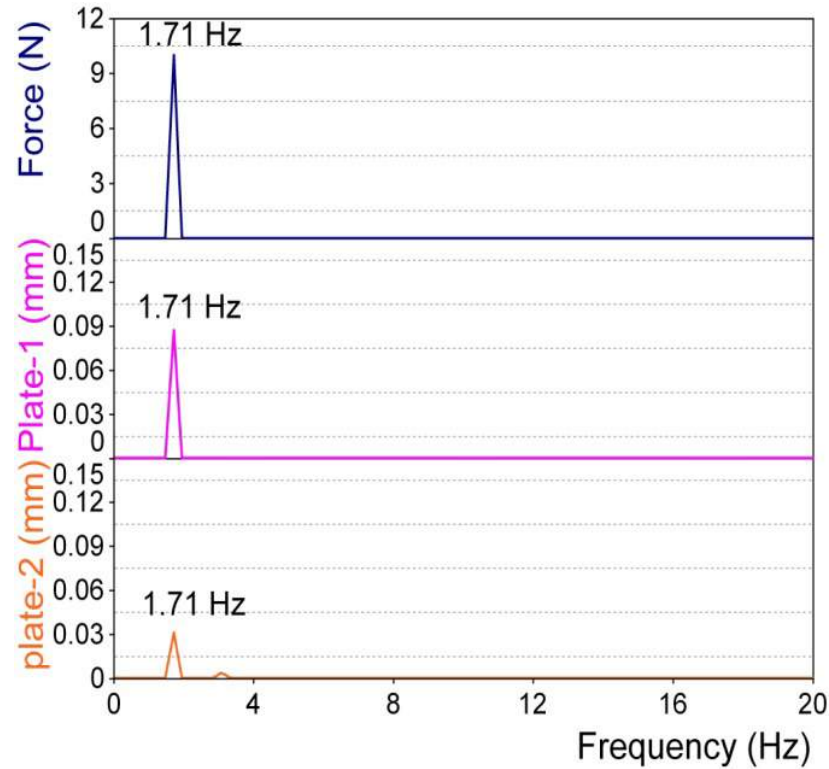
Fig. 4.22 Force, excitation and response of the plates for (d/l) =0.3 from CAST3M

Discrete excitation of the plates

In this study, instead of giving continuous excitation, a discrete excitation was given in simulation to the plate-1 and the response of the plate-2 is investigated to understand the phenomenon. Simulation was carried out for all the three cases for different (d/l) ratios. Fig.4.23, Fig. 4.24 and Fig. 4.25 show the results of discrete input of excitation for the plate-1 for all the cases with (d/l) = 0.3. It can be seen that the plate first vibrates at the excitation frequency and then vibrates at its damped frequency. Damping of 2% is assumed in the simulation. This simulation shows that the variation of amplitude of vibration of the plates is due to the superimposition of the back wall reflected waves over the plates resulting in coupled vibration (fluid and plate).
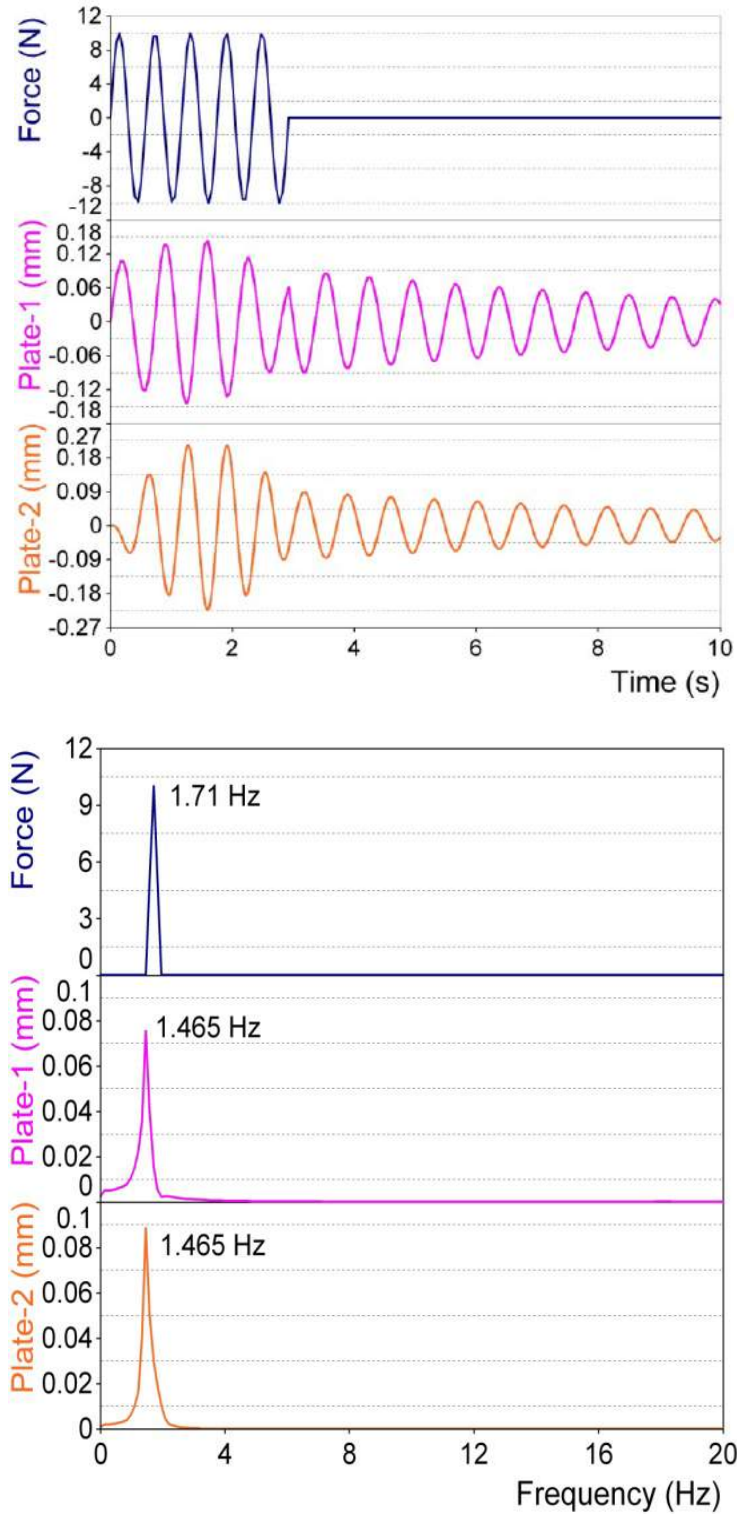
Fig. 4.23 Force, excitation and response of the plates for the case-1
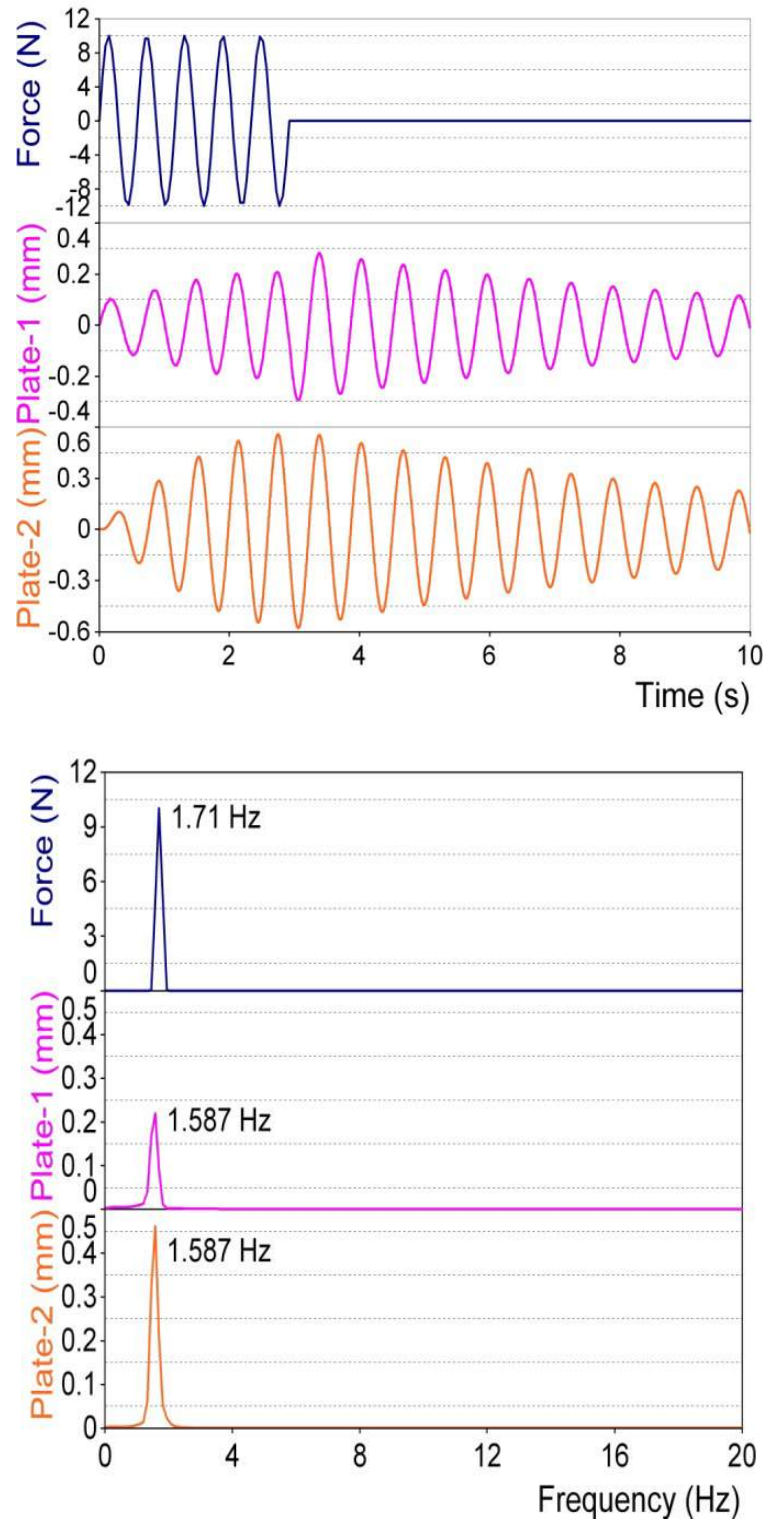
Fig. 4.24 Force, excitation and response of the plates for the case-2
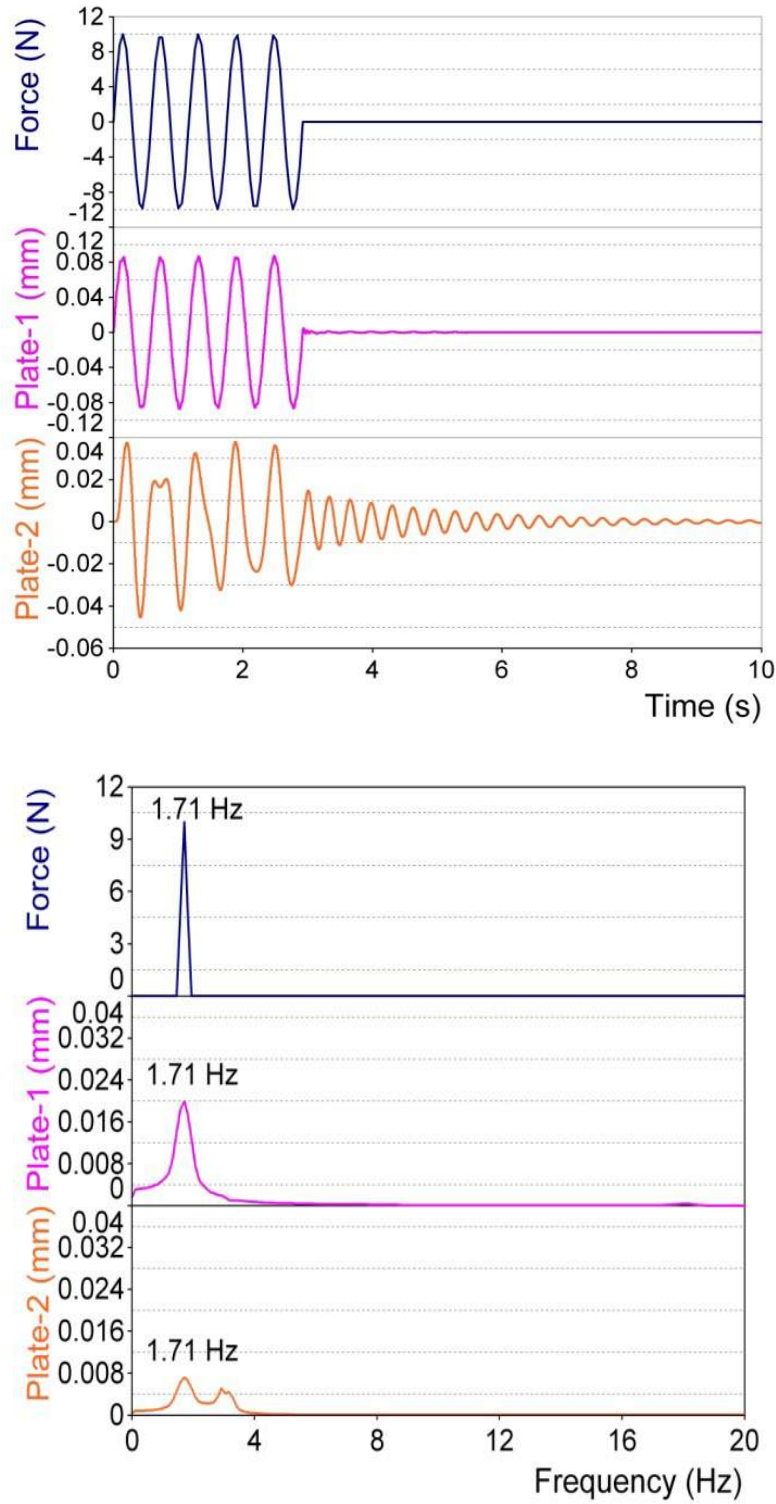
Fig. 4.25 Force, excitation and response of the plates for the case-3

Important conclusions from the present studies are:

1. Predicted results using CAST3M code and the results obtained through experiments are closely matching.

2. Natural frequency decreases with increase in the depth of immersion of the plates. With change in the width of the plate for same thickness, the natural frequency remains the same in air and it increases with decrease in the width of the plate.

3. Amplitude of vibration of response plate will be higher when the plates are excited close to its resonance frequency and it is much lower when gets excited far away from its resonance frequency.

4. Irregularity in the amplitude of vibration of the excited and response plates is due to the oscillations in the contained fluid in case of continuous excitation. For discrete excitation, such irregularity is not observed.

5. A typical practical event is where the Intermediate heat exchanger immersed in the liquid sodium in a pool type fast reactor will get excited due to a sudden transient event like sodium water reaction with high pressure waves. When the frequency of excitation matches with the fundamental frequency, the energy transmission may play an important role.

4.3 VIBRATION BETWEEN PLATE AND TUBE STRUCTURES

4.3.1 Experimental Setup

Vibrations between tube and plate structures close to resonance frequency (tubes) have been studied experimentally. A rectangular tank (500 x 500 x 750 mm) with opposite two walls made using thin plates compared to the other two walls was fabricated

as a part of experimental setup. The thin walls are considered as plate-1 (excited plate) and plate-2 (response plate).

Three tubes are made and located centrally inside the tank. The schematic of a single tube arrangement with the tank is shown in Fig. 4.26. The tubes are fixed at one end. The tubes are arranged in linear fashion with uniform distance. Miniature accelerometers (axial) are attached to the tubes to measure the displacement. LVDT has been used to measure the displacement of the plates. Under water accelerometers are also used. Electro dynamic shaker is used to excite the plate in the tank through stringer rod and the response of the tubes immersed in fluid is observed. Technical specifications of miniature and underwater accelerometers used are listed in Table 4.8. The actual experimental setup is shown in Fig. 4.27.

Table 4.8 Technical specifications of Accelerometers

Miniature Accelerometers	
Make	PCB Piezotronics
Model	357 B22
Range	± 1500 g pk
Sensitivity	3.1 pC/m/s^2 or 30 pC/g
Frequency range	8.5 kHz
Resonant frequency	≥ 23 kHz
Purpose	Acceleration measurement

Under water Accelerometers	
Make	DJB Instruments
Model	A/28/E Micro-miniature Piezoelectric
Charge Sensitivity	0.04 pC/(m/s^2)
Resonant frequency	45 kHz
Typical Frequency Response ±5%	1Hz- 10kHz
Size & weight	5.7xØ3.5x2.3 mm & 0.19 gram
Purpose	Acceleration measurement
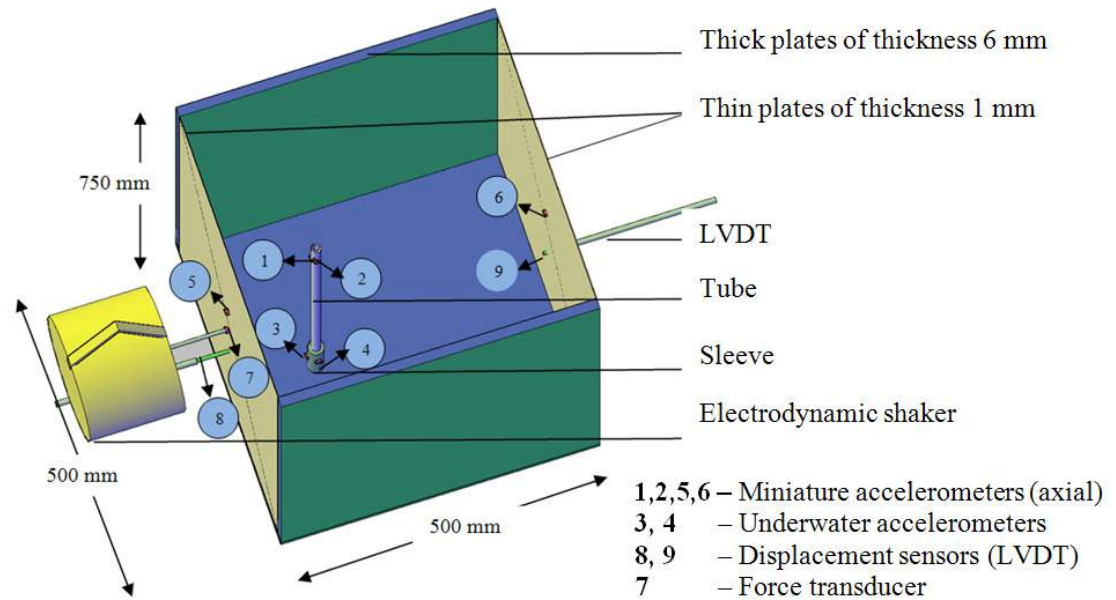
Fig. 4.26 Schematic of the experimental setup
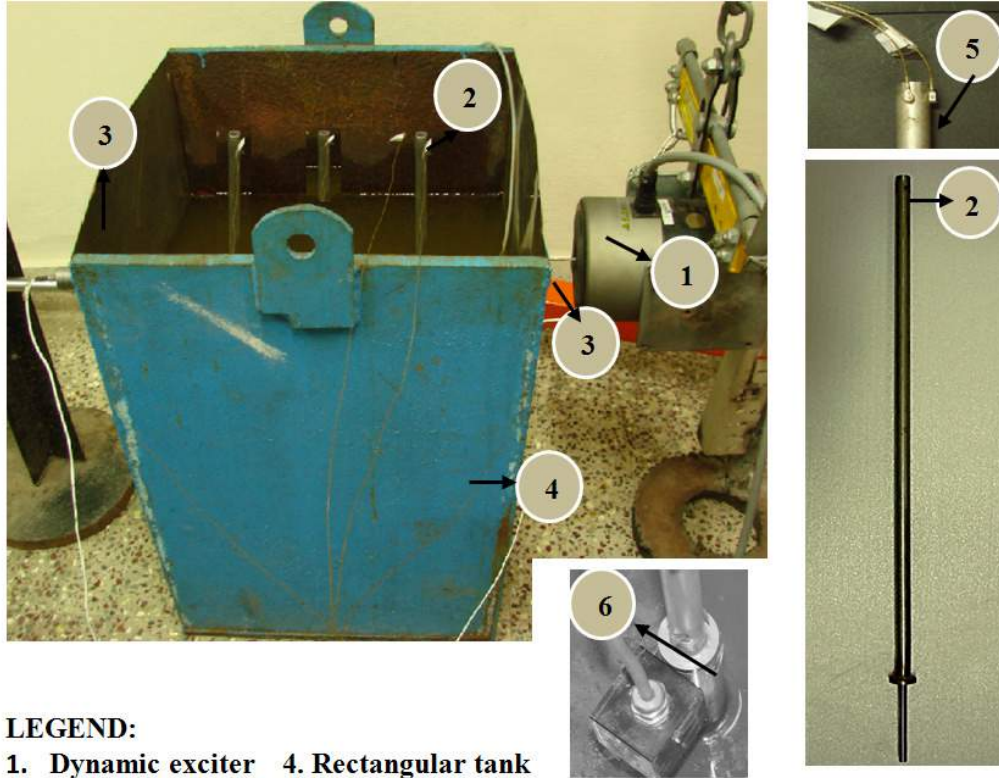
LEGEND:
1. Dynamic exciter   4. Rectangular tank
2. Cantilever tube   5. Sensor position
3. LVDT on plates   6. Sleeve with sensor

Fig. 4.27 Experimental setup

Sine sweep from 10 – 80 Hz was experimentally carried out to find the natural frequency of the tubes. Three immersion depths ratios (d/h) = 0.27, (d/h) = 0.53, (d/h) = 0.80 are considered for the study. From sine sweep, the natural frequencies of the tubes in both X and Y directions were found out. Fig. 4.28 to Fig. 4.31 show the experimental results from sine sweep. Fig. 4.27 (b) shows phase and coherence spectrum (d/h) = 0.27. It can be observed that additional frequencies are involved in the immersed conditions in comparison with air. The natural frequency with air is largest and with increase in fluid level the frequency is decreased. Same frequency in both X and Y direction is observed in Tube-2 and Tube-3, which shows that the tube is circular. The values were also compared with CAST3M results. The frequencies are tabulated in Table 4.9.
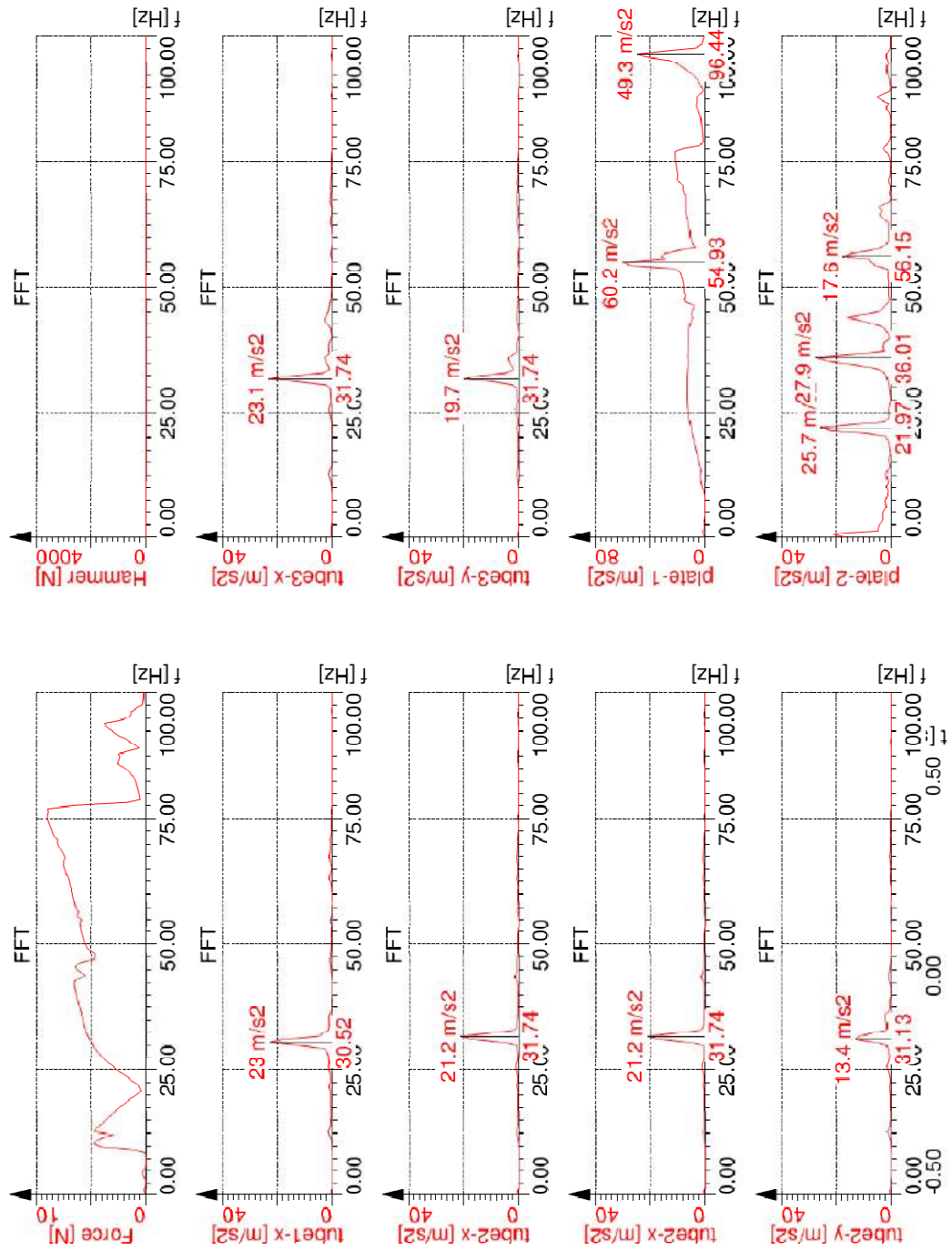
Fig. 4.28 Sine sweep in Air
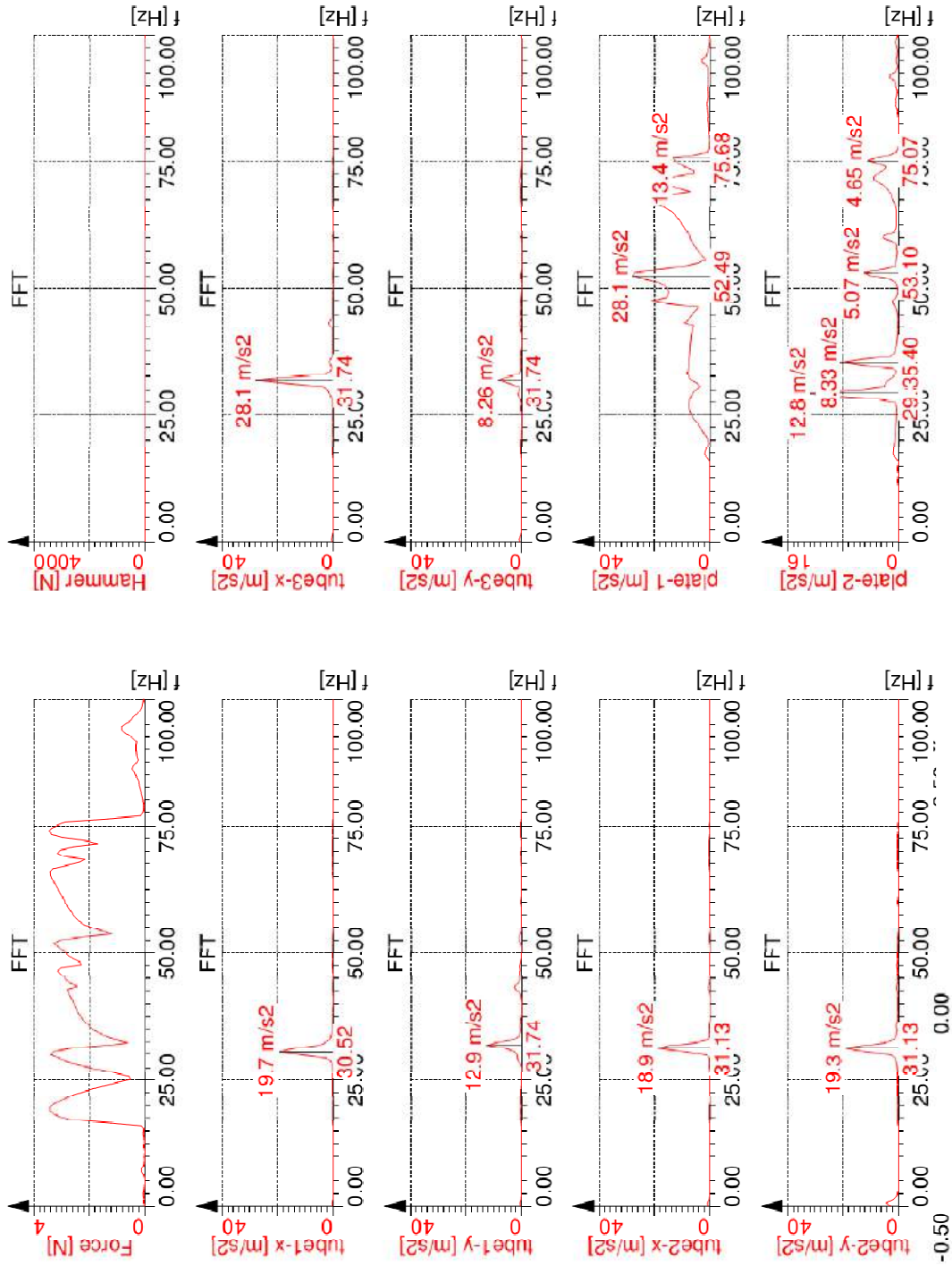
Fig. 4.29 (a) Sine sweep for (d/h) = 0.27

116
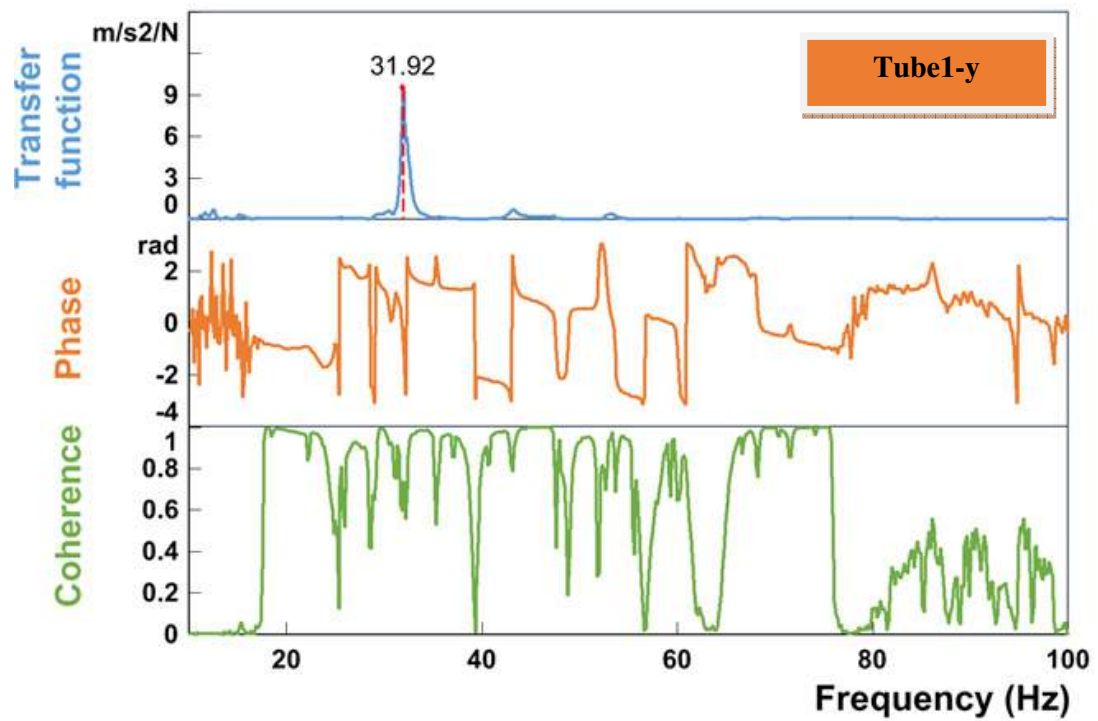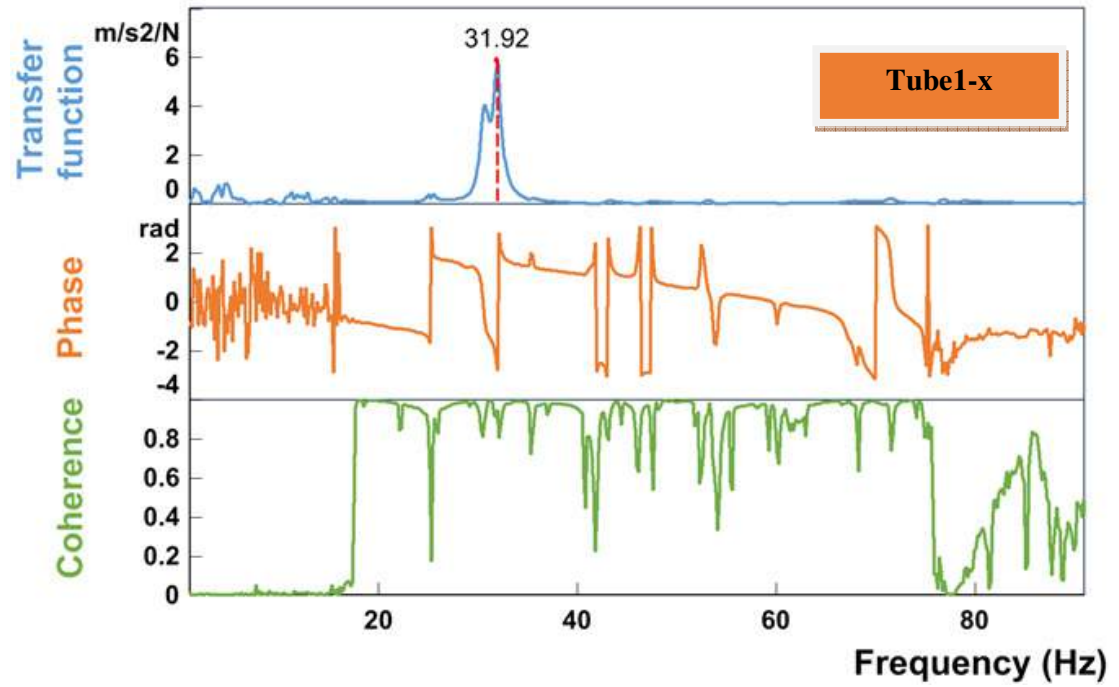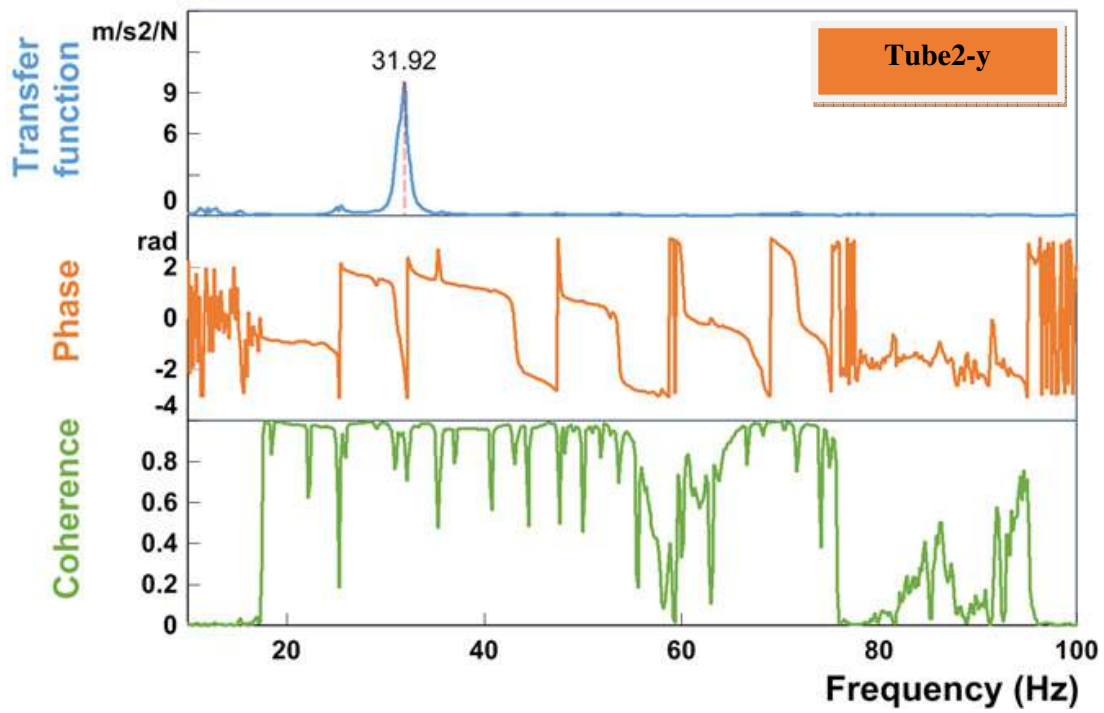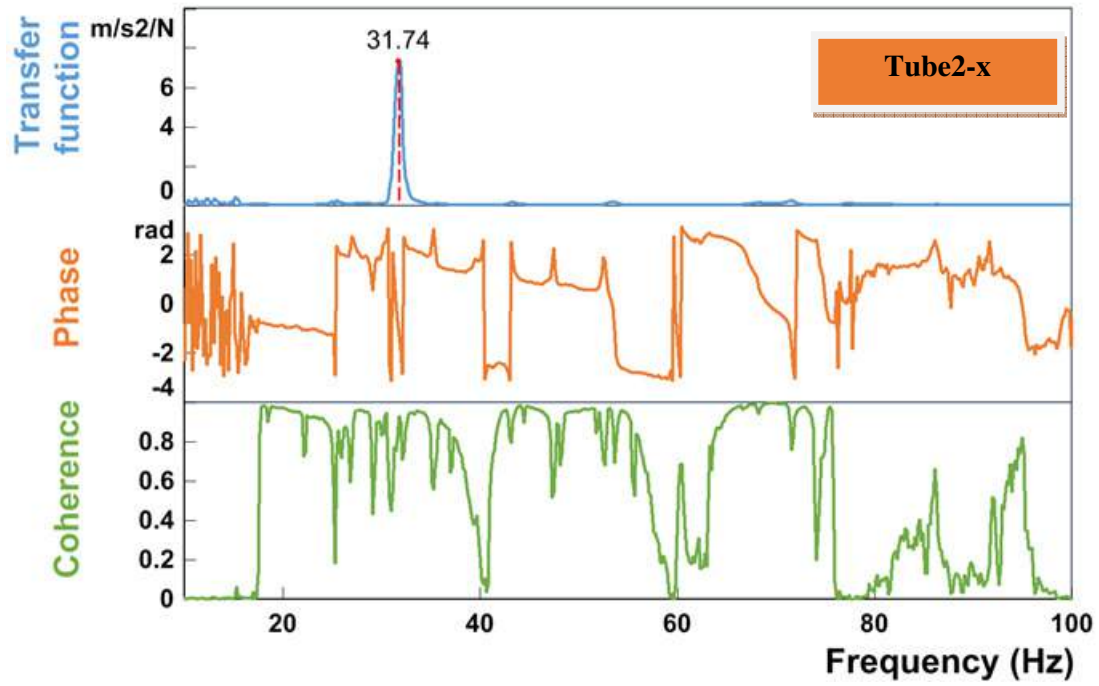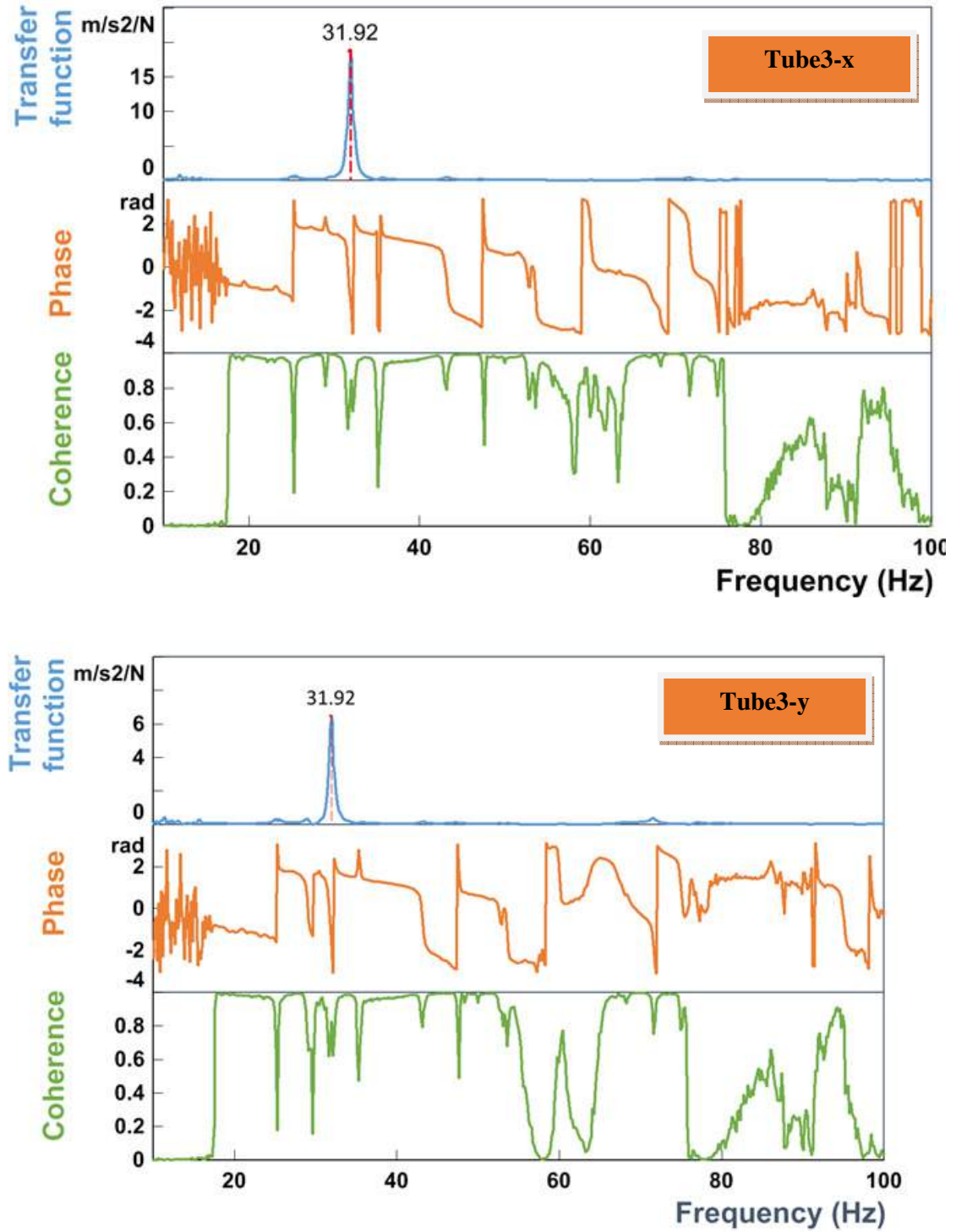
Fig. 4.29 (b) Phase and coherence spectrum for (d/h) = 0.27
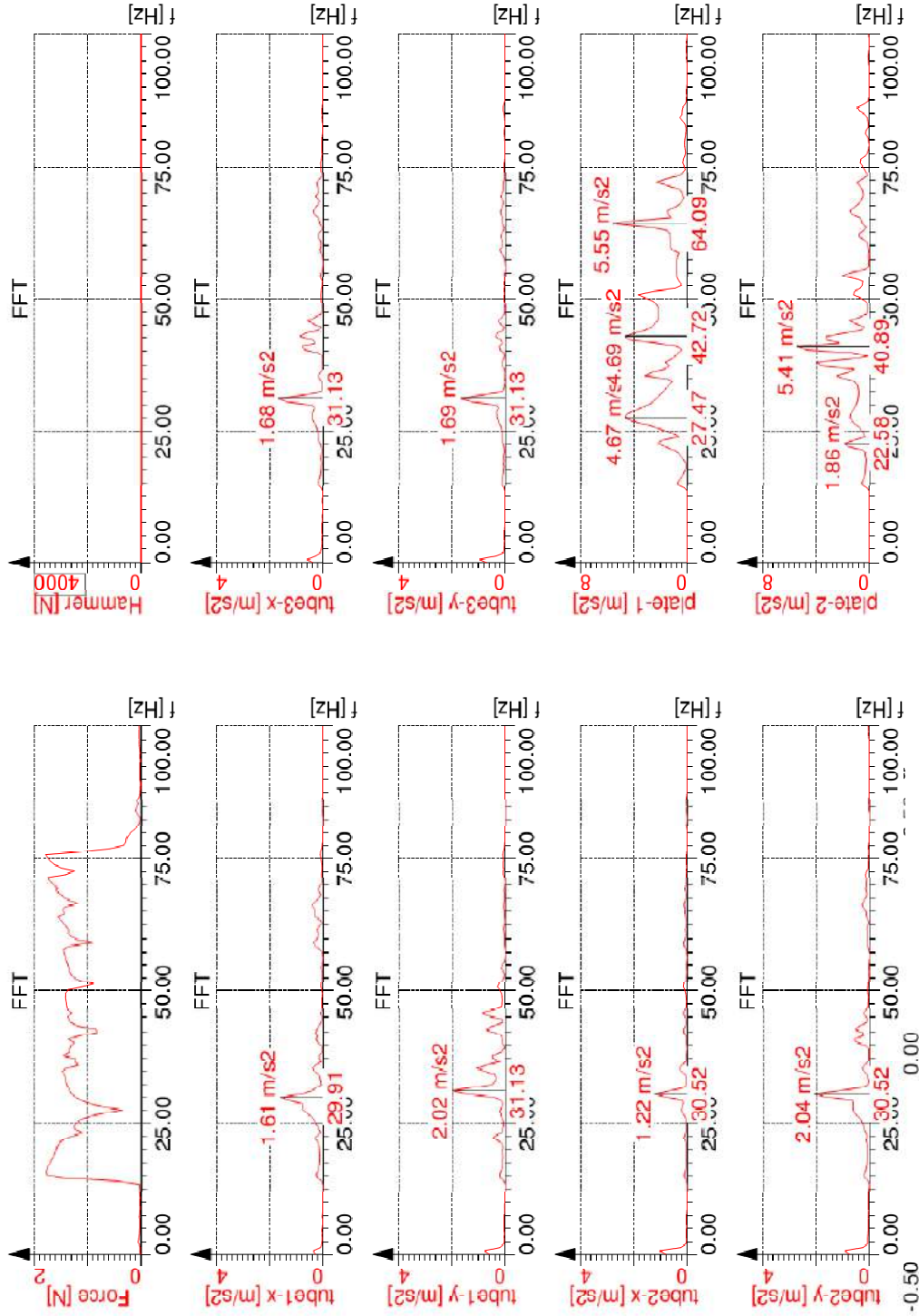
Fig. 4.30 Sine sweep for (d/h) = 0.53
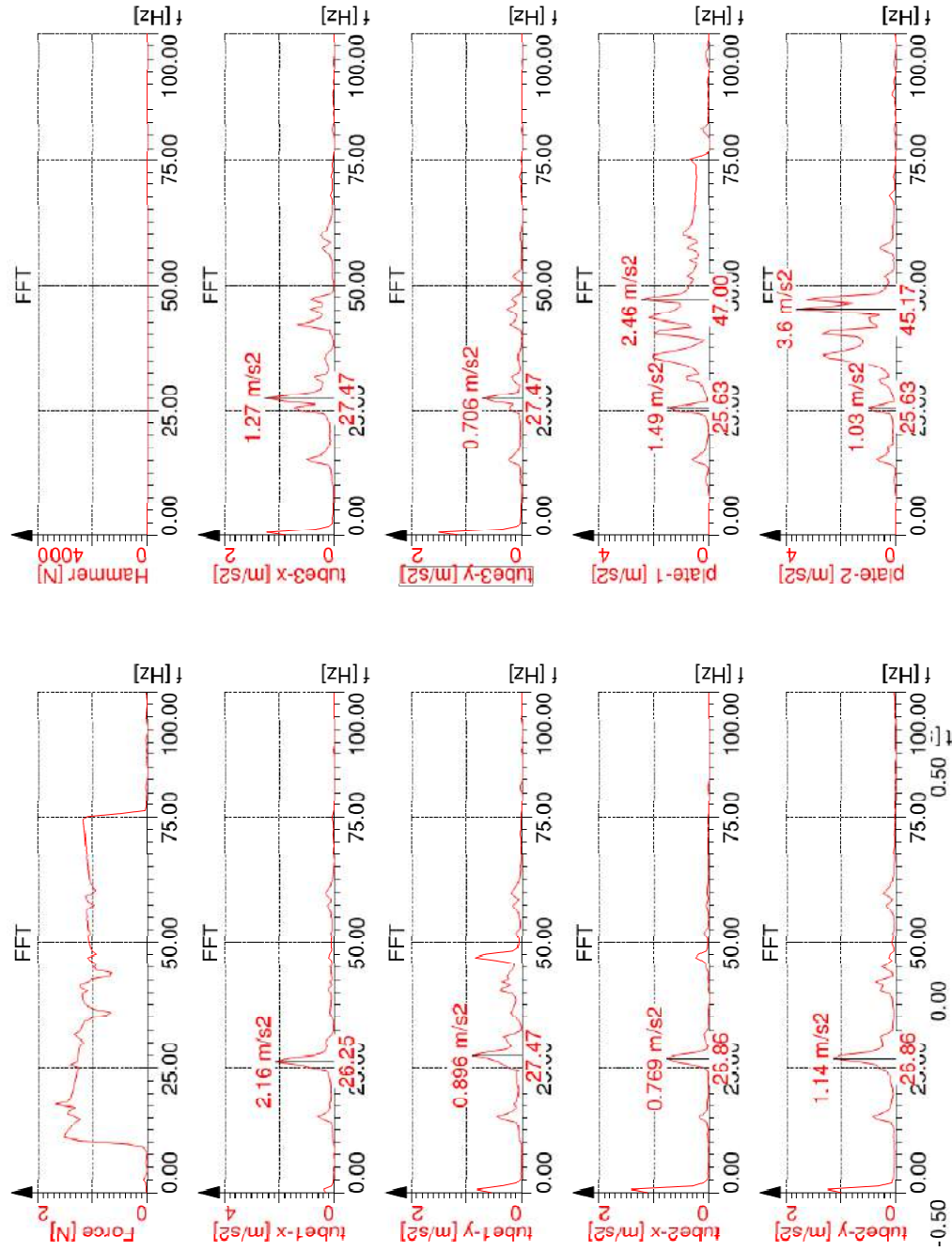
Fig. 4.31 Sine sweep for (d/h) = 0.87

Table 4.9 Natural frequency of tubes in Hz

Immersion depth (d/h)	Tube-1		Tube-2		Tube-3		CAST3M
	x	y	x	y	x	y	
Air	30.54	31.74	31.74	31.13	31.74	31.74	33.76
0.27	30.52	31.74	31.13	31.13	31.74	31.74	33.56
0.53	29.91	31.13	30.52	30.52	31.13	31.13	29.74
0.80	26.25	27.47	26.86	26.86	27.47	27.47	27.05

4.3.2 Results and discussion

To study vibration transmission from plate to tube structures, one of the thin walls of the tank (plate-1) is excited in the frequency range of 26-32 Hz, which is the resonance frequency of the tubes at different immersion depth ratios. Transmission ratio tu-1/pl-1 refers the ratio between excited plate and tube-1, tu-2/tu-1 refers the ratio between tube-2 and tube-1, tu-3/tu-2 refers the ratio between tube-3 to tube-2. The transmissibility ratio between the plates/tube and tube/tube for different immersion depth ratios is shown in Fig. 4.32.

(i)

(ii)

(iii)

(iv)
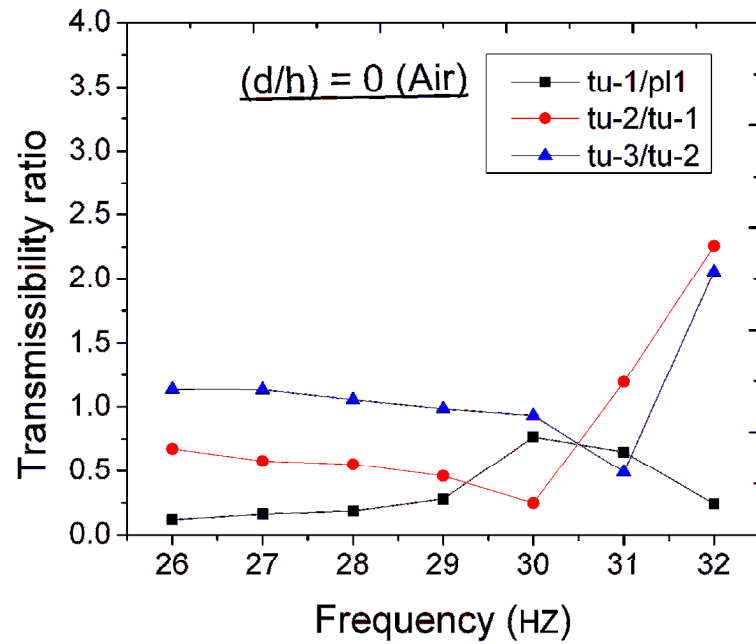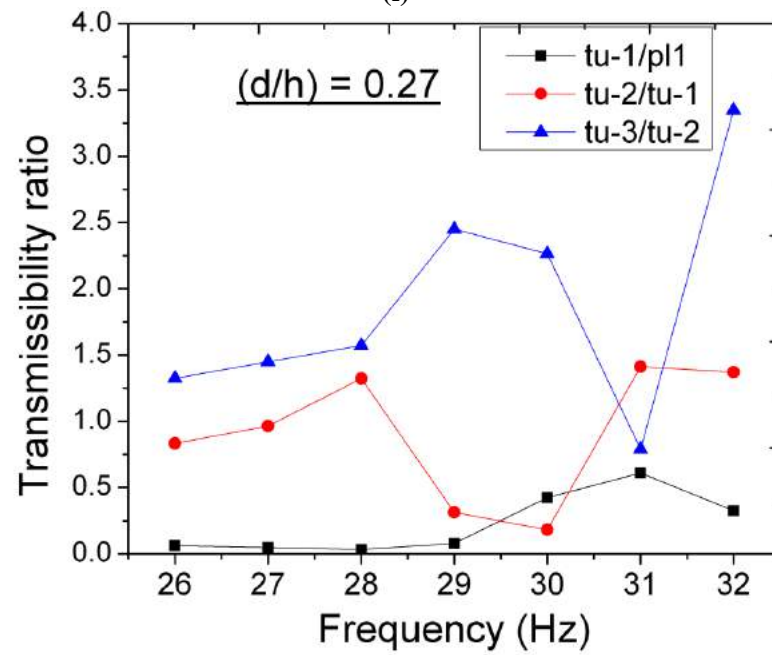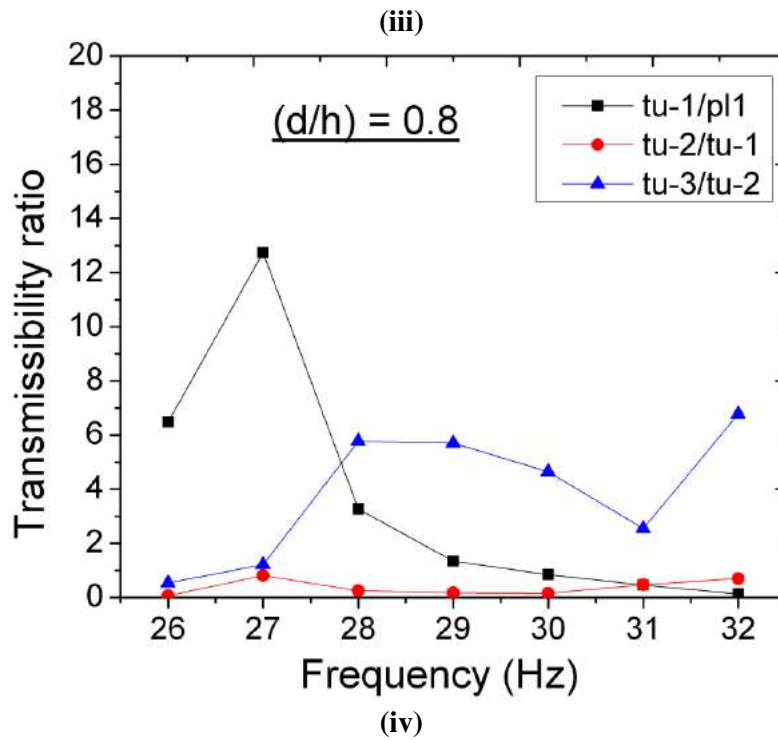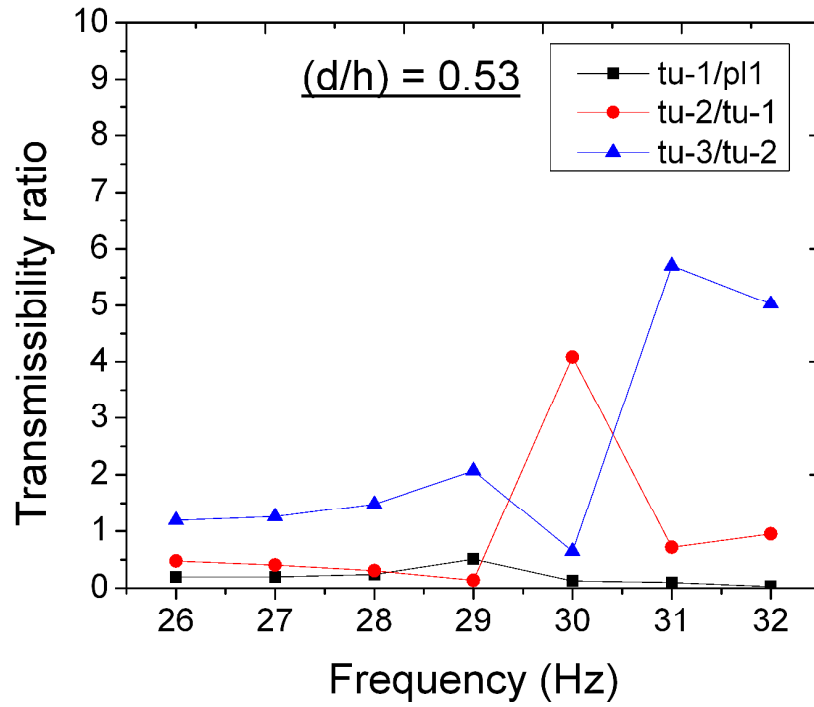
Fig. 4.32 Transmissibility ratio (i) (d/h) =0 (air); (ii) (d/h)=0.27; (iii) (d/h)=0.53; (iv) (d/h)=0.80

It was observed that the transmission ratios between the tubes are found to be higher than between the plate and the tube. Maximum ratio is found in the resonance region of tubes for all immersion depths.

4.4   CLOSURE

Vibration transmission between side walls of a rectangular tank is studied. It is found that transmission ratio increases and then decreases after a particular depth, and this is due to the participation of higher modes at increased depth of immersion. Natural frequency of cantilever plate structures for different aspect ratio and immersion depth was found experimentally and numerically. It is observed that in air the resonance frequency of the plates is not affected by change in width of the plates. The same is not applicable in the fluid medium. When the plate is excited close to its resonance frequency, the amplitude of vibration of the response plate is found to be higher and it is much lower when excited far away from its resonance frequency in immersed conditions. It is found that the movement of plates when excited close to resonance frequency follows sudden increase and decrease in amplitude of motion of the plates in a finite fluid. This is mainly due to the superimposition of vibration due to fluid wave and structural vibration. Fluid damping increases with increase in the depth of immersion as expected. Further in the study of tubular structures, the natural frequencies of the tubes were found experimentally and, the vibration transmission between and plate and tube were studied. Transmissibility ratios close to resonance frequency showed higher values between the tubes than between tube and plate.

* * *

CHAPTER 5

Investigation of Vibration in Core for Design Basis Sodium - Water Reaction 5

5.0 INTRODUCTION

Sodium-water reaction in LMFBR has been studied extensively by various countries having/had active fast breeder reactor programme. Both numerical as well as experimental studies have been carried out. Computer codes have been developed to predict the pressure wave propagation in the secondary sodium circuit due to a large sodium water reaction in the Steam Generator. These codes have been validated using experimental results. Investigation of subassemblies displacement and consequent changes in the reactivity in a fast breeder reactor in case of design basis leak sodium water reaction is discussed in detail in this chapter

5.1 LARGE LEAK SODIUM-WATER REACTION EVENT

In LMFBR Steam Generator (Fig. 5.1) heat is transferred from sodium to water to produce steam. The hot sodium flows in the shell side from top to bottom. Water enters the tubes at the bottom, gets evaporated and superheated and leaves at the top as superheated steam. The pressure on the sodium side is low (usually around 4 to 5 bars), while the pressure on the water/steam side is high (usually around 170 bars) to feed steam to the turbine. The sodium and water are separated by the single wall of the heat transfer tubes. Therefore, if there is a hole or breach in the heat-transfer tube, leakage of water into sodium will occur, resulting in sodium-water reaction.
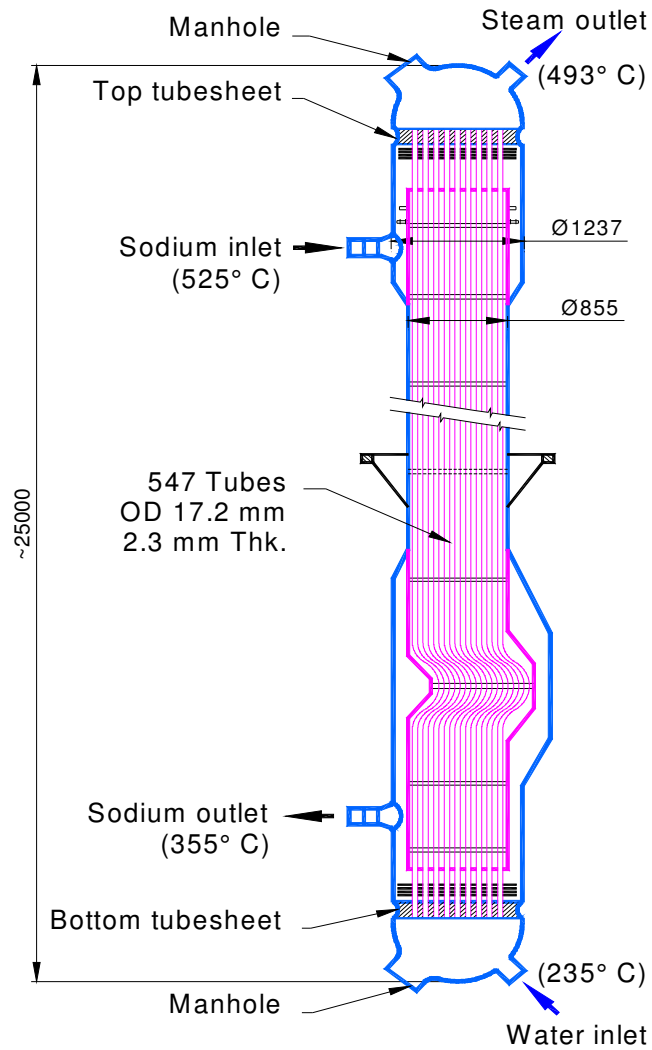
Fig. 5.1 Steam Generator

The reaction between sodium and water is rapid and violent. The leakage of water from the heat transfer tubes will cause various phenomena, depending on the amount of water coming out, and will have different effects on the Steam Generator. Since the sodium-water reaction is highly exothermic and caustic producing, the leaks can expand rapidly. The major cause for sodium-water reaction has been singled out as flow induced vibration in tubes and poor quality of welds (Rajput, 1983). The sodium-water reaction produces heat and other reaction products NaOH, Na_2O and NaH. These products cause

corrosion and erosion of nearby tubes leading to further escalation of water/steam leak rates. The dominant threat and the approximate diameter of the hole due to the leak has been presented in Table 1.1.

In the plant, sodium-water reaction is immediately identified in the small leak range itself through in sodium and in argon hydrogen detectors and safety actions are automatically initiated to stop further sodium-water reaction. These include isolation of water/steam side of the steam generator and rapidly expelling water from the tubes by opening water dump and nitrogen purging gas valves. A surge tank is provided on the up-stream of the Steam Generator to mitigate the initial pressure spike.

5.2 PRESSURE TRANSIENTS

Using the SWEPT(Sodium Water Event and Pressure Transients) code, the peak pressures in the secondary sodium circuit components including the leaking and adjacent Steam Generators are estimated and the components are designed to withstand these pressures (Chellapandi et al., 2003)(Chetal et al., 2011). The SWEPT code has been developed for this purpose. SWEPT is a generalized code which can be applied to any sodium circuit.

5.2.1 Modeling details of SWEPT

For designing the secondary sodium circuit (Fig. 5.2) components viz. Pump, Intermediate Heat Exchanger, Surge tank, Steam Generator, isolation valves and pipelines, the maximum pressure seen by them due to large leak sodium-water reaction needs to be determined. The SWEPT code consists of four main modules in which the various aspects of steam generator tube leaks, sodium-water reaction and pressure wave propagation effect are computed.
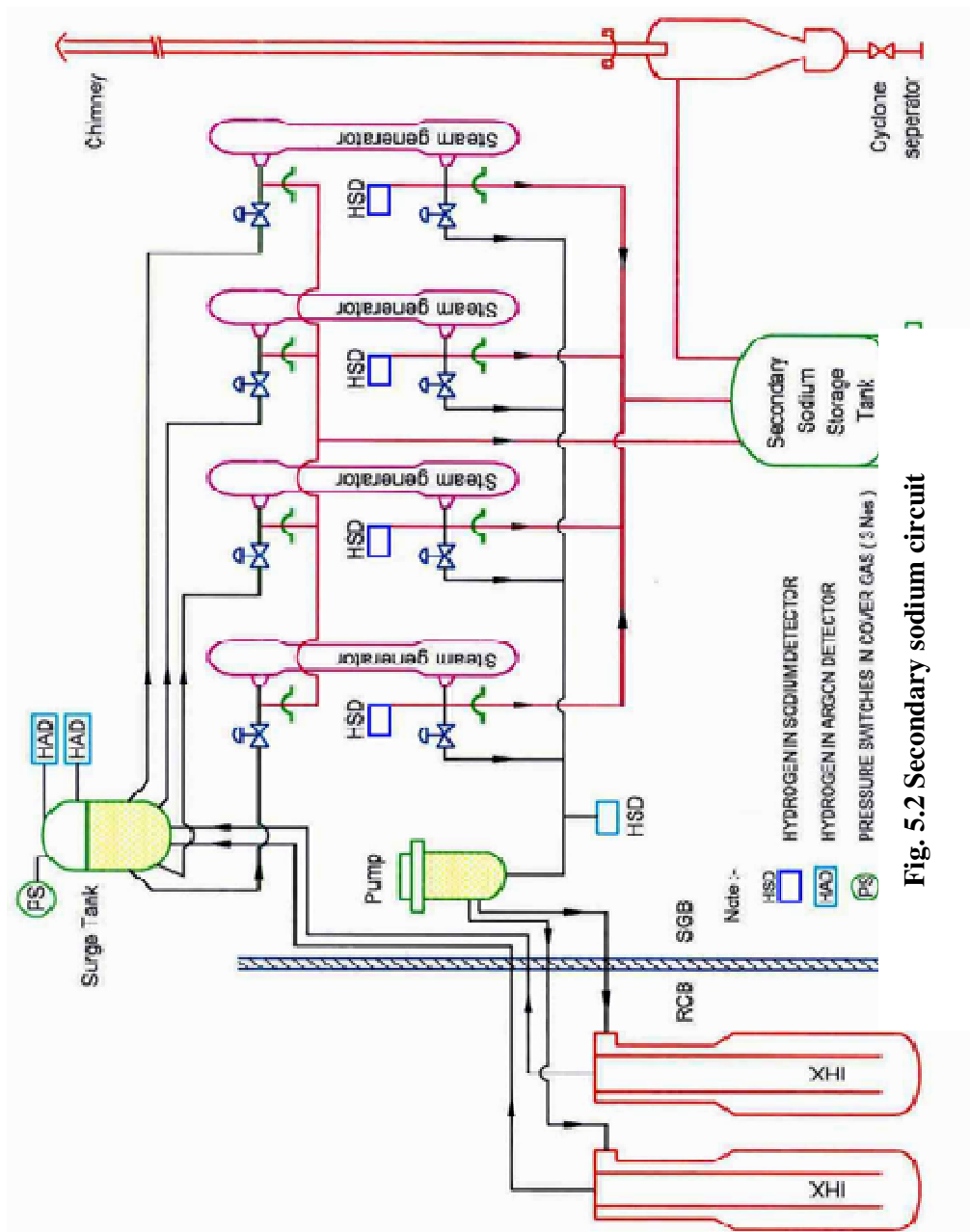
Fig. 5.2 Secondary sodium circuit

Reaction bubble dynamics: The derivations of the governing equations are based on the following features. The reaction between sodium and water is represented by the following general reaction equation:

$aNa + b\ H_2O \rightarrow c\ NaOH + d\ Na_2O + e\ NaH + f\ H_2$
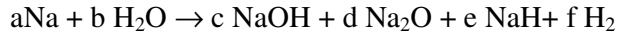
where 'f' is the moles of hydrogen produced to the moles of water reacted. This ratio and also the temperature at which hydrogen is generated are based on data used by different countries derived from their experimental programs (IAEA, 1983). The maximum value is 0.7 for f and 1660 K for hydrogen temperature has been used in the calculations and accepted internationally (Hori, M., 1980).
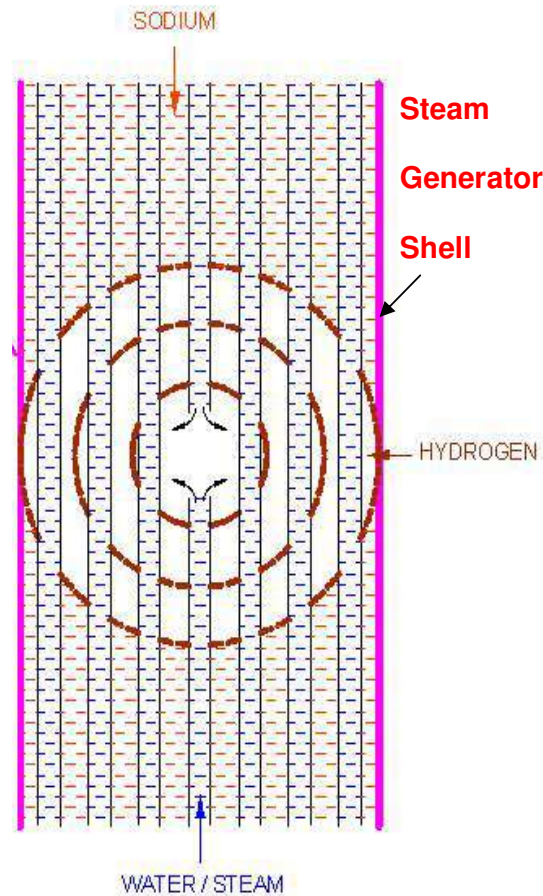
Fig. 5.3 Reaction Site

Hydrogen is taken to behave like an ideal gas and its expansion at reaction site is assumed to be adiabatic. This assumption is valid as the expansion process is very fast. The hydrogen bubble growth (Fig. 5.3) is analyzed using a combined model (a) spherical bubble growth in an incompressible liquid in the vicinity of the reaction site and (b) a one dimensional axial motion in a compressible liquid away from the reaction site.

Sodium side system transients: Pressure waves emanating from sodium-hydrogen interfaces of the bubble in the Steam Generator get transmitted throughout the secondary circuit (Fig. 5.2) and interact with its components like sodium headers on the bottom of Steam Generator, Surge tank, Pump tank etc. This phenomenon of pressure wave propagation is described mathematically by the simultaneous solution of one-dimensional transient equations of mass balance and momentum balance utilizing the numerical method "Method of Characteristics (MOC)" with appropriate boundary conditions described by circuit components (E.B Wylie and V.L Streeter, 1978). The velocity of pressure wave propagation is lower than the sonic velocity, because a part of its energy is used in straining the pipe material. The pump is modeled using homologous pump characteristics covering all four zones of operation.

Water/steam side system transients: Two different leak rate models are used for leak rate of water and that of steam for rupture in economizer and super heater portions respectively.

Water leak model: This inertia controlled model, assumes the fluid to be incompressible and considers forces acting on an element of water in the tube. Water leaks from both the ruptured ends and it accelerates up to critical velocity given by Burnell's relation (S. T. Revankar et al., 2013).

Steam leak model: Following a rupture in super heater portion steam flows towards both the broken ends in upstream and downstream portions of ruptured tube. Frictional adiabatic flow of steam (Fano flow) has been assumed, since, during a period of few hundred millisecond practically no heat gets transferred to steam flowing in the tube.

Discharge Circuit System Transient: At the sodium inlet and outlet of each Steam Generator rupture discs have been provided. When the sodium pressure at these rupture discs goes above the set pressure, these rupture discs will rupture and dump the sodium and sodium-water reaction products into the storage tank through the discharge circuit. Till the rupture disc breaks no calculation has been carried out for the discharge circuit. When the rupture disc breaks, initially only sodium flows through the rupture disc and in discharge circuit till the sodium-hydrogen interface reaches the rupture disc junction. Up to this, time calculations are carried out. When the interface reaches rupture disc junction, two-phase sodium-hydrogen flow through rupture disc and discharge circuit has been carried out. This is based on Greene's model(Greene, D.A., 1972), (S Srinivas and P.S Chopra, 1977).It is a homogeneous flow model in which the fluid is composed of an incompressible liquid and a compressible gas. No phase changes occur in the two components of the fluid. Depending on the available pressure drop, calculations are carried out either for critical two-phase flow or non- critical two-phase flow.

Solution Technique: For finding the pressure and velocity of sodium in the pipes, the governing equations of mass and momentum balance are solved using the MOC. Using the numerical method, the partial differential equations are converted into ordinary differential equations and these are solved by finite difference method. The reaction site equations, characteristic equations for sodium flow adjacent to the reaction site and the water/steam leak rate equations are solved together using the Hamming's modified

predictor-corrector method. The capabilities and the mathematical details of the SWEPT code are discussed in detail in (Selvaraj P. et al., 1996).

5.2.2 Results from SWEPT

The experimental result for comparison is taken from literature (J. Biscarel et.al, 1982). This experiment was conducted to study the effects of large leak sodium-water reaction due to guillotine failure of a single tube. The effects on the pressure and temperature variations and tube bundle deformations were studied. The pressure at the reaction site is at the injection level, measured experimentally and compared with the SWEPT code (Selvaraj et al., 1990). SWEPT code gives conservative values compared to experiment.

For designing the secondary sodium circuit components, an upper bound of leak rate called design basis leak needs to be defined. Overheating of tubes occurs at the sodium hydrogen interface. If the interface is stationary or moves very slowly there will be enough time to cause continuous failure due to overheating. On the other hand if the interface moves faster, there will be little or no time for overheating. In this way additional tube failures are prevented.

Steam Generator leaks generally start in the range of micro leaks or small leaks. They then escalate into intermediate leak range due to wastage of neighboring tubes. In the intermediate leak range many of the surrounding tubes gets heated up and failure occurs due to overheating. Since the process is very complex, it is difficult to predict the evolution of a steam generator leak event. The safety action is initiated by providing two rupture discs one at the top and one at the bottom of the steam generator. The Design

Basis Leak is selected such that the leak rate at which both the rupture discs should break almost simultaneously leading to a fast movement of sodium–hydrogen interface.

A study has been carried out with the SWEPT code to estimate the number of simultaneous Double Ended Guillotine (DEG) failures required to ensure rupture of both rupture discs as well as pushing sodium away from the reaction site. From the study it has been found that the design basis leak is instantaneous DEG failure of 3 tubes at the top of the Steam Generator (for leak at the middle of the Steam Generator the value is 4 and for leak at the bottom the value is 5). For the design basis leak (13 Kg/s), it takes only 5 s for all the sodium to move out of the Steam Generator. Experimental results indicate that it takes more than 20 s for overheating failure to occurs (G. Ruloff and R.Hubner, 1990).
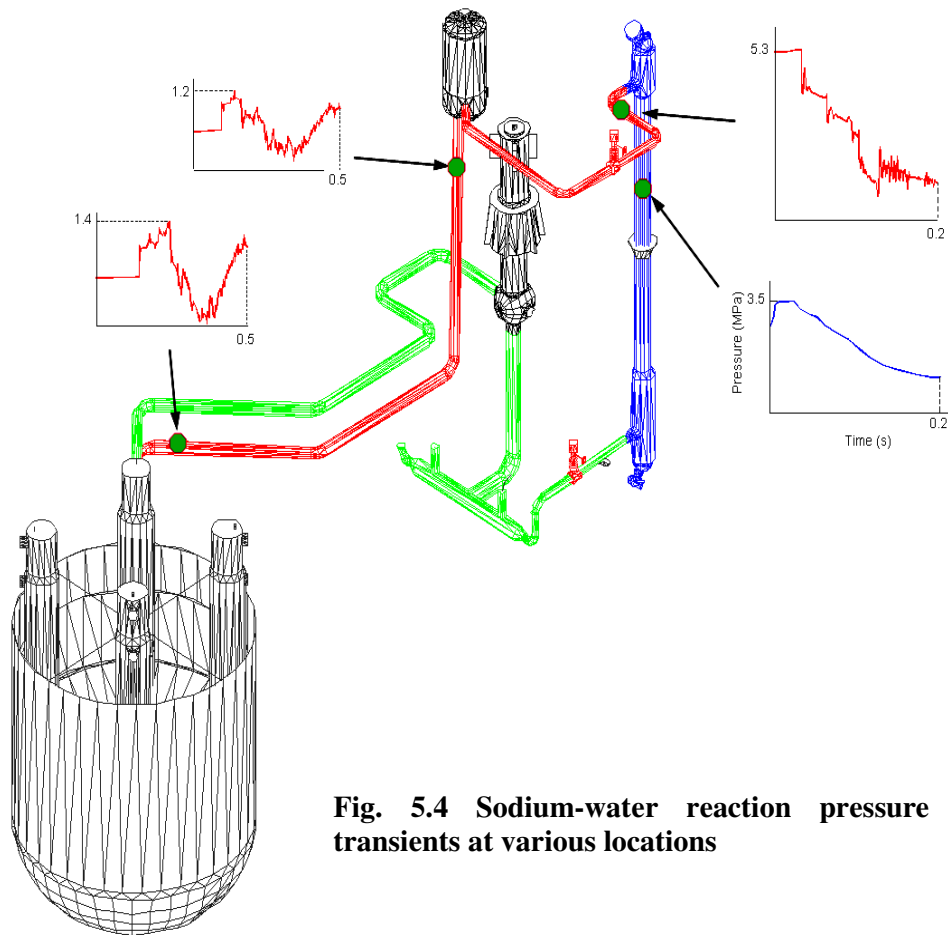
Fig. 5.4 Sodium-water reaction pressure transients at various locations

Table – 5.1 Maximum design basis leak sodium-water reaction pressures

	Maximum Pressure (MPa abs)			
	IHX bottom	**Surge tank cover gas**	**Steam Generator leaking**	**Steam Generator adjacent unit**
Steady state values	0.98	0.40	0.40	0.40
Rupture of both rupture discs	1.76	0.68	5.38	1.18
Rupture of only top rupture disc	1.99	0.86	5.38	1.20
Rupture of only bottom rupture disc	2.50	1.62	5.38	1.34

Table- 5.1 (Selvaraj et.al, 1996) gives the maximum pressure values in the secondary sodium circuit components due to Design Basis Leak sodium-water reaction calculated using the SWEPT code. Fig. 5.4 gives the results of pressure wave propagation in the secondary sodium circuit at different locations.

The maximum pressure predicted due to large sodium-water reactions is 1.8 MPa at IHX (Bhoje, 2003). Fig. 5.5 shows the maximum pressure load acting on the IHX due to Design Basis leak sodium-water reaction event in the Steam Generator.
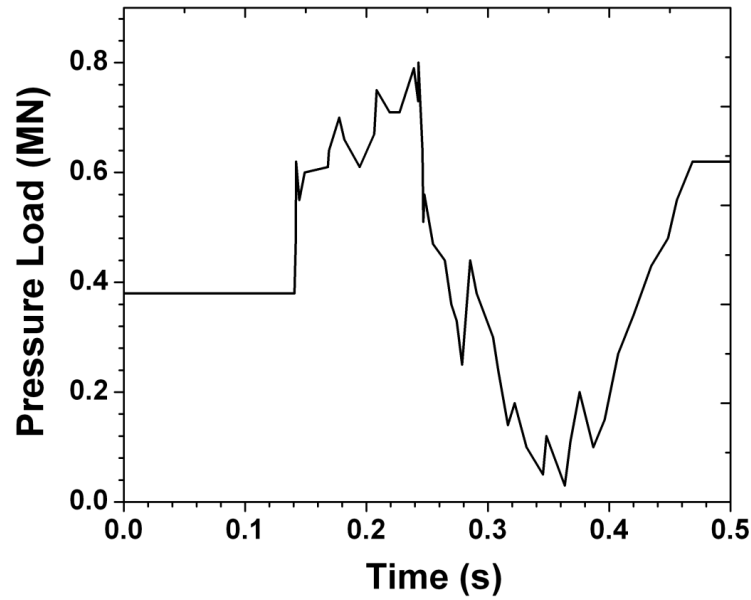
Fig. 5.5 Pressure load at IHX due to Design Basis sodium-water reaction

5.3 CORE SUBASSEMBLY VIBRATION

In pool type LMFBR the IHX is supported on the roof slab and is guided at the Inner vessel. There is a possibility of IHX vibration when the pressure wave due to sodium-water reaction passes through IHX. These vibrations may get transmitted through sodium and Inner vessel to core subassemblies leading to vibration of core subassemblies (Verma et al., 2017). This may cause reactivity perturbations. In the present study, this phenomenon has been studied using CAST3M computer code. When the frequency of pressure pulse resulting at the IHX due to large leak sodium-water reaction matches with the fundamental frequency of other components/structures immersed in reactor vessel, the response of the components/structures during such an event is important to be investigated.

5.3.1 Modeling of Reactor Assembly Components
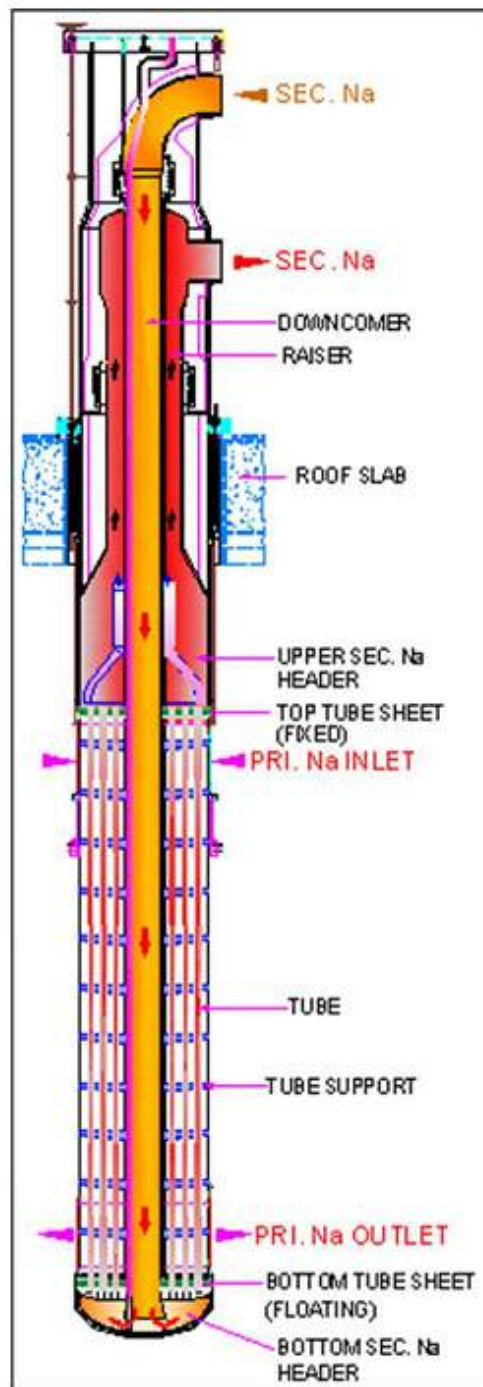
Fig. 5.6 Schematic of Intermediate heat exchanger

The components of interest for the defined problem are the Intermediate Heat Exchangers, Inner vessel and subassemblies which are fully immersed inside the liquid sodium. The Inner vessel is immersed in the liquid sodium which sees the hot and cold sodium during reactor operation. Inner vessel consists of two cylindrical structures and connected by a conical structure with extension of standpipes to the Inner vessel for the passage of IHX.

Intermediate Heat Exchanger (IHX) (Fig. 5.6) is a shell and tube vertical counter flow heat exchanger with primary sodium on the shell side and secondary sodium on the tube side. It is an important heat exchanging component as it transfers heat from radioactive primary sodium in the pool to the non-radioactive secondary sodium. It is supported on the roof slab and is freely hanging from the top and it is partially immersed in the sodium. It is part of the secondary circuit transporting heat to Steam Generator. The outer shell of the IHX is supported at the roof slab and the down comer inside it is freely hanging from the top. The fundamental frequency of IHX is 4.01 Hz (Srinivasan, et. al., 2003). Simplified IHX is modelled with actual thickness with its various parts (top and bottom tube sheet, down comer pipe, inlet & outlet nozzle, Inner & outer shell) excluding the tube bundle. The tube bundle is considered as additional mass. The finite element model is shown in Fig. 5.8. Adding the tube bundle portion as equivalent mass, the natural frequency of simplified IHX model is matched with IHX fundamental frequency. Now the stiffness simulation is carried out for the cylindrical shell by varying the value of Young's modulus to get equal deflection in simplified IHX and cylindrical shell, thereby to achieve same 1st natural frequency. Mass and stiffness are uniformly distributed in the cylindrical shell.
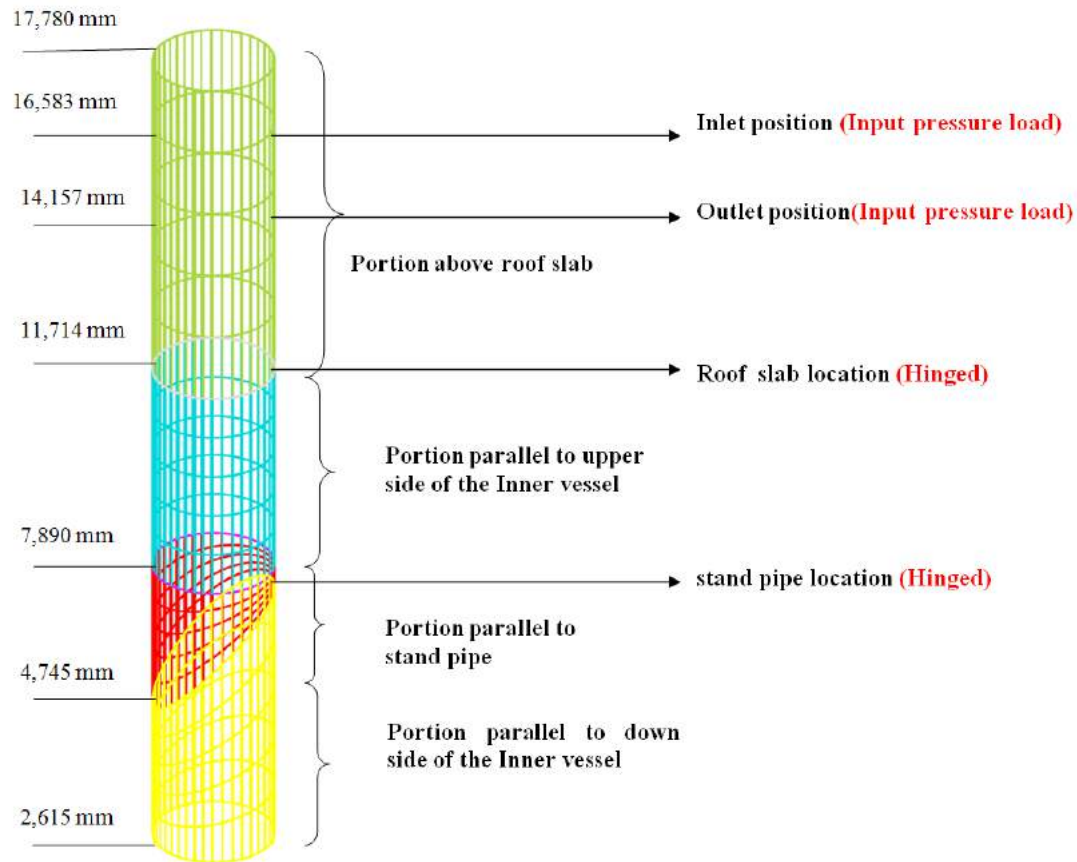
Fig. 5.7 Support positions of IHX

The total height of the IHX is around 16 meters and it is supported from the top and hinged to the conical portion of the Inner vessel through stand pipes.IHX connected to the secondary sodium circuit will experience high pressure fluctuations during large sodium-water reaction in the steam generator. The secondary sodium inlet is at the top of the IHX and the outlet is just below the inlet. Both the inlet and outlet end of IHX will experience the pressure load due to sodium-water reaction.
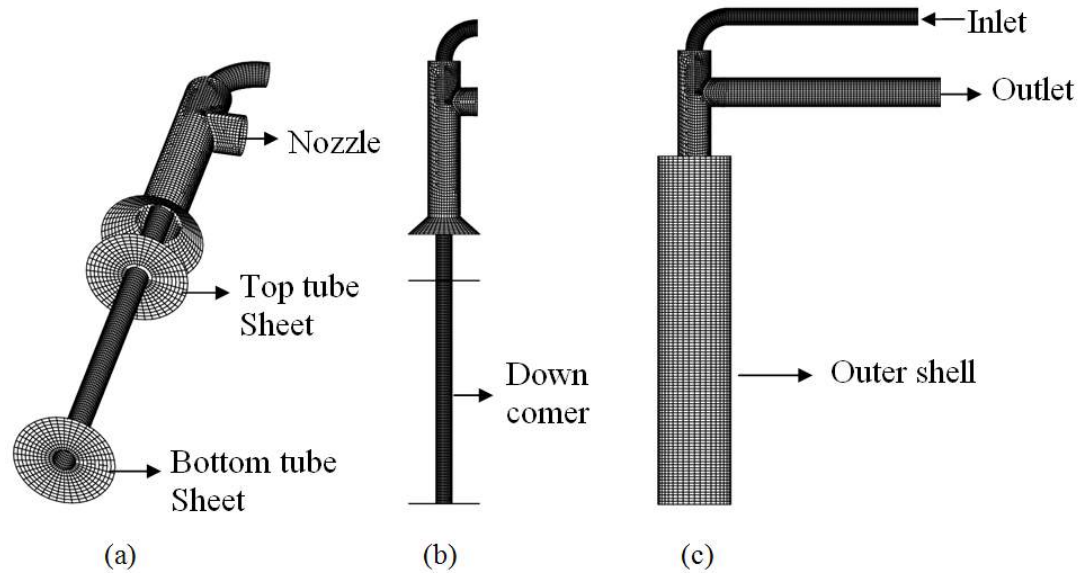
Fig.5.8 FEM model of Intermediate Heat Exchanger (a) Isometric view; (b) front view; (c) front view with sodium inlet and outlet

Fig. 5.9 shows the core configuration. The innermost subassemblies are the fuel subassemblies and the extreme outer are the shielding subassemblies. Since the inner vessel is very near to the outer subassemblies, the last two rows of them are modeled in the analysis. To observe the response of the fuel subassemblies, the inner fuel subassemblies are modeled in the analysis. For easiness in modeling and analysis, 180 degree sector of the Reactor has been modeled with last two rows of subassemblies and inner core subassemblies. Outer two rows of subassemblies are shielding subassemblies and the inner core subassemblies are the fuel subassemblies. Fluid elements between the subassemblies have also been modeled. Two rows of subassemblies in 180 degree model of the reactor assembly comprise of 76 subassemblies in a row, thus totally 152 subassemblies have been modeled in the outer core and the fuel inner core are with 51 subassemblies.

Fig. 5.10 shows the schematic of a subassembly. The foot of the subassembly is freely inserted inside the grid plate. Since the subassemblies are freely standing, they are more prone to vibrations. This is taken care in the simulation also. The base of the grid plate is fixed and the subassemblies are hinged to it. Mass simulation for the subassemblies has also been done. To investigate the behavior of subassemblies, the core is divided into four zones as shown in Fig. 5.11.
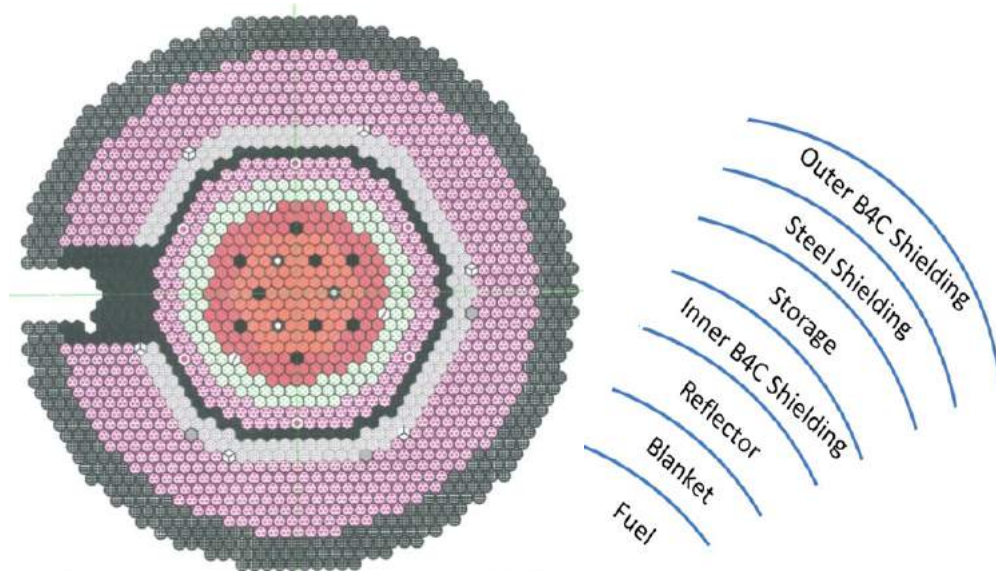
SYMBOL	TYPE OF SUBASSEMBLY
	FUEL (INNER)
	FUEL (OUTER)
	CONTROL AND SAFETY ROD
	DIVERSE SAFETY ROD
	BLANKET
	SOURCE
	STEEL REFLECTOR
	PURGER
	B_4C SHIELDING (INNER)
	STORAGE LOCATION
	STORAGE FOR SOURCE
	FAILED FUEL STORAGE LOCATION
	STEEL SHIELDING
	B_4C SHIELDING (OUTER)
	TOTAL SUBASSEMBLIES

Fig.5.9 Core configuration

Head

Shielding pin bundle

Fuel pin bundle

Diffuser

Orifice

Foot

Coolant entry slots

Discriminator

Handling Head

Top Shield

Push buttons

Fuel Pins

Fuel Pin Support

Foot

Coolant Entry Slots

Discriminator
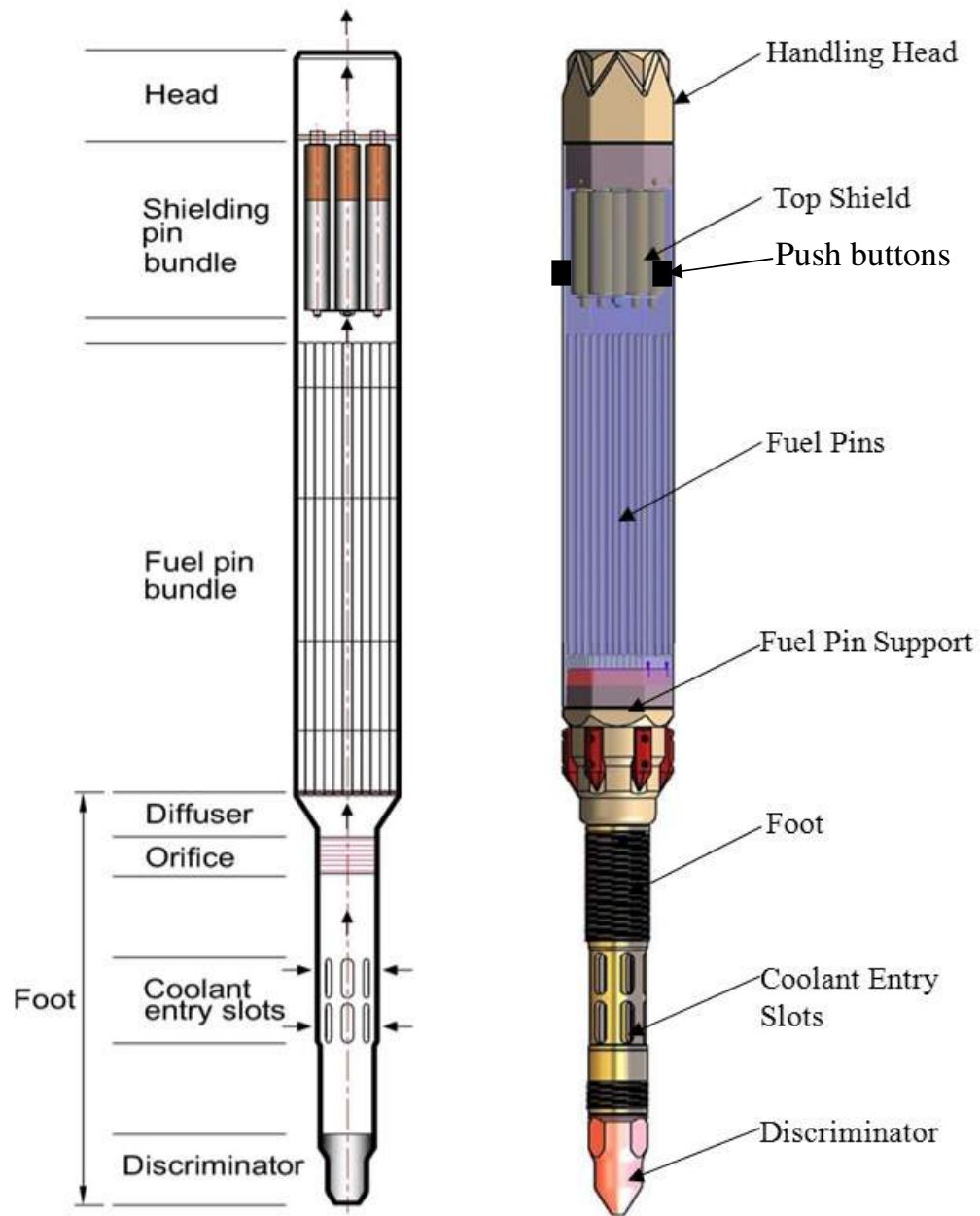
Fig. 5.10 Schematic of a subassembly
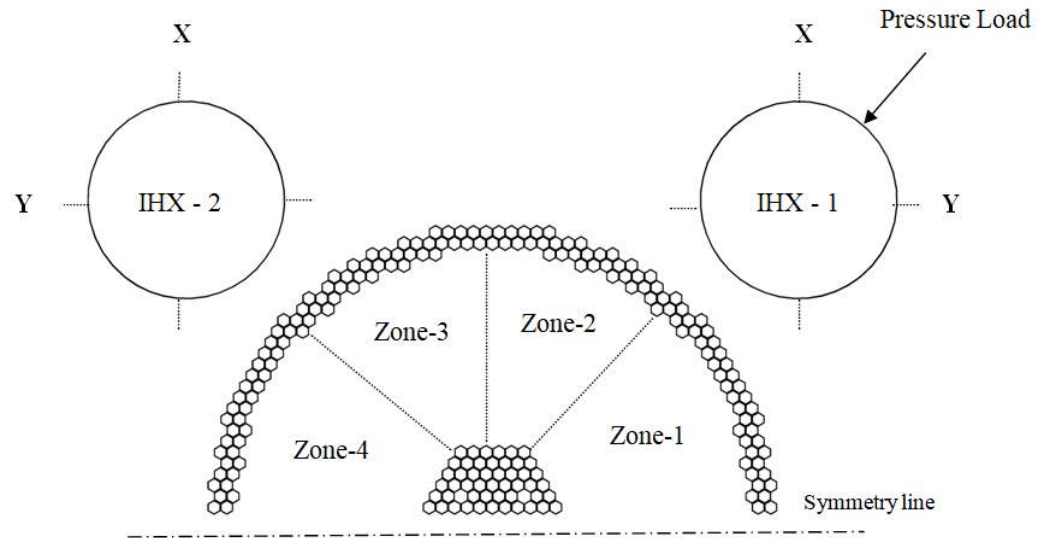
Fig. 5.11 Zone separation with direction of impulse

The components are modeled using four noded element and three nodded shell element with six degrees of freedom. The fluid volume is modeled using eight noded and six nodded brick element. At the fluid-solid interface, the fluid and the solid nodes are joined by liquid shell transition element. Fluid damping of 1% is used in the simulation. The FEM model with grid plate and subassemblies, Inner vessel with Intermediate Heat Exchanger and the reactor assembly combining all is shown in Fig. 5.12. The material properties are listed in Table 5.2.

Table 5.2 Material properties

Property	Value
Density of Steel (ρ_s)	7800 kg/m^3
Modulus of Elasticity (E)	1.61 x 10^{11} N/m^2
Density of Sodium (ρ_f)	857 kg/m^3
Poisson's ratio (μ)	0.3
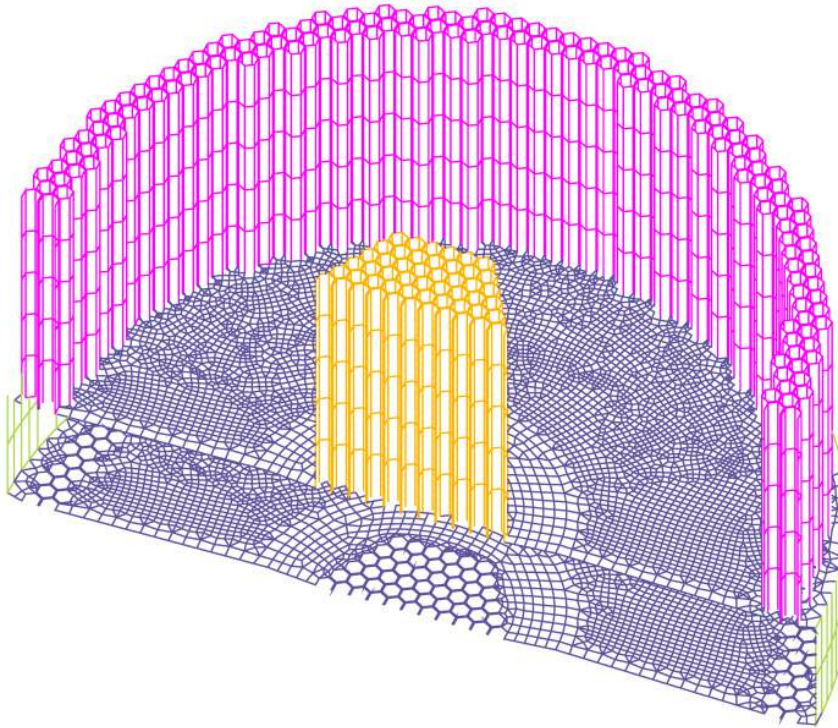
(a)
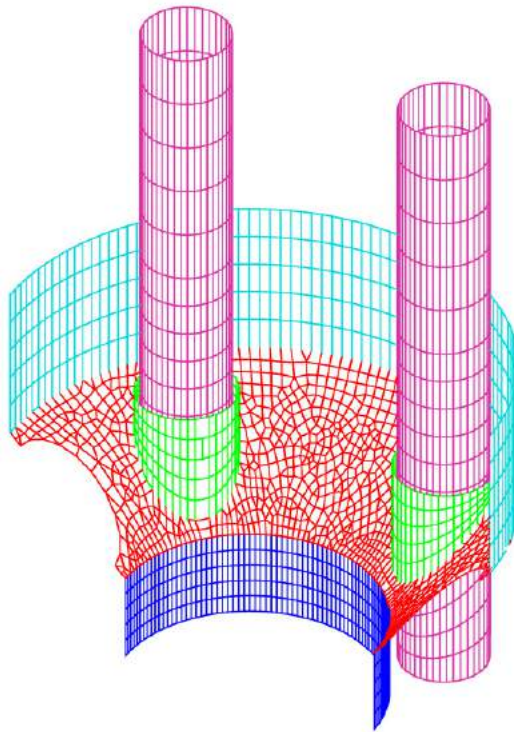
(b)
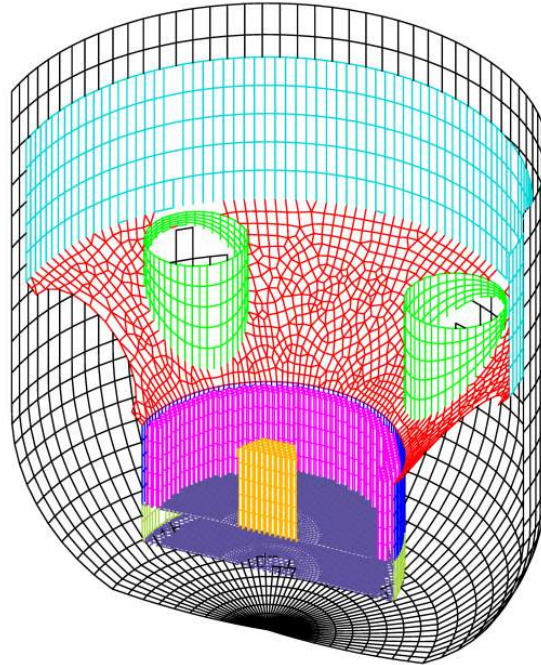
(c)
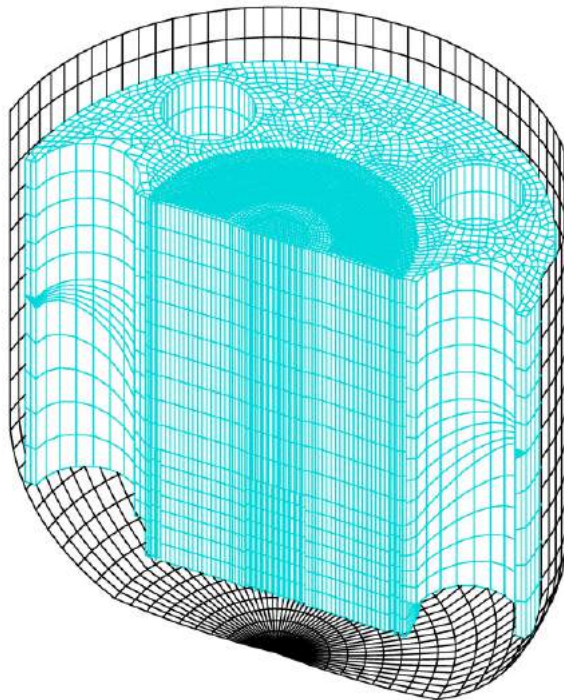
(d)

Fig. 5.12 (a) Grid plate with subassemblies; (b) Inner vessel with IHX; (c) Reactor assembly with main vessel; (d) Fluid elements in the reactor assembly

5.3.2 Results and Discussion

Due to sharp pressure rise, the inlet and outlet of IHX experience a sudden impact pressure load in the direction of the flow of liquid sodium. From the structural dynamics analysis of IHX, the natural frequency is found to be 4.48 Hz. The frequency of pressure load shows a maximum frequency of (50-70) Hz. Hence the frequency of input to the IHX is away from the resonant frequency of the IHX. When the pressure load acts on the inlet and outlet of the IHX, the response displacement of IHX, Inner vessel and subassemblies are calculated.
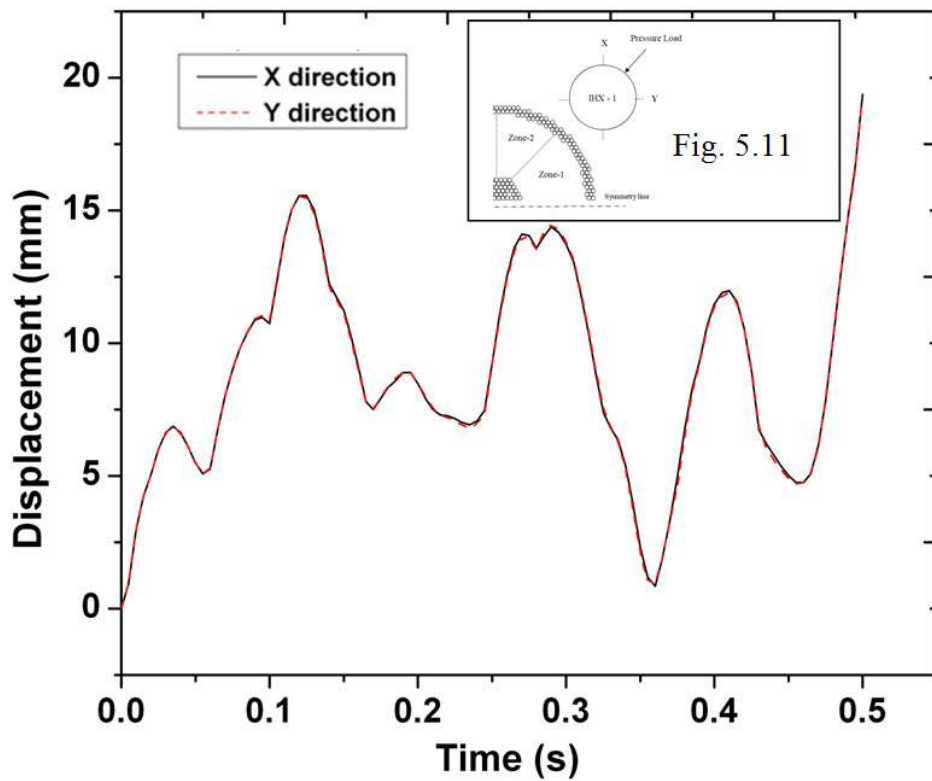
Fig. 5.13 IHX-1 displacement
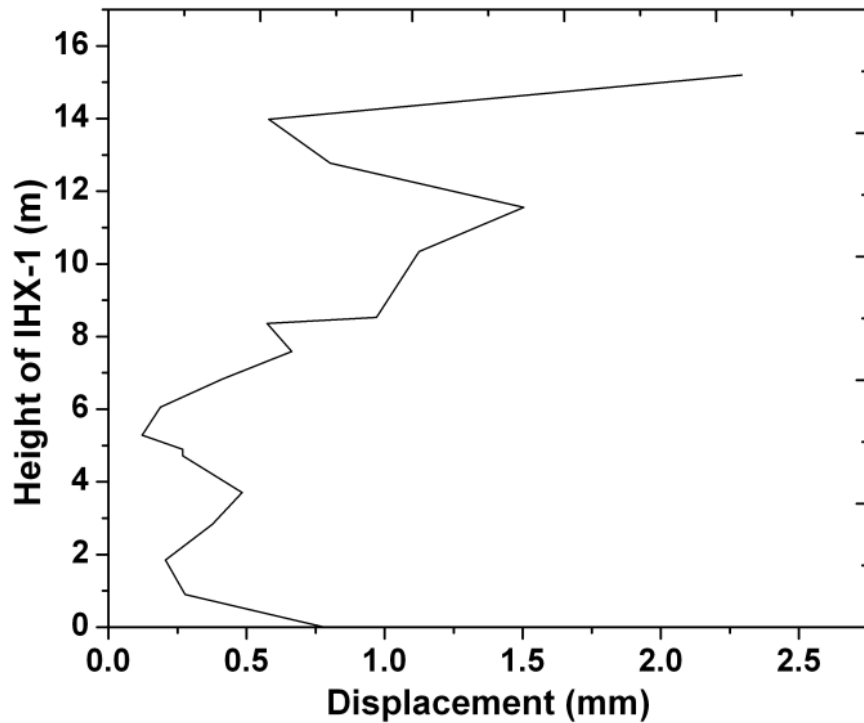
Fig.5.14 Displacement of IHX-1 along the height

Fig. 5.13 shows the displacement of IHX-1 in the X and Y direction. The maximum displacement of the IHX-1 is found to be 20.0 mm due to sudden impact. As the pressure load to IHX-1 is symmetric to both the directions, the displacement is almost found to be the same in both the directions. IHX-2 displacement is found to be less because major pressure load is acting towards the IHX-1 and also the position of IHX-2 is far from the loading area. Fig. 5.14 shows the displacement of the IHX-1 along the height. The graph is plotted for the dynamic displacement at 0.3 s. Since the IHX is hinged to the roof slab and at its mid height with the inner vessel through the stand pipe, it behaves like an overhanging beam along its height, and the displacement is found to be less at the middle and maximum near the roof slab end. The dynamic deflection at 0.3 s is found to be 0.7 mm at the bottom. Fig. 5.15 shows the contour plot of maximum displacement at 0.3 s. Peak displacement occurs above the roof slab elevation.
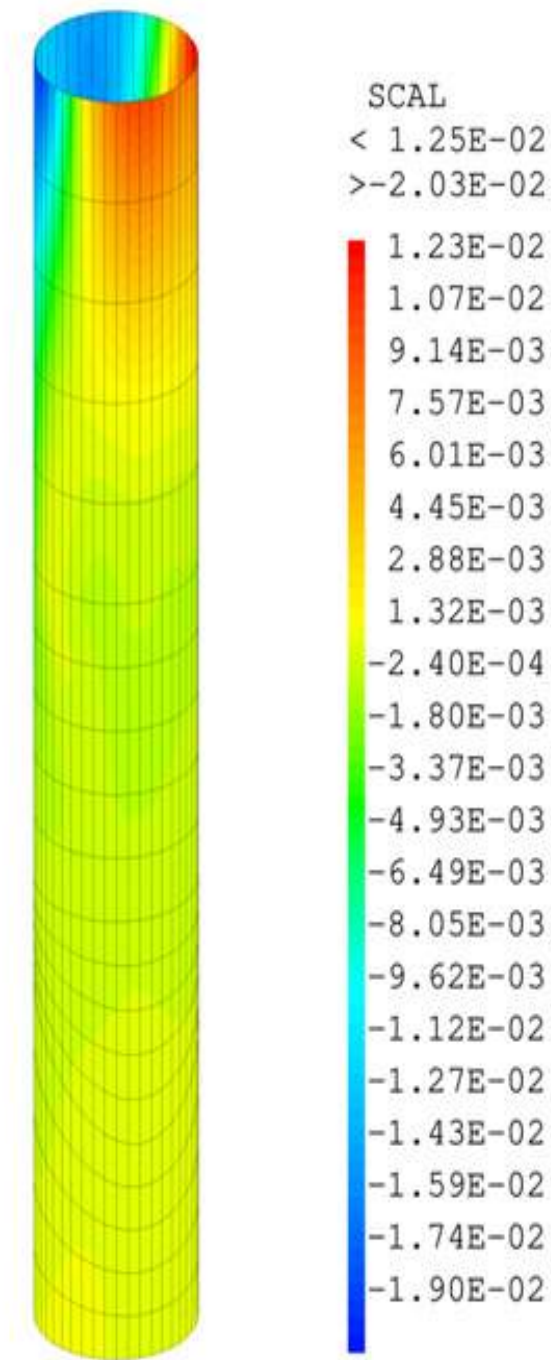
Fig. 5.15 Maximum displacement of IHX-1 in m
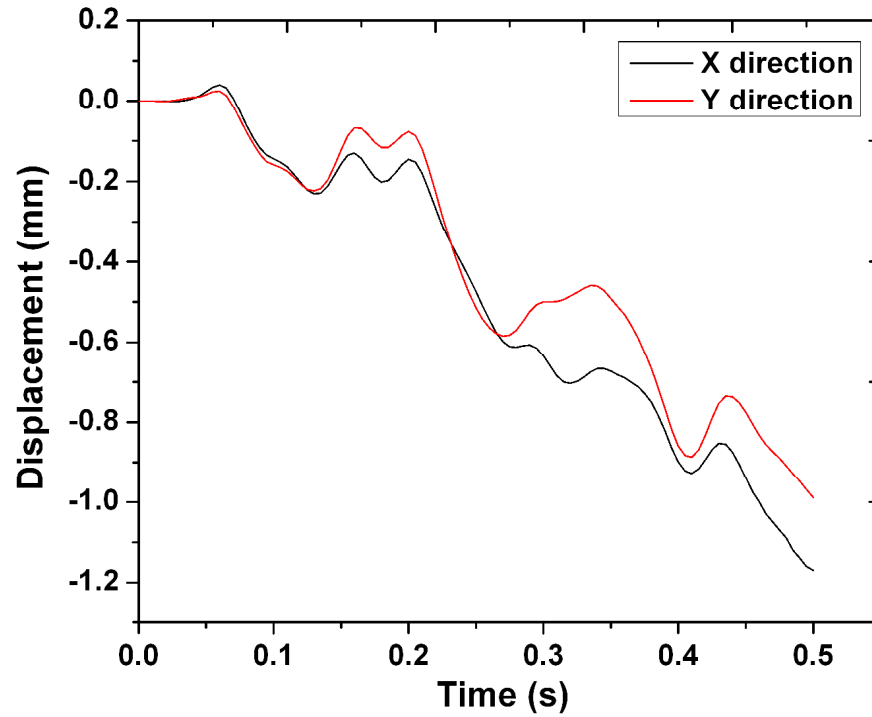
Fig. 5.16 Inner Vessel displacement

Fig. 5.16 shows the displacement of the Inner vessel in X and Y direction at the upper cylindrical position, which nearer to the IHX-1. At 0.3 s, peak pressure load is seen from Fig. 5.5, due to this there is monotonic increase in the displacement of the inner vessel. Fig. 5.17 shows the contour plot of displacement of Inner vessel at 0.3 s. Peak displacement occurs at stand pipe location, where the IHX is hinged to the Inner vessel.

```
SCAL
<  1.15E-03
>-1.44E-03

   1.13E-03
   1.01E-03
   8.86E-04
   7.62E-04
   6.39E-04
   5.15E-04
   3.92E-04
   2.69E-04
   1.45E-04
   2.19E-05
  -1.01E-04
  -2.25E-04
  -3.48E-04
  -4.72E-04
  -5.95E-04
  -7.18E-04
  -8.42E-04
  -9.65E-04
  -1.09E-03
  -1.21E-03
  -1.34E-03
```
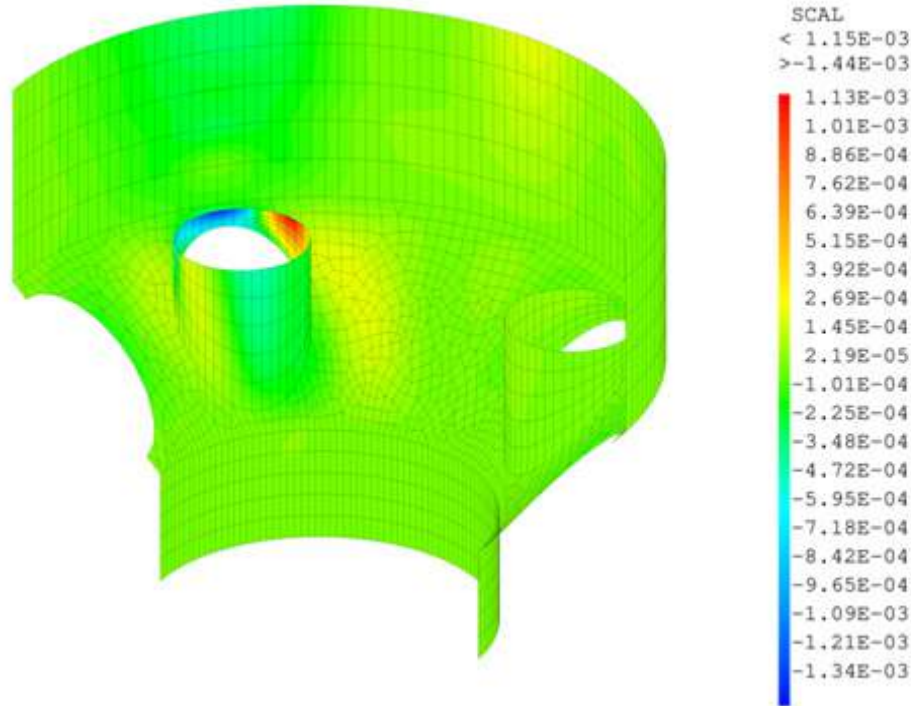
Fig. 5.17 Displacement of Inner vessel at 0.3 s in m

The maximum displacement of the subassemblies in the X and Y direction is shown in Fig. 5.18 and Fig. 5.19 respectively. The maximum displacement at the top of the subassemblies is found to be 0.07 mm. Maximum displacements are found between zone 1 and zone 2. This is due to excitation of IHX with the pressure load which is near to the zone 1. Displacements of the inner fuel core subassemblies are directly due to the impact pressure load from IHX to the top of the subassemblies. This displacement is found to be less.

Since the subassemblies are separated by a fluid gap of 3.4 mm between them, when the displacement is more than 3.4 mm only the second row of assemblies will be

influenced due to neighbouring subassemblies. So the displacement will be limited to first

row of subassemblies only during such transient events.
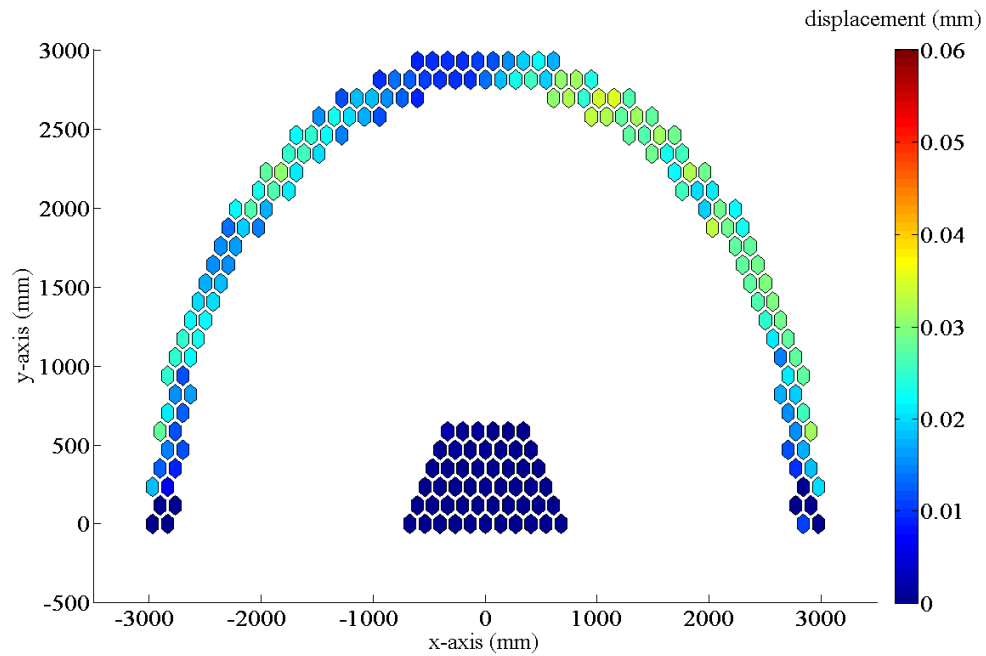
Fig. 5.18 Displacement of subassemblies in X direction
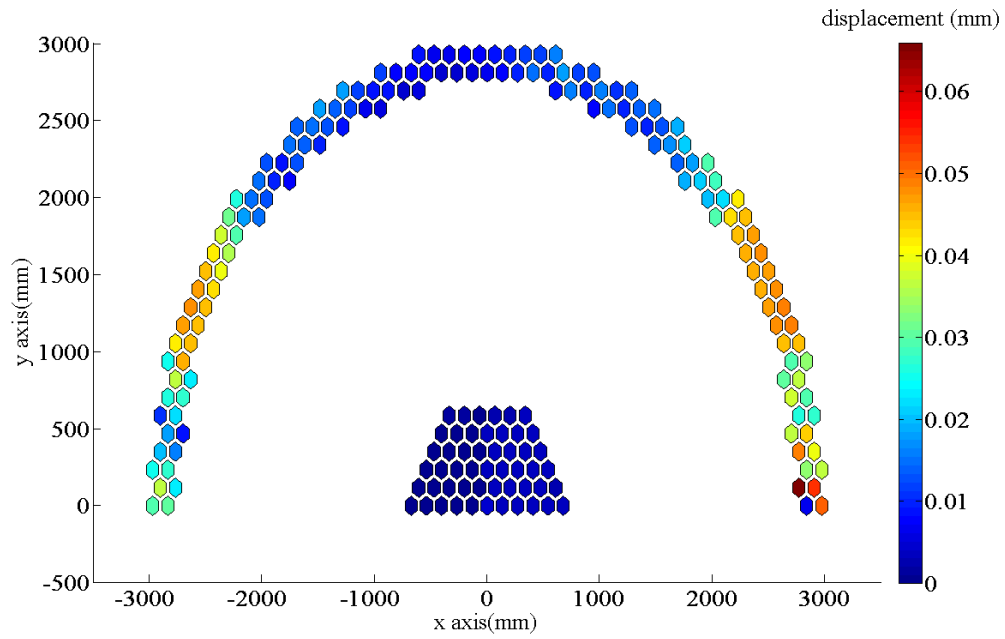
Fig. 5.19 Displacement of subassemblies in Y direction
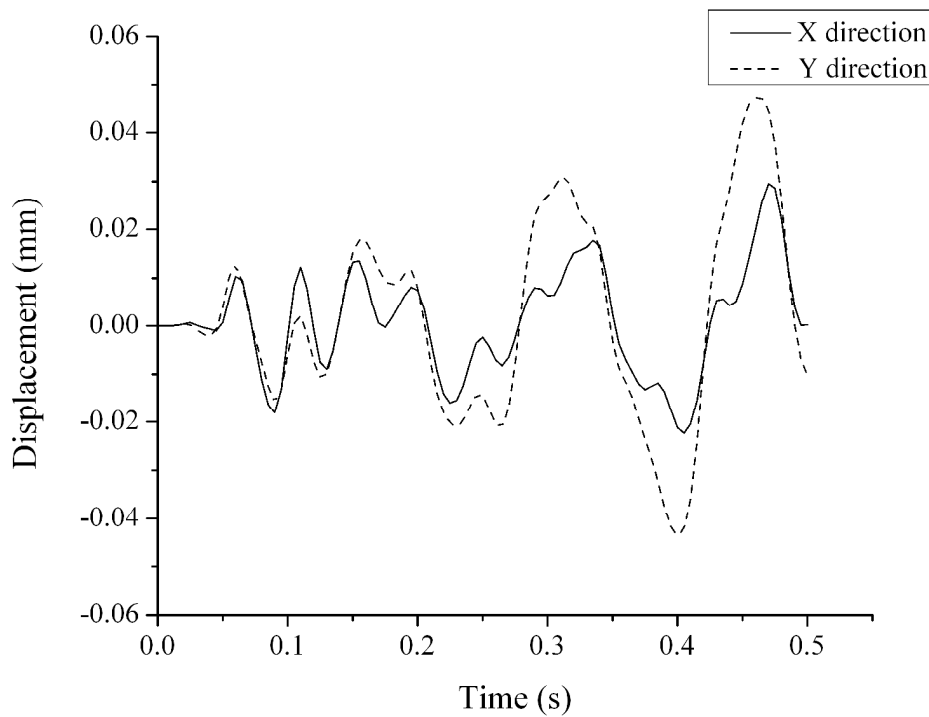
Fig. 5.20 Displacement of a subassembly

Fig. 5.20 shows the displacement of a single subassembly in zone-1 in X and Y direction which shows the maximum displacement of 0.05 mm. Also frequency of vibration of the subassembly is found to be 15 Hz, which is far away from the fundamental frequency of individual subassembly (5.42 Hz).

5.3.3 Effect on reactivity of the core due to displacement of subassemblies

Reactivity feedback is defined as the reactivity changes that occur in the reactor core to due to change in temperature/void. Reactivity feedback in a nuclear reactor core can be studied in terms of fuel Doppler coefficient, coolant density, Fuel axial expansion, core radial expansion and control rod driveline expansion (Raj et al., 2015) In case of core radial expansion, if core subassemblies move outward in the radial direction, increasing the effective diameter of the core, a negative reactivity feedback is generated. Conversely, if the core subassemblies move inward, a positive reactivity feedback will be resulted. In the present study, reactivity feedbacks due to the displacement of fuel subassemblies in case of pressure wave transmission have been studied.

In power reactors, the distortion or movement of subassemblies in the core can be observed usually as the reactivity feedback. The reactivity feedback from sub-assembly bowing has been calculated by considering it as a radial boundary movement of one zone of sub-assemblies to the next zone. The reactivity change caused by the radial outward movement of a particular zone in the inner core by 1 mm is calculated (Gautama Hebbar A, 2012) using first order perturbation analysis.
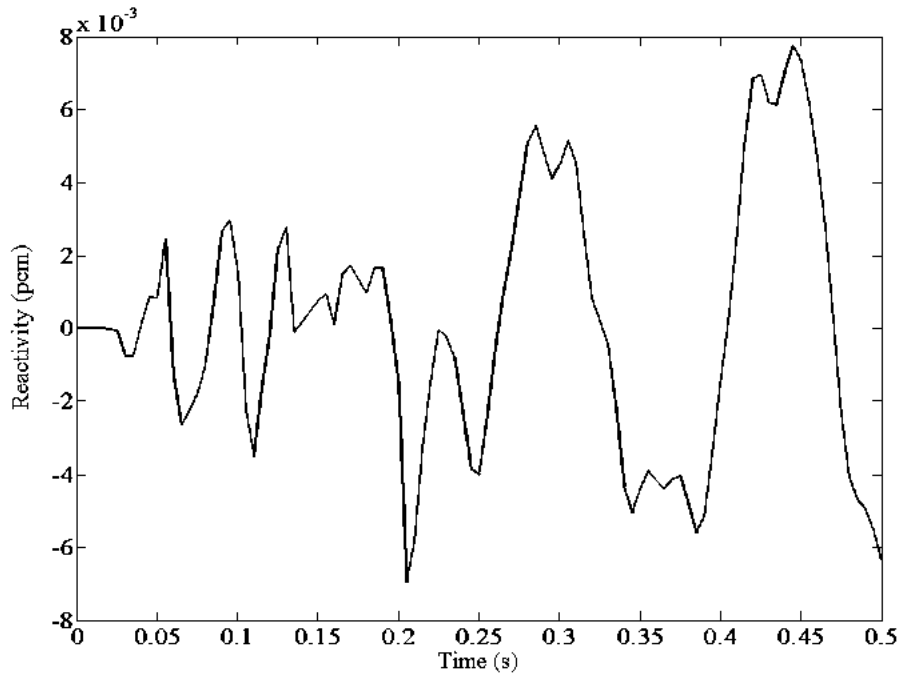
Fig. 5.21 Change in reactivity in the core

From the observed displacements in the inner core subassemblies, the reactivity is calculated by interpolation for the Design Basis Event sodium-water reaction. The reactivity changes due to subassembly displacement for the given period of time shows a maximum of 0.008 pcm as shown in Fig. 5.21. The graph shows both the positive and negative reactivity in the core due to displacement of subassemblies.
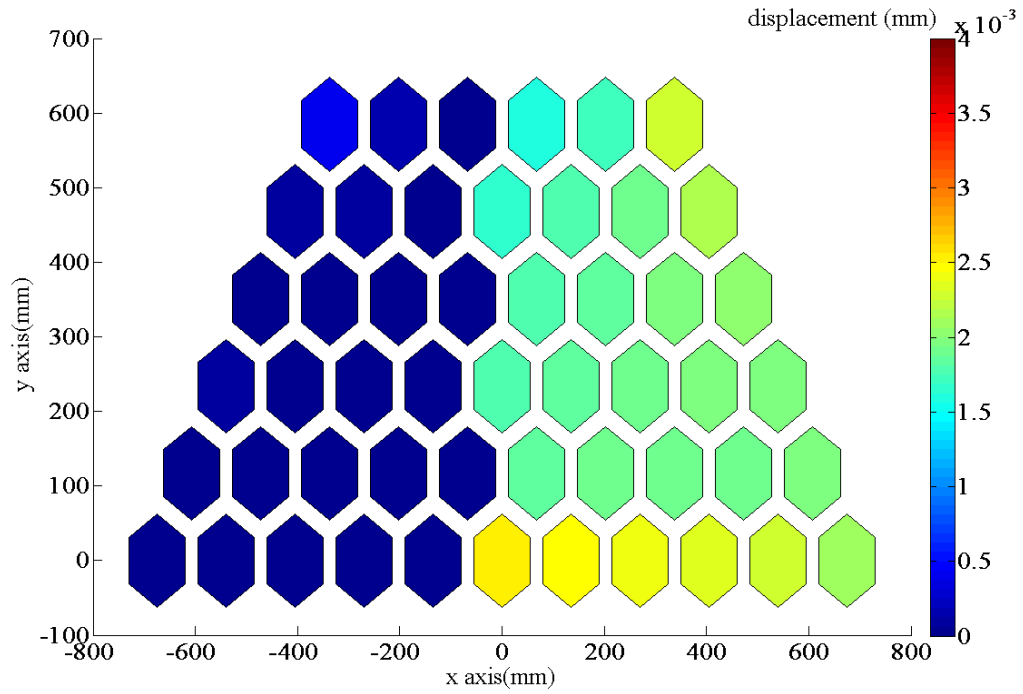
Fig. 5.22 Displacement of core at 0.35 s
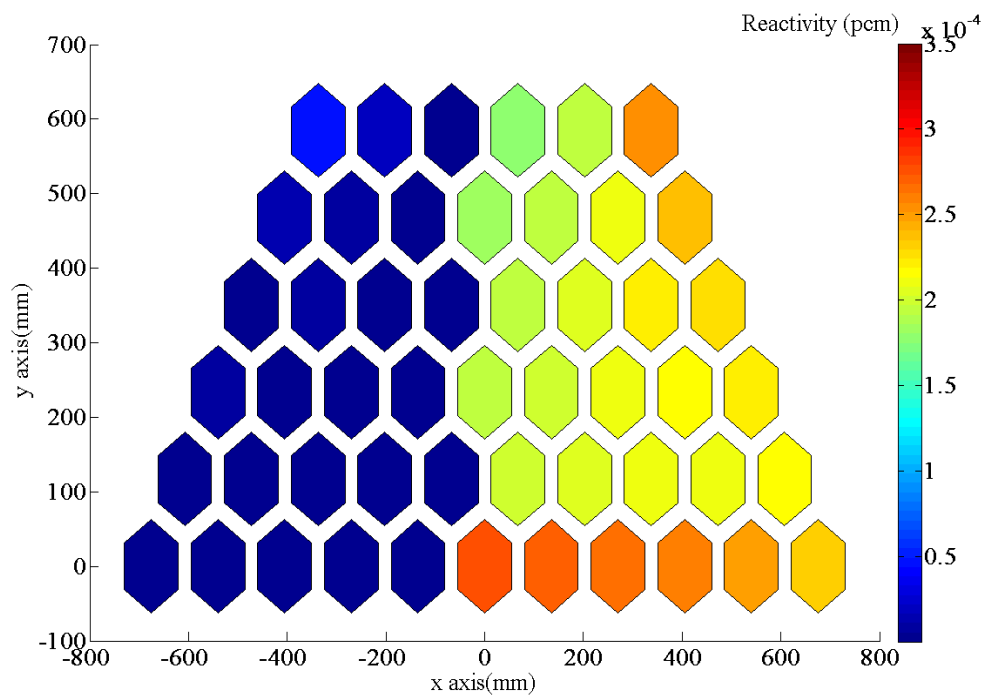
Fig. 5.23 Reactivity of core at 0.35 s

The displacement and the corresponding reactivity change in the fuel subassemblies are plotted for the particular time step of 0.35 s as shown in the Fig. 5.22 and Fig. 5.23 respectively. Negligible displacement and change in reactivity is observed from the other half of the fuel core, and this is due to the transient event taking place only in one loop of the Steam Generator resulting in the excitation of IHX-1. Due to outward displacement of the subassembly at that time step, the net reactivity of the subassembly is found to be positive. The values obtained are within the design limits for displacement and reactivity obtained due to Design Basis sodium-water reaction.

5.4 CLOSURE

Evaluation of the vibration of subassemblies in the reactor core for Design Basis leak sodium-water reaction event in the Steam Generator is performed using CAST3M. Due to dynamic pressure load at the Intermediate Heat Exchanger (IHX), the responses of the subassemblies are studied. The study shows maximum displacement in the subassemblies as 0.07 mm for Design Basis leak sodium-water reaction. The change in reactivity in the inner core subassemblies for the observed displacement is presented. Due to this displacement there is negligible change in the reactivity of the core.

* * *

CHAPTER 6

Investigation of Vibration in Core for Beyond Design Basis Sodium-Water Reaction

6

6.0 INTRODUCTION

The operating experiences of Steam Generators indicate that tube leakage affects the availability of the plant. Every effort is being made during design, material procurement and manufacture of Steam Generator to ensure that tube leak probability is minimum. In case of a tube leak, various provisions as mentioned in chapter 5.1 have been made to detect the leak and terminate sodium-water reaction as early as possible. Hence the possibility of a large leak sodium-water reaction is very low. However in line with the approach of defense in depth, a design basis water/steam leak is defined. Further in order to study any possibility of cliff edge effect, large scale sodium-water reaction analyses beyond the design basis leak have been carried out using the SWEPT and CAST3M computer codes, and the details are given in this chapter.

6.1 LARGE SCALE SODIUM-WATER REACTION STUDIES

Steam/water leaks ranging from small to large leaks have occurred in fast reactor steam generators, which influenced the plant availability and safety of the installation. In the plant, sodium-water reaction is immediately identified within the small leak range itself through in-sodium and in argon hydrogen detectors and safety actions are automatically initiated to stop further sodium-water reaction. These include simultaneous isolation of water and steam side (3 s), isolation of sodium inlet and outlet (10 s) and

dumping of water/steam inside the steam generator into a dump tank. When the water/steam pressure reduces from 17.2 MPa to 0.9 MPa, nitrogen is injected to flush out the remaining water/steam inside the Steam Generator (50 s). These actions stop further sodium-water reaction. In the intermediate leak range, pressure switches are provided in the surge tank. When the Surge tank cover gas pressure increases above the threshold value, automatic actions are initiated to terminate further sodium-water reaction. In the large leak range (> 2 kg/s) the major effect is the increased pressure in the sodium system. A Surge tank is provided on the up-stream of the Steam Generator to mitigate the initial pressure spike. Further, rupture discs are provided both at sodium inlet and outlet of the Steam Generator. When the sodium pressure at the rupture disc increases above the set pressure, the rupture disc will burst and relieve the system pressure. Sodium leak detectors provided down-stream of the rupture discs initiates the safety actions to terminate further sodium-water reaction.

Even though the design basis leak generates a peak pressure of 5.4 MPa at the top rupture disc and 2.7 MPa at the bottom rupture disc, the set pressure for the rupture discs has been selected as 1.2 MPa. This is to ensure the breaking of the rupture disc at the earliest. The formation of hydrogen bubble at the reaction site and the quick opening of the rupture discs ensure that the possibility of multiple simultaneous tube failures beyond the design basis leak is highly unlikely. However in order to avoid any cliff edge effect the following studies have been carried out.

6.1.1 Failure of more number of tubes than Design Basis Leak

In 1987, an incident of sodium water reaction has occurred in Prototype Fast Reactor (PFR) Dounreay, UK (Currie et al., 1990). In this event 40 tubes have failed each

one is equivalent to a DEG (Double Ended Guillotine) failure. The 39 secondary failures have occurred in a time of about 10 s. A similar study has been carried out using the SWEPT code. In this study it is assumed that one tube fails after every 0.1 s. Fig. 6.1 gives the pressure rise at the reaction site. It can be seen from figure that the pressure rise at the reaction site is higher for the design basis leak. For the other case even though there is a failure of 100 tubes in 10 s, the maximum pressure occurred is lower than that of design basis leak. This is mainly because the maximum pressure has occurred due to one tube failure only. Immediately afterwards the maximum pressure reduces due to rarefaction wave from surge tank. Failure of second tube coincides with the breaking of top rupture disc. Once the top rupture disc breaks, it opens a permanent relief path through storage tank. The system now becomes open. Hence any failure of further tubes could not increase the pressure above the initial peak value. The pressure drop near the time 5s is induced by the emptying of Steam Generator. Even after emptying Steam Generator, there is further sodium-water reaction in the discharge circuit connecting the Steam Generator and storage tank. The pressure rise after 5 s is mainly due to this reaction. The maintenance of secondary pressure of around 1.6 MPa is due to the resistance offered by the discharge circuit.
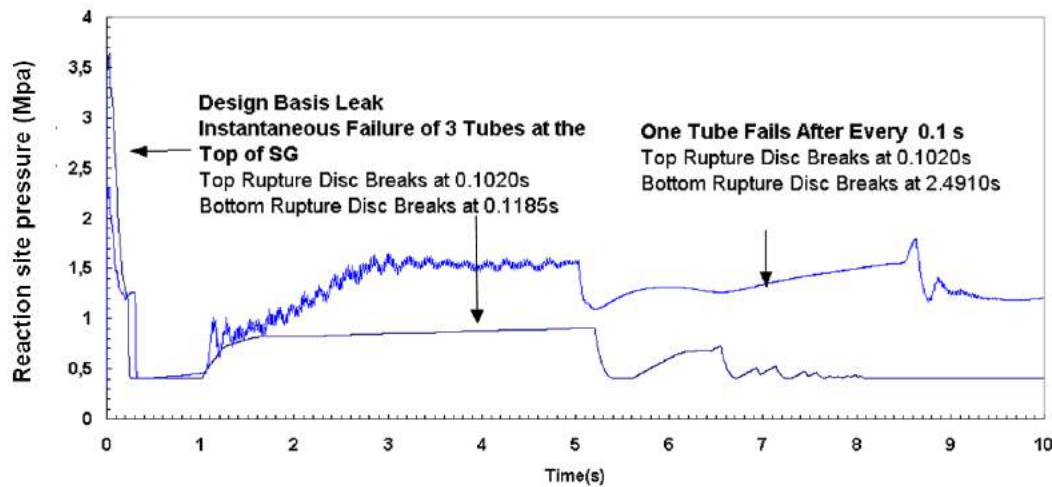
Fig. 6.1 Multiple tube sodium-water reaction studies

6.1.2 Simultaneous failure of more tubes than the design basis leak

Another study has been carried out where the number of simultaneous double ended guillotine failure of tubes has been increased beyond the design basis leak. IHX is designed (maximum pressure equal to 1.8 MPa) for RCC-MR (RCC-MR, 2007) level A criteria for the design basis leak case (simultaneous failure of 4 tubes in the middle of IHX). In this case it is planned to reuse IHX after a design basis leak sodium-water reaction. Under level D condition the maximum pressure IHX can withstand is 2.5 MPa (Fig.6.2). Using the SWEPT code it is found that it takes simultaneous DEG failure of 15 tubes in the Steam Generator to cause a pressure rise of 2.5 MPa in the IHX. Hence IHX can withstand up to 15 DEG failures of tubes. In this case IHX will not be reused.
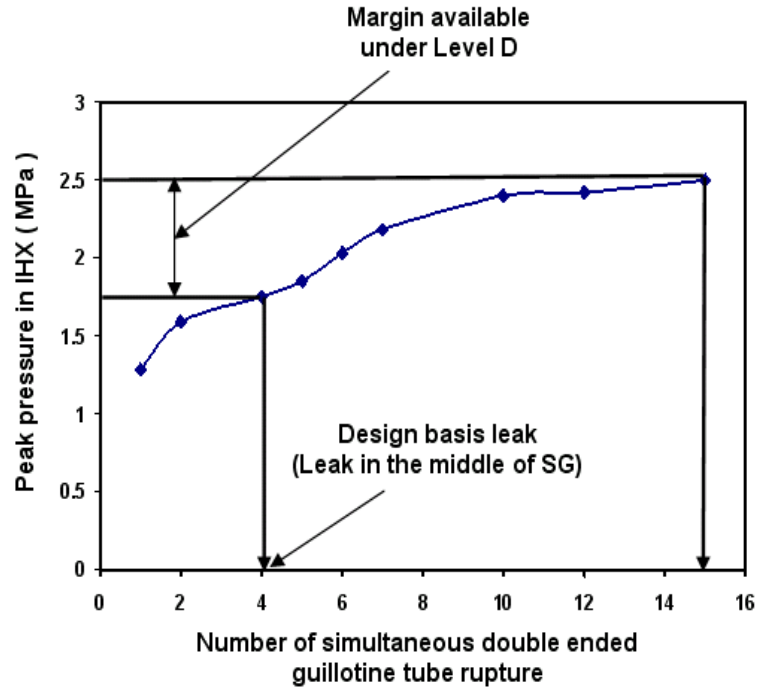
Fig. 6.2 Pressure rise in Intermediate Heat Exchanger
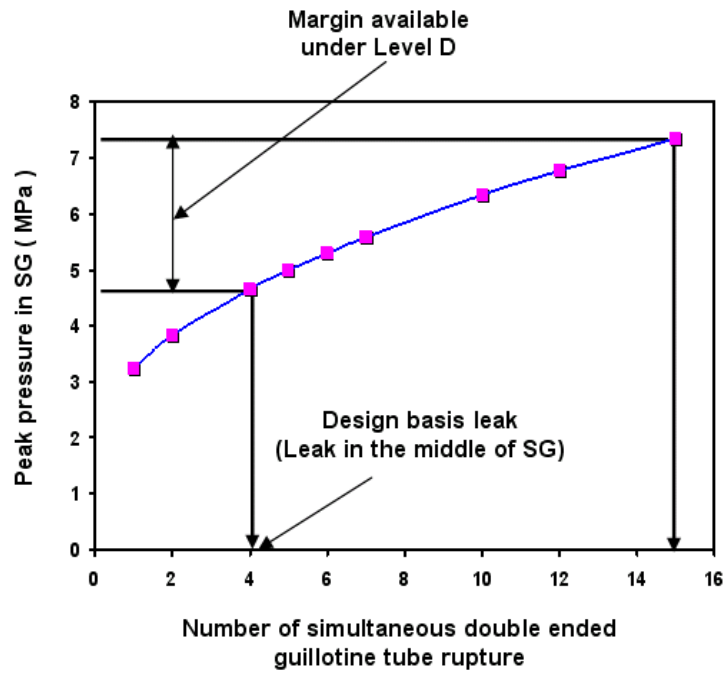
Fig.6.3 Pressure rise in Steam Generator

Similarly it is found that the Surge tank (1.74 MPa) and Steam generator (7.6 MPa) also can withstand the pressure rise due to simultaneous double ended guillotine failure of 15 tubes. The results are given in Fig. 6.3 for the Steam Generator. Hence it is concluded that sufficient margin exist in the design to take care of any large scale sodium-water reaction event.

6.2 FEM FORMULATION IN CAST3M

The modeling and material properties details remain the same as design basis leak event. From SWEPT code, for the beyond design basis sodium-water reaction (simultaneous DEG failure of 15 tubes in the steam generator), pressure-time history at IHX is obtained. Fig. 6.4 shows the pressure load-time history.
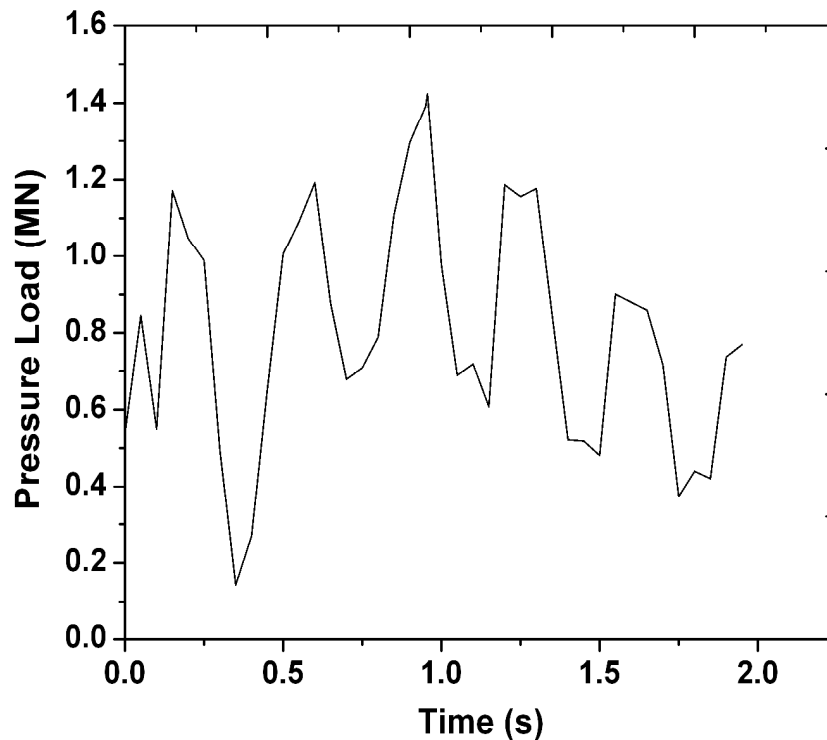
Fig. 6.4 Pressure-load time history

6.2.1Results and Discussion

When the pressure load acts at the inlet and outlet of the Intermediate Heat Exchanger, the displacement of Inner vessel and IHX are given in Fig. 6.5, and Fig. 6.6 respectively. The maximum displacement is found to be 6.5 mm, 35 mm and 0.16 mm respectively for inner vessel, IHX-1 and IHX-2. The bottommost point of IHX-1 experiences a displacement of 9 mm. Since the inlet and outlet of IHX are the pressure loading points and they are located above the roof slab elevation, maximum displacement occurs at the topmost position of IHX-1. Since the pressure load is acting only in IHX-1, the IHX-2 displacements are very less.


```
SCAL
<  6.66E-03
>-5.24E-03
   6.56E-03
   6.00E-03
   5.43E-03
   4.86E-03
   4.30E-03
   3.73E-03
   3.16E-03
   2.60E-03
   2.03E-03
   1.47E-03
   8.99E-04
   3.32E-04
  -2.34E-04
  -8.00E-04
  -1.37E-03
  -1.93E-03
  -2.50E-03
  -3.07E-03
  -3.63E-03
  -4.20E-03
  -4.77E-03
```
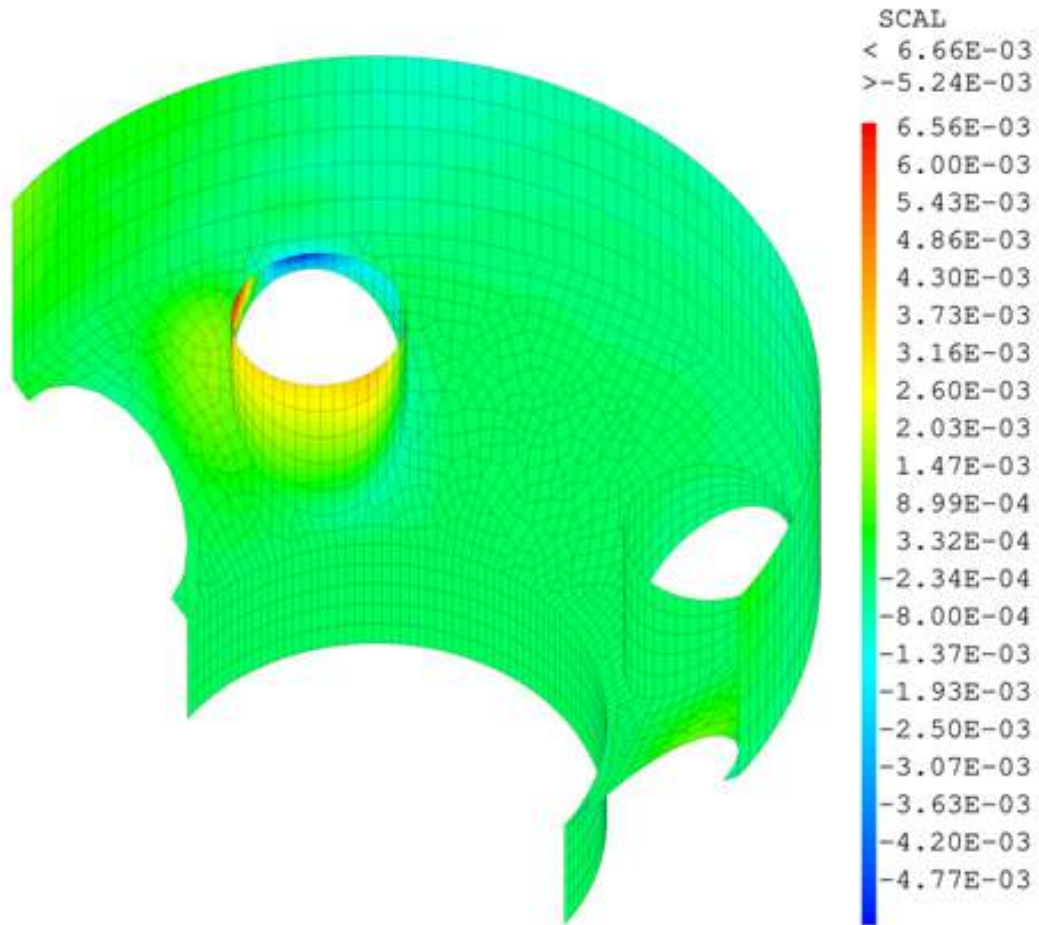
Fig. 6.5 Displacement of inner vessel (m) at 1.4 s
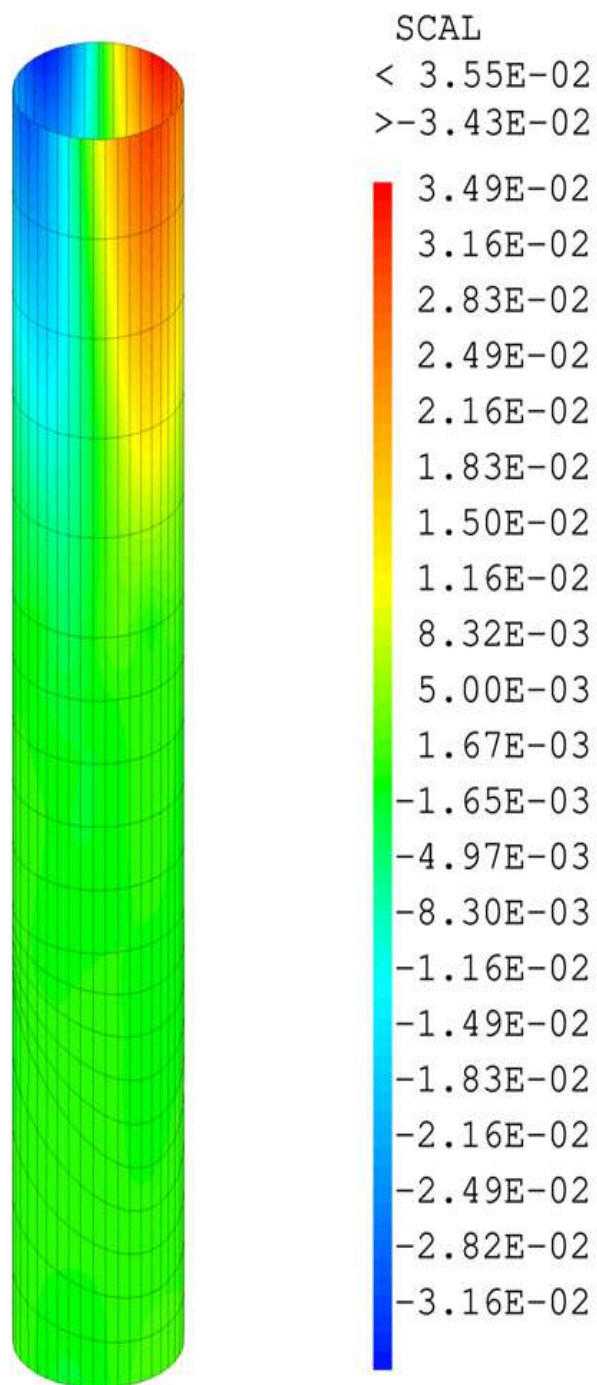
Fig.6.6 Displacement of IHX-1 (m) at 1.48 s

The maximum displacement observed at the top of the outer shield subassemblies is depicted in Fig. 6.7 and Fig. 6.8 for X and Y direction respectively. The maximum displacement is found to be 0.3 mm from the outer row of subassemblies. The displacement absorbed in the inner fuel subassemblies was very small, in the order of microns. The displacement of the fuel subassemblies at a particular time step of 1.0 s is shown in Fig. 6.9. The maximum displacement is found to be 0.008 mm
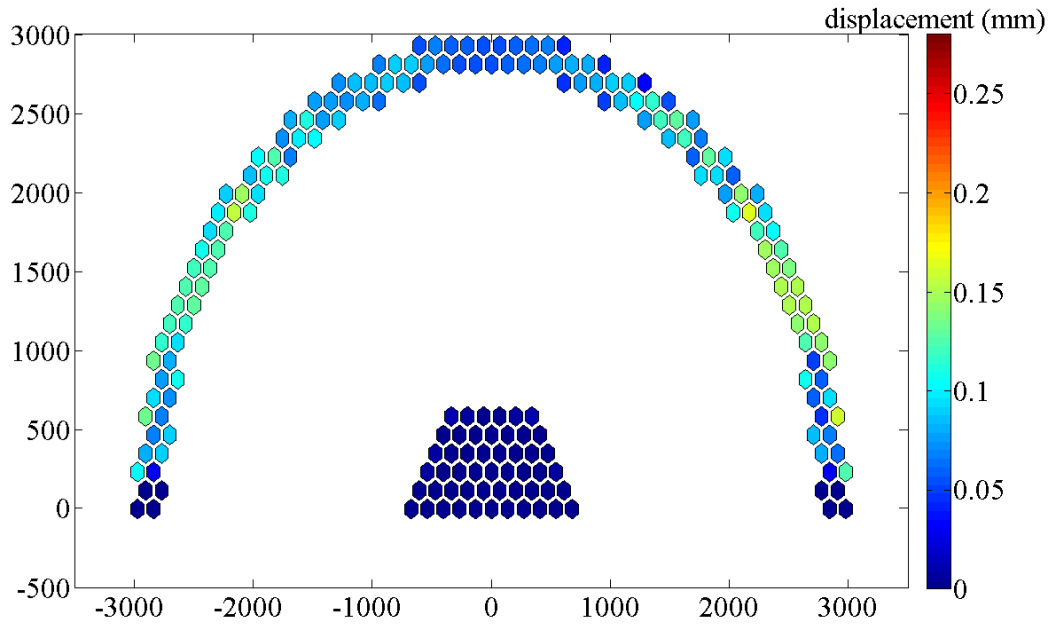
Fig. 6.7 Displacement of subassemblies in X direction
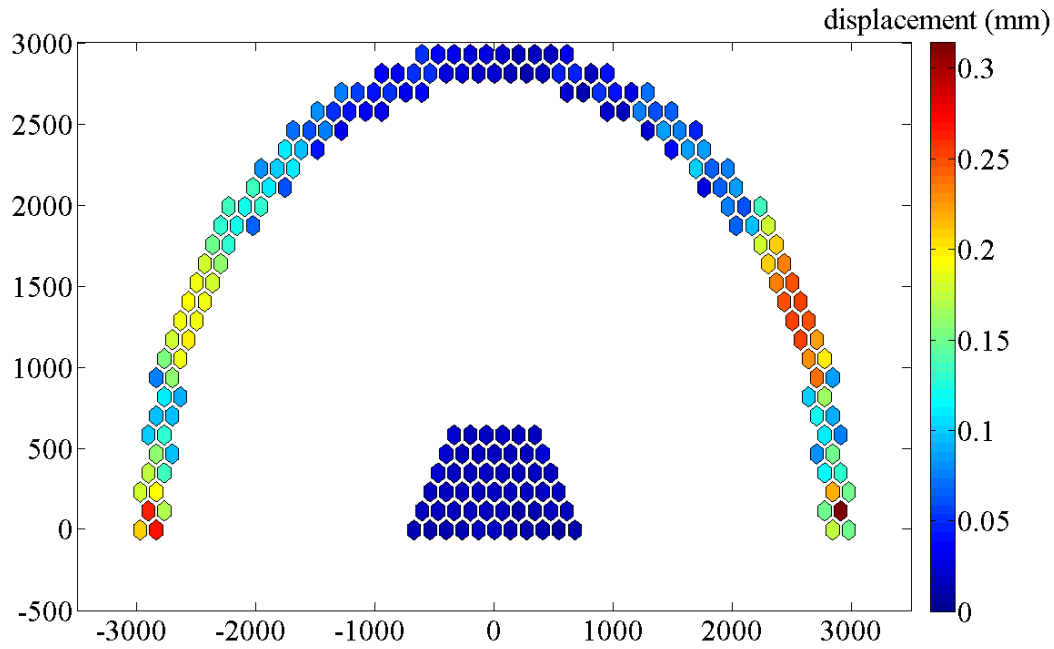
Fig. 6.8 Displacement of subassemblies in Y direction
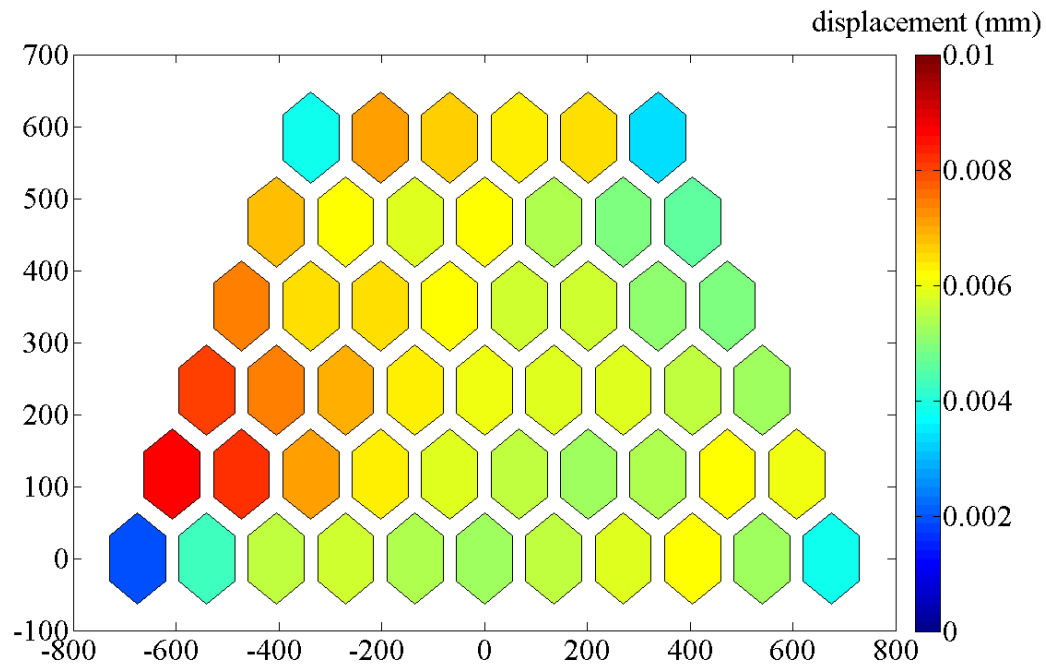
Fig. 6.9 Resultant displacement of fuel subassemblies at 1.0 s

6.2.2 Effect on reactivity perturbations

The reactivity feedbacks from sub-assemblies have been calculated by considering them as a radial boundary movement of one zone of sub-assemblies to the next zone. The reactivity change caused by the radial outward movement of a particular zone in the inner core by 1 mm is calculated (Gautama Hebbar, 2012) using first order perturbation analysis. From the observed displacements in the inner core subassemblies, the reactivity is calculated. The net reactivity change due to subassemblies displacement at 1.0 s is 0.033 pcm which is negligible. Fig. 6.10 shows reactivity distribution in the core at 1.0 s.
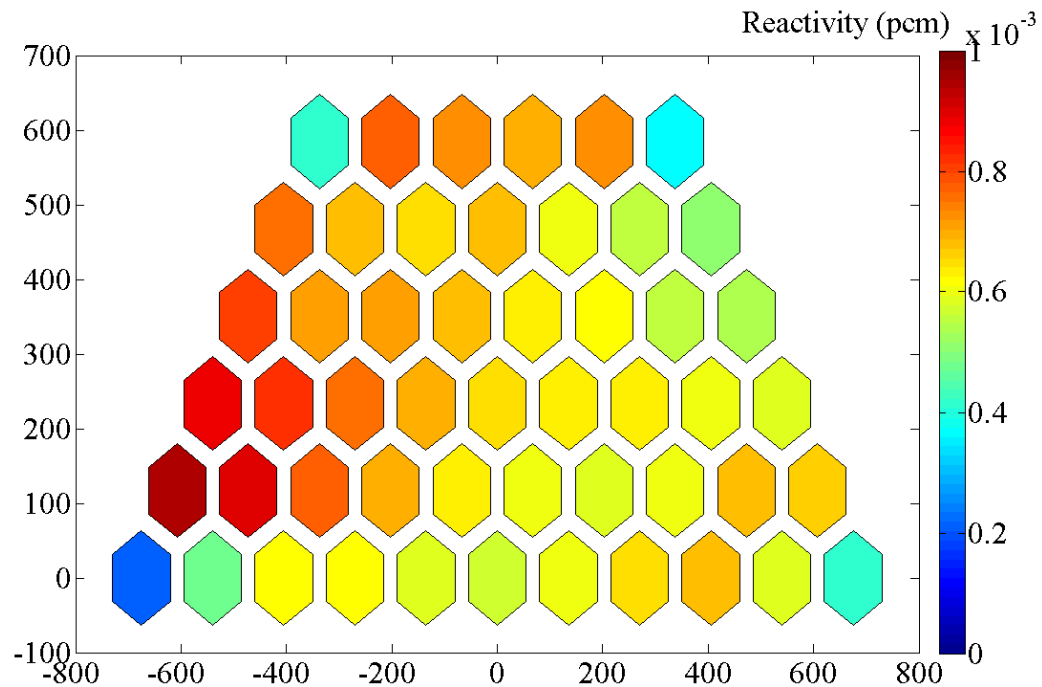
Fig. 6.10 Reactivity of fuel subassemblies at 1.0 s

6.3 CLOSURE

Steam/water leaks ranging from small to large leaks have occurred in fast reactor steam generators which influenced the plant availability and safety of the installation. In

case of a leak, necessary automatic safety actions will be initiated in the plant to quickly terminate sodium-water reaction. As a defense in depth, design basis leak sodium-water reaction has been considered in the design of secondary sodium system. A computer code SWEPT has been developed to study the pressure transients in the secondary sodium circuit due to large leak sodium-water reaction. Using the SWEPT code it is found that the design basis leak is instantaneous DEG failure of 3 tubes at the top of the Steam Generator. Further beyond the design basis leak, the possibility of more number of simultaneous and sequential tube failures have also been studied using the SWEPT code. The results for the sequential tube failures show that even though there is a failure of 100 tubes in 10 s, the maximum pressure occurred is lower than that of design basis leak. For the simultaneous failure case it is found that the IHX can withstand up to 15 DEG failures.

Since the IHX is free to vibrate at the bottom, the possibility of its vibration during the large scale sodium-water reaction and also the transmission of vibration to core subassemblies are assessed using the CAST3M computer code. Simulation for the reactor shows a maximum displacement of 9 mm for the IHX bottom point. The maximum displacement is found to be 0.3 mm for the outer row of shielding subassemblies. Very less displacement of the order of microns is observed in the inner fuel subassemblies. Reactivity perturbations due to displacement of subassemblies are found to be negligible. From the above studies it is concluded that sufficient margin exists in the design to take care of large scale sodium-water reaction events to the extent of simultaneous DEG failure of 15 tubes in the Steam Generator.

* * *

CHAPTER 7

Conclusion and Scope for Future Studies

7

7.0 CONCLUSIONS

As a part of this research work, the dynamics of structures immersed in fluid has been studied using experiments and numerical analyses. The phenomenon of Fluid Structure Interaction (FSI) Vibration of immersed structures in a finite volume of fluid is studied. Use of the numerical tool CAST3M for FSI vibration problems has been demonstrated. For the plate and tube structures, the transmission of vibration between structures for instance, from one plate to adjacent plate immersed in a finite volume of fluid is scarcely reported. Vibration transmissions between plate and tube structures have been studied using experiment and numerical simulation. The focus of the study has been to investigate the vibration in core subassemblies due to large leak sodium water reaction event. Effect of pressure transients due to sodium water reactions on reactor assembly components and vibration in core subassemblies are discussed. In the present chapter, the major observations and conclusions drawn from the results of Chapters 3 to 6 are summarized.

7.1 FSI VIBRATION BETWEEN IMMERSED STRUCTURES

➢ Free vibration analyses of plate and tube structures have been carried out and the results are compared with CAST3M results.

➢ The results are closely matching, and it provides validation of / applicability of CAST3M for the present study.

➢ Natural frequency decreases with increase in the depth of immersion for plate and tube structures in the fluid medium due to added mass. Vibration transmission between side walls of a rectangular tank is studied. It is found that transmission ratio increases and then decreases after a particular depth, this is due to the participation of higher modes at increased depth of immersion.

➢ Natural frequency of the cantilevered plate structures have been found experimentally. Parametric studies were carried out with change in width and depth of plates immersed in medium. It is observed that the resonance frequency of the plates is not affected by change in width of the plates in air. The same is not applicable in the fluid medium.

➢ Vibration transmission between two cantilevered plate structures has been studied. Transmissibility ratio is found to be higher when the plate is excited close to resonance frequency of the response plate.

➢ When the plate is excited close to its resonance frequency, the amplitude of vibration of the response plate is found to be higher and it is much lower when excited far away from its resonance frequency in immersed conditions. It is also found that the movement of plates when excited close to resonance frequency follows sudden increase and decrease in amplitude of motion of the plates in a finite fluid. This is mainly due to the superimposition of fluid wave and structural vibration

➢ Fluid damping increases with increase in the depth of immersion as expected. Further in the study of tubular structures, the natural frequencies of the tubes were found experimentally.

➢ Vibration transmission between and plate and tube were studied. Transmissibility ratios when excited close to resonance frequency of tubes showed higher values than when excited at plate resonance frequency.

7.2 FSI VIBRATION IN CORE SUBASSEMBLIES FOR DESIGN BASIS EVENT

➢ Investigations on the response of various reactor assembly components due to design basis sodium water reactions have been studied.

➢ For design basis leak event, the maximum displacement of IHX and Inner vessel is found to be 20 mm and 2 mm respectively.

➢ The displacement at the IHX bottom is found to be 0.7 mm during peak load.

➢ Maximum displacement in outer subassemblies is found to be 0.07 mm. The displacement in the fuel core subassemblies is very less, in the order of microns. Displacement from fuel subassemblies is due to direct transmission of pressure waves from IHX.

➢ Reactivity perturbations due to displacement of subassemblies are found to be negligible. Also the responses of other reactor components are also within the design limits.

7.3 FSI VIBRATION IN CORE SUBASSEMBLIES FOR BEYOND DESIGN BASIS EVENT

➢ For beyond design basis leak event, the maximum displacement of IHX and Inner vessel is found to be 35 mm and 6.5 mm respectively.

➢ The bottommost point of IHX-1 experiences a maximum displacement of 9 mm.

➢ Maximum displacement in outer subassemblies is found to be 0.3 mm. The displacement in the fuel core subassemblies is very less. Reactivity perturbations due to less displacement is found to be negligible.

➢ From these investigations, it is concluded that sufficient margin exists in the design to take care of fast transient event like large scale sodium water reactions to the extent of simultaneous double-ended guillotine failure of 15 tubes in the steam generator.

7.4 SCOPE FOR FUTURE STUDIES

➢ Three-dimensional simulation of the whole core during such a transient event can be studied.

➢ Experimental demonstration of similar event can be studied with scaled-up reactor assembly components.

➢ FSI vibration studies for hollow cylindrical shells and fluid flow between thin gaps of the structures can be studied.

∗ ∗ ∗

REFERENCES

1. Abassi, W., El Baroudi, A., Razafimahery, F., 2016. Vibration Analysis of Euler-Bernoulli Beams Partially Immersed in a Viscous Fluid. Phys. Res. Int. 2016, 1–14. https://doi.org/10.1155/2016/6761372

2. Ahn, S.J., Ha, K.-S., Chang, W.-P., Kang, S.H., Lee, K.L., Choi, C.-W., Lee, S.W., Yoo, J., Jeong, J.-H., Jeong, T., 2016. Evaluation of a Sodium–Water Reaction Event Caused by Steam Generator Tubes Break in the Prototype Generation IV Sodium-cooled Fast Reactor. Nucl. Eng. Technol. 48, 952–964. https://doi.org/10.1016/j.net.2016.02.016

3. Aizawa, K., 1998. Consideration on safety research strategy toward commercialization of FBRs. Prog. Nucl. Energy 32, 255–262.

4. Amabili, M., Frosali, G., Kwak, M.K., 1996. Free vibrations of annular plates coupled with fluids. J. Sound Vib. 191, 825–846.

5. Aoto, K., Dufour, P., Hongyi, Y., Glatz, J.P., Kim, Y., Ashurko, Y., Hill, R., Uto, N., 2014. A summary of sodium-cooled fast reactor development. Prog. Nucl. Energy 77, 247–265. https://doi.org/10.1016/j.pnucene.2014.05.008

6. Arellano Castro, R.F., Guillamot, L., Cros, A., Eloy, C., 2014. Non-linear effects on the resonant frequencies of a cantilevered plate. J. Fluids Struct. 46, 165–173. https://doi.org/10.1016/j.jfluidstructs.2014.02.001

7. Banerjee, S., Gupta, H.P., 2017.The evolution of the Indian nuclear power programme. Prog.Nucl.Energy. https://doi.org/10.1016/j.pnucene.2017.02.008

8. Bermúdez, A., Durán, R., Rodríguez, R., 1997. FINITE ELEMENT SOLUTION OF INCOMPRESSIBLE FLUID-STRUCTURE VIBRATION PROBLEMS. Int. J. Numer. Methods Eng. 40, 1435–1448. https://doi.org/10.1002/(SICI)1097-0207(19970430)40:8<1435::AID-NME119>3.0.CO;2-P

9. Bermúdez, A., Hervella-Nieto, L., Rodríguez, R., 2001. Finite element computation of the vibrations of a plate-fluid system with interface damping. Comput. Methods Appl. Mech. Eng. 190, 3021–3038.

10. Bermúdez, A., Rodríguez, R., 1999. Finite element analysis of sloshing and hydroelastic vibrations under gravity. ESAIM Math. Model. Numer. Anal. 33, 305–327.

11. Bhardwaj, S.A., 2013. Indian nuclear power programme – Past, present and future. Sadhana 38, 775–794. https://doi.org/10.1007/s12046-013-0187-4

12. Bhoje, S.B., 2003. Structural Dynamics in FBR, in: 17th International Conference on Structural Mechanics in Reactor Technology (SMiRT 17). pp. 1–10.

13. Cast3M: A general purpose code for solving partial differential equations by the finite element method. Developed by the French Atomic Energy Commission (CEA), http://wwwcast3m.cea.fr/index.php

14. CAST3M, 2000: User Guide for CAST3M. Developed by French Atomic Energy Commission (CEA), http://wwwcast3m.cea.fr/index.php

15. Canales, F.G., Mantari, J.L., 2017. Laminated composite plates in contact with a bounded fluid: Free vibration analysis via unified formulation. Compos. Struct. 162, 374–387.

16. Chambers, D.H., 2013. Acoustically Driven Vibrations in Cylindrical Structures. Lawrence Livermore National Laboratory (LLNL), Livermore, CA.

17. Chan, K.-T., Zhang, J.-Z., 1995. Free vibration of a cantilever tube partially filled with liquid. J. Sound Vib. 182, 185–190.

18. Chellapandi, P., Chetal, S.C., Raj, B., 2012. Numerical simulation of fluid–structure interaction dynamics under seismic loadings between main and safety vessels in a sodium fast reactor. Nucl. Eng. Des. 253, 125–141. https://doi.org/10.1016/j.nucengdes.2012.08.005

19. Chellapandi, P., Chetal, S.C., Raj, B., 2007. Effects of nuclear island connected buildings on seismic behaviour of reactor internals in a pool type fast breeder reactor. Nucl. Eng. Des. 237, 2250–2264. https://doi.org/10.1016/j.nucengdes.2007.04.002

20. Chellapandi, P., Jalaldeen, S., Srinivasan, R., Chetal, S.C., Bhoje, S.B., 2003. Vibration analysis of reactor assembly internals for prototype fast breeder reactor, in: Transaction of the 17th International Conference on Structural Mechanics in Reactor Technology (SMiRT 17), Prague, Czech Republic.

21. Chen, S.-S., 1985. Flow-induced vibration of circular cylindrical structures. Argonne National Lab., IL (USA). International Atomic Energy (IAEA) collection. http://www.iaea.org/inis/collection/NCLCollectionStore/_Public/17/036/17036539.pdf

22. Chetal, S.C., Balasubramaniyan, V., Chellapandi, P., Mohanakrishnan, P., Puthiyavinayagam, P., Pillai, C.P., Raghupathy, S., Shanmugham, T.K., Pillai, C.S., 2006. The design of the Prototype Fast Breeder Reactor. Nucl. Eng. Des. 236, 852–860. https://doi.org/10.1016/j.nucengdes.2005.09.025

23. Chetal, S.C., Chellapandi, P., Puthiyavinayagam, P., Raghupathy, S., V.Balasubramaniyan, Selvaraj, P., Mohanakrishnan, P., Raj, B., 2011. Current Status of Fast Reactors and Future Plans in India. Energy Procedia 7, 64–73. https://doi.org/10.1016/j.egypro.2011.06.009

24. Cho, D.S., Kim, B.H., Kim, J.-H., Vladimir, N., Choi, T.M., 2015a. Frequency response of rectangular plate structures in contact with fluid subjected to harmonic point excitation force. Thin-Walled Struct. 95, 276–286.

25. Cho, D.S., Kim, B.H., Vladimir, N., Choi, T.M., 2015b. Natural vibration analysis of rectangular bottom plate structures in contact with fluid. Ocean Eng. 103, 171–179. https://doi.org/10.1016/j.oceaneng.2015.04.078

26. Combescure, A., Glbert, R.J., Jeanpierre, F., Hoffmann, A., Livolant, M., 1980. Fluid-structure interaction: A general method used in the ceasemt computer programs. Comput. Struct. 12, 471–474.

27. Combescure, A., Hoffmann, A., Pasquet, P., 1982. The CASTEM Finite Element System, in: Brebbia, C.A. (Ed.), Finite Element Systems: A Handbook. Springer Berlin Heidelberg, Berlin, Heidelberg, pp. 115–125. https://doi.org/10.1007/978-3-662-07229-5_8

28. Cummings, G.E., 1978. Dynamic Response of a Cylindrical Shell Immersed in a Potential Fluid. U. of Calif., Davis. International Atomic Energy (IAEA) collection. http://www.iaea.org/inis/collection/NCLCollectionStore/_Public/09/408/9408493.pdf

29. Currie, R. Linekar, G.A.B. , Edge, D.M., 1990. The under sodium leak in the PFR Superheater 2 in February 1987, Proceedings of the specialists' meeting on steam generator failure and failure propagation experience, Aix-en-provence, France, IWGFR/78, pp.107-132.

30. Da Lozzo, E., Auricchio, F., Calvi, G.M., 2012. Added mass model for vertical circular cylinder partially immersed in water. Proc. 15th WCEE Lisb.

31. E.B Wylie and V.L Streeter, 1978. Fluid Transients. McGraw-Hill Inc.

32. Ergin, A., Uğurlu, B., 2003. Linear vibration analysis of cantilever plates partially submerged in fluid. J. Fluids Struct. 17, 927–939. https://doi.org/10.1016/S0889-9746(03)00050-1

33. Espinosa, H.D., Lee, S., Moldovan, N., 2006. A Novel Fluid Structure Interaction Experiment to Investigate Deformation of Structural Elements Subjected to Impulsive Loading. Exp. Mech. 46, 805–824. https://doi.org/10.1007/s11340-006-0296-7

34. Frendi, A., Maestrello, L., Bayliss, A., 1992. Coupling between plate vibration and acoustic radiation.
https://ntrs.nasa.gov/search.jsp?R=19930009581

35. Fu, Y., Price, W.G., 1987. Interactions between a partially or totally immersed vibrating cantilever plate and the surrounding fluid. J. Sound Vib. 118, 495–513.

36. Fujita, K., 1990. Flow-induced vibration and fluid-structure interaction in nuclear power plant components. J. Wind Eng. Ind. Aerodyn. 33, 405–418.

37. G. Ruloff and R.Hubner, 1990. SNR-300 Steam generator accident philosophy-Assessment due to new understanding in sodium-water reaction. (No. IAEA, IWGFR/78), Steam generator failure and failure propagation experience, Aix-en-province.

38. GauravVerma, M.Eswaran, SamiranSengupta, G.R.Reddy, ShajiMammen, 2017. Dynamic characteristics of immersed plate-type fuel assemblies under seismic excitation. Nucl. Eng. Des. 314, 11–28. https://doi.org/10.1016/j.nucengdes.2017.01.005

39. Gautama Hebbar A, 2012. Design optimization of core restraint system for a fast breeder reactor. M.Tech Thesis in Nuclear Engineering, Manipal Institute of Technology.

40. Greene, D.A., 1972. Steam generator vessel pressures resulting from a sodium-water reaction: a computer analysis with the Swear code. IAEA/INIS 3, 218–231.

41. Grzegorz Kępisty, Cyril Patricot, Daniel Broc, Guillaume Campioni, 2017, SFR mechanical scenarios and neutron transport transients with CAST3M code, Annals of Nuclear Energy, Vol 101, March, page 226-236.

42. Han, R.P., others, 1996. A simple and accurate added mass model for hydrodynamic fluid—Structure interaction analysis. J. Frankl. Inst. 333, 929–945.

43. Hori, M., 1980. Sodium/water reactions in steam generators of liquid metal fast breeder reactors. Int. At. Energy Agency IAEA 12, 707–778.

44. Horiuchi, T., Nakagawa, M., Kasai, H., 1995. Development of SAFA, a seismic analysis program for FBR core components. Nucl. Eng. Des. 157, 37–48. https://doi.org/10.1016/0029-5493(95)00984

45. Hossain, A., Humphrey, L., Mian, A., 2012. Prediction of the dynamic response of a mini-cantilever beam partially submerged in viscous media using finite element method. Finite Elem. Anal. Des. 48, 1339–1345. https://doi.org/10.1016/j.finel.2011.08.004

46. Hosseini Hashemi, S., Karimi, M., Rokni Damavandi Taher, H., 2010. Vibration analysis of rectangular Mindlin plates on elastic foundations and vertically in contact with stationary fluid by the Ritz method. Ocean Eng. 37, 174–185. https://doi.org/10.1016/j.oceaneng.2009.12.001

47. Hosseini-Hashemi, S., Karimi, M., Rokni, H., 2012. Natural frequencies of rectangular Mindlin plates coupled with stationary fluid. Appl. Math. Model. 36, 764–778. https://doi.org/10.1016/j.apm.2011.07.007

48. IAEA, 1983. Proc. Specialists' Meeting on Theoretical and Experimental Work on LMFBR Steam Generator Integrity and Reliability with a particular reference to Leak Development and Detection, Hague, IAEA IWGFR/50

49. Inaba, S., Akaishi, K., Mori, T., Hane, K., 1993. Analysis of the resonance characteristics of a cantilever vibrated photothermally in a liquid. J. Appl. Phys. 73, 2654–2658.

50. Intartaglia, C., Soria, L., Porfiri, M., 2013. Hydrodynamic coupling of two sharp-edged beams vibrating in a viscous fluid. Proc. R. Soc. Math. Phys. Eng. Sci. 470, 20130397–20130397. https://doi.org/10.1098/rspa.2013.0397

51. J. Biscarel et.al, 1982. Pressure wave effects and steam generator tube bundle deformations following guillotine failure of a tube, in: Proc. of LMFBR Safety Topical Meeting. Lyon, pp. 62–70.

52. Jeong, K.-H., Kang, H.-S., 2013. Free vibration of multiple rectangular plates coupled with a liquid. Int. J. Mech. Sci. 74, 161–172. https://doi.org/10.1016/j.ijmecsci.2013.05.011

53. Jeong, K.-H., Kim, J.-W., 2009. Hydroelastic vibration analysis of two flexible rectangular plates partially coupled with a liquid. Nucl. Eng. Technol. 41, 335–346.

54. Jeong, K.-H., Yoo, G.-H., Lee, S.-C., 2004. Hydroelastic vibration of two identical rectangular plates. J. Sound Vib. 272, 539–555. https://doi.org/10.1016/S0022-460X(03)00383-3

55. Joseph, P., Muthuveerappan, G., Ganesan, N., 1990. Vibrations of generally orthotropic plates in fluids. Compos. Struct. 15, 25–42. https://doi.org/10.1016/0263-8223(90)90079-T

56. Kadlec, J., Appelt, K.D., 1970. Flow induced rod vibrations of fast reactor subassemblies. Nucl. Eng. Des. 14, 136–150. https://doi.org/10.1016/0029-5493(70)90091-9

57. Kakodkar, A., 2008. Evolving Indian Nuclear Program: Rationale and Perspectives. Lecture at Indian Academy of Sciences.

58. Kapoor, S., 2015. Book Review: India's Nuclear Programme-Future Plans, Prospects and Concerns. Proc. Indian Natl. Sci. Acad. 81. https://doi.org/10.16943/ptinsa/2015/v81i2/48107

59. Kara, F., Vassalos, D., 2007. Hydroelastic analysis of cantilever plate in time domain. Ocean Eng. 34, 122–132. https://doi.org/10.1016/j.oceaneng.2005.12.008

60. Kerboua, Y., Lakis, A.A., Thomas, M., Marcouiller, L., 2008. Vibration analysis of rectangular plates coupled with fluid. Appl. Math. Model. 32, 2570–2586. https://doi.org/10.1016/j.apm.2007.09.004

61. Khorshidi, K., Akbari, F., Ghadirian, H., 2017. Experimental and analytical modal studies of vibrating rectangular plates in contact with a bounded fluid. Ocean Eng. 140, 146–154. https://doi.org/10.1016/j.oceaneng.2017.05.017

62. Kim, J.O., Chun, H.Y., 2003. Interaction Between the Torsional Vibration of a Circular Rod and an Adjacent Viscous Fluid. J. Vib. Acoust. 125, 39. https://doi.org/10.1115/1.1525004

63. Kim, J.O., Wang, Y., Bau, H.H., 1991. The effect of an adjacent viscous fluid on the transmission of torsional stress waves in a submerged waveguide. J. Acoust. Soc. Am. 89, 1414–1422. https://doi.org/10.1121/1.400541

64. Kishore, S., Ashok Kumar, A., Chandramouli, S., Nashine, B.K., Rajan, K.K., Kalyanasundaram, P., Chetal, S.C., 2012. An experimental study on impingement wastage of Mod 9Cr 1Mo steel due to sodium water reaction. Nucl. Eng. Des. 243, 49–55. https://doi.org/10.1016/j.nucengdes.2011.11.008

65. Kopmaz, O., Telli, S., 2002. FREE VIBRATIONS OF A RECTANGULAR PLATE CARRYING A DISTRIBUTED MASS. J. Sound Vib. 251, 39–57. https://doi.org/10.1006/jsvi.2001.3977

66. Kramer, M.R., Liu, Z., Young, Y.L., 2013. Free vibration of cantilevered composite plates in air and in water. Compos. Struct. 95, 254–263. https://doi.org/10.1016/j.compstruct.2012.07.017

67. Kwon, Y.W., Priest, E.M., Gordis, J.H., 2013. Investigation of vibrational characteristics of composite beams with fluid–structure interaction. Compos. Struct. 105, 269–278. https://doi.org/10.1016/j.compstruct.2013.05.032

68. Li, J., Guo, X.H., Luo, J., Li, H.Y., Wang, Y.Q., 2013. Analytical study on inherent properties of a unidirectional vibrating steel strip partially immersed in fluid. Shock Vib. 20, 793–807.

69. Liang, C.-C., Liao, C.-C., Tai, Y.-S., Lai, W.-H., 2001. The free vibration analysis of submerged cantilever plates. Ocean Eng. 28, 1225–1245.

70. Marcus M.S, 1978. A finite-element method applied to the vibration of submerged plates. Journal of Ship Research 22, 94–99.

71. Meylan, M.H., 1997. The forced vibration of a thin plate floating on an infinite liquid. J. Sound Vib. 205, 581–591.

72. Muthuveerappan, G., Ganesan, N., Veluswami, M.A., 1980. Influence of fluid added mass on the vibration characteristics of plates under various boundary conditions. J. Sound Vib. 69, 612–615. https://doi.org/10.1016/0022-460X(80)90631-8

73. Muthuveerappan, G., Ganesan, N., Veluswami, M.A., 1979. A note on vibration of a cantilever plate immersed in water. J. Sound Vib. 63, 385–391.

74. Narita, Y., 1982. Vibration of a non-uniform cantilever beam partially immersed in an ideal liquid. J. Sound Vib. 81, 583–586. https://doi.org/10.1016/0022-460X(82)90299-1

75. Padmakumar, G., Vinod, V., Pandey, G.K., Krishnakumar, S., Chandramouli, S., Vijaykumar, G., Rajendra Prasad, R., Mourya, R.K., Madankumar, P., Shanmugasundaram, M., Ramakrishnan, V., Meikandamurthy, C., Rajan, K.K., 2013. SADHANA facility for simulation of natural convection in the SGDHR system of PFBR. Prog. Nucl. Energy 66, 99–107. https://doi.org/10.1016/j.pnucene.2013.03.019

76. Paraz, F., Eloy, C., Schouveiler, L., 2014. Experimental study of the response of a flexible plate to a harmonic forcing in a flow. Comptes Rendus Mécanique 342, 532–538. https://doi.org/10.1016/j.crme.2014.06.004

77. Phan, C.N., Aureli, M., Porfiri, M., 2013. Finite amplitude vibrations of cantilevers of rectangular cross sections in viscous fluids. J. Fluids Struct. 40, 52–69. https://doi.org/10.1016/j.jfluidstructs.2013.03.013

78. Planchard, J., 1985. Vibrations of nuclear fuel assemblies: a simplified model. Nucl. Eng. Des. 86, 383–391.

79. Prakash, V., Thirumalai, M., Prabhakar, R., Vaidyanathan, G., 2009. Assessment of flow induced vibration in a sodium–sodium heat exchanger. Nucl. Eng. Des. 239, 169–179. https://doi.org/10.1016/j.nucengdes.2008.10.007

80. Puthiyavinayagam, P., Selvaraj, P., Balasubramaniyan, V., Raghupathy, S., Velusamy, K., Devan, K., Nashine, B.K., Padma Kumar, G., Suresh kumar, K.V., Varatharajan, S., Mohanakrishnan, P., Srinivasan, G., Bhaduri, A.K., 2017. Development of fast breeder reactor technology in India. Prog. Nucl. Energy. https://doi.org/10.1016/j.pnucene.2017.03.015

81. Qu, T., Avachat, S., Zhou, M., 2017. Response of Cylindrical Composite Structures Subjected to Underwater Impulsive Loading: Experimentations and Computations. J. Eng. Mater. Technol. 139, 021020. https://doi.org/10.1115/1.4035767

82. Raj Baldev, Chellapandi, P., Vasudeva Rao, P.R., Taylor and Francis Group, LLC, 2015. Sodium fast reactors with closed fuel cycle. (ISSN: 978-1-4665-8769-4)

83. Rajput, A.K., 1983. 122 pressure transients resulting from sodium-water reaction following a large leak in lmfbr steam generator. Theor. Exp. Work lmfbr steam Gener. Integr. Reliab. Part. Ref. Leak Dev. Detect. 122.

84. Rao, S.N., Ganesan, N., 1985. Vibration of plates immersed in hot fluids. Comput. Struct. 21, 777–787. https://doi.org/10.1016/0045-7949(85)90154-3

85. Ray W. Clough, J.P., 1975. Dynamics of Structures, 1st edition. ed. McGraw-Hill Inc.

86. RCC-MR, Section-1, Subsection B: Class 1 components, RB 3250 (Edition 2007).

87. S. T. Revankar, Brian Wolf, Anand VadlamaniBrian Wolf, 2013. Assessment of Leak Rates through Steam Generator Tubes (No. RSP-0294, PU/NE-13-11). Canadian Nuclear Safety Commission, PURDUE UNIVERSITY, School of Nuclear Engineering.

88. S Srinivas, P.S Chopra, 1977. ANALYSIS OF EBR-II SECONDARY SODIUM NETWORK FOR PRESSURES PULSES DUE TO LEAKS OF STEAM OR WATER INTO SODIUM. N.-Holl. Publ. Co. 313–325.

89. Selvaraj P., Vaidyanathan G., Chetal S.C., 1996. Review of design basis accident for large leak sodium-water reaction for PFBR, in: ICONE -PROCEEDINGS. Presented at the International Conference on Nuclear Engineering, American Society of Mechanical Engineers, United States, pp. 567–574.

90. Selvaraj, P., Seetharamu, K.N., Vaidyanathan, G., 1990. Large leak sodium-water reaction analysis of an LMFBR steam generator using a variable temperature spherical bubble model. Nucl. Eng. Des. 123, 87–90.

91. SeyunKim, Jae-HyukEoh, Seong-OKim, 2007. Development of a numerical analysis methodology for the multi-dimensional and multi-phase phenomena of a sodium–water reaction in an SFR steam generator. Annals of Nuclear Energy 34, 839–848. https://doi.org/10.1016/j.anucene.2007.04.001

92. Shabani, R., Hatami, H., Golzar, F.G., Tariverdilo, S., Rezazadeh, G., 2013. Coupled vibration of a cantilever micro-beam submerged in a bounded incompressible fluid domain. Acta Mech. 224, 841–850. https://doi.org/10.1007/s00707-012-0792-z

93. Shin, Y.W., Wiedermann, A.H., Eichler, T.V., Youngdahl, C.K., Ockert, C.E., 1988. An analytical model for dynamics of a sodium/water reaction bubble in an LMFBR steam generator and the coupled response of the intermediate heat transport system. Nucl. Eng. Des. 106, 221–230. https://doi.org/10.1016/0029-5493(88)90279-8

94. Shoei-sheng Chen, 1975. Vibration of nuclear fuel bundles. Nucl. Eng. Des. 35, 399–422. https://doi.org/10.1016/0029-5493(75)90071-0

95. Song, C., Li, X., Zhou, G., Wei, C., 2017. Research on FSI effect and simplified method of PCS water tank of nuclear island building under earthquake. Prog. Nucl. Energy 100, 48–59. https://doi.org/10.1016/j.pnucene.2017.05.025

96. Srinivasan, R. et.al. Structural Mechanics Analysis of Intermediate Heat exchanger for Prototype Fast Breeder Reactor. Transactions of the 17th International conference on Structural Materials in Reactor Technology (SMiRT-17) Prague, Czech Republic, August 17-22, 2003.

97. Srinivasan, G., Suresh Kumar, K.V., Rajendran, B., Ramalingam, P.V., 2006. The Fast Breeder Test Reactor—Design and operating experiences. Nucl. Eng. Des. 236, 796–811. https://doi.org/10.1016/j.nucengdes.2005.09.024

98. Stenius, I., Fagerberg, L., Kuttenkeuler, J., 2016. Experimental eigenfrequency study of dry and fully wetted rectangular composite and metallic plates by forced vibrations. Ocean Eng. 111, 95–103. https://doi.org/10.1016/j.oceaneng.2015.10.047

99. S.Wang, M.Flad, W.Maschek, P.Agostini, D.Pellini, G.Bandini, T.Suzuki, K.Morita, 2008. Evaluation of a steam generator tube rupture accident in an accelerator driven system with lead cooling. Progress in Nuclear Energy 50, 363–369. https://doi.org/10.1016/j.pnucene.2007.11.018

100. Tubaldi, E., Amabili, M., 2013. Vibrations and stability of a periodically supported rectangular plate immersed in axial flow. J. Fluids Struct. 39, 391–407. https://doi.org/10.1016/j.jfluidstructs.2013.03.003

101.   U.S. Lindholm, D.D. Kana, W.H. Chu, et al., 1965. Elastic vibration characteristics of cantilever plates in water. J. Ship Research 9(1), 11–22.

102.   Van Eysden, C.A., Sader, J.E., 2009. Frequency response of cantilever beams immersed in compressible fluids with applications to the atomic force microscope. J. Appl. Phys. 106, 094904. https://doi.org/10.1063/1.3254191

103.   Van Eysden, C.A., Sader, J.E., 2006. Resonant frequencies of a rectangular cantilever beam immersed in a fluid. J. Appl. Phys. 100, 114916. https://doi.org/10.1063/1.2401053

104.   Venkataramana, K., Kawano, K., 1995. Nonlinear dynamics of offshore structures under sea wave and earthquake forces. Sadhana 20, 501–512. https://doi.org/10.1007/BF02823205

105.   Zhang, Z., Hu, F., Li, Z., Hua, H., 2012. Modeling and control of the vibration of two beams coupled with fluid and active links. Shock Vib. 19, 653–668.

106.   Zhou, D., 1993. Vibration of uniform columns with arbitrarily shaped cross-sections partially submerged in water considering the effects of surface wave and compressibility of water. Comput. Struct. 46, 1049–1054. https://doi.org/10.1016/0045-7949(93)90091-Q

* * *

APPENDIX - RCCMR CRITERIA FOR DESIGN OF COMPONENETS (RCCMR, 2007)

Level-A criteria

where $P_m < S_m$; $P_l < 1.5 \, S_m$; $P_l + P_b < 1.5 \, S_m$ for elastic analysis

have been chosen for normal loading and working conditions.

Level C criteria

where $P_m < 1.35 \, S_m$; $P_l < 2.02 \, S_m$; $P_l + P_b < 2.02 \, S_m$ for elastic analysis

have been chosen for events like concurrent loading associated with either normal plant operation or Operational Basis Earthquake; loading associated with design basis accident.

Level D criteria

where $P_m < 2.4 \, S_m$; $P_l < 3.6 \, S_m$; $P_l + P_b < 3.6 \, S_m$ for elastic analysis

have been chosen for events like concurrent loading associated with either the normal plant operation or the upset plant condition and Safe Shutdown Earthquake.

For Level A criteria the component will be reused without inspection.

For Level C criteria the component will be reused after inspection.

For Level D criteria the component will not be reused.

P_m Primary membrane stress

P_b Primary bending stress

P_l Local primary membrane stress

S_m Allowable stress

NOMENCLATURE

English Alphabets

C   Sound velocity

F   Surface force

g   Acceleration due to gravity

K   Stiffness matrix

M   Mass matrix

P   Pressure

s   second

u   Displacement

Z   Fluid level

Greek symbols

$\boldsymbol{\rho_f}$ Fluid density

$\boldsymbol{\rho_s}$ Structure density

μ   Poisson's ratio

ω   Natural frequency

Acronyms

CFD   Computational Fluid Dynamics

DBE   Design Basis Event

DEG   Double Ended Guillotine

FBR   Fast Breeder Reactor

FBTR	Fast Breeder Test Reactor
FEM	Finite Element Method
FIV	Flow Induced Vibration
FSI	Fluid Structure Interaction
FRF	Frequency Response Function
GFR	Gas cooled Fast Reactor
IHX	Intermediate Heat Exchanger
LFR	Lead cooled Fast Reactor
LMFBR	Liquid Metal Fast Breeder Reactor
LVDT	Linear Variable Displacement Transformer
MOC	Method of Characteristics
PHWR	Pressurized Heavy Water Reactor
pcm	Percent milli
RMS	Root Mean Square
SFR	Sodium cooled Fast Reactor
SWEPT	Sodium Water reaction Event and Pressure Transients